Electrochemical methods for processes in polymer solvents

Hotchen, Christopher

Award date:
2015

Awarding institution:
University of Bath

Electrochemical methods for processes in polymer solvents

Christopher Edward Hotchen

A thesis submitted for the degree of Doctor of Philosophy

University of Bath
Department of Chemistry

August 2015

Table of contents

Acknowledgements

The completion of this thesis would not have been possible without the help and support of friends, family and colleagues. Firstly, I would like to thank my family for their continued support and encouragement throughout my PhD. I am grateful to John Mitchels and Ursula Potter for helping me to acquire high quality SEM images and teaching me how to use the equipment. I am grateful to Begbroke Science Park (Oxford) for allowing XPS measurements to be taken with their equipment and to Geoff Nelson, who performed all analysis of XPS data. I would like to thank Phil Jones for making and amending various pieces of glassware with great skill, including the sealed electrochemical cell for voltammetry *in vacuo* used in Chapter 3. I am very grateful to Paul Frith for manufacturing the rotating drum apparatus with high precision allowing the completion of hydrodynamic experiments. I am grateful for the COMSOL Multiphsics® simulations developed by Adrian Fisher and Viet Nguyen to model Couette flow conditions in a microgap, which provide important complementary datasets to experimental results. I would like to thank Ian Maybury for his work as a summer placement student on grafting poly(ethylene glycol) to glassy carbon and boron-doped diamond surfaces, and Khadijeh (Rahil) Nekoueian for her contribution as a visiting student towards the modification of carbon electrodes with Kolliphor® EL. I would like to thank Gary Attard for sharing his knowledge of platinum electro-catalysis and advising improvements to my experimental design.

The help and support from friends and colleagues has been invaluable. A particular thanks to Sunyhik Ahn, Pete Bush, Petra Cameron, Sara Dale, Jane Davies, Andrew Gross, Jonny Halls, Daping He, Gabriela Kissling, Pete Kubiak, Grace Lewis, Elena Madrid, Adam Pockett, Yuanyang Rong, Tom Risbridger and James Weber.

I would like to thank Prof. Frank Marken and Dr. Steve Bull for their endless support, advice and supervision throughout the course of my PhD. The many discussions have led to numerous new ideas and have been invaluable in my understanding of electrochemistry. Finally, I would like to thank the University of Bath for funding my research in the form of a University Research Studentship and providing me with the opportunity to complete a PhD.

Abbreviations

Roman symbols

Symbol	Meaning	Units
a_j	Activity of species *j*	None
A	Area	m
C	Capacitance	F
C_{dl}	Double layer capacitance	F
C_j	Concentration of species *j*	mol m^{-3}
C_j^*	Bulk concentration of species *j*	mol m^{-3}
$C_{j(x=0)}$	Surface concentration of species *j*	mol m^{-3}
D_j	Diffusion coefficient of species *j*	m^2 s^{-1}
E	Potential	V
E°	Standard reduction potential	V
$E^{\circ\prime}$	Formal reduction potential	V
F	Faraday's constant	96485 C mol^{-1}
f	Frequency	Hz
$G^\ddagger$	Gibbs energy of transition state	kJ mol^{-1}
ΔG	Change in Gibbs Free Energy	kJ mol^{-1}
h	Distance between electrode and rotating drum	m
I	Current	A
J	Flux	mol m^{-2} s^{-1}
j	Current density	A cm^{-2}
k_0	Standard heterogeneous rate constant	cm s^{-1}
k_B	Boltzmann constant	J K^{-1}
m	Mass	kg
N_A	Avagadro's number	6.023×10^{23} mol^{-1}
n	Stoichiometric number of electrons transferred	None
R	(i) Universal gas constant	8.314 J K^{-1} mol^{-1}
	(ii) Resistance	Ω
r	(i) Radius of disc electrode	m

	(ii) Radial component in cylindrical coordinates	
Re	Reynolds number	None
T	Absolute temperature	K
t	Time	s
U_0	Limiting velocity at rotating disk	m s^{-1}
V	Volume	m^3
v	Scan rate	V s^{-1}
v_j	Component velocity in *j* direction	m s^{-1}
w_e	Width of electrode	m
X_C	Capacitive reactance	Ω
x_e	Length of electrode	m
Y	Admittance	S or Ω^{-1}
y	Axial component in cylindrical coordinates	
Z	Impedance	Ω

Greek symbols

α	Transfer coefficient	None
β	Tunnelling parameter	$Å^{-1}$
γ	Activity coefficient	mol^{-1} m^3
δ	Diffusion layer thickness	m
ε	Dielectric constant	None
ε_0	Permittivity of free space	C^2 N^{-1} m^{-2}
η	(i) overpotential	V
	(ii) Dynamic viscosity	g m^{-1} s^{-1}
θ	Dimensionless voltage ($= \frac{nF(E-E^\circ)}{RT}$)	
μ_{bond}	Bond dipole moment	Debye
ν	Kinematic viscosity	m^2 s^{-1} (or Pa.s)
ρ	Density	kg m^{-3}
Φ	Electrode potential	V
φ	(i) Azimuthal angle in cylindrical coordinates	degrees (or rad)
	(ii) Phase angle	degrees (or rad)
ω	Angular frequency	rad s^{-1}

Chemical abbreviations

AQS	Anthraquinone sulfonic acid (sodium salt) monohydrate
AROP	Anionic ring-opening polymerisation
BDD	Boron doped diamond
BuFc	*n*-butyl ferrocene
CA	Chronoamperometry
CE	Counter electrode
CROP	Cationic ring-opening polymerisation
CV	Cyclic voltammetry
Fc	Ferrocene
Fc(AcOH)	Ferrocene acetic acid
$Fc(CH_2CN)$	Ferrocene acetonitrile
$Fc(CH_2NMe_2)$	Dimethylaminomethyl ferrocene
$Fc(CH_2OH)_2$	1,1'-ferrocene dimethanol
$Fc(COOH)_2$	1,1'-ferrocene dicarboxylic acid
FESEM	Field emission scanning electron microscopy
GC	Glassy carbon
H_2SO_4	Sulfuric acid
$HClO_4$	Perchloric acid
HOMO	Highest occupied molecular orbital
$K_3Fe(CN)_6$	Potassium ferricyanide(III)
$K_4Fe(CN)_6$	Potassium ferrocyanide(II)
KNO_3	Potassium nitrate
$LiClO_4$	Lithium perchlorate
LSV	Linear sweep voltammetry
LUMO	Lowest unoccupied molecular orbital
MeCN	Acetonitrile
MeOH	Methanol
PEG	Poly(ethylene glycol)
PEG200	Poly(ethylene glycol) with average M_w 200 g mol^{-1}
PEG400	Poly(ethylene glycol) with average M_w 400 g mol^{-1}
PEG600	Poly(ethylene glycol) with average M_w 600 g mol^{-1}

RDE	Rotating disk electrode
RE	Reference electrode
SCE	Saturated calomel electrode
S_N1	Unimolecular nucleophilic substitution
S_N2	Bimolecular nucleophilic substitution
SEM	Scanning tunnelling microscopy
WE	Working electrode
XPS	X-ray photoelectron spectroscopy

Abstract

It is becoming increasingly important to find "green" solvents for chemical and electrochemical purposes. Poly(ethylene glycol) has been identified as an environmentally benign, non-volatile, viscous solvent with interesting properties that could be beneficial in many applications. For example, poly(ethylene glycol) is known to be a strong absorber of carbon dioxide, which could lead to applications in carbon capture and utilisation technologies. The electrochemical properties of poly(ethylene glycol) are therefore of interest.

Voltammetry in poly(ethylene glycol) was performed. Diffusion coefficients for both oxidised and reduced forms of several redox species were determined and verified using a combination of double potential step experiments, cyclic voltammetry and computer simulations using the commercial electrochemical software DigiElch™. The optimised diffusion coefficients were approximately two orders of magnitudes smaller compared with aqueous solution, which was attributed to the higher viscosity of the polymer solvent.

The slow diffusion in viscous poly(ethylene glycol) gives low measured currents in voltammetry. To overcome the slow mass transport, a hydrodynamic technique based upon a laminar Couette flow in a microgap was developed. An increase in current of over two orders of magnitude was observed. A Levich-type equation was derived and was consistent with experimental data for the reduction of $Fe(CN)_6^{3-}{}_{(aq)}$ under Couette flow conditions. Studies in poly(ethylene glycol) could indicate complex interactions between the polymer solvent and the platinum electrode. A proposed mechanism involves the reversible adsorption of poly(ethylene glycol) to the platinum electrode above +0.4 V (*vs*. SCE).

The grafting ability of poly(ethylene glycol) was investigated by anodic coupling to glassy carbon and boron-doped diamond surfaces. Modification of carbon substrates with poly(ethylene glycol) caused a suppression in the apparent rate of electron transfer for the $Fe(CN)_6^{3-/4-}$ redox couple. The apparent rate of electron transfer after poly(ethylene glycol) attachment correlated with grafting potential, time and polymer

chain length. It is proposed that the hydrophilic redox species cannot diffuse far into the poly(ethylene glycol) layer, which slows the apparent rate of electron transfer. However, the apparent rate of electron transfer for a more hydrophobic redox species, 1,1'-ferrocene dimethanol ($Fc(CH_2OH)_2$, was not affected by grafting potential, time or chain length. The apparent selectivity of the PEG-modified electrode enabled the mediated oxidation of potassium ferrocyanide ($K_4Fe(CN)_6$) using a $Fc(CH_2OH)_2$ mediator. This mediated oxidation approach enhanced the voltammetric response for micromolar concentrations of the mediator, which could have potential uses in sensing applications.

The electrochemical grafting of a PEGylated castor oil, Kolliphor® EL, is also demonstrated. A similar suppression in the voltammetric response for the $Fe(CN)_6^{3-/4-}$ redox couple was observed and five ferrocene mediators were assessed in their ability to mediate electron transfer to $Fe(CN)_6^{3-/4-}$. The electron shuttle ability for the five ferrocene mediators decreased in the order: dimethylaminomethyl ferrocene > *n*-butyl ferrocene > ferrocene dimethanol > ferrocene acetonitrile > ferrocene acetic acid. It is proposed that the electron shuttle ability is influenced by (i) the reversible potential for the mediator molecule, (ii) the heterogeneous electron transfer kinetics for the mediator molecule, (iii) electrostatic interactions, and (iv) mediator aggregation at the modified surface.

Finally, a one-step electroless deposition method is developed, which utilises the reducing ability of poly(ethylene glycol). A platinum salt precursor solution is prepared in PEG200 and heated at 500 °C for 30 min in atmospheric conditions. PEG200 acts as both the solvent and as the reducing agent. The high temperature causes PEG200 to evaporate, which results in the formation of metallic Pt nano-fibrous deposits. The electrochemically active surface area and the electro-catalytic activity of the Pt nano-fibrous deposits was determined. Only a slight increase in catalytic activity is observed for the nano-fibrous deposits compared with a bulk polycrystalline Pt disc.

Aims

The aims of this thesis are:

- To investigate the use of low molecular weight poly(ethylene glycol)s as inexpensive, non-volatile, environmentally benign solvents in electrochemical applications. Develop a methodology using voltammetric measurements coupled with computer simulations to determine the diffusion coefficients for a range of redox species in poly(ethylene glycol) under mixed diffusion (planar and hemi-spherical) conditions.

- To develop a novel hydrodynamic method suitable for electro-synthetic processes in highly viscous media. Derive theory to compliment the hydrodynamic process to enable the technique to be used as a quantitative tool. Verify theoretical models with experiment using low molecular weight poly(ethylene glycol) as the viscous solvent.

- To develop an electrochemical attachment method for modifying the surface of carbon electrodes with poly(ethylene glycol) derivatives. Provide evidence for attachment and investigate the electrochemical properties of the poly(ethylene glycol) modified electrodes. For example, investigating changes in the rate of electron transfer for different redox species at poly(ethylene glycol) modified electrodes.

- To use a mediated oxidation mechanism at poly(ethylene glycol) modified electrodes to enhance currents of redox species at low concentrations. This approach could be adapted for use in electrochemical sensing devices.

- To develop a novel, one-step, electroless deposition of metal nanoparticles using poly(ethylene glycol) as both the solvent and reducing agent. The electrochemical surface area and catalytic activity of metal nanoparticles will be explored.

Chapter 1: Introduction to electrochemical solvents

Chapter abstract

The quest to discover and use environmentally benign solvents is becoming increasingly more important. This chapter gives an overview of the significant role that solvents have in chemical and electrochemical processes, and highlights the advantages and disadvantages of aqueous, organic and ionic liquid media in electrochemical processes. Poly(ethylene glycol) is a non-toxic, non-volatile, inexpensive polyether that has been identified as an environmentally benign solvent with potential uses in electrochemical applications. The physical properties of poly(ethylene glycol) are discussed and applications for increasing the solubility of therapeutics and its use as an additive in electroplating solutions are described. Previous literature using poly(ethylene glycol) based electrolytes in electrochemistry has been reviewed and the suitability of the polymer solvent for such purposes has been highlighted.

Chapter contents

1. Introduction to electrochemical solvents

Many organic solvents have detrimental effects on the environment and it is becoming increasingly important to use alternative, less damaging materials for chemical or electrochemical processes. Poly(ethylene glycol) (PEG) is well documented to be environmentally benign and to have a low toxicity.[1,2] It is an inexpensive solvent made from the polymerisation of ethylene glycol or ethylene oxide and has many applications, for example as a suppressor in electroplating solutions,[3] as a lubricant,[4] and was sprayed on the Mary Rose to prevent degradation of the wooden ship.[5] The polyether has also been shown to exhibit anti-biofouling properties, increase the solubility of pharmaceuticals in the body, and is known to be a good absorber of carbon dioxide with uses in carbon capture and utilisation technologies.[6-8] Despite the wide ranging applications for poly(ethylene glycol), the electrochemical properties of the material have received limited attention in the literature. However, the low toxicity of poly(ethylene glycol) implies that the polymer could have potential future uses in chemical and electrochemical technologies. This thesis seeks to explore the use of poly(ethylene glycol) as the solvent in electrochemical processes and develop a novel hydrodynamic method to enhance currents. An electrochemical attachment of poly(ethylene glycol) to carbon surfaces will also be investigated and the electrochemical properties of PEG-modified electrodes examined. Finally, poly(ethylene glycol) will be used as the solvent and reducing agent for the synthesis of platinum nanoparticles using a thermolysis method.

1.1. Chemical solvents

The success of any chemical reaction can be influenced by many experimental parameters, such as temperature, pressure, the use of a catalyst and the solvent. In liquid phase chemical reactions, the solvent provides the medium in which a reaction can occur. For a solvent to be useful for a particular chemical reaction, it must dissolve the starting materials, reagents and any reaction intermediates. Generally polar solvents will solubilise polar molecules and ionic species, whereas non-polar solvents will solubilise non-polar molecules. The dielectric constant (ε) reflects a solvent's ability to

stabilise electrostatic charges in a solution and can be used as a measure of the polarity of the solvent. Solvents with a large dielectric constant are considered to be polar and those with a low dielectric constant are considered to be non-polar.[7] The dielectric constant (or relative permittivity) is defined as the dimensionless ratio between the permittivity of the material (ε_μ) and the permittivity of free space (ε_0):

$$\varepsilon = \frac{\varepsilon_\mu}{\varepsilon_0} \tag{1.1}$$

The polarity of a solvent can also be measured using the molecular dipole moment (μ), which is the vector sum of the dipole moment for each bond in the molecule. A dipole moment for a bond (μ_{bond}) is the product of the charge (q) and the bond distance (d):

$$\mu_{bond} = q \times d \tag{1.2}$$

Water (H_2O) is a polar solvent with a large dielectric constant ($\varepsilon = 80$ at 25 °C) and a molecular dipole moment of 1.85 D.[9,10] The oxygen atom is more electronegative than hydrogen and attracts electron density in the O-H bonds. The oxygen atom therefore accumulates a partial negative charge (δ^-) and each hydrogen a partial positive charge (δ^+). The molecular dipole exists due to the bent shape of the water molecule (Figure 1.1A). Ionic salts, such as potassium nitrate (KNO_3), can fully dissociate in water to form K^+ cations and NO_3^- anions, which are surrounded by the solvent molecules. The surrounding water molecules orient themselves such that the $O^{\delta-}$ atoms are facing the K^+ cations and the $H^{\delta+}$ atoms on water are facing the NO_3^- anions (Figure 1.1B). If water molecules are considered as dipoles, the molecular dipole moments will point towards the K^+ cations and away from the NO_3^- anions. This arrangement helps to stabilise the electrostatic charges on the dissociated ionic species. The layer of solvent surrounding a dissolved species is known as a solvation shell.

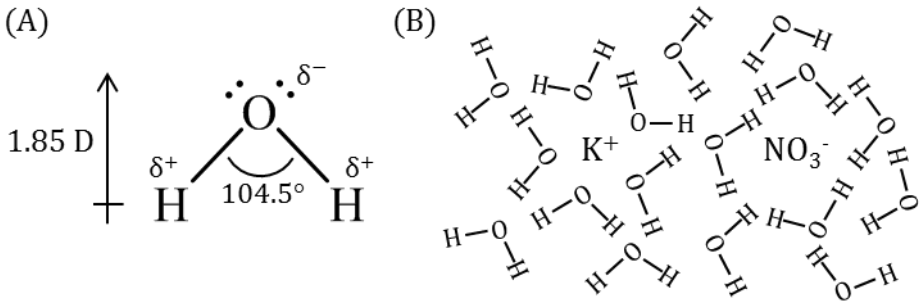

Figure 1.1. (**A**) The structure of a water molecule showing the bond angle and dipole moment. (**B**) A schematic diagram of how water molecules might arrange themselves around dissociated KNO_3 ions.

A simple, one step liquid phase chemical reaction can be described as:

$$A_{(aq)} + B_{(aq)} \longrightarrow C \qquad (1.3)$$

The starting materials (A and B) are solubilised by the solvent and are free to move through the solution. When molecules A and B collide in the correct orientation and with enough energy to overcome the activation energy barrier a chemical reaction will take place and product C will be formed. It is necessary for the solvent to solubilise the starting materials, which allows for collisions, and hence the reaction, to occur. However, the solvent can also affect the rate and mechanism of the reaction. For example, the unimolecular nucleophilic substitution (S_N1) reaction of a tri-substituted alkyl, such as *tert*-butyl bromide, will occur at a faster rate in more polar solvents.[11] The S_N1 mechanism proceeds through a charged carbocation intermediate, the formation of which is the rate determining step for the reaction. The transition state for the formation of the carbocation intermediate is stabilised to greater extents by more polar solvents. Consequently the activation energy for the rate determining step is lower in more polar solvents and the rate of the reaction is increased (Figure 1.2).

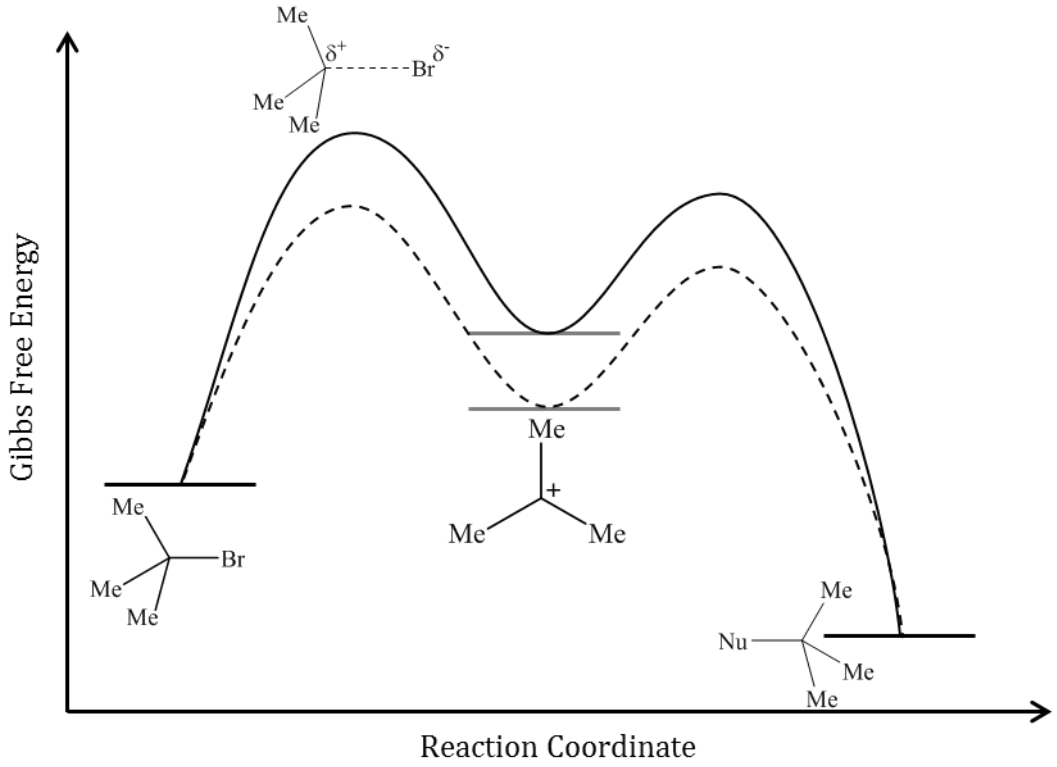

Figure 1.2. A reaction profile for the unimolecular nucleophilic substitution (S_N1) of *tert*-butyl bromide. The formation of the carbocation intermediate is the rate determining step. The transition state and carbocation intermediate is stabilised by polar solvents (dashed line).

1.2. Solvents in electrochemistry

The importance of the solvent in chemical processes has already been highlighted and extends even further for electrochemical processes. Electrochemical processes typically involve the immersion of at least two electrodes into a solution and passing a current between them. The solution must therefore provide a conductive pathway between the electrodes in order to form a complete electrical circuit. The conductivity of the solution is usually achieved by dissolving an ionic salt, such as KNO_3, in a polar solvent, such as water. As the potential difference between the electrodes is changed, oxidation and reduction processes can occur at the surface of the electrodes. At some stage the potential between the electrodes will be great enough to cause oxidation or reduction of the solvent. The potentials at which the solvent is oxidised and reduced defines the usable potential window for the solvent. For a redox process to be studied effectively

using voltammetry, it is important that the oxidation or reduction potential for the redox species falls within the usable potential window for the solvent.

Since electrochemical reactions only take place at the electrode surface, the rate of the reaction, and therefore the current, is often limited by the flux of redox material to and away from the electrode. In a static electrolyte the flux of material to the electrode surface is usually determined by the rate of diffusion, where faster diffusion leads to higher currents. The Stokes-Einstein equation (equation 1.4) indicates that the diffusion coefficient of a species (D) in a solvent is inversely proportional to the dynamic viscosity (η) of the solvent.

$$D = \frac{k_B T}{6\pi\eta a} \tag{1.4}$$

Here k_B is the Boltzmann constant, T is the absolute temperature (in K) and a is the hydrodynamic radius. Consequently, solvents with a low viscosity are better suited as solvents for electrochemical applications.

To maintain a constant and known concentration of redox analyte throughout the course of an electrochemical investigation is often important for analytical purposes. In some cases the concentration of analyte could change due to evaporation of the solvent. Solvents with a high vapour pressure should therefore be avoided. For this reason voltammetry under reduced pressure is not possible in aqueous media. However, aqueous electrolytes provide an important medium for many electrochemical processes.

1.2.1. Aqueous electrolytes

The low toxicity, high abundance and low cost of water makes it a good solvent for a wide range of electrochemical processes, such as for biosensors; wastewater treatment, analysis and purification, in corrosion studies, and as the solvent in lead acid batteries.[12-17] The number and diversity of processes performed and studied in aqueous electrolytes highlights the importance of water as a solvent.

Pure water has a high resistivity (> 18 MΩ.cm), which makes voltammetry in pure water problematic, however, a supporting electrolyte may be dissolved to lower the resistance of the solution. The ionic conductivity through a solution is achieved by

charge separation of the dissolved species, which allows free migration of ions in an electric field to carry the charge. The supporting electrolyte is typically an electrochemically inert ionic species, such as potassium nitrate (KNO_3), which carries the electric charge through the solution and is added in high concentrations (0.1 – 1 M) to ensure the solution resistance is reduced sufficiently for voltammetry. Furthermore, the supporting electrolyte also helps to prevent the movement of charged redox species under the influence of an electric field, which is known as mass transport by migration.[18] The concentration of the supporting electrolyte is generally in large excess compared with the redox species under investigation. Consequently, if a negative charge is applied to an electrode, the cations from the more abundant supporting electrolyte will move towards the electrode by electrostatic interactions and form a double layer at the electrode surface. Equally, if a positive charge is applied to an electrode, the anions of the supporting electrolyte will move towards the electrode surface. The accumulation of ions at the electrode surface screens the electric field from penetrating into the bulk solution. As a result, the electric field in the bulk solution is minimal and charged species do not move via migration. Assuming mass transport by migration to be an insignificant process allows many electrochemical theories to be simplified.

One of the major advantages of using an aqueous electrolyte is the availability of reference electrodes that have a well-defined and stable potential. A good reference electrode should have a low impedance such that a large change in current does not change the potential to a significant degree. An electrode that exhibits this behaviour is known as an ideal non-polarisable electrode. The silver/silver chloride (Ag/AgCl) electrode and KCl-saturated calomel (Hg/Hg_2Cl_2) electrode approach this ideal non-polarisable behaviour at low currents and are therefore commonly used as reference electrodes in aqueous electrolytes. A KCl-saturated calomel electrode (SCE) is comprised of a column of mercury in contact with calomel (Hg_2Cl_2) immersed in a saturated KCl solution (Figure 1.3).[19] The SCE electrode has a well-defined potential due to the fast equilibrium established at the liquid mercury | calomel | solution triple phase boundary.

$$2Hg + 2Cl^- \rightleftharpoons Hg_2Cl_2 + 2\,e^- \qquad (1.5)$$

The reference electrode is usually separated from the working and counter electrodes by a porous glass frit or a Luggin capillary to avoid contamination between the electrolyte for the reference electrode and the bulk electrolyte.

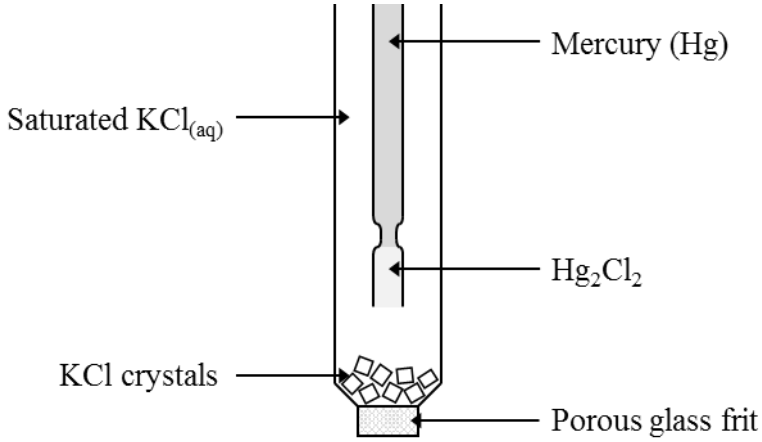

Figure 1.3. The structure of a KCl-saturated calomel reference electrode.

The usable potential window for aqueous electrolytes depends on several factors including pH and electrode material. However, the reduction of water to form hydrogen (hydrogen evolution reaction) or the oxidation of water to form oxygen (oxygen evolution reaction) often determine this usable potential range for aqueous solutions. The hydrogen evolution reaction (HER) occurs at 0 V (*vs.* SHE) at a platinum working electrode immersed in 1 M $HClO_{4(aq)}$.[20] However, the driving force for hydrogen evolution is lower in more basic solutions, and the process occurs at more negative potentials. For example, the hydrogen evolution reaction occurs at -1.15 V (*vs.* SCE) in 1 M NaOH.[20] Furthermore, the potential required for the hydrogen evolution reaction is highly dependent upon the electrode material. For example, the overpotential for hydrogen evolution at a mercury electrode is larger than for a platinum electrode.[21,22] For this reason mercury is used in voltammetric analysis of water samples with trace metal impurities, although alternative less toxic electrode materials are being developed.[23-25] Some electrochemical processes occur at similar potentials to the hydrogen evolution reaction (or oxygen evolution reaction). For example, the reduction of carbon dioxide has been widely studied on a range of different metal and alloy surfaces in potassium carbonate buffer and often occurs at similar potentials to the hydrogen evolution reaction.[26] There are numerous reaction pathways for carbon dioxide reduction, which are dependent upon solvent, electrolyte concentration and pH.

However, the Faradaic efficiency for carbon dioxide reduction is often low due to the competing hydrogen evolution reaction. In these instances aprotic, polar organic solvents, such as dimethyl formamide (DMF), can be useful alternatives.[27]

Water has many advantages as a solvent in electrochemistry but not all redox processes are suitable for study in aqueous media. For example, materials used in photovoltaic devices are often highly air and water sensitive. Water can often degrade the photoactive materials in the solar cell resulting in reduced cell efficiency and lifetime.[28,29] It is therefore important to exclude water from these cells and the use of alternative solvents is necessary. Non-aqueous solvents may also be required to study organic redox species that are insoluble in aqueous solutions, such as anthraquinone.

1.2.2. Organic solvents in electrochemistry

Electrochemistry in polar organic solvents, such as acetonitrile (MeCN) and dimethylsulfoxide (DMSO), allows for some redox molecules that are insoluble in aqueous solution to be studied but also allows investigation of some redox species that exhibit electrochemistry outside of the usable solvent potential window for water. [30] Electrochemistry in organic solvents has been widely developed and has applications in electro-organic synthesis, electro-polymerisation reactions,[31] Li-ion battery technology[32] and in dye-sensitised solar cells.[33]

Similar to aqueous electrolytes, the conductivity of organic solvents must be provided by the intentional addition of supporting electrolyte, which carries the charge through the solution. However, due to the lower dielectric constant for most organic solvents, the conductivities observed in organic solvents generally do not match those observed in aqueous media. This results in electrochemical systems with a higher solution resistance, which are less ideal for voltammetry. Organic electrolytes are often based upon tetraalkylammonium salts, such as tetrabutylammonium hexafluorophosphate ($[NBu_4]^+$ $[PF_6]^-$), which can provide sufficient conductivity (and solubility) in a range of polar organic solvents.[34]

Reference electrodes used in aqueous voltammetry are often not suitable for use in non-aqueous solvents, even if they are separated by a porous glass frit. The organic

electrolyte may diffuse into the aqueous reference electrolyte and affect the potential. Equally, the aqueous electrolyte surrounding the reference electrode may diffuse into the organic electrolyte and contaminate the solution. If water is immiscible with the organic electrolyte a liquid-liquid phase boundary would result, where a potential drop is observed across the phase boundary, which adds an uncompensated resistance to the system. Consequently, alternative pseudo-reference electrodes, such as a silver wire, are often used in non-aqueous media. However, the potential of a metal wire in solution can be affected by water content and proton concentration. Pseudo-reference electrodes are often calibrated by spiking the organic solution with ferrocene (Fc). The potential of the redox analyte of interest can then be recorded in reference to the one-electron $Fc^{0/+}$ redox couple, which would be expected to have a fixed reversible potential.

Although organic solvents allow the electrochemical investigation of a wide range of compounds, and methods have been developed to find stable reference electrodes, there are some drawbacks to using organic solvents. Many organic solvents have a high vapour pressure and high volatility, which makes devices containing these compounds inflammable and often restricts their useful lifetime. When considered with the often harmful effects of organic solvents to living organisms and the environment, alternatives should be found for electrochemical applications.

1.2.3. Ionic liquids in electrochemistry

Room temperature ionic liquids (RTILs) are a relatively modern class of compounds with interesting, unusual and potentially useful properties in many areas of chemistry. They are defined as "materials composed of cations and anions, that melt around 100 ºC or below as an arbitrary temperature limit."[35] Literature sources often claim ionic liquids to be non-volatile,[36] non-flammable,[37] thermally stable[38] and have good solvation properties for a range of polar and non-polar compounds.[39]

The first ionic liquids were reported independently by Siegmund Gabriel in 1888 and by the Latvian chemist Paul Walden in 1914.[40,41] Walden used ethylammonium nitrate, which has a melting point of 12 ºC, for conductivity measurements. [42] However, further work on room temperature ionic liquids was limited until the discovery of pyridinium- and imidazolium-based haloaluminate room temperature ionic melts. Chum et al.

reported the "first use of a room temperature, high Lewis acid molten salt system" for electrochemistry, which was based on a 2:1 mix of aluminium chloride : ethylpyridinium bromide and observed a solvent potential window of -0.2 V to +1.8 V (*vs.* Al reference electrode).[43] However, the haloaluminate ionic liquids were highly moisture and oxygen sensitive and needed to be handled in glove box conditions to avoid oxidation of the aluminium halide. However, the development of non-haloaluminate ionic liquids created a 'new' class of room temperature ionic liquids that showed improved air and water stability. The first of these were based on the 1-ethyl-3-methylimidazolium (EMIm) cation with a range of inorganic anions, such as nitrate (NO_3^-), tetrafluoroborate (BF_4^-) and sulfate (SO_4^-).[44] Despite still being hygroscopic, these first non-haloauluminate ionic liquids could be dried in an oven at 80 °C.[44] Over 300 room temperature ionic liquids are now commercially available, and more could be designed based on an ever increasing library of suitable anions and cations (Figure 1.4), each with individual and unique properties.[45] Further developments have also seen the discovery of deep eutectic solvents (DES), which can be categorised as a sub-class of ionic liquids. Deep eutectic solvents are low melting point materials typically composed of quaternary ammonium salts and either metal salts or hydrogen bond donors.[46]

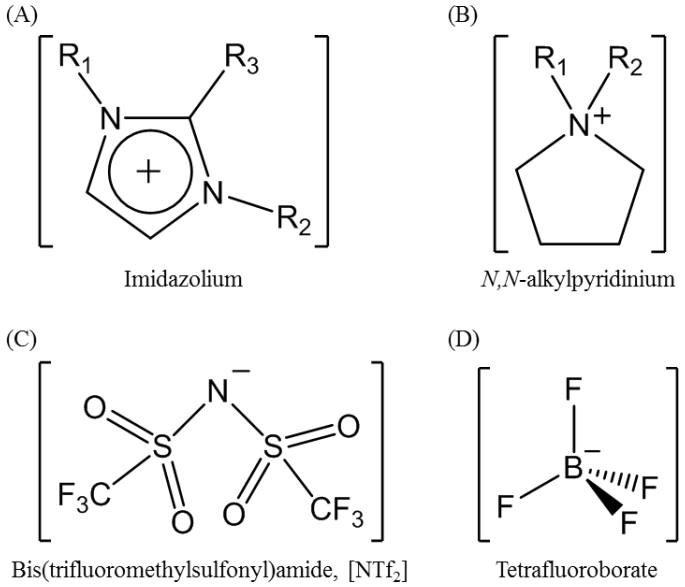

Figure 1.4. The chemical structure of (**A**) imidazolium and (**B**) *N*,*N*-dialkylpyrrolodinium cations, and (**C**) bis(trifluoromethylsulfonyl)amide, $[NTf_2]^-$ and (**D**) tetrafluoroborate anions, $[BF_4]^-$, which are commonly used as constituents for room temperature ionic liquids.

By definition ionic liquids have a high charge density and all exhibit intrinsic conductivity due to the free movement of ions. Consequently the intentional addition of an ionic salt is not required for electrochemistry in ionic liquids. However, the conductivity of the ionic liquid is usually significantly lower compared with aqueous electrolytes and is dependent upon ion size, anionic charge delocalisation, viscosity and density.[47-50] In general, cations based on the imidazolium structure tend to exhibit the highest conductivities (~10 mS cm^{-1}), whereas quaternary ammonium salts are less conductive (~2 mS cm^{-1}).[42] The conductivity of the ionic liquids can be increased by adding molecular organic solvents, water and in some cases Li^+ ions.

Highly pure and dry room temperature ionic liquids can exhibit a broad usable electrochemical potential window. Suarez *et al*. reported a potential window for [BMIm][BF_4] of up to 7 V where the negative and positive limits were determined by the reduction of the cation and the oxidation of the anion respectively.[51] However, impurities will often lower the usable potential limits.[52] Ionic liquids are often hygroscopic, but the addition of even 3 wt. % water can severely decrease the electrochemical solvent window, in some instances by more than 2 V.[53] This can reduce the usefulness of the ionic liquid solvent.

The viscosity of ionic liquids can be up to three orders of magnitude higher than for conventional molecular solvents.[54] Consequently, the rate of mass transport within ionic liquids can be slow, which could impact the currents recorded in voltammetric experiments. In addition, extensive purging must be performed prior to electrochemical experimentation to remove all traces of oxygen from the system. Sufficient purging will take longer in more viscous solvents.

Pure room temperature ionic liquids have many advantages, such as low-volatility, large usable potential window and intrinsic conductivity. However, the synthesis and purification of ionic liquids is often expensive and their hygroscopic nature can lead to water impurities, which can be detrimental to the desired properties. The very high viscosity can make handling ionic liquids troublesome and the environmental and health risks remain largely unknown.[55,56] A less expensive and environmentally benign alternative to ionic liquids should be found as solvents in electrochemistry.

1.3. Poly(ethylene glycol)

1.3.1. Chemical and physical properties of poly(ethylene glycol)

Poly(ethylene glycol) is generally considered to be an inexpensive, environmentally benign, non-toxic, non-volatile, highly viscous polymer, which has many interesting properties including bio-fouling resistance when attached to surfaces.[57-59] Poly(ethylene glycol) is also known to absorb carbon dioxide (CO_2) well, which could suggest potential applications as a solvent for the electrochemical capture and conversion of carbon dioxide.[7,60] These advantageous properties could make poly(ethylene glycol) suitable for use as a solvent in electrochemical investigations. The polymer already has many uses in a wide range of applications, for example as a material to control the viscosity of printer inks[61], and as a spray to maintain the structure of wooden archaeological objects[62]. Poly(ethylene glycol) derivatives are also used as electrolyte materials in battery technology[63], as a calibration compound for mass spectrometry[64], as a plasticiser, and as a moiety added to pharmaceuticals to increase the bioavailability of drug molecules.[65]

Poly(ethylene glycol), poly(ethylene oxide) and poly(oxyethylene) are synonymous names for the polyether molecule with a structure shown in Figure 1.5. However, the preferred name typically depends on the chain length of the polymer. If the average molecular weight of the polymer is less than ~100,000 g mol^{-1}, poly(ethylene glycol) (PEG) is the preferred choice, however, if the average molecular weight is greater than ~100,000 g mol^{-1} poly(ethylene oxide) (PEO) is usually favoured.[66] Poly(oxyethylene) (POE) can be used to refer to any chain length. The average molecular weight frequently suffixes the abbreviated polymer name. For example, a poly(ethylene glycol) with an average molecular weight of 200 g mol^{-1} would be denoted as PEG200.

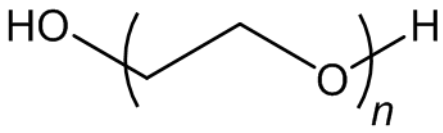

Figure 1.5. The chemical structure of poly(ethylene glycol), where *n* denotes the degree of polymerisation. $n \approx 4$ for PEG with an average molecular weight of 200 g mol^{-1} (PEG200).

The appearance of poly(ethylene glycol) depends largely on the chain length of the polymer. PEG is a clear, viscous liquid at room temperature when the average molecular weight is less than 600 g mol^{-1}. However, at higher molecular weights the polymer exists as a white, waxy solid. The melting point of the polymer increases with chain length due to increasing van der Waals forces, and reaches a limiting value at 67 °C.[66] Hydrogen bonding can occur between the terminal hydroxyl groups and the ether oxygen atoms, in particular for low molecular weight PEGs due to the greater abundance of terminal hydroxyl groups. The polymer is completely miscible with water and dissolves in polar organic solvents such as methanol, ethanol, and acetonitrile. However, PEG is insoluble in non-polar organic solvents, such as diethyl ether and hexane.[67]

In 1859, Lourenco and Wurtz independently synthesised poly(ethylene glycol) for the first time. Lourenco vigorously heated ethylene glycol with ethylene dibromide to give short chain polymers, whilst Wurtz reacted ethylene oxide (also known as oxirane) to give a white solid that melted at 56 °C. [68,69] The production of poly(ethylene glycol) was industrialised by the Union Carbide Corporation in 1958 using an alkaline metal carbonate in order to give higher average molecular weights. [67,68]

Poly(ethylene glycol) can be synthesised by the cationic[70-73] or anionic[74,75] polymerisation of ethylene oxide. The polymerisation conditions have been studied to lower the polydispersity index of the product.[76] One method involves the anionic ring opening polymerisation (AROP) of ethylene oxide. The polymerisation is described as "anionic" because the end group of the growing chain carries an anionic (negative) charge during chain propagation.[77] The AROP of ethylene oxide typically proceeds through a three step mechanism: (i) an initiation step, (ii) a propagation step, and (iii) a termination step (Figure 1.6).[75] An initiator molecule, often a strong base, such as a metal alkoxide, reacts with the ethylene oxide monomer via a bimolecular nucleophilic substitution (S_N2) reaction to generate a reactive species with an anionic end group. This reactive species becomes the growing chain and can react with a second monomer species via another S_N2-type reaction to increase the chain length by one monomer unit and regenerate the reactive site. The polymerisation is terminated by the addition of either alcohol or water.[75]

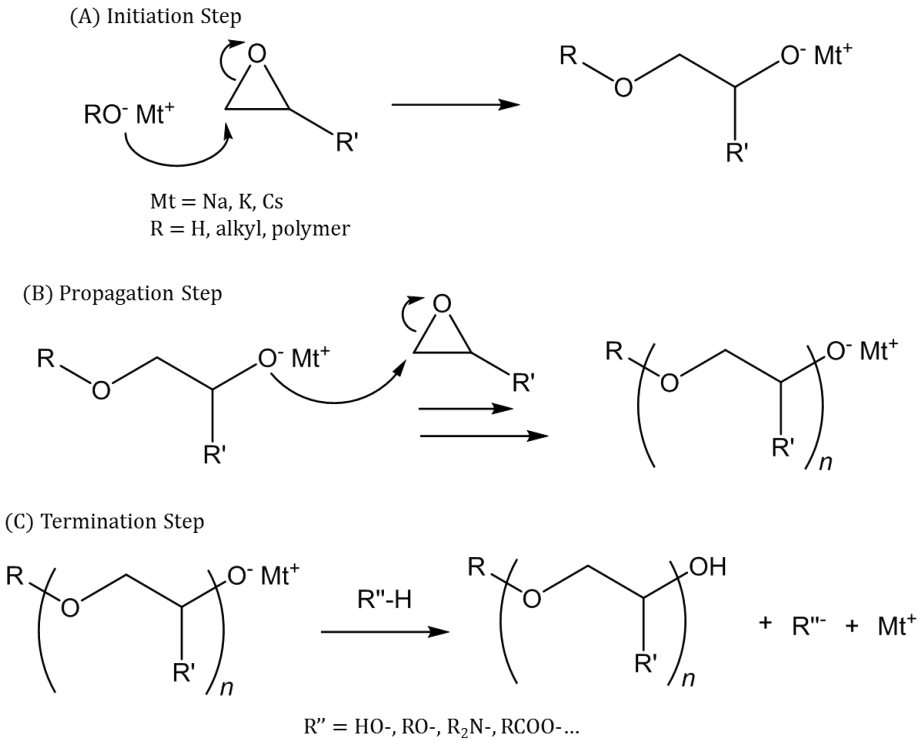

Figure 1.6. The three-step mechanism for anionic ring-opening polymerisation of ethylene oxide to form poly(ethylene glycol) initiated by a metal alkoxide. Figure taken from reference 75.

The reactivity of PEGs is largely determined by the functionality on the end group of the polymer chain and many mono- or di-substituted PEG molecules are commercially available. In its most simplistic form, the terminal functional groups are two hydroxyl (-OH) groups. These hydroxyl end groups are susceptible to oxidation and PEG can be considered as a mild reducing agent.[78] The reducing ability of PEG increases with temperature, however, the PEG chains decompose above 250 °C.[79]

1.3.2. Poly(ethylene glycol) as a suppressor in electroplating solutions

Electroplating involves the electrochemical reduction of metal ions from solution to form metallic deposits on the electrode surface and is an important technique in many applications, such as the fabrication of nano-electronic devices and in corrosion resistance.[80] In order to improve the uniformity of the deposited metal, organic additives are often incorporated in the plating bath. These can generally be classed as accelerators/brighteners, levellers and suppressors/inhibitors.[81] Accelerators provide growth sites to allow the electrodeposition process to occur at a faster rate. They often diffuse easily to the bottom of crevices, which can help to fill trenches and flatten

concave regions of the substrate. Suppressors are species, usually poly(alkylene glycols), which inhibit the electrodeposition rate by binding to areas of high current density. They will accumulate at the top of trenches and prevent further deposition in this region until the trench has been filled (Figure 1.7).[82] Levellers, such as the nitrogen rich Janus Green dye, also inhibit the rate of electrodeposition but in areas of high mass transport.[83,84] The synergistic effect of accelerators, suppressors and levellers is important to fill trenches from the bottom without forming voids.[84]

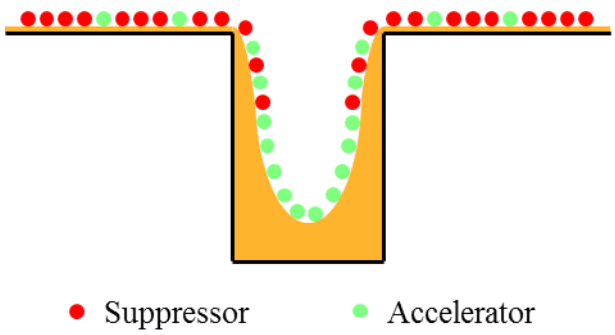

Figure 1.7. A schematic of a pit in electrodeposition. Accelerators diffuse to the bottom of the pit, whilst suppressors inhibit growth at the surface. This results in bottom-up deposition to fill the trench.[82]

The electrodeposition of copper has important applications in the fabrication of electronic devices and the quality of the copper deposit is strongly influenced by the concentration and nature of the additives present in the plating solution.[85] For the fabrication of electronic devices it is important for any trenches to be completely filled without voids to ensure high conductivity in the copper deposits, which often act as wires.[81] The plating bath usually consists of sulfuric acid (H_2SO_4), copper sulfate ($CuSO_4$), ~1 mM chloride ions (Cl^-), an accelerator and a suppressor,[81] which is often poly(ethylene glycol) with an average molecular weight of greater than 1000 g mol^{-1}.[83] The effects of the plating bath composition on the electrodeposition has been studied extensively, in particular for the superconformal filling (or superfilling) of trenches.[84,86-88] A mechanism as to how poly(alkylene glycols), in particular poly(ethylene glycol), inhibits copper deposition was proposed by Garrido and Pritzker.[87] Their model developed from earlier work by Hebert[89] where an adsorbed complex comprising of Cl^-, PEG and Cu^+ (herein referred to as $ClCuPEG_{(ads)}$) is considered to be the active suppressor species. Surface-enhanced Raman spectroscopy (SERS) has provided evidence for the formation of the $ClCuPEG_{(ads)}$ species.[90,91] The

formation of the $ClCuPEG_{(ads)}$ is thought to proceed via the following pathway in the presence of chloride ions:

$$Cu^{2+}_{(aq)} + Cl^- + e^- \rightleftharpoons CuCl_{(ads)} \quad (1.6)$$

$$CuCl_{(ads)} + PEG \rightleftharpoons ClCuPEG_{(ads)} \quad (1.7)$$

Feng *et al*. suggest the adsorbed ClCuPEG complex binds to the copper substrate by a bridging chloride bond,[90] however, others propose a model where poly(ethylene glycol) binds directly to the metal substrate.[92] When the ClCuPEG complex is adsorbed, an active site is filled and the deposition of metallic copper is obstructed, which causes the rate of deposition to decrease. Copper deposition can only occur when the ClCuPEG complex has desorbed. Poly(ethylene glycol) is an effective inhibitor in electroplating systems because it can reversibly adsorb onto metallic surfaces. The reversible adsorption of PEG on platinum has also been reported, where the terminal hydroxyl groups are suspected to bind with the metallic surface.[93] Chapter 4 discusses the adsorption of PEG on platinum in further detail.

1.3.3. PEGs in medicinal applications

Due to their low toxicity and resistance to bio-fouling, PEGs have found many applications in medicinal applications. They have been used to modify proteins[94] and drug molecules to increase the solubility of therapeutics *in vivo*,[95] and modify liposomes for drug delivery systems.[96] There are many drug molecules modified with poly(ethylene glycol) that are commercially available, such as Pegasys®[1] and Krystexxa®[2], which are used to treat hepatitis C and chronic gout respectively.[97-99]

Without any modification poly(ethylene glycol) induces a laxative effect when ingested and is poorly metabolised by the human body. For this reason PEGs have been administered to children prior to colonoscopies to clean and improve visualisation of the bowel.[100] A PEG3500 treatment prior to colonoscopy was deemed significantly more "effective" when compared with another preparative method using a senna laxative.[100] The use of PEG as a medicinal tool for children highlights the low toxicity of the compound.

[1] Also known as PEG-interferon-α2a.
[2] Also known as PEG-Uricase or Pegloticase.

Protein and peptide drugs are useful therapeutic compounds, however, many are poorly soluble in water and can generate an immune response (immunogenic), which makes their use problematic. Abuchowski *et al*. tackled this issue in the 1970s by developing a process known as PEGylation. Poly(ethylene glycol) was used to modify the surface of two proteins – bovine serum albumin and bovine liver catalase. The immunogenicity and circulating life was improved, and the activity of the enzyme was maintained after PEGylation.[101,102] PEG covalently binds to the polypeptide and shrouds the protein, which helps to camouflage the antigen *in vivo* and slow down an immune response.[103] The pharmacological properties of the PEGylated proteins are dependent upon the number and length of the PEG chains attached. Typically, proteins modified with a greater number of PEG chains have a longer circulatory half-life and are less prone to an immune response.[103]

For PEGylation to be successful, the poly(ethylene glycol) chain must attach to a protein molecule at a suitable binding site. Due to the complex structure of proteins each polypeptide has a range of suitable binding sites, which often include the *N*-terminus and the *C*-terminus of free amino acids. Typically the terminal hydroxyl groups on poly(ethylene glycol) need to be converted to more reactive functionality prior to covalent attachment to a protein molecule.[104] A range of activated PEGs have been designed and synthesised to target the various surface functionalities of proteins.[105] Lysine is the most abundant amino acid and has an amine containing side chain that can be targeted as a PEGylation binding site (Figure 1.8).[106] Site specific protein PEGylation has also been reported in order to synthesise well-defined protein-polymer conjugates.[107]

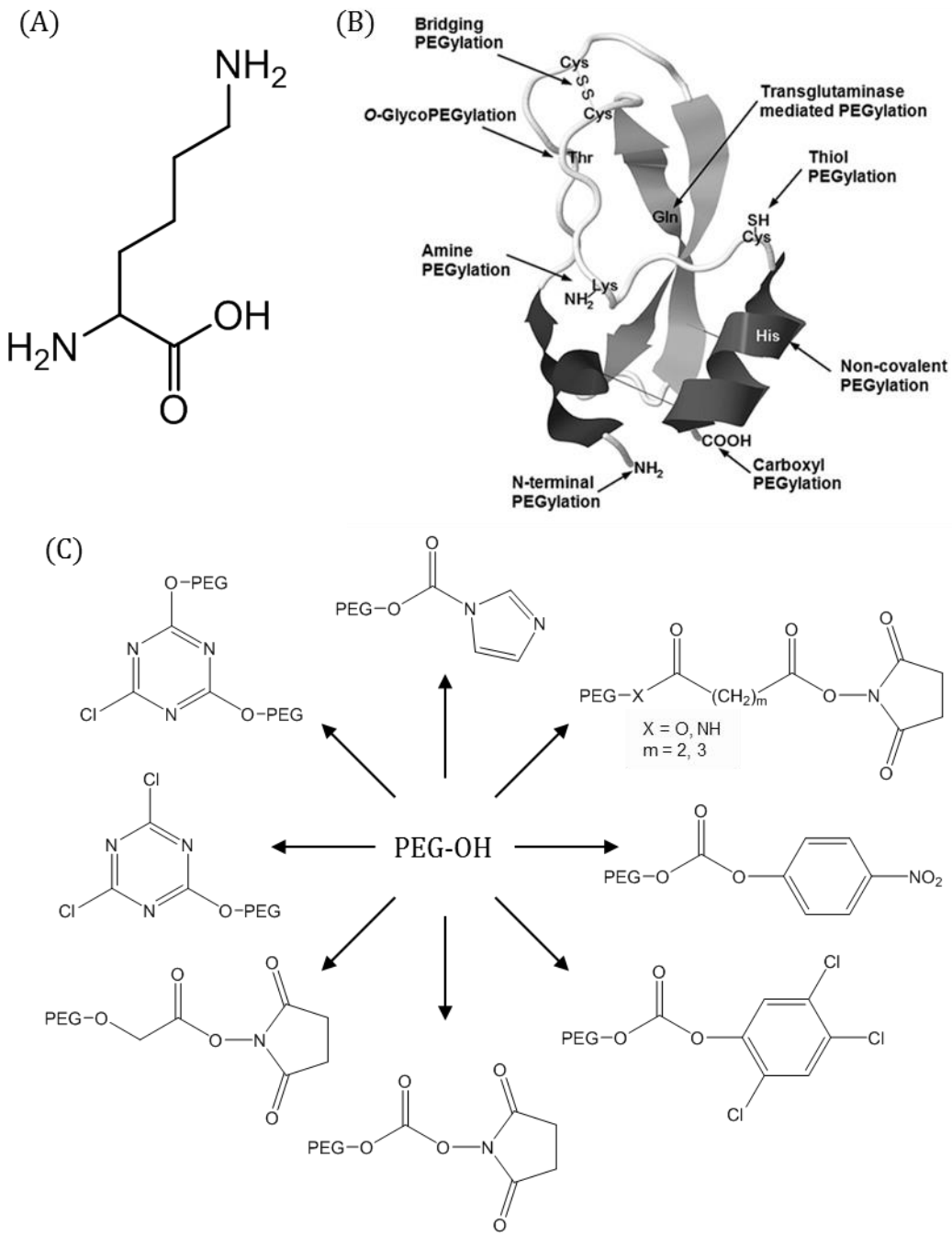

Figure 1.8. (**A**) The chemical structure of lysine. (**B**) An illustration showing the diverse functionality on proteins suitable for PEGylation (reprinted from reference 106) (**C**) A range of activated PEG molecules used for PEGylation of proteins (adapted from reference 105).

A general mechanism for PEGylation involves a chemical activation of a PEG derivative, such as a mono-methoxylated-PEG, followed by the formation of a covalent bond with the therapeutic. The PEG activation step converts the unprotected terminal hydroxyl group into a more reactive species such as a carbonate, aldehyde or tresylate.[105] The active group can then form a covalent linkage to the polypeptide chain.

Despite the wide range of synthetic routes developed for the chemical PEGylation of proteins, the prospect of using electrochemical techniques to modify surfaces with poly(ethylene glycol) has received little attention. PEG-modified surfaces could be important biofouling resistant materials and will be discussed in more detail in Chapters 5 and 6.

1.3.4. Poly(ethylene glycol) in electrochemistry

High molecular weight poly(ethylene oxide) is commonly used as a gel or solid polymer electrolyte. The low lattice energy of poly(ethylene oxide) and its good ability to solvate alkali metal salts[108] makes it a useful electrolyte material in solar cells[109] and in battery technologies.[110] A solid polymer electrolyte eliminates the risk of leakages in the cell, which can improve the safety and robustness of the device.[111]

There are fewer reports of electrochemical investigations in low molecular weight polymer solvents. However, some fundamental studies at a metal | polymer electrolyte interface were performed by Dong and Zhou in the mid-1990s.[112-120] They used both steady state and non-steady state methods to determine the diffusion coefficients (D) and standard heterogeneous rate constants for electron transfer (k_s) for several ferrocene derivatives in polyethylene glycols.[116] They suggest the apparent diffusion coefficient (D_{app}) is larger at higher ferrocene concentrations and if the supporting electrolyte cation has a larger radius.[117] The ether oxygen atoms on the poly(ethylene glycol) chain are thought to coordinate to the cation of the supporting electrolyte. A larger cation has a lower surface charge density, which results in weaker coordination with the ether oxygen atoms. Weaker coordination allows for a larger degree of polymer chain mobility, which results in a lower viscosity and a higher apparent diffusion coefficient for the redox species.[118] The same authors found that an electrolyte with a smaller anion radius led to a larger apparent diffusion coefficient in a polymer solvent electrolyte.[119] A similar rationale was used to explain this finding: a smaller electrolyte anion has a higher surface charge density and can coordinate more strongly to the cation of the electrolyte. Consequently, the electrolyte cations binds more weakly to the

polymer chains, which increases the chain mobility leading to a lower viscosity and higher diffusion coefficient for the redox species.[119]

The effect of temperature and chain length was also investigated.[117,120] Higher molecular weight pol(ethylene glycols) were observed to have higher viscosities and exhibit lower diffusion coefficients. Increasing the temperature was found to increase the diffusion coefficients.[116,120] However, a sharp increase in the diffusion coefficient was observed when a threshold temperature was reached (20-25 °C for PEG600).[120] This temperature coincided with the melt transition temperature (T_m) for the polymer. It is expected that at temperatures greater than T_m the polymer exists in an amorphous state. However, at temperatures lower than T_m crystalline regions are expected to form, which act to impede the diffusion of species in the solution.[120,121]

The high decomposition temperature of poly(ethylene glycol) allows for voltammetric studies to be performed across a wide temperature range. Ohno reports the reversible redox responses of PEG modified haem-proteins, such as haemoglobin and myoglobin, in a poly(ethylene glycol) solvent between -10 °C and 140 °C.[122] The PEG-modified proteins were stable for over 10 h at 80 °C in PEG solutions, however, denatured within 20 minutes at 60 °C in aqueous solution.[123] The beneficial thermal stability provided by the polymer solvent was rationalised by a less vigorous molecular motion of the polymer chains compared with molecular solvents.[122]

The diffusion of species in polymer solvent electrolytes is primarily dependent upon (i) the size of the diffusing species and (ii) the interactions between the species and the polymer chain.[116] Poly(ethylene glycol) with an average molecular weight of 200 g mol^{-1} (PEG200) exists as a liquid, amorphous polymer at room temperature ($T_{m(PEG200)}$ < 20 °C) and the diffusion coefficient (D) is considered to be related to the viscosity (η) by the Stokes-Einstein relation (equation 1.4). PEG200 has a low viscosity compared to other members of the poly(ethylene glycol) family, has a large dipole moment and can solubilise a wide variety of substrates, which makes it a suitable solvent for voltammetric experiments.[122]

Low molecular weight poly(ethylene glycols) could be useful solvents for electrochemical processes due to their low toxicity, low cost and low volatility. However, the solvents have been shown to have a high viscosity, which is responsible for the low diffusion coefficients of redox species previously reported in the literature (10^{-8}–10^{-7} cm^2 s^{-1}).[116,124] This thesis explores methods using poly(ethylene glycol) as a solvent in electrochemical investigations. A computer simulation method is used to determine diffusion coefficients of species under a mixed diffusion regime (Chapter 3), and a new hydrodynamic method is developed to overcome slow diffusion in highly viscous media (Chapter 4). An electrochemical method is developed to modify carbon electrodes with poly(ethylene glycol) derivatives and the electrochemical properties of these PEG-modified electrodes is investigated (Chapters 5 and 6). Finally, a one-step method to synthesise metal nano-catalysts from a metal salt precursor solution is developed using poly(ethylene glycol) as both the solvent and reducing agent (Chapter 7).

1.4. References

1. S. K. Sharma and A. Mudhoo, eds., *Green Chemistry for Environmental Sustainability*, CRC Press, 2011.
2. J. Chen, S. K. Spear, J. G. Huddleston and R. D. Rogers, *Green Chemistry*, 2005, **7**, 64-82.
3. C.-C. Hung, W.-H. Lee, Y.-L. Wang, D.-Y. Chan and G.-J. Hwang, *Journal of Vacuum Science & Technology A*, 2008, **26**, 1109-1114.
4. M. Kobayashi, T. Koide and S.-H. Hyon, *Journal of the Mechanical Behavior of Biomedical Materials*, 2014, **38**, 33-38.
5. J. Preston, A. D. Smith, E. J. Schofield, A. V. Chadwick, M. A. Jones and J. E. M. Watts, *Plos One*, 2014, **9**.
6. K. Holmberg and J. M. Harris, *First International Congress on Adhesion Science and Technology - Invited Papers: Festschrift in Honor of Dr. K.L. Mittal on the Occasion of His 50th Birthday*, 1998, 443-460.
7. Z.-Z. Yang, Q.-W. Song and L.-N. He, *Capture and Utilization of Carbon Dioxide with Polyethylene Glycol*, Springer, 2012.
8. Y. Tanaka, K. Matin, M. Gyo, A. Okada, Y. Tsutsumi, H. Doi, N. Nomura, J. Tagami and T. Hanawa, *Journal of Biomedical Materials Research Part A*, 2010, **95A**, 1105-1113.
9. C. G. Malmberg and A. A. Maryott, *Journal of Research of the National Bureau of Standards*, 1956, **56**, 1-8.
10. A. I. Vogel, *Vogel's textbook of practical organic chemistry*, Longman, Suffolk, 4th ed / revised by B. S. Furniss, A. J. Hannaford, V. Rogers, P. W. G. Smith and A. R. Tatchell edn., 1979.

11. P. Sykes, *A guidebook to mechanism in organic chemistry*, Harlow : Pearson Prentice Hall, Harlow, 6th ed. edn., 1986.
12. C. Shan, H. Yang, J. Song, D. Han, A. Ivaska and L. Niu, *Analytical Chemistry*, 2009, **81**, 2378-2382.
13. G. H. Chen, *Separation and Purification Technology*, 2004, **38**, 11-41.
14. K. Sipila, M. Bojinov, W. Mayinger, T. Saario and M. Stanislowski, *Electrochimica Acta*, 2015, **173**, 757-770.
15. S. Vasudevan and M. A. Oturan, *Environmental Chemistry Letters*, 2014, **12**, 97-108.
16. F. Fu and Q. Wang, *Journal of Environmental Management*, 2011, **92**, 407-418.
17. C. A. Martinez-Huitle and E. Brillas, *Applied Catalysis B-Environmental*, 2009, **87**, 105-145.
18. A. J. Bard and L. R. Faulkner, *Electrochemical methods : fundamentals and applications*, John Wiley, New York ; Chichester, 2nd edn., 2001.
19. R. Compton and C. Banks, *Understanding Voltammetry*, Imperial College Press, 2nd edn., 2011.
20. Š. Komorsky-Lovrić, Electrolytes in *Electroanalytical Methods: Guide to Experiments and Applications*, eds. F. Scholz, A. M. Bond, R. G. Compton, D. A. Fiedler, G. Inzelt, H. Kahlert, Š. Komorsky-Lovrić, H. Lohse, M. Lovrić, F. Marken, A. Neudeck, U. Retter, F. Scholz and Z. Stojek, Springer, Berlin Heidelberg, 2010, pp. 309-330.
21. F. Scholz, A. J. Bard and G. Inzelt, *Electrochemical Dictionary*, Springer-Verlag, Berlin, Heidelberg, 2008.
22. A. Wieckowski, *Interfacial electrochemistry : theory, experiment and applications*, Dekker, New York, 1999.
23. P. Surmann and H. Zeyat, *Analytical and Bioanalytical Chemistry*, 2005, **383**, 1009-1013.
24. W. Yantasee, L. A. Deibler, G. E. Fryxell, C. Timchalk and Y. H. Lin, *Electrochemistry Communications*, 2005, **7**, 1170-1176.
25. A. Manivannan, R. Kawasaki, D. A. Tryk and A. Fujishima, *Electrochimica Acta*, 2004, **49**, 3313-3318.
26. M. Azuma, K. Hashimoto, M. Hiramoto, M. Watanabe and T. Sakata, *Journal of the Electrochemical Society*, 1990, **137**, 1772-1778.
27. D. Niu, H. Wang, H. Li and X. Zhang, *Electrochemistry Communications*, 2015, **52**, 58-62.
28. I. Hwang, I. Jeong, J. Lee, M. J. Ko and K. Yong, *ACS applied materials & interfaces*, 2015, **7**, 17330-17336.
29. H.-L. Lu, T. F. R. Shen, S.-T. Huang, Y.-L. Tung and T. C. K. Yang, *Solar Energy Materials and Solar Cells*, 2011, **95**, 1624-1629.
30. F. Scholz and SpringerLink (Online service), Springer Berlin Heidelberg, Berlin, Heidelberg, Editon edn., 2010.
31. P. S. Kubiak, S. Awhida, C. Hotchen, W. Deng, B. Alston, T. O. McDonald, D. J. Adams and P. J. Cameron, *Chemical Communications*, 2015, **51**, 10427-10430.
32. L. J. Hardwick and P. G. Bruce, *Current Opinion in Solid State & Materials Science*, 2012, **16**, 178-185.
33. B. Oregan and M. Gratzel, *Nature*, 1991, **353**, 737-740.
34. M. Ue, K. Ida and S. Mori, *Journal of the Electrochemical Society*, 1994, **141**, 2989-2996.
35. C. Reichardt, *Organic Process Research & Development*, 2007, **11**, 105-113.

36. M. J. Earle, J. Esperanca, M. A. Gilea, J. N. C. Lopes, L. P. N. Rebelo, J. W. Magee, K. R. Seddon and J. A. Widegren, *Nature*, 2006, **439**, 831-834.
37. M. Smiglak, W. M. Reichert, J. D. Holbrey, J. S. Wilkes, L. Y. Sun, J. S. Thrasher, K. Kirichenko, S. Singh, A. R. Katritzky and R. D. Rogers, *Chemical Communications*, 2006, 2554-2556.
38. J. Patra, P. P. Dahiya, C.-J. Tseng, J. Fang, Y.-W. Lin, S. Basu, S. B. Majumder and J.-K. Chang, *Journal of Power Sources*, 2015, **294**, 22-30.
39. M. J. Neto, R. Leones, F. Sentanin, J. M. S. S. Esperanca, M. J. Medeiros, A. Pawlicka and M. M. Silva, *Journal of Electroanalytical Chemistry*, 2014, **714**, 63-69.
40. G. Khashayar, *Green and Sustainable Chemistry*, 2014, **04**, 44.
41. B. Kirchner, Preface in *Ionic Liquids*, ed. B. Kirchner, Berlin : Springer, Berlin, 1st edn., 2010, pp. xi-xiii.
42. P. Hapiot and C. Lagrost, *Chemical Reviews*, 2008, **108**, 2238-2264.
43. H. L. Chum, V. R. Koch, L. L. Miller and R. A. Osteryoung, *Journal of the American Chemical Society*, 1975, **97**, 3264-3265.
44. J. S. Wilkes and M. J. Zaworotko, *Journal of the Chemical Society-Chemical Communications*, 1992, 965-967.
45. N. V. Plechkova and K. R. Seddon, *Chemical Society Reviews*, 2008, **37**, 123-150.
46. E. L. Smith, A. P. Abbott and K. S. Ryder, *Chemical Reviews*, 2014, **114**, 11060-11082.
47. P. Bonhote, A. P. Dias, N. Papageorgiou, K. Kalyanasundaram and M. Gratzel, *Inorganic Chemistry*, 1996, **35**, 1168-1178.
48. A. B. McEwen, H. L. Ngo, K. LeCompte and J. L. Goldman, *Journal of the Electrochemical Society*, 1999, **146**, 1687-1695.
49. J. Sun, M. Forsyth and D. R. MacFarlane, *Journal of Physical Chemistry B*, 1998, **102**, 8858-8864.
50. H. Tokuda, K. Hayamizu, K. Ishii, M. Susan and M. Watanabe, *Journal of Physical Chemistry B*, 2005, **109**, 6103-6110.
51. P. A. Z. Suarez, C. S. Consorti, R. F. de Souza, J. Dupont and R. S. Goncalves, *Journal of the Brazilian Chemical Society*, 2002, **13**, 106-109.
52. B. D. Fitchett, T. N. Knepp and J. C. Conboy, *Journal of the Electrochemical Society*, 2004, **151**, E219-E225.
53. U. Schroder, J. D. Wadhawan, R. G. Compton, F. Marken, P. A. Z. Suarez, C. S. Consorti, R. F. de Souza and J. Dupont, *New Journal of Chemistry*, 2000, **24**, 1009-1015.
54. S. Zhang, N. Sun, X. He, X. Lu and X. Zhang, *Journal of Physical and Chemical Reference Data*, 2006, **35**, 1475-1517.
55. D. Zhao, Y. Liao and Z. Zhang, *Clean-Soil Air Water*, 2007, **35**, 42-48.
56. B. Kudlak, K. Owczarek and J. Namiesnik, *Environmental Science and Pollution Research*, 2015, **22**, 11975-11992.
57. M. Q. Zhang, T. Desai and M. Ferrari, *Biomaterials*, 1998, **19**, 953-960.
58. A. J. Downard and A. bin Mohamed, *Electroanalysis*, 1999, **11**, 418-423.
59. H. Maeda, M. Itami, K. Katayama, Y. Yamauchi and H. Ohmori, *Analytical Sciences*, 1997, **13**, 721-727.
60. Z.-Z. Yang, L.-N. He, Y.-N. Zhao, B. Li and B. Yu, *Energy & Environmental Science*, 2011, **4**, 3971-3975.
61. H. H. Lee, K. S. Chou and K. C. Huang, *Nanotechnology*, 2005, **16**, 2436-2441.
62. R. M. Seborg and Inverari.Rb, *Science*, 1962, **136**, 649-&.

63. Y. Kusachi, J. Dong, Z. Zhang and K. Amine, *Journal of Power Sources*, 2011, **196**, 8301-8306.
64. J. T. Watson, *Introduction to mass spectrometry instrumentation, applications and strategies for data interpretation*, Chichester : Wiley, Chichester, 4th ed. edn., 2007.
65. F. M. Veronese and G. Pasut, *Drug Discovery Today*, 2005, **10**, 1451-1458.
66. S. Aldrich, *Poly(ethlene glycol) and Poly(ethylene oxide)*, http://www.sigmaaldrich.com/materials-science/material-science-products.html?TablePage=20204110, Accessed 12 June 2015.
67. J. K. Gao, *Polyethylene Glycol as an Embedment for Microscopy and Histochemistry*, CRC, Florida, 1993.
68. F. E. Bailey and J. V. Koleske, *Poly(ethylene oxide)*, Academic Press Inc., 1976.
69. F. E. Bailey, *Alkylene Oxides and Their Polymers*, Taylor & Francis, 1990.
70. O. Nuyken and S. D. Pask, *Polymers*, 2013, **5**, 361-403.
71. M. Bednarek, P. Kubisa and S. Penczek, *Macromolecules*, 1999, **32**, 5257-5263.
72. S. Penczek, *Journal of Polymer Science Part a-Polymer Chemistry*, 2000, **38**, 1919-1933.
73. R. Tokar, P. Kubisa, S. Penczek and A. Dworak, *Macromolecules*, 1994, **27**, 320-322.
74. B. Esswein, N. M. Steidl and M. Moller, *Macromolecular Rapid Communications*, 1996, **17**, 143-148.
75. A.-L. Brocas, C. Mantzaridis, D. Tunc and S. Carlotti, *Progress in Polymer Science*, 2013, **38**, 845-873.
76. L. M. Broomfield, R. M. Sebastian, J. Marquet and R. Schoenfeld, *Polymer*, 2012, **53**, 5632-5640.
77. S. Penczek and G. Moad, *Pure and Applied Chemistry*, 2008, **80**, 2163-2193.
78. C. C. Luo, Y. H. Zhang, X. W. Zeng, Y. W. Zeng and Y. G. Wang, *J. Colloid Interface Sci.*, 2005, **288**, 444-448.
79. J.-F. Li, Z.-L. Xu, H. Yang, C.-P. Feng and J.-H. Shi, *Journal of Applied Polymer Science*, 2008, **107**, 4100-4108.
80. J. Ji, Z. Zhou, X. Yang, W. Zhang, S. Sang and P. Li, *Small*, 2013, **9**, 3014-3029.
81. C. Gabrielli, P. Mocoteguy, H. Perrot, D. Nieto-Sanz and A. Zdunek, *Electrochimica Acta*, 2006, **51**, 1462-1472.
82. P. M. Vereecken, R. A. Binstead, H. Deligianni and P. C. Andricacos, *Ibm Journal of Research and Development*, 2005, **49**, 3-18.
83. L. T. Koh, G. Z. You, S. Y. Lim, C. Y. Li and P. D. Foo, *Microelectronics Journal*, 2001, **32**, 973-977.
84. M. Hasegawa, Y. Negishi, T. Nakanishi and T. Osaka, *Journal of the Electrochemical Society*, 2005, **152**, C221-C228.
85. M. Tan and J. N. Harb, *Journal of the Electrochemical Society*, 2003, **150**, C420-C425.
86. D. Stoychev and C. Tsvetanov, *Journal of Applied Electrochemistry*, 1996, **26**, 741-749.
87. M. E. H. Garrido and M. D. Pritzker, *Journal of the Electrochemical Society*, 2009, **156**, D175-D183.
88. T. P. Moffat, D. Wheeler and D. Josell, *Journal of the Electrochemical Society*, 2004, **151**, C262-C271.
89. K. R. Hebert, S. Adhikari and J. E. Houser, *Journal of the Electrochemical Society*, 2005, **152**, C324-C329.

90. Z. V. Feng, X. Li and A. A. Gewirth, *Journal of Physical Chemistry B*, 2003, **107**, 9415-9423.
91. B. Bozzini, L. D'Urzo, C. Mele and V. Romanello, *Journal of Materials Science-Materials in Electronics*, 2006, **17**, 915-923.
92. L. Yang, A. Radisic, J. Deconinck and P. M. Vereecken, *Journal of the Electrochemical Society*, 2014, **161**, D269-D276.
93. T. Y. Safonova, N. V. Smirnova and O. A. Petrii, *Russian Journal of Electrochemistry*, 2006, **42**, 995-1000.
94. S. Jevsevar, M. Kunstelj and V. G. Porekar, *Biotechnology Journal*, 2010, **5**, 113-128.
95. T. Ueda, *Biochimica Et Biophysica Acta-Proteins and Proteomics*, 2014, **1844**, 2053-2057.
96. T. Zhao, Y. Liu, Z. Gao, D. Gao, N. Li, Y. Bian, K. Dai and Z. Liu, *Materials Science & Engineering C-Materials for Biological Applications*, 2015, **53**, 196-203.
97. G. Pasut and F. M. Veronese, *Journal of Controlled Release*, 2012, **161**, 461-472.
98. K. R. Reddy, M. W. Modi and S. Pedder, *Advanced Drug Delivery Reviews*, 2002, **54**, 571-586.
99. M. R. Sherman, M. G. P. Saifer and F. Perez-Ruiz, *Advanced Drug Delivery Reviews*, 2008, **60**, 59-68.
100. N. A. Terry, M. L. Chen-Lim, E. Ely, M. Jatla, D. Ciavardone, S. Esch, L. Farace, F. Jannelli, A. Puma, D. Carlow and P. Mamula, *Journal of Pediatric Gastroenterology and Nutrition*, 2013, **56**, 215-219.
101. A. Abuchowski, T. Vanes, N. C. Palczuk and F. F. Davis, *Journal of Biological Chemistry*, 1977, **252**, 3578-3581.
102. A. Abuchowski, J. R. McCoy, N. C. Palczuk, T. Vanes and F. F. Davis, *Journal of Biological Chemistry*, 1977, **252**, 3582-3586.
103. M. J. Roberts, M. D. Bentley and J. M. Harris, *Advanced Drug Delivery Reviews*, 2002, **54**, 459-476.
104. A. Kolate, D. Baradia, S. Patil, I. Vhora, G. Kore and A. Misra, *Journal of Controlled Release*, 2014, **192**, 67-81.
105. J. M. Harris and R. B. Chess, *Nature Reviews Drug Discovery*, 2003, **2**, 214-221.
106. D. Pfister and M. Morbidelli, *Journal of Controlled Release*, 2014, **180**, 134-149.
107. W. Zhao, F. Liu, Y. Chen, J. Bai and W. Gao, *Polymer*, 2015, **66**, A1-A10.
108. S. Das and A. Ghosh, *Aip Advances*, 2015, **5**.
109. Y. Yang and W. Wang, *Journal of Power Sources*, 2015, **285**, 70-75.
110. D. Devaux, D. Gle, T. N. T. Phan, D. Gigmes, E. Giroud, M. Deschamps, R. Denoyel and R. Bouchet, *Chemistry of Materials*, 2015, **27**, 4682-4692.
111. Y. V. Baskakova, O. V. Yarmolenko and O. N. Efimov, *Russian Chemical Reviews*, 2012, **81**, 367-380.
112. H. F. Zhou, N. Y. Gu and S. J. Dong, *Journal of Solid State Electrochemistry*, 1999, **3**, 82-86.
113. H. F. Zhou and S. J. Dong, *Electrochimica Acta*, 1997, **42**, 1801-1807.
114. H. F. Zhou and S. J. Dong, *Journal of Electroanalytical Chemistry*, 1997, **425**, 55-59.
115. H. F. Zhou and S. J. Dong, *Electrochimica Acta*, 1996, **41**, 2395-2398.

116. H. F. Zhou, N. Y. Gu and S. J. Dong, *Journal of Electroanalytical Chemistry*, 1998, **441**, 153-160.
117. S. J. Dong and H. F. Zhou, *Journal of Electroanalytical Chemistry*, 1996, **403**, 117-123.
118. S. J. Dong, N. Y. Gu and H. F. Zhou, *Journal of Electroanalytical Chemistry*, 1998, **441**, 95-101.
119. N. Y. Gu, H. F. Zhou, L. M. Ding, Z. Shi and S. J. Dong, *Solid State Ionics*, 2000, **138**, 123-133.
120. H. F. Zhou and S. J. Dong, *Journal of Electroanalytical Chemistry*, 1996, **414**, 121-125.
121. M. A. Ratner and D. F. Shriver, *Chemical Reviews*, 1988, **88**, 109-124.
122. H. Ohno, *Electrochimica Acta*, 1998, **43**, 1581-1587.
123. N. Y. Kawahara and H. Ohno, *Electrochimica Acta*, 1998, **43**, 1493-1497.
124. Y. Guo, K. Aoki, J. Chen and T. Nishiumi, *Electrochimica Acta*, 2011, **56**, 3727-3730.

Chapter 2: Introduction to electrochemical techniques

Chapter abstract

This chapter explains some of the fundamental aspects underpinning electrochemical processes, such as thermodynamics of electrode processes, electrode kinetics and mass transport. Discussions on electrode kinetics are based upon the Butler-Volmer model where a mass transport corrected Butler-Volmer equation is developed for systems with controlled mass transport, such as hydrodynamic techniques. Practical methods, such as potential step voltammetry, cyclic voltammetry, voltammetry at microelectrodes, rotating disc voltammetry and electrochemical impedance spectroscopy are also introduced. The Levich equation for rotating disc voltammetry is derived from first principles.

Chapter contents

2 Introduction to electrochemical techniques

2.1 Introduction

Electrochemistry is the study of oxidation and reduction reactions that are driven by an applied electrical potential to an electrode in solution. Static electricity was first discovered by Otto von Guericke in the 17th century, however, it was not until the development of the Volta pile in 1800 before electrical currents could be produced.[1] Extensive research was carried out during the 19th century by A. Volta, J. W. Ritter, M. Faraday, J. Daniell and W. Nernst, providing the founding principles and terminology used today in electrochemistry.[1] The field has flourished in the last century with important developments in battery technology, biological sensors, supercapacitors, fuel cells, solar cells, corrosion studies and organic synthesis.[2-6] Electrochemistry is usually performed in a three electrode arrangement (Figure 2.1) with the reaction of interest occurring at the working electrode (WE). The applied potential is controlled with respect to a low impedance reference electrode (RE), which has an invariable potential. No current passes between the WE and the RE, but instead is directed through the third electrode – the counter electrode (CE). In order for current to flow through the external circuit, there must be a reaction at the CE that is complementary to the reaction occurring at the WE. The area of the CE is typically over 100 times larger than the working electrode, which prevents the reaction at the WE being limited by the reaction at the CE. Therefore, the processes at the CE are generally not considered in most electrochemical studies.

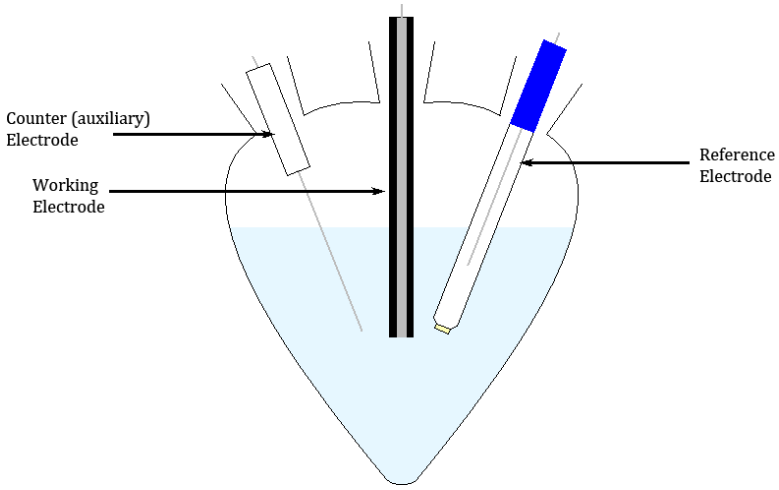

Figure 2.1. A schematic diagram showing a three-electrode arrangement in a typical electrochemical cell.

Electrochemical methods can either be performed potentiostatically, where the potential between the WE and RE is controlled whilst the current is measured, or galvanostatically, where the current is controlled whilst the potential is measured. Most electrochemical measurements use a potentiostatic approach.

2.2 Electrode dynamics

2.2.1 Thermodynamics of electrode processes

An electrochemical reaction involves the transfer of one or more electrons between a redox active species and an electrode via an electron tunnelling process. For electron transfer to occur the redox analyte must be close to the electrode surface (< 20 Å) and there must be a favourable change in the Gibbs energy (ΔG) associated with the process ($\Delta G < 0$).[7] A negative ΔG corresponds to the favourable movement of electrons from a high energy level to a lower energy level. The Fermi level of a metal is the most energetically filled energy level at 0 K. If the Fermi level of the electrode is higher in energy than the lowest unoccupied molecular orbital (LUMO) of the analyte, it is favourable for an electron to be transferred from the electrode to the analyte. This causes reduction of the analyte in solution (Figure 2.2). Conversely, an oxidation process will be favoured if the HOMO of the analyte is higher in energy than the Fermi level of the electrode, causing a flow of electrons from the analyte to the electrode. A flow of electrons is observed as a current. It should be noted that the direction of current flows in opposite directions for reduction and oxidation processes. By convention, oxidation and reduction processes have different signs.[8] In this thesis a positive current corresponds to an oxidation process.

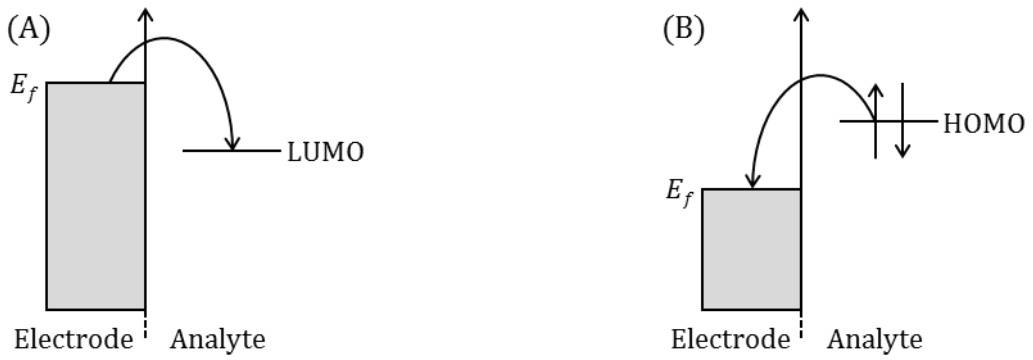

Figure 2.2. (**A**) The Fermi level of the electrode is higher than the LUMO of the analyte; therefore a reduction reaction is favoured. (**B**) The Fermi level of the electrode is lower in energy than the HOMO of the analyte, favouring an oxidation reaction. The transfer of electrons to or from the electrode generates a current and sets up a potential difference between the electrode and the solution ($\phi_m - \phi_s$). There is no net current flow at dynamic equilibrium.

If a metal strip, such as platinum, is placed into a solution containing an equal concentration of Fe^{2+} and Fe^{3+} ions, the following dynamic equilibrium will be established at the electrode surface:

$$Fe^{3+}_{(aq)} + e^-_{(m)} \rightleftharpoons Fe^{2+}_{(aq)}$$

The equilibrium only occurs near the electrode surface because electrons from the metal are required to balance the reaction. If the equilibrium lies to the left hand side of the equation, electrons will have been transferred from Fe^{2+} in solution to the metal electrode and there will be a net negative charge on the electrode. Alternatively, if the equilibrium lies to the right, electrons will have transferred away from the metal electrode into the solution resulting in a net positive charge on the electrode with respect to the solution. In both instances a potential difference between the electrode and the solution ($\phi_M - \phi_S$) is set-up, which is known as the *electrode potential*. ϕ_M is the potential of the electrode and ϕ_S is the potential of the solution. These individual parameters are not measureable directly, and must always be measured with respect to a second potential.[7]

At dynamic equilibrium, the forward and backward electrochemical reactions occur at the same rate and therefore there is no overall current flow. The open circuit potential (OCP) is the potential, relative to a reference electrode, where there is no overall net current flow. The cell potential (E) measured when no current is flowing through a circuit is described by the Nernst equation (equation 2.1).

$$E = E^\circ + \frac{RT}{nF}\ln\left(\frac{a_{Ox}}{a_{Red}}\right) \quad (2.1)$$

Here E° is the *standard reduction potential* for the redox couple, R is the universal gas constant (8.314 J K^{-1} mol^{-1}), T is the temperature, n is the number of electrons transferred, F is Faraday's constant (96485 C mol^{-1}), a_{ox} is the activity of oxidised species, and a_{red} is the activity of reduced species. The activity of solids and pure liquids is defined as unity ($a_{solid} = a_{liquid} = 1$). The activity of a species, x, dissolved in solution is proportional to the concentration ($[x]$) (equation 2.2), where the constant of proportionality (the activity coefficient, γ) is dependent upon temperature, pressure and solvent interactions.[7, 9]

$$a_x = \gamma_x[x] \quad (2.2)$$

The Nernst equation can therefore be expressed in terms of concentration (equation 2.3).

$$E = E^{\circ\prime} + \frac{RT}{nF}\ln\left(\frac{[Ox]_{bulk}}{[Red]_{bulk}}\right) \quad (2.3)$$

In this equation, $[Ox]_{bulk}$ is the bulk concentration of oxidised species, $[Red]_{bulk}$ is the bulk concentration of reduced species, and $E^{\circ\prime}$ is the *formal reduction potential*, which can be expressed as:[10]

$$E^{\circ\prime} = E^\circ + \frac{RT}{nF}\ln\left(\frac{\gamma_{Ox}}{\gamma_{Red}}\right) \quad (2.4)$$

If an electrode is immersed in a solution containing equimolar concentrations of reduced and oxidised forms of a redox couple, for example an equimolar solution of $Fe(CN)_6^{3-}$ and $Fe(CN)_6^{4-}$, the logarithmic term from the Nernst equation (2.3) will equal zero. Consequently, at equilibrium the open circuit potential will therefore also correspond to the formal reduction potential for the redox system.

When equilibrium has been established, no changes will be observed in the system unless an external force is applied to drive the equilibrium either to the right or the left. Applying a potential to the electrode (with respect to a reference) causes the Fermi level of the electrode to change and hence initiate electron transfer reactions. A positive potential lowers the Fermi level of the electrode, which favours oxidation of the redox analyte, whilst a negative potential raises the Fermi level of the electrode favouring reduction of the analyte (Figure 2.3). Applying an external potential therefore changes the ratio of $[Ox]$ and $[Red]$ at the electrode surface as dictated by the Nernst equation.

The Nernst equation only indicates the thermodynamic viability of an electrochemical process but does not consider the kinetics of the reaction.

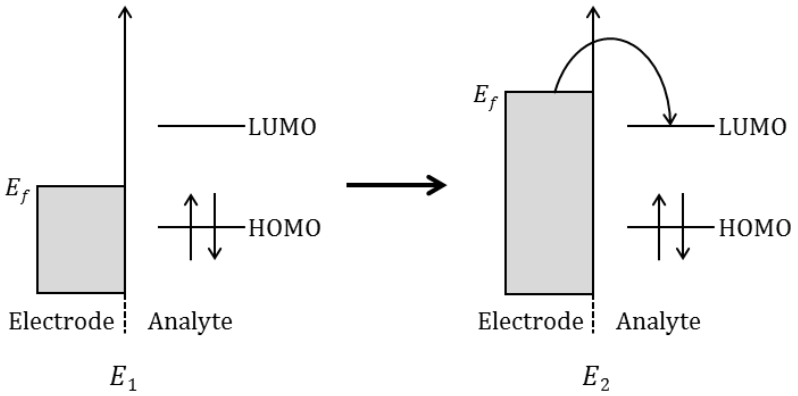

Figure 2.3. Applying a potential to the electrode causes a shift in the Fermi level and hence shifts the position of the equilibrium causing either oxidation or reduction. E_2 is a more negative potential than E_1 and therefore the reduction of the analyte is more favourable.

2.2.2 Kinetics of electrode processes

A simplified mechanism for an electrochemical reaction can be described as a five step process, with any of the steps being rate determining (Figure 2.4):

(i) Redox active analyte moves to the electrode by mass transport.

(ii) Analyte adsorbs onto the electrode surface.

(iii) Electron transfer.

(iv) Product desorbs from the electrode surface.

(v) Product moves away from the electrode by mass transport.

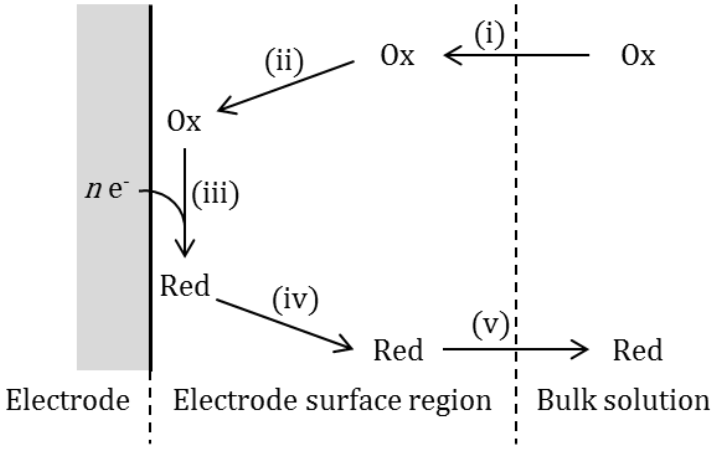

Figure 2.4. A schematic diagram showing the general mechanism for an electro-reduction process: (i) mass transport of reactant to the electrode, (ii) adsorption of reactant, (iii) electron transfer, (iv) desorption of product and (v) product moves away from electrode by mass transport.[10]

For a reduction (cathodic) reaction, electrons are transferred from the electrode to the reactant. A net movement of electrons through the circuit is observed as a measurable current. The magnitude of the cathodic current (I_c) is proportional to the number of electrons transferred per molecule (n), the area of the electrode (A), and the concentration of the analyte at the electrode surface ($[Ox]_0$) (equation 2.5). The constant of proportionality is the rate constant for electron transfer (k_c). A similar expression can be obtained for an anodic reaction (equation 2.6).

$$I_c = -nFAk_c[\mathrm{Ox}]_0 \tag{2.5}$$

$$I_a = nFAk_a[\mathrm{Red}]_0 \tag{2.6}$$

Here I_a is the anodic current, and F is Faraday's constant – the charge of 1 mole of electrons. The negative sign for the cathodic current is the convention to indicate the direction of the current. The quantities $k_a[\mathrm{Red}]_0$ and $k_c[\mathrm{Ox}]_0$ correspond to the flux of material to the electrode surface (J) and, similar to chemical rate laws, also correspond to the rate of the electrochemical reaction. Since the current is proportional to the flux, the current gives an indication of the rate of the electrochemical reaction. The measured net current (I_{total}) is the sum of the anodic and cathodic currents.

$$I_{total} = I_a + I_c \tag{2.7}$$

$$I_{total} = nFA(k_a[\mathrm{Red}]_0 - k_c[\mathrm{Ox}]_0) \tag{2.8}$$

A better understanding of the rate constants k_a and k_c can be gained based on kinetic models, such as the Butler-Volmer model.

2.2.3 The Butler-Volmer model

If the rate of electron transfer is the rate determining step, the Butler-Volmer model can be used to calculate the rate of electron transfer in the electrochemical reaction. Consider a generic heterogeneous electrochemical reaction involving the transfer of one electron occurring at a metal electrode:

$$Ox^{n+1} + e^- \underset{k_a}{\overset{k_c}{\rightleftharpoons}} Red^n \tag{2.9}$$

In this expression, k_c and k_a represent the electrochemical rate constants for the cathodic and anodic process respectively. Analogous to chemical reactions, an energy barrier must be overcome for an electrochemical process to take place. The peak of the barrier corresponds to a transition state (denoted using a superscript ‡) and the

magnitude of the reaction energy barrier ($\Delta G^{\ddagger}$) is related to the electrochemical rate constant by the Eyring equation:

$$k \propto \exp\left(\frac{-\Delta G^{\ddagger}}{RT}\right) \tag{2.10}$$

At dynamic equilibrium (or at the formal electrode potential, $E^{\circ\prime}$) the rates of the anodic and cathodic reaction are the same ($k_a = k_c$). Therefore the energy barrier at equilibrium for the anodic ($\Delta G_a^{\circ\ddagger}$) and cathodic ($\Delta G_c^{\circ\ddagger}$) process must also be equivalent. An energy profile diagram can be used to visualise the energy barriers associated with the electrochemical reaction (Figure 2.5A).

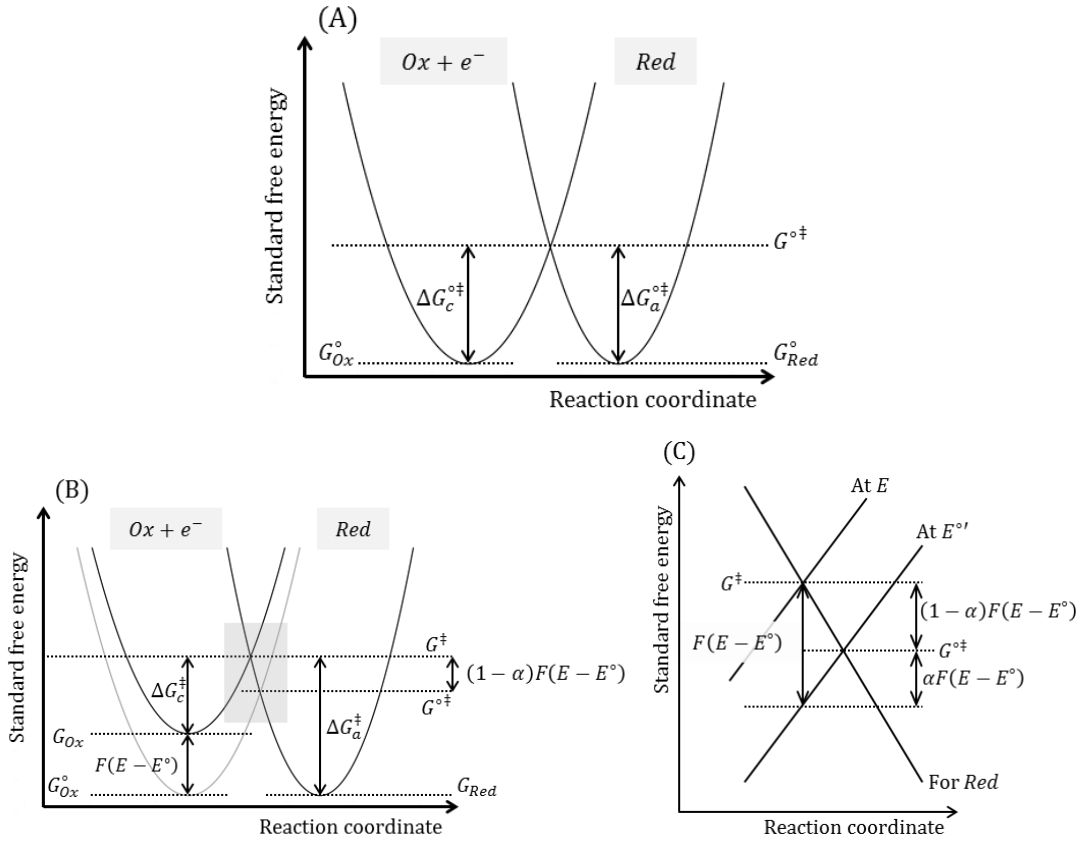

Figure 2.5. Energy profile diagrams for (**A**) a system at equilibrium (or the formal reduction potential) and (**B**) for a system subject to a *negative* applied potential (E). The applied potential causes the total Gibbs energy for "$Ox + e^-$" to change by $F(E - E^{\circ\prime})$, which lowers the barrier for the cathodic reaction ($\Delta G_c^{\ddagger}$). The shaded rectangle represents the points of intersection, which is enlarged in (**C**).[10]

From Figure 2.5A, the right hand parabola represents the total Gibbs energy for the reduced species (Red) and the left hand parabola represents the total Gibbs energy for the oxidised side of the reaction ($Ox + e^-$) at the standard potential E°. The point at which the curves intersect represents the transition state. The Gibbs energy of the

species in solution (Red and Ox) depends upon the solution potential but is not directly affected by an applied potential to the electrode. However, the Gibbs energy of the electron resident on the metal electrode (e^-) varies with applied potential as described by equation 2.11.

$$\Delta G = -nF\Delta E = -nF(E - E^\circ) \quad (2.11)$$

In this expression n is the stoichiometric number of electrons transferred, which is 1 in this example. $(E - E^\circ)$ is known as the overpotential and is often given the symbol η. The total Gibbs free energy of the reactants ($Ox + e^-$) can therefore be expressed as a function of the applied potential (E) (equation 2.12).

$$G_{Ox} = G^\circ_{Ox} - F(E - E^\circ) \quad (2.12)$$

Figure 2.5B shows that the Gibbs energy of the transition state also changes with the applied potential. In most electrochemical systems the change in standard free energy due to an applied potential is small. Therefore the energy profiles at the points of intersection may be considered as straight lines at least in first approximation (Figure 2.5C). The change in the standard free energy of the transition state ($G^\ddagger - G^{\circ\ddagger}$) can be expressed as a fraction of the applied potential (equation 2.13).

$$G^\ddagger - G^{\circ\ddagger} = -(1 - \alpha)F(E - E^\circ) \quad (2.13)$$

In this expression α is a dimensionless parameter known as the *transfer coefficient*, and has a value between 0 and 1. The value of α corresponds to whether the transition state more closely resembles the reactants ($Ox + e^-$) or the products (Red). If $\alpha = 0$, the transition state resembles the reactants, and if $\alpha = 1$ the transition state will resemble the products. Generally, for metallic species, $\alpha \approx 0.5$ because the electron transfer takes place without structural reorganisation of the molecule. For example, $Fe(CN)_6^{3-}$ and $Fe(CN)_6^{4-}$ are both octahedral in shape. Using the expression for the Gibbs energy of the transition state (equation 2.13) and equations for the Gibbs free energies of reactants (equation 2.12) and products, it is possible to find expressions relating the applied potential to the cathodic and anodic energy barrier, $\Delta G_c^\ddagger$ and $\Delta G_a^\ddagger$ respectively.

$$\Delta G_c^\ddagger = \Delta G_c^{\circ\ddagger} + \alpha F(E - E^\circ) \quad (2.14)$$

$$\Delta G_a^\ddagger = \Delta G_a^{\circ\ddagger} - (1 - \alpha)F(E - E^\circ) \quad (2.15)$$

The expressions for $\Delta G_c^\ddagger$ and $\Delta G_a^\ddagger$ can be substituted into the Eyring equation (equation 2.10) to allow the cathodic (k_c) and anodic (k_a) rate constants to be determined.

$$k_c = A_c \exp\left(\frac{-\Delta G_c^{\circ\ddagger}}{RT}\right) \exp\left(\frac{-\alpha F(E-E^\circ)}{RT}\right) \quad (2.16)$$

$$k_a = A_a \exp\left(\frac{-\Delta G_a^{\circ\ddagger}}{RT}\right) \exp\left(\frac{(1-\alpha)F(E-E^\circ)}{RT}\right) \quad (2.17)$$

In these expressions, A_c and A_a are pre-exponential constants that relate to the frequency of collisions between species in solution and the electrode surface.[11] The first exponential term is independent of the applied potential and is therefore also a constant for a particular reaction at a fixed temperature. The second exponential term is dependent upon the applied potential. In general, a more positive applied potential increases the rate of the anodic reaction, whilst decreasing the rate of the cathodic process.

At equilibrium ($E = E^\circ$), the rate of the cathodic and anodic reactions are equal ($k_c = k_a$), which defines the standard heterogeneous rate constant for electron transfer (k_0). Equations 2.16 and 2.17 can therefore be combined and simplified to yield the potential independent expression 2.18.

$$k_0 = A_c \exp\left(\frac{-\Delta G_c^{\circ\ddagger}}{RT}\right) = A_a \exp\left(\frac{-\Delta G_a^{\circ\ddagger}}{RT}\right) \quad (2.18)$$

Appropriate substitution of equation 2.18 into equations 2.16 and 2.17 allows the cathodic and anodic rate constants (k_c and k_a respectively) to be expressed with regards to the standard heterogeneous rate constant for electron transfer (k_0).

$$k_c = k_0 \exp\left(\frac{-\alpha \mathrm{F}(\mathrm{E}-\mathrm{E}^\circ)}{RT}\right) \quad (2.19)$$

$$k_a = k_0 \exp\left(\frac{(1-\alpha)F(E-E^\circ)}{RT}\right) \quad (2.20)$$

These expressions for the cathodic and anodic rate constants (equations 2.19 and 2.20) can be related to the current measured by substituting into equation 2.8, which yields a form of the Butler-Volmer equation for a single electron transfer process:

$$I_{total} = FAk_0\left([Red]_0 \exp\left(\frac{(1-\alpha)F(E-E^\circ)}{RT}\right) - [Ox]_0 \exp\left(\frac{-\alpha F(E-E^\circ)}{RT}\right)\right) \quad (2.21)$$

Since there is no net current at dynamic equilibrium ($E = E^\circ$), the cathodic and anodic processes must be occurring at the same rate. The current due to either the anodic or cathodic process at equilibrium is known as the *exchange current*, I_0.

$$I_0 = FAk_0[Red]_0 \exp\left(\frac{(1-\alpha)F(E-E^\circ)}{RT}\right) \quad (2.22)$$

$$I_0 = -FAk_0[Ox]_0 \exp\left(\frac{-\alpha F(E-E^\circ)}{RT}\right) \quad (2.23)$$

At dynamic equilibrium, the concentration of species must be constant throughout the solution. That is to say, the surface concentration of species is equal to the bulk concentration, which can be described by the Nernst equation (2.24).

$$\frac{F(E-E^\circ)}{RT} = \ln\left(\frac{[Ox]_{bulk}}{[Red]_{bulk}}\right) \quad (2.24)$$

Equation 2.24 can therefore be directly substituted into either equation 2.22 or 2.23 when the system is at equilibrium and the exchange current simplifies to equation 2.25.

$$I_0 = FAk_0[Red]^{\alpha}_{bulk}[Ox]^{(1-\alpha)}_{bulk} \quad (2.25)$$

If equation 2.25 is rearranged to make k_0 the subject, it can be substituted into equations 2.19 and 2.20. Simplification yields equations 2.26 and 2.27.

$$k_c = \frac{I_0}{FA[Ox]_{bulk}} \quad (2.26)$$

$$k_a = \frac{I_0}{FA[Red]_{bulk}} \quad (2.27)$$

Finally, equations 2.26 and 2.27 can be substituted back into equation 2.8 to yield a second form of the Butler-Volmer equation, which includes the exchange current (I_0):

$$I = I_0\left(\frac{[Red]_0}{[Red]_{bulk}}\exp\left(\frac{(1-\alpha)F(E-E^\circ)}{RT}\right) - \frac{[Ox]_0}{[Ox]_{bulk}}\exp\left(\frac{-\alpha F(E-E^\circ)}{RT}\right)\right) \quad (2.28)$$

The Butler-Volmer equation (or current overpotential equation)[10] is an important equation in order to determine the rate of electron transfer in electrochemical reactions. However, one should be reminded that it is only applicable if the rate of electron transfer is the rate determining step. In many electrochemical systems this is not the case and the rate of mass transport to the electrode surface will limit the rate of the reaction.

2.2.4 Mass transport

Mass transport is the movement of analyte towards and away from the active area of the electrode and has three forms – convection, migration and diffusion. Convection is the movement of a species through a solution due to density gradients or from mechanical stirring.[10] For example, a rotating disc electrode (RDE) controls the flow of solution to the surface of the electrode using forced convection (see section 2.3.4).

Migration is the movement of charged ions in an electric field.[10] The charge at an electrode surface will vary as the potential is changed and will cause electrostatic

interactions with charged bodies in solution. Positive ions in solution move towards a negatively charged electrode, whilst being repelled by an electrode with a positive charge. The movement of ions via migration is difficult to model mathematically but the effects can be minimised by adding a high concentration of background electrolyte to the solution.

Background electrolyte is a redox inactive salt dissolved in solution, for example potassium chloride (KCl), which increases the ionic conductivity of the solution. When a negative charge is applied to the electrode, the cations of the salt align at the electrode surface to form a layer that shields the electric field from the rest of the solution. Consequently, there is a potential drop across the double layer and migration effects are minimised. A higher concentration of background electrolyte leads to a more compressed double layer and more effective screening of the electric field. It is important to use a high enough concentration of electrolyte to cause a compact double layer, which allows the analyte to diffuse close enough to the electrode for electron transfer to take place before the analyte is affected by the electric field.[7]

The third mechanism of mass transport is diffusion, which is the random movement of molecules through a solution, where a species moves from a region of high concentration to low concentration until the species is uniformly dispersed. Fick's first law of diffusion (in one dimension) states that the flux (J) of a species, B, is proportional to the concentration gradient $\left(\frac{\partial[B]}{\partial x}\right)$:

$$J_B = -D_B\left(\frac{\partial[B]}{\partial x}\right) \tag{2.29}$$

Here D_B is the diffusion coefficient for the species B, which has a typical value of $\approx 10^{-5}$ cm^2s^{-1} in aqueous solutions. In many instances, reactions occurring at the electrode are limited by the rate of mass transport (or flux) of analyte to the electrode surface and the measured current can be expressed as:

$$I = nFAJ_B \tag{2.30}$$

If the rate of the diffusion is the limiting process for mass transport, equation 2.30 can be expressed as:

$$I = -nFAD_B\left(\frac{\partial[B]}{\partial x}\right) \tag{2.31}$$

The derivative of J gives Fick's second law of diffusion, which states that the rate of change of concentration is proportional to the change in the concentration gradient.

$$\frac{\partial[B]}{\partial t} = D_B\left(\frac{\partial^2[B]}{\partial x^2}\right) \tag{2.32}$$

Solving Fick's second law for one-dimensional (planar) diffusion leads to the Cottrell equation (equation 2.33), which can be used to determine diffusion coefficients from currents measured from potential step experiments at macroelectrodes.

$$|I| = \frac{nFA[B]_{bulk}\sqrt{D_B}}{\sqrt{\pi t}} \tag{2.33}$$

In this equation n is the number of electrons transferred in the electrochemical reaction, F is Faraday's constant, A is the active surface area of the electrode, $[B]_{bulk}$ is the concentration of B in the bulk solution and t is time. A plot of current versus $\frac{1}{\sqrt{t}}$ gives a linear plot (known as a Cottrell plot), which can be used to determine the diffusion coefficient under planar diffusion conditions if the concentration is known.

2.2.5 Mass transport corrected Butler-Volmer equation

The Butler-Volmer equation derived in Section 2.2.3 can be modified to include effects from mass transport where the mass transport is constant, for example in hydrodynamic voltammetry where the flow of solution to the electrode is controlled.[12] Consider a fully reversible, one-electron oxidation process under controlled mass transport where only the reduced species (Red) is initially present in bulk solution.

$$Red \rightleftharpoons Ox + e^-$$

At a fixed oxidising potential under hydrodynamic conditions, a steady state concentration gradient will be established where the concentration of starting material (Red) will be depleted to some extent at the electrode surface. If the diffusion coefficients (D) for the reduced and oxidised species are assumed to be the same, an equal magnitude concentration gradient for the product (Ox) will also arise (Figure 2.6).[7] Consequently, the flux of starting material moving towards the electrode must equal the flux of product moving away from the electrode.

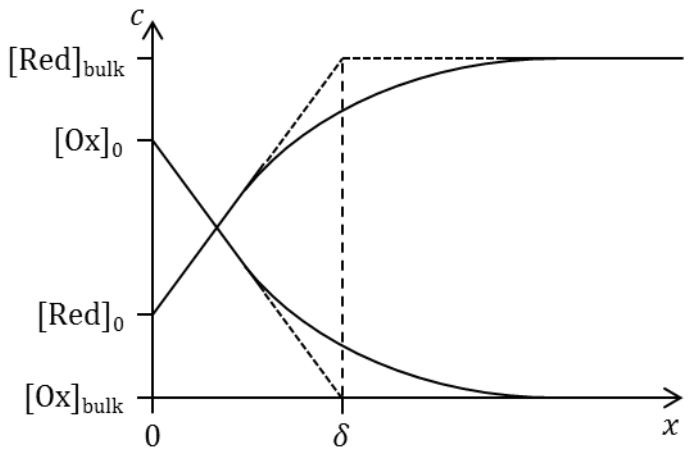

Figure 2.6. Concentration profiles for the oxidation of $Red \rightarrow Ox + e^-$ under steady state conditions when no Ox is initially present in the bulk solution. δ is the diffusion layer thickness.

The current for the redox process is dependent upon the flux of material reaching the electrode and the electrode kinetics, and can be expressed as (*cf.* equation 2.30):

$$I = nFADJ_{Red} = -nFADJ_{Ox} \tag{2.34}$$

In this expression, J_{Red} and J_{Ox} are the flux of the reduced and oxidised species respectively. If the concentration gradient across the diffusion layer is assumed to be linear the flux J_{Red} and J_{Ox} can be calculated by solving Fick's first law of diffusion to give equations 2.35 and 2.36 respectively.

$$I = nFAD\,\frac{[Red]_{bulk} - [Red]_0}{\delta} \tag{2.35}$$

$$I = -nFAD\,\frac{[Ox]_{bulk} - [Ox]_0}{\delta} \tag{2.36}$$

In these expressions, δ is the diffusion layer thickness, which is assumed to be equal for oxidised and reduced species, and $[Ox]_{bulk} = 0$. At high oxidising overpotentials a limiting current (I_{lim}) will be reached when the steady state diffusion layer has the steepest concentration gradient. This corresponds to when all reactant is consumed at the electrode surface ($[Red]_0 = 0$). An expression for the limiting current can therefore be attained (equation 2.37).

$$I_{lim} = \frac{nFAD[Red]_{bulk}}{\delta} \tag{2.37}$$

The Butler-Volmer equation (equation 2.21) can be used to model the current as a function of potential, however, the surface concentration of species ($[Red]_0$ and $[Ox]_0$) is usually unknown. Equations 2.35 – 2.37 can be rearranged and substituted into equation 2.21 to eliminate $[Red]_0$, $[Ox]_0$ and $[Red]_{bulk}$:

$$\frac{I}{nFAk_0} = \frac{I_{lim}\delta}{nFAD}\exp[(1-\alpha)\theta] - \frac{I\delta}{nFAD}\{\exp[(1-\alpha)\theta] + \exp(-\alpha\theta)\} \qquad (2.38)$$

In this equation $\theta = \frac{nF(E-E^{\circ\prime})}{RT}$. Further rearrangement and simplification leads to equation 2.39.

$$\frac{I}{I_{lim}} = \frac{\frac{\delta}{D}\exp[(1-\alpha)\theta]}{\frac{1}{k_0} + \frac{\delta}{D}\{\exp[(1-\alpha)\theta] + \exp(-\alpha\theta)\}} \qquad (2.39)$$

If fast electrode kinetics are assumed ($\frac{1}{k_0} \ll \frac{\delta}{D}$) equation 2.39 may be simplified further to yield equation 2.40.

$$\frac{I}{I_{lim} - I} = \exp(\theta) = \exp\left(\frac{nF(E-E^{\circ})}{RT}\right) \qquad (2.40)$$

The exponential term is a constant dependent upon the applied potential. Consequently a plot of $\log\left(\frac{I}{I_{lim}-I}\right)$ versus applied potential (E) gives a linear plot with a slope of $\frac{nF}{RT} \approx \frac{1}{59\,\mathrm{mV}}$ for fully reversible redox systems with fast electron transfer kinetics.

2.3 Electrochemical methods

2.3.1 Potential step experiments

Potential step or chronoamperometry experiments can be used to gather information concerning the rate of diffusion of a redox species in solution. In the simplest case, the initial potential, E_1, is fixed at a value where no redox processes are occurring. The potential is then stepped to a second value, E_2, where reactant is converted into product. The potential is held at E_2 for a period of time whilst the current is measured (Figure 2.7). E_2 is usually chosen to be a potential where the rate of electron transfer is fast.

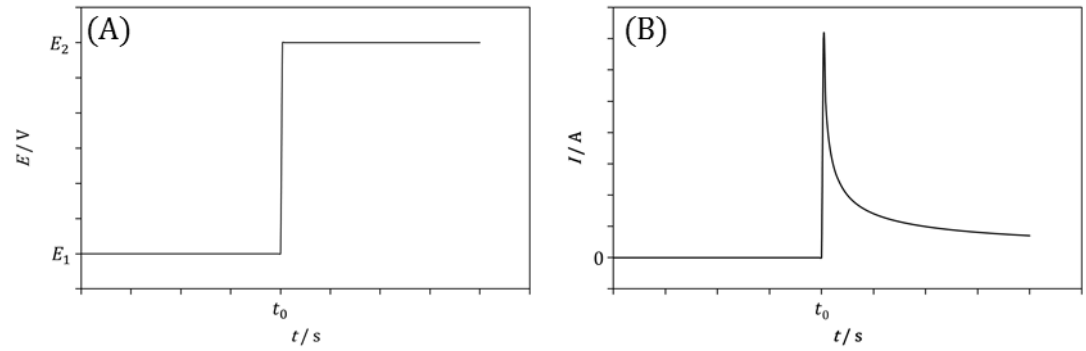

Figure 2.7. (**A**) A graph showing the change in potential with time for a potential step experiment and (**B**) a typical current response for a 1-electron process limited by planar diffusion.

At E_1 no redox processes are occurring, so the current remains at 0 A. As the potential is stepped to E_2, all of the reactant near the electrode surface is converted into product generating a sharp increase in current. This leads to a large concentration gradient between the unreacted starting material in the bulk and the product near the electrode surface. As time progresses, the concentration gradient becomes shallower, which lowers the flux to the electrode and causes the current to decay accordingly. The current response is governed by Fick's second law of diffusion. The Cottrell Equation (equation 2.33) can be used to model the current response from potential step experiments, and can be linearised by plotting $\frac{1}{i^2}$ against t. The slope of the linear fit can be used to determine the diffusion coefficient of the species.

2.3.2 Linear sweep and cyclic voltammetry

Rather than potential step experiments, it is often useful to change the potential of the electrode gradually using a technique called linear sweep voltammetry (Figure 2.8).

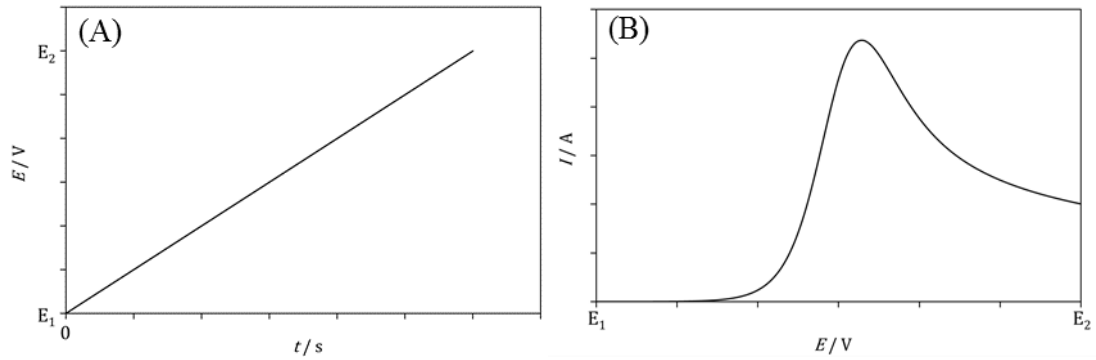

Figure 2.8. (**A**) A curve showing the gradual change of potential with time for a linear sweep experiment and (**B**) a typical current response for a fully reversible system limited by planar diffusion.

Analogous to potential step experiments, linear sweep experiments are designed to begin at a potential where no redox reactions are occurring, E_1. The potential is then gradually changed to a potential, E_2, which lies at a value where the redox reaction of interest is occurring with fast electron transfer. As the potential is changed, the ratio of oxidised species to reduced species changes as predicted by the Nernst equation (equation 2.3). This leads to an exponential increase in the current. However, this exponential increase does not continue indefinitely as all of the starting material near the electrode surface will be consumed. Assuming fast electron transfer, a situation will occur where the rate of influx of reactant material will not be sufficient to satisfy the Nernst equation concentration conditions. The voltammogram therefore reaches a peak, where the rate of diffusion begins to limit the rate of the reaction. Beyond the peak, the curve can be described by the Cottrell equation (equation 2.33).

The peak current, I_p, is mathematically described using the Randles-Ševčík equation and corresponds to the point at which the reactant is fully depleted at the electrode surface. The equation shows that the peak current is proportional to the square root of the sweep rate (v).

$$I_p = 0.4463nFAc\left(\frac{nFvD}{RT}\right)^{\frac{1}{2}} \qquad (2.41)$$

n is the number of electrons transferred, F is Faraday's constant, A is the active surface area of the electrode, c is the concentration of reactant in the bulk solution, v is the scan rate, D is the diffusion coefficient, R is the Universal gas constant and T is the temperature (in K).

The sweep rate, or scan rate, is the rate of change of potential. The potentials where electron transfer processes occur rapidly are therefore reached more quickly at faster scan rates. Consequently there is less time for the diffusion layer thickness to grow and the concentration gradient is steeper for the duration of the potential sweep. A steeper concentration gradient results in a higher flux of material to the electrode, which leads to higher peak current at faster scan rates.

Cyclic voltammetry uses continuous forward and backward linear sweeps in order to provide information concerning both oxidised and reduced species in the solution. Figure 2.9 shows how the potential is varied with time for a cyclic voltammetry experiment. The shape of the forward (anodic) scan is identical to the LSV experiment described above; however, a hysteresis loop is observed on the return (cathodic) sweep. At the maximum potential (E_2), there is a high concentration of oxidised species at the electrode surface. As the potential is lowered, the oxidised species is reduced, which generates a negative current. For a fully reversible system a peak will also be observed on the reverse scan. The Nernst equation predicts that the potential between the anodic and cathodic peaks (ΔE_p) for a fully reversible, single electron redox process will be 57 mV.[11]

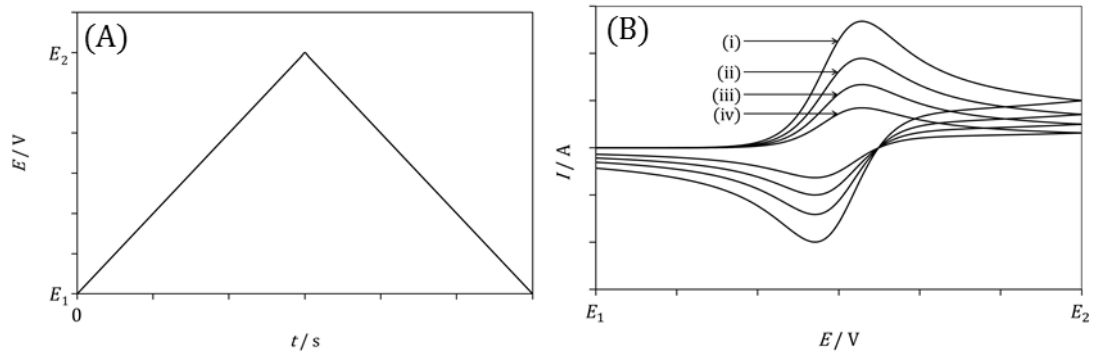

Figure 2.9. (**A**) A graph of potential against time for a cyclic voltammogram. The gradient of the graph is the scan rate (v). (**B**) A typical cyclic voltammogram for a fully reversible redox system at a macroelectrode at (i) 100 mVs^{-1}, (ii) 50 mVs^{-1}, (iii) 25 mVs^{-1} and (iv) 10 mVs^{-1}.

2.3.3 Voltammetry at a microelectrode

So far all electrochemical reactions have been considered on a macroelectrode, where planar diffusion to the electrode surface limits the rate of the reaction. However, if the electrode area is significantly reduced, for example to < 100 μm diameter disc, it is possible to start to crowd the active electrode surface and initiate hemi-spherical (or radial) diffusion (Figure 2.10).

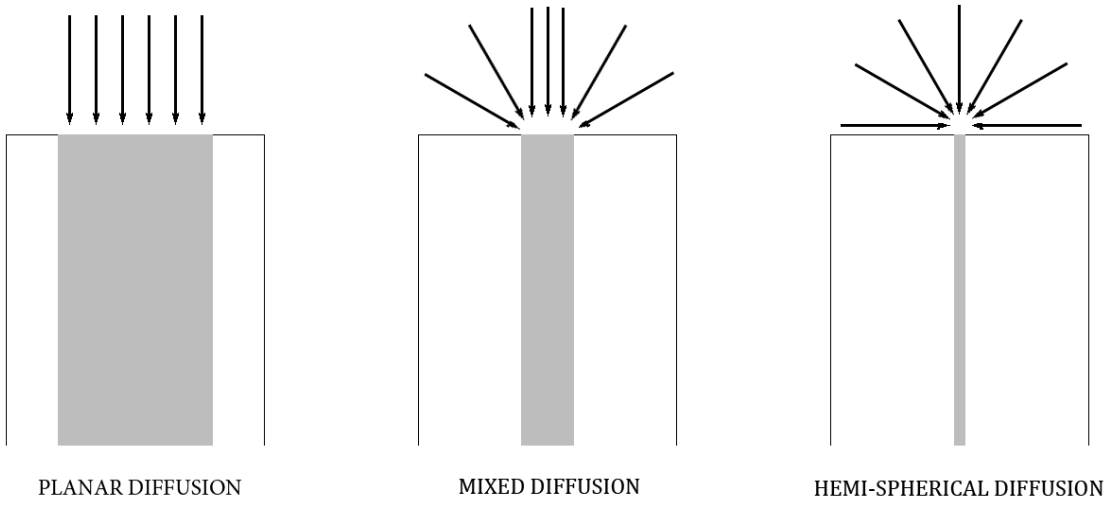

Figure 2.10. A schematic diagram showing the change from planar to hemi-spherical diffusion as the electrode area is reduced.

Due to the small area of the electrode, very small currents are produced. Consequently, it can be possible to run electrochemical experiments using a two-electrode arrangement rather than the typical three-electrode set-up. The CE and RE are joined in a two-electrode arrangement. Usually no current passes through the RE as this can affect the potential of the RE. However, since the currents are usually very small at microelectrodes (< 10 nA), it is possible to connect the CE and RE without significantly shifting the potential of the RE. The small area of the electrode also greatly reduces the capacitance of the electrode when compared to a macroelectrode, and hence reduces the capacitative charging current during cyclic voltammetry. As a result it is possible to use higher scan rates for cyclic voltammetry. Furthermore, higher quality data, with less distortion in cyclic voltammograms, can be attained for systems with high solution resistance. If there is high solution resistance at a macroelectrode, the flux of current will not be uniformly dispersed across the electrode surface, causing distortions in

cyclic voltammograms. However, distortions in cyclic voltammograms due to resistance effects are minimised at microelectrodes.[10] Again due to the very small working area of the electrode, a much steeper concentration gradient can be created leading to faster mass transport to the electrode surface of a microelectrode when compared to a macroelectrode at long timescales. Consequently, it is possible to gather kinetic information for fast rates of electron transfer, which is inaccessible when using a macroelectrode.[11] The change in nature of diffusion to the electrode surface leads to a different solution to Fick's second law (equation 2.32). In this instance the diffusion considered forms a hemi-spherical diffusion layer around the microelectrode and the current reaches a steady state value rather than tending to zero. Fick's laws change form for hemi-spherical diffusion and diffusion at a circular disc, and when solved show that the current is dependent upon timescale (equations 2.42). At short timescales, the current can be modelled using the Cottrell equation; however, at long timescales, the current will reach a steady state rather than tending to zero.

$$J = Dc\left(\frac{1}{\sqrt{D\pi t}} + \frac{1}{r}\right) \tag{2.42}$$

$$\lim_{t\to 0} I = \frac{nFAc\sqrt{D}}{\sqrt{\pi t}} \tag{2.43}$$

$$\lim_{t\to \infty} I = \frac{nFADc}{r} \tag{2.44}$$

Hemi-spherical: $I_{lim} = 2nFrDc$ (2.45)

Disc: $I_{lim} = 4nFDrc$ (2.46)

Here r is the radius of the electrode and c is the bulk concentration.

The dependence of current on timescale causes a change in the shape of cyclic voltammograms. When a voltammogram is limited by spherical diffusion, the current reaches a limiting value as described by equation 2.46 rather than being described by the Cottrell equation. The cyclic voltammogram therefore does not have a peak, but reaches a steady state value. This has a knock-on effect of removing the hysteresis from the voltammogram (Figure 2.11).

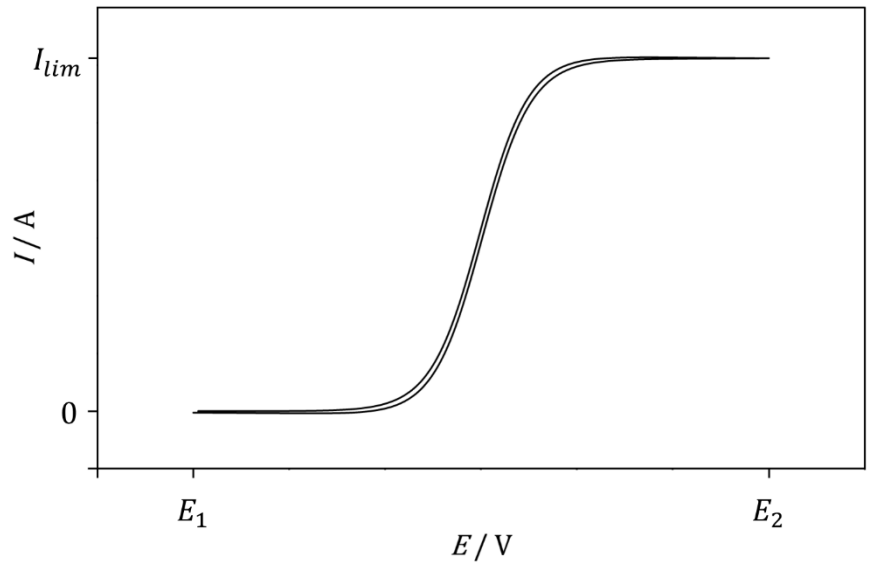

Figure 2.11. A cyclic voltammogram for a fully reversible system at a microelectrode. The curve is sigmoidal in shape rather than having a well-defined peak.

2.3.4 Hydrodynamic methods: Rotating Disc Electrode

Hydrodynamic electrochemical methods encompass a range of electrochemical techniques where forced convection is used to control the mass transport of material to the electrode. Forced convection is usually achieved by either moving the working electrode, for example in the rotating disc electrode, or by controlling the flow of solution across a static electrode, for example in channel flow electrochemistry.[13] The increased mass transport under hydrodynamic conditions causes an enhancement in the measured currents (often resulting in a limiting current being reached) and removes capacitive charging currents from cyclic voltammograms.[7, 10]

The most commonly used and studied hydrodynamic method is the rotating disc electrode (RDE). The apparatus typically consists of a three-electrode arrangement where the working electrode (a disc electrode) is rotated about the vertical axis (*y*-axis) during the electrochemical measurement (Figure 2.12).

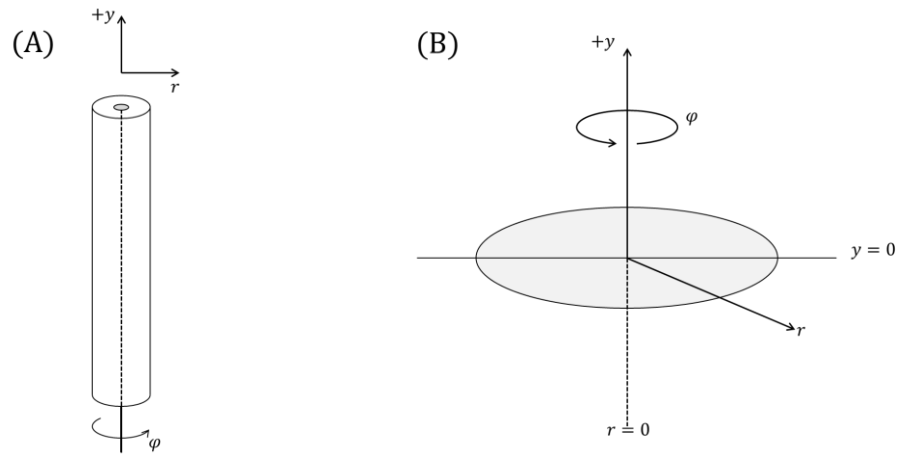

Figure 2.12. (**A**) A rotating disc electrode and (**B**) a representation of the electrode surface with cylindrical coordinates (r, φ, y).

Experiments performed under hydrodynamic control are usually designed such that laminar flow (as opposed to turbulent flow) occurs across the electrode surface as this helps to simplify mathematical models. A dimensionless parameter known as the Reynolds number (Re) is often used to determine whether the flow is laminar or turbulent. The Reynolds number is dependent upon a characteristic velocity of the fluid (v_{ch}), the length of flow (L) and the kinematic viscosity of the solution (ν)[10]:

$$Re = \frac{v_{ch}L}{\nu} \tag{2.47}$$

The flow is assumed to be laminar at low Reynolds numbers but if the Reynolds number exceeds a critical value (Re_{cr}) the flow will become turbulent.[10]

For a rotating disc electrode, with radius r, the Reynolds number is dependent upon the frequency of rotation (f, in Hz) and can be expressed as:

$$Re = \frac{fr^2}{\nu} \tag{2.48}$$

The critical Reynolds number for a rotating disc electrode is *ca.* 2×10^3.[7] The Reynolds number is proportional to the rotation frequency, where high rotation frequencies can cause the Reynolds number to exceed its critical value, which may result in turbulent flow or vortex formation.

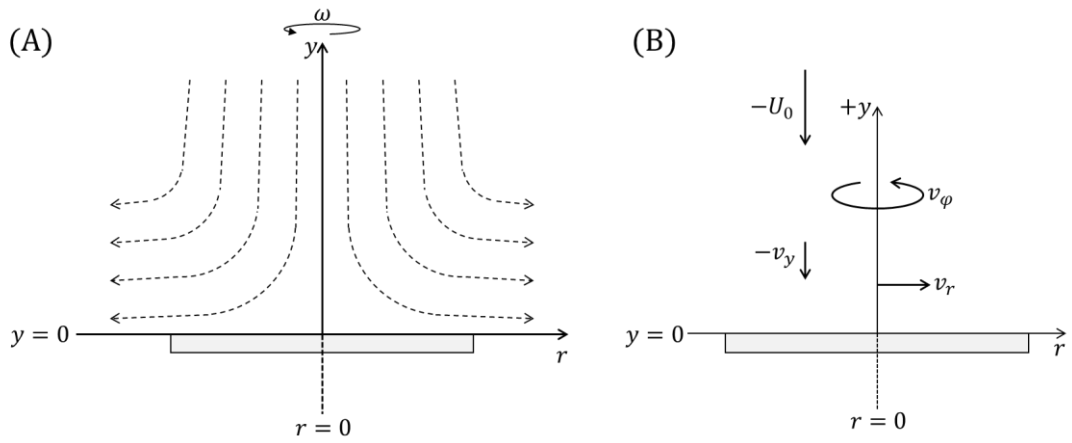

Figure 2.13 (**A**) The 2-dimensional laminar flow pattern at a rotating disc with angular frequency ω. Dashed arrows represent the flow of solution. (**B**) A vector representation of the flow velocities. A negative v_y corresponds to flow towards the rotating disc.

The 2-dimensional flow profile for a rotating disc is shown in Figure 2.13A. As the electrode rotates, solution very near to the electrode surface is expelled radially outwards from the axis of rotation (i.e. away from the centre of the disc) due to centrifugal forces. To replenish the expelled solution near the spinning surface, material from the bulk solution is dragged perpendicularly towards the electrode. This flow pattern results in superior mass transport to the electrode when compared with a static solution and leads to enhanced currents in voltammetric measurements. At a static macroelectrode under diffusion control, a potential step into a region where redox processes occur will result in the current to decay towards zero due to the change in concentration gradient over time and the thickening of the diffusion layer. However, an analogous potential step experiment at a rotating disc electrode will cause the current to decay towards a steady state value, which is independent of time. This implies a steady state concentration profile is set up at a rotating disc with a constant diffusion layer thickness. The constant diffusion layer thickness is also apparent in cyclic voltammetry at a rotating disc electrode. As the potential is gradually increased a limiting current (rather than a peak) is observed when redox processes occur.

To quantitatively understand electrochemical processes at a rotating surface and the current responses observed, the general convective-diffusion equation (equation 2.49) must be solved.

$$\frac{\partial C_j}{\partial t} = D_j \nabla^2 C_j - \boldsymbol{v} \cdot \boldsymbol{\nabla} C_j \qquad (2.49)$$

The general convective-diffusion equation is comprised of Fick's second law of diffusion in three dimensions ($\frac{\partial C_j}{\partial t} = D_j \nabla^2 C_j$) with an additional convective term ($-\boldsymbol{v} \cdot \boldsymbol{\nabla} C_j$) due to the rotation of the electrode. It is assumed that mass transport due to migration is negligible due to an addition of excess electrolyte to the solution and is therefore not considered. The del operator ($\boldsymbol{\nabla}$) is used here to denote the concentration gradient in three-dimensions and ∇^2 denotes the Laplace operator. In cylindrical coordinates these are expressed as follows[10]:

$$\boldsymbol{\nabla} = \frac{\partial}{\partial r}\boldsymbol{\mu_1} + \frac{1}{r}\frac{\partial}{\partial \varphi}\boldsymbol{\mu_2} + \frac{\partial}{\partial y}\boldsymbol{\mu_3} \tag{2.50}$$

$$\nabla^2 = \frac{1}{r}\frac{\partial}{\partial r}\left(r\frac{\partial}{\partial r}\right) + \frac{1}{r^2}\frac{\partial^2}{\partial \varphi^2} + \frac{\partial^2}{\partial y^2} \tag{2.51}$$

Here $\boldsymbol{\mu_1}$, $\boldsymbol{\mu_2}$ and $\boldsymbol{\mu_3}$ are unit vectors in r, φ and y respectively.

The vector $\boldsymbol{v}$ corresponds to the flow velocity in three dimensions at a given point. It is therefore important to understand the full velocity profile at a rotating disc in order to solve the general convective-diffusion equation (equation 2.49). The velocity profiles are often expressed in cylindrical coordinates due to the symmetry of a rotating circular disc. The three key parameters are: (i) the radial velocity (v_r), which is the velocity away from the axis of rotation, (ii) the tangential (or angular) velocity (v_φ), which is the linear velocity at a tangent to a flow with a circular path, and (iii) the axial velocity (v_y), which is the velocity normal to the surface of the rotating disc, where a negative v_y corresponds to a flow towards the spinning surface.[14] The boundary conditions used to determine each velocity component are:

(i) At the electrode surface ($y = 0$), $v_r = 0$, $v_\varphi = \omega r$, and $v_y = 0$.

(ii) Far from the electrode surface ($y \to \infty$), $v_r = 0$, $v_\varphi = 0$ and $v_y = -U_0$.

The first boundary condition suggests the flow of solution at the spinning surface is completely determined by the angular velocity of the rotating disc (ωr). There is no radial or axial component to the velocity. The second boundary condition implies negligible radial or tangential velocity components as $y \to \infty$. Instead the solution flows perpendicularly towards the electrode surface at a limiting velocity $-U_0$.

The work of von Kármán and Cochran[15] led to expressions indicating how the three velocity components (v_r, v_φ and v_y) vary as a function of the dimensionless parameter ζ, where ζ is proportional to the distance normal to the surface of the spinning disc (y):

$$\zeta = \left(\frac{\omega}{\nu}\right)^{\frac{1}{2}} y \tag{2.52}$$

The expression for each velocity component was found to take the form of an infinite series as a function of ζ[15]:

$$v_r = r\omega \mathrm{F}(\zeta) = r\omega \left(a\zeta - \frac{\zeta^2}{2} - \frac{b\zeta^3}{3} - \frac{b^2\zeta^4}{12} - \frac{a\zeta^5}{60} + \left(\frac{1}{360} - \frac{ab}{90}\right)\zeta^6 + \left(\frac{b}{315} + \frac{ab^2}{1260}\right)\zeta^7 + \cdots\right) \tag{2.53}$$

$$v_\varphi = r\omega \mathrm{G}(\zeta) = r\omega \left(1 + b\zeta + \frac{a\zeta^3}{3} - \frac{(ab-1)\zeta^4}{12} - \frac{b\zeta^5}{15} - \left(\frac{a^2}{90} + \frac{b^2}{45}\right)\zeta^6 + \left(\frac{a}{315} - \frac{b^3}{315} - \frac{a^2 b}{252}\right)\zeta^7 + \cdots\right) \tag{2.54}$$

$$v_y = (\omega\nu)^{\frac{1}{2}} \mathrm{H}(\zeta) = -(\omega\nu)^{\frac{1}{2}} \left(a\zeta^2 - \frac{\zeta^3}{3} - \frac{b\zeta^4}{6} - \frac{b^2\zeta^5}{30} - \frac{a\zeta^6}{180} + \cdots\right) \tag{2.55}$$

In these expressions a and b are coefficients with values 0.51023 and -0.6159 respectively.

The functions F(ζ), G(ζ) and H(ζ) are proportional to v_r, v_φ and v_y respectively and are shown graphically in Figure 2.14. It is important to note that v_y does not depend on the radial distance from the axis of rotation. This implies that at a particular distance from the disc (y), the axial velocity (v_y), and therefore the flux, will be uniform across the entire surface of the disc. When $\zeta < 3.6$ there are significant contributions from all three velocity components to the net flow. However, when $\zeta > 3.6$, both v_r and v_φ have negligible contributions to the overall flow. The distance from the electrode at which v_r and v_φ become insignificant is known as the hydrodynamic (or Prandtl) boundary layer thickness, and is defined when $\zeta = 3.6$.[10]

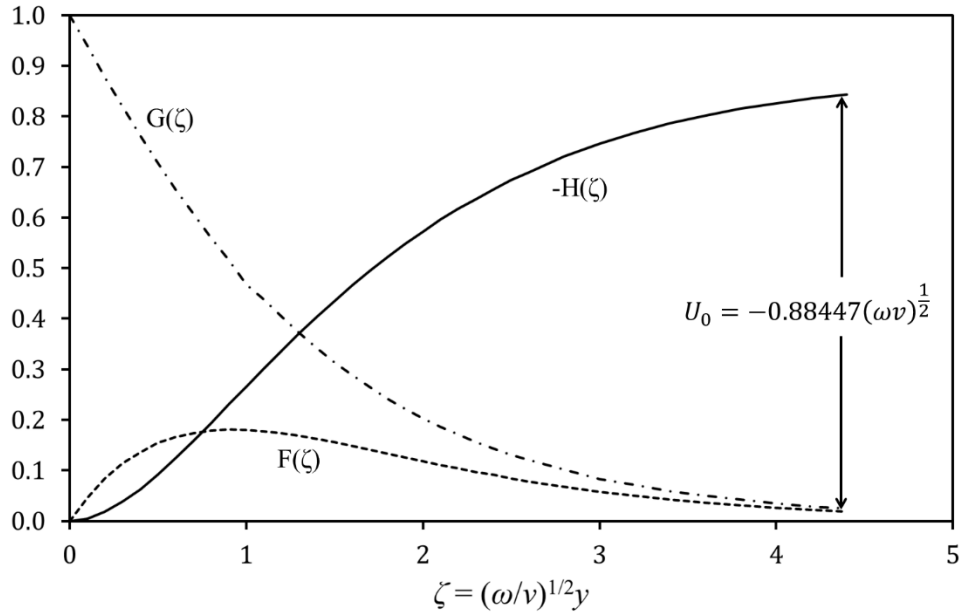

Figure 2.14. A graphical representation of how F(ζ), G(ζ) and H(ζ) vary as a function of ζ. It should be noted that $\zeta \propto y$ and therefore the *x*-axis reflects the perpendicular distance away from the surface of the rotating disc.

Having determined the velocity profile in cylindrical coordinates these expressions can be substituted into the general convective-diffusion equation (equation 2.49) to give:

$$\frac{\partial C_j}{\partial t} = D_j \left[\frac{1}{r}\frac{\partial C_j}{\partial r} + \frac{\partial^2 C_j}{\partial r^2} + \frac{1}{r^2}\frac{\partial^2 C_j}{\partial \varphi^2} + \frac{\partial^2 C_j}{\partial y^2}\right] - \left[v_r \frac{\partial C_j}{\partial r} + \frac{v_\varphi}{r}\frac{\partial C_j}{\partial \varphi} + v_y \frac{\partial C_j}{\partial y}\right] \qquad (2.56)$$

The velocity profile expressions (equations 2.53-2.55) are independent of time and therefore indicate that at a fixed ω, a steady state velocity profile (and hence steady state concentration profile) is reached. Since the concentration profile is independent of time, $\frac{\partial C_j}{\partial t} = 0$. Due to the rotational symmetry of a circular disc, the concentration must be independent of the azimuthal angle (φ). That is to say, at a fixed y and r, the concentration is constant for all φ, which implies $\frac{\partial C_j}{\partial \varphi} = \frac{\partial^2 C_j}{\partial \varphi^2} = 0$. At the surface of the electrode ($y = 0$) it is assumed all regions of the electrode have the same fast rate of electron transfer and therefore the concentration is uniform across the entire surface of the disc ($\frac{\partial C_j}{\partial r} = \frac{\partial^2 C_j}{\partial r^2} = 0$). Since v_y is also independent of r, there is a uniform influx of material towards the electrode across all parts of the disc. It can therefore be concluded that the concentration is independent of the radial distance r at any fixed distance y from the electrode ($\frac{\partial C_j}{\partial r} = \frac{\partial^2 C_j}{\partial r^2} = 0$ for all y). Equation 2.56 can therefore be simplified:

$$v_y \frac{\partial C_j}{\partial y} = D_j \frac{\partial^2 C_j}{\partial y^2} \tag{2.57}$$

From equation 2.55, v_y can be expressed as an infinite series in terms of y. However, as $y \to 0$ the first term in the infinite series is a good approximation for v_y and the other terms can be ignored.

$$v_y = -(\omega v)^{\frac{1}{2}} \times a\zeta^2 \tag{2.58}$$

$$v_y = -a\omega^{\frac{3}{2}} v^{-\frac{1}{2}} y^2 \tag{2.59}$$

$$-a\omega^{\frac{3}{2}} v^{-\frac{1}{2}} y^2 \frac{\partial C_j}{\partial y} = D_j \frac{\partial^2 C_j}{\partial y^2} \tag{2.60}$$

$$\frac{-a\omega^{\frac{3}{2}}}{D_j v^{\frac{1}{2}}} y^2 \frac{\partial C_j}{\partial y} = \frac{\partial^2 C_j}{\partial y^2} \tag{2.61}$$

The second order differential equation (2.61) can be solved by integration by making the following substitutions:

Let $$B = \frac{a\omega^{\frac{3}{2}}}{D_j v^{\frac{1}{2}}} \tag{2.62}$$

$$X = \frac{\partial C_j}{\partial y} \tag{2.63}$$

$$X_{y=0} = \left(\frac{\partial C_j}{\partial y}\right)_{\mathrm{y=0}} \tag{2.64}$$

and $$\frac{\partial X}{\partial y} = \frac{\partial^2 C_j}{\partial y^2} \tag{2.65}$$

$$-By^2 X = \frac{\partial X}{\partial y} \tag{2.66}$$

$$-B \int_0^y y^2 \partial y = \int_{X_{y=0}}^{X} \frac{1}{X} \partial X \tag{2.67}$$

$$\frac{-By^3}{3} = \ln\left(\frac{X}{X_{y=0}}\right) \tag{2.68}$$

$$X = X_{y=0} \exp\left(\frac{-By^3}{3}\right) \tag{2.69}$$

Substitute back in for X and $X_{y=0}$ to give:

$$\frac{\partial C_j}{\partial y} = \left(\frac{\partial C_j}{\partial y}\right)_{\mathrm{y=0}} \exp\left(\frac{-By^3}{3}\right) \tag{2.70}$$

$$\int_{C_{j,y=0}}^{C_{j,bulk}} dC_j = \left(\frac{\partial C_j}{\partial y}\right)_{\mathrm{y=0}} \int_0^{\infty} \exp\left(\frac{-By^3}{3}\right) dy \tag{2.71}$$

If the applied potential is in the current limiting region, the species *j* will undergo fast electron transfer at the electrode surface. It can therefore be assumed $C_{j,y=0} = 0$. The

definite integral with limits between 0 and ∞ can be solved by making an appropriate substitution:

Let $z = \frac{By^3}{3}$ (2.72)

Rearranging equation 2.72 gives:

$$y^2 = \left(\frac{3z}{B}\right)^{\frac{2}{3}} \quad (2.73)$$

Differentiating equation 2.72 and then substituting for y using equation 2.73 gives:

$$\frac{dz}{dy} = B\left(\frac{3z}{B}\right)^{\frac{2}{3}} \quad (2.74)$$

Equations 2.72 and 2.74 can then be used to substitute into equation 2.71, which yields:

$$\int_0^{C_{j,bulk}} dC_j = \left(\frac{\partial C_j}{\partial y}\right)_{\mathrm{y=0}} (3^2B)^{-\frac{1}{3}} \int_0^{\infty} z^{-\frac{2}{3}} \exp(-z)\, dz \quad (2.75)$$

Equation 2.75 can be solved using the gamma function:

$$\Gamma(t) = \int_0^{\infty} x^{t-1} \exp(-x)\, dx \quad (2.76)$$

$$C_{j,bulk} = \left(\frac{\partial C_j}{\partial y}\right)_{\mathrm{y=0}} (9B)^{-\frac{1}{3}} \Gamma\left(\frac{1}{3}\right) \quad (2.77)$$

$$\Gamma\left(\frac{1}{3}\right) = 2.67894$$

$$C_{j,bulk} = 1.28790 \left(\frac{\partial C_j}{\partial y}\right)_{\mathrm{y=0}} B^{-\frac{1}{3}} \quad (2.78)$$

$$C_{j,bulk} = 1.28790 \left(\frac{\partial C_j}{\partial y}\right)_{\mathrm{y=0}} \left(\frac{a\omega^{\frac{3}{2}}}{D_j \nu^{\frac{1}{2}}}\right)^{-\frac{1}{3}} \quad (2.79)$$

From the velocity profile expressions (equations 2.53-2.55), $a = 0.51023$. Rearrangement and simplification of equation 2.79 to make the concentration gradient at the electrode surface the subject gives:

$$\left(\frac{\partial C_j}{\partial y}\right)_{\mathrm{y=0}} = 0.62045 \times D_j^{-\frac{1}{3}} \nu^{-\frac{1}{6}} \omega^{\frac{1}{2}} C_{j,bulk} \quad (2.80)$$

In this case where electrode kinetics are fast and the rate of mass transport is limiting the reaction, the limiting current observed is proportional to the flux of material reaching the electrode:

$$I_{lim} = nFAJ_j \quad (2.81)$$

Similar to equation 2.30, I is the limiting current, n is the number of electrons transferred, F is Faraday's constant, A is the electrode area and J_j is the flux of species

j to the electrode. Using Fick's First Law of diffusion, equation 2.81 can also be expressed as:

$$I_{lim} = nFAD_j \left(\frac{\partial C_j}{\partial y}\right)_{y=0} \quad (2.82)$$

Substituting equation 2.80 for $\left(\frac{\partial C_j}{\partial y}\right)_{y=0}$ yields the Levich equation for a rotating disc electrode (equation 2.83):

$$I_{lim} = 0.62045 \times nFAD_j^{\frac{2}{3}} v^{-\frac{1}{6}} \omega^{\frac{1}{2}} C_{j,bulk} \quad (2.83)$$

Here A is the electrode area (in m^2), D_j is the diffusion coefficient of species j (in $m^2\ s^{-1}$), v is the kinematic viscosity of the solution (in $m^2\ s^{-1}$), ω is the angular frequency of the rotating electrode (in rad s^{-1}) and $C_{j,bulk}$ is the bulk concentration of species j (in mol m^{-3}).

The Levich equation indicates that the limiting current is proportional to the square root of the angular frequency. A plot of I_{lim} against $\omega^{\frac{1}{2}}$ will give a linear graph where the slope can be used to determine the diffusion coefficient of the species.

Consider a solution containing only the reduced form of a fully reversible redox species that can undergo a 1-electron oxidation. Cyclic voltammetry of this solution at a *static* macroelectrode will result in an oxidation and reduction peak on the forward (positive) and backward (negative) scans respectively (Figure 2.9B). In contrast, cyclic voltammetry of the same system at a rotating disc would not give redox peaks but rather a steady state limiting current at high overpotentials. As the potential is gradually increased from E_1 to E_2, the change in surface concentration of the redox species changes as predicted by the Nernst equation, with a corresponding exponential increase in the current. However, the laminar flow pattern at a rotating disc results in the product (oxidised species) to be forced away from the electrode and unreacted material (reduced species) to be dragged towards the electrode. Consequently a steady state concentration profile is set up very quickly with the uniform layer known as the *hydrodynamic layer*.

2.3.5 Electrochemical impedance spectroscopy

Electrochemical impedance spectroscopy (EIS) is a powerful technique used to study electrochemical systems in a steady state. The technique allows determination of the double layer capacitance, charge transfer resistance, uncompensated resistance, diffusion coefficients, and gives access to kinetic information.[10, 16] Impedance (Z) is the resistance, in Ohms (Ω), to the flow of electrical current (I) in a system when an AC potential (E) is applied:

$$Z = \frac{\Delta E}{\Delta I} \tag{2.84}$$

An AC potential is generated by sinusoidal perturbations of the potential and can be expressed either mathematically (equation 2.85) or pictorially using phasor diagrams (Figure 2.15).

$$E_t = E_0 \sin \omega t \tag{2.85}$$

E_t is the potential at time t, E_0 is the amplitude of the perturbation and ω is the angular frequency of the phasor ($\omega = 2\pi f$).

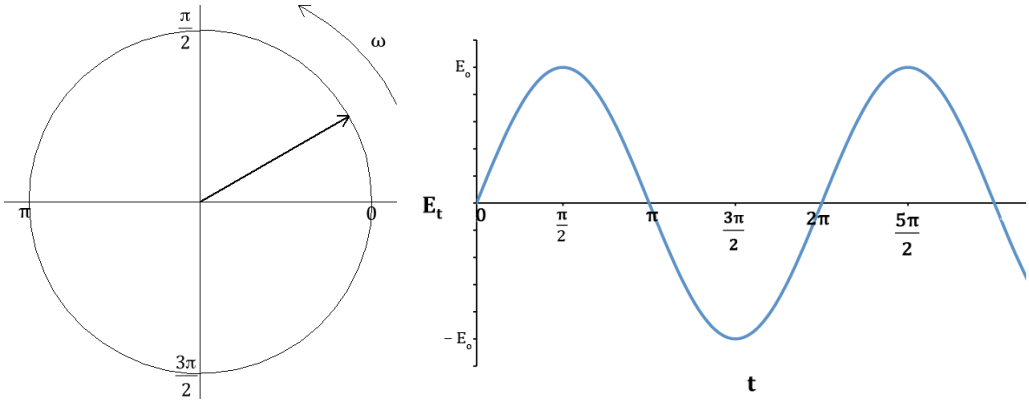

Figure 2.15. The sine wave is generated from a projection on the x-axis of the phase diagram and is representative of an AC potential.[10]

If an AC potential is applied to a pure electrical component, for example an ideal resistor or capacitor, an alternating current will result.

$$I_t = I_0 \sin(\omega t + \varphi) \tag{2.86}$$

This AC current will have the same angular frequency as the AC potential but may have a different amplitude and phase. If visualised as a phasor, it can be seen that the phase

angle (φ) between E_t and I_t will be constant because the angular frequency for the input AC potential and the AC current response is the same (Figure 2.16).

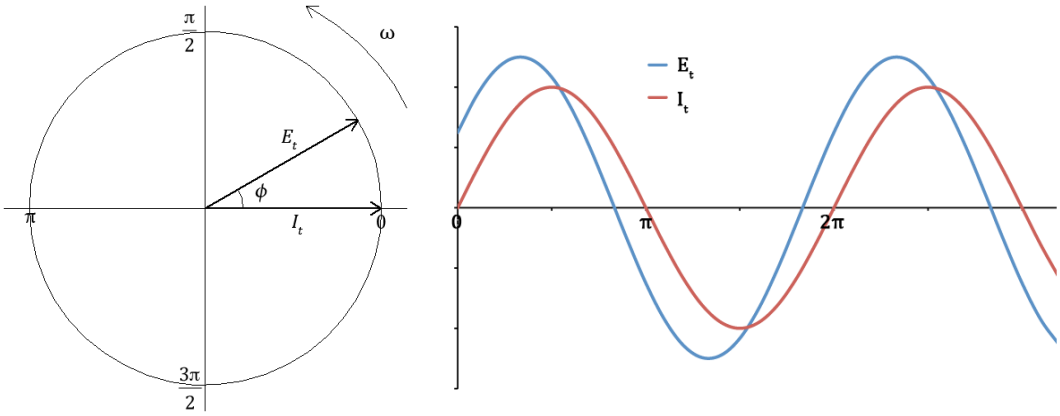

Figure 2.16. A phasor diagram showing E_t (blue) and I_t (red). E_t and I_t have the same frequency resulting in a constant phase angle (φ = 30˚) at all times.[10]

The impedance can therefore be expressed as:

$$Z = \frac{E_t}{I_t} = \frac{E_o}{I_o}\frac{\sin(\omega t)}{\sin(\omega t + \varphi)} \tag{2.87}$$

On phasor diagrams, it is a generally accepted practice to draw the current on the abscissa (horizontal axis) and the potential on the ordinate (vertical) axis to allow easy measurement of the phase angle between the two vectors. It is also common convention to multiply any value on the ordinate axis by *j*, where $j = \sqrt{-1}$. Therefore any vector that is phase shifted ($\varphi \neq 0$) will have an imaginary component to the impedance. Furthermore, if the phase shift is exactly 90˚ there will be no real component to the impedance. Hence the total impedance can be described as:

$$Z_{tot} = Z(Re) + Z(Im) \tag{2.88}$$

Euler's formula (equation 2.89) can be used to express E_t and I_t in polar form, which can help to simplify the mathematics:

$$z = x + jy = |z|(\cos\phi + j\sin\phi) = |z|\exp(j\phi) \tag{2.89}$$

$$\text{where } |z| = \sqrt{x^2 + y^2} \text{ and } j = \sqrt{-1}$$

$$E_t = E_0\sin(\omega t) \rightarrow E_t = E_0\exp(j\omega t) \tag{2.90}$$

$$I_t = I_0\sin(\omega t + \varphi) \rightarrow I_t = I_0\exp(j\omega t + \varphi) \tag{2.91}$$

The impedance of an ideal resistor obeys Ohm's Law and is therefore independent of perturbation frequency. Additionally, there is no phase shift between the applied

potential and the current response. Consequently, the impedance of a pure resistor is equivalent to the *resistance* of the component.

If $\varphi = 0$,

$$Z = \frac{E_o}{I_o}\frac{\exp\left(j\omega t\right)}{\exp\left(j\omega t\right)}$$

$$Z = \frac{E_o}{I_o} \equiv R \tag{2.92}$$

If a capacitor is considered, the current across the component can be evaluated as follows:

$$E_t = E_0 \exp(j\omega t)$$

$$Q(t) = CE_t = CE_0 \exp(j\omega t)$$

$$I = \frac{dQ}{dt} = C\frac{dE}{dt}$$

$$I = j\omega CE_0 \exp(j\omega t) = \frac{jE_0}{X_C}\exp(j\omega t)$$

$$Z = \frac{E}{I} = \frac{X_C E_0 \exp(j\omega t)}{jE_0 \exp(j\omega t)} = -jX_C \tag{2.93}$$

Here $$X_C = \frac{1}{\omega C} \tag{2.94}$$

X_C is known as the capacitive reactance, which represents the opposition of current with a change in voltage across a capacitor. X_C is analogous to the resistance of a resistor and has the units of Ohms. The above analysis shows that the impedance of a pure capacitor is purely imaginary and has no real part at any frequency. This corresponds to a -90° phase shift of the voltage compared to the current.[16] From equation 2.94 it is also revealed that the impedance of a capacitor is dependent upon the frequency of modulation.

In the two examples examined there has been a linear relationship between current and potential. Unfortunately, the current response in electrochemical cells is usually non-linear when the potential is varied. However, if the change in potential is small enough, typically < 10 mV, a pseudo-linear current response can be observed and the system can be treated using the methods discussed above. In electrochemical impedance spectroscopy, the frequency of a sinusoidal AC potential is varied and the current is measured. The impedance is calculated as a function of frequency and can be displayed

graphically using either a Nyquist plot (complex plane) or a Bode plot. A Nyquist plot shows the imaginary impedance (Z'') against the real impedance (Z'). It is the convention to keep the scales on both horizontal and vertical axes the same to aid interpretation of the Nyquist plot. The frequency dependency of the system cannot be obtained from the Nyquist plot alone and is therefore often presented with a corresponding Bode plot. A Bode plot shows how the absolute impedance ($|Z|$) and the phase shift (φ) vary with frequency. The absolute impedance and the frequency are plotted using logarithmic scales (Figure 2.17).

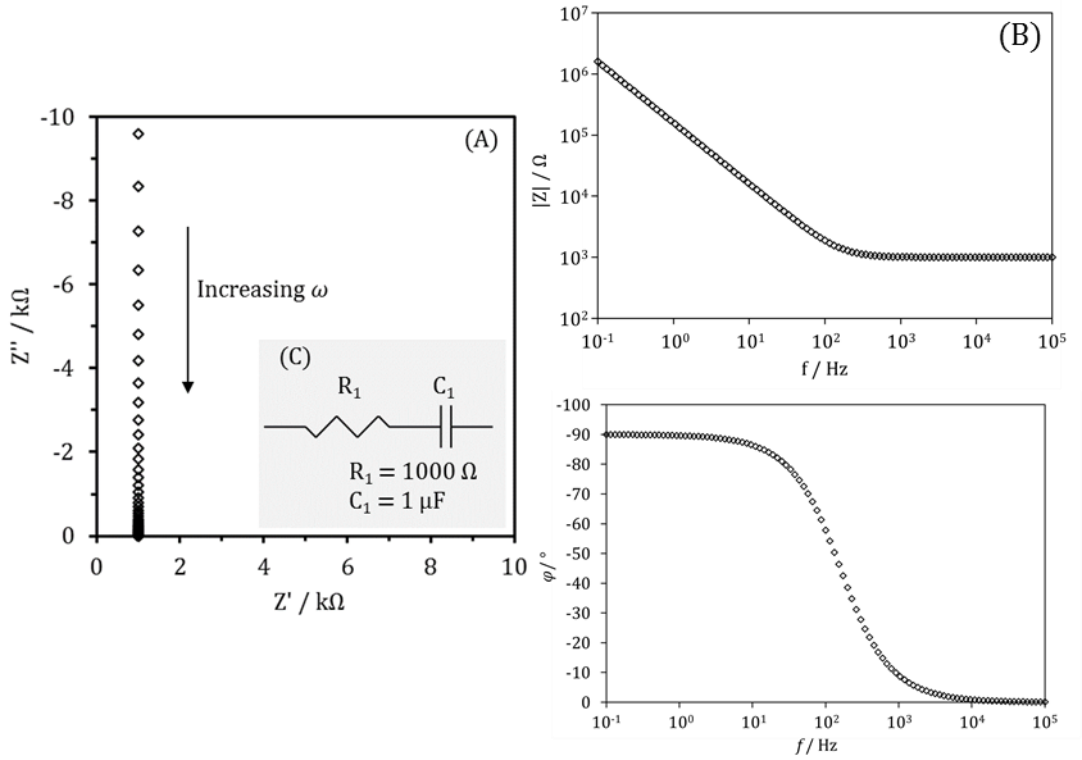

Figure 2.17. (**A**) A Nyquist plot and (**B**) a Bode plot for an RC circuit (**C**). R = 1 kΩ and C = 100 nF.

In order to extract useful values from these graphical plots, an electrically equivalent circuit is constructed and non-linear fitting methods are employed to optimise the values of each component in the circuit. In general, there are four main components used in equivalent circuits: resistors, capacitors, inductors and memristors. Resistors and capacitors are often sufficient to describe most scenarios. It must be emphasised that each component in the equivalent circuit must have a real physical relationship with the electrochemical cell under investigation. In most cases there will be a solution resistance (represented by a resistor) in series with the double layer capacitance (represented by a capacitor) and possibly some additional complexity. For example,

electron transfer processes may become diffusion limited at low frequencies in a static solution. The semi-infinite diffusion layer is modelled by an open Warburg element. However, a closed Warburg element can be used if the diffusion layer has a finite thickness, for example in hydrodynamic systems. A commonly misused circuit element is the constant phase element (CPE), where the phase shift (φ) is independent of frequency. A pure resistor has $\varphi = 0°$, a pure capacitor has $\varphi = -90°$, and a constant phase element typically has a phase angle between the two. The use of CPEs should generally be avoided as they often do not have a physical meaning. However, they can be used to represent the non-ideal nature of a double layer capacitance for a non-homogeneous electrode surface. Values for constant phase elements should be treated with caution.

2.4 References

1. F. Scholz, A. J. Bard and G. Inzelt, *Electrochemical Dictionary*, Springer-Verlag, Berlin, Heidelberg, 2008.
2. M. Winter and R. J. Brodd, *Chemical Reviews*, 2004, **104**, 4245-4269.
3. T. G. Drummond, M. G. Hill and J. K. Barton, *Nature Biotechnology*, 2003, **21**, 1192-1199.
4. B. Oregan and M. Gratzel, *Nature*, 1991, **353**, 737-740.
5. W. J. Lorenz and F. Mansfeld, *Corrosion Science*, 1981, **21**, 647-672.
6. L.-X. Wu, H. Wang, L. He, L. Wu, A.-J. Zhang, H. Kajiura, Y.-M. Li and J.-X. Lu, *International Journal of Electrochemical Science*, 2012, **7**, 5616-5625.
7. R. Compton and C. Banks, *Understanding Voltammetry*, 2nd edn., Imperial College Press, 2011.
8. E. R. Cohen, T. Cvitas, J. G. Frey, B. Holmstrom, K. Kuchitsu, R. Marquardt, I. Mills, F. Pavese, M. Quack, J. Stohner, H. L. Strauss, M. Takami and A. J. Thor, *Quantities, Units and Symbols in Physical Chemistry*, IUPAC Green Book, 3rd edition, 2nd printing edn., IUPAC & RSC Publishing, Cambridge, 2008.
9. C. M. A. Brett and A. M. O. Brett, *Electrochemistry : principles, methods, and applications*, Oxford University Press, Oxford, 1993.
10. A. J. Bard and L. R. Faulkner, *Electrochemical methods : fundamentals and applications*, 2nd edn., John Wiley, New York ; Chichester, 2001.
11. A. C. Fisher, *Electrode dynamics*, Oxford University Press, Oxford, 1996.
12. I. Streeter and R. G. Compton, *Electrochimica Acta*, 2007, **52**, 4305-4311.
13. J. A. Cooper and R. G. Compton, *Electroanalysis*, 1998, **10**, 141-155.
14. V. G. Levich, *Physicochemical hydrodynamics*, Prentice-Hall, 1962.

15. W. G. Cochran and S. Goldstein, *Mathematical Proceedings of the Cambridge Philosophical Society*, 1934, **30**, 365.
16. D. Pletcher, R. Greef, R. Peat, L. M. Peter and J. Robinson, *Instrumental methods in electrochemistry*, Horwood, Chichester, 2001.

Chapter 3: Methods for the determination of diffusion coefficients in poly(ethylene glycol)

Chapter abstract

Poly(ethylene glycol) has been identified as a non-toxic, non-volatile, inexpensive and environmentally benign solvent. In this study, poly(ethylene glycol) with an average molecular weight of 200 g mol^{-1} (PEG200) is used as the solvent in electrochemical processes. The low volatility of PEG200 is utilised and voltammetry is performed *in vacuo* in order to remove all gases and to control the humidity levels of the solution. Double potential step experiments are employed to determine the diffusion coefficients for oxidised and reduced forms of four redox species (anthraquinone-2-sulfonate, ferrocene, 1,1'-ferrocene dimethanol and 1,1'-ferrocene dicarboxylic acid) under mixed diffusion conditions at a 100 μm diameter platinum disc electrode. Diffusion coefficients were optimised using the data fitting tool on the commercial electrochemical simulation software package DigiElch™ Professional. Optimised values were verified by comparing experimental and simulated cyclic voltammograms and reasons for deviations are discussed. Diffusion coefficients were found to be $\sim 1 - 2 \times 10^{-7}$ cm^2 s^{-1} for all the redox systems employed and the hydrodynamic radius for each species was approximated using the Stokes-Einstein relation. The low diffusion coefficients in PEG200 is attributed to the high viscosity of the polymer electrolyte.

Chapter publications

Parts of this chapter have been published in:
C. E. Hotchen, H. V. Nguyen, A. C. Fisher, P. E. Frith and F. Marken, *ChemPhysChem*, 2015, **16**, 2789-2796.

Special acknowledgements

I would like to thank Philip Jones, the glassblower at the University of Bath, for making the sealed glass cell, which enabled me to perform electrochemical measurements *in vacuo*.

Chapter Contents

3. Methods for the determination of diffusion coefficients in poly(ethylene glycol)

3.1 Voltammetric methods to determine diffusion coefficients

It is increasingly more important to find environmentally benign solvents for uses in chemical processes. Water is environmentally benign, however, it is not always practical to use aqueous solutions due to a narrow potential window, high volatility (especially at elevated temperatures) and an inability to solvate many organic species. Organic alternatives are generally more hazardous to the environment and require more careful disposal. Ionic liquids have some favourable properties for electrochemical purposes, such as a large solvent potential window, however, they are often hygroscopic, where water impurities severely decrease the usable potential limits of the solvent. Ionic liquids are also expensive to synthesise and their toxicological properties are still largely unknown. It is therefore of interest to investigate alternative solvents that are inexpensive and environmentally benign. Poly(ethylene glycol) (PEG) is commonly regarded as an environmentally 'green' solvent, due to its low toxicity and its suitability as a solvent for voltammetry will be investigated.[1]

The determination of diffusion coefficients by electrochemical methods is commonly practised and a number of voltammetric techniques, such as cyclic voltammetry and potential step experiments, can be used.[2-4] However, in some cases, the reported values for diffusion coefficients show significant variation. For example the diffusion coefficient for copper salts in aqueous solution has been reported in a range from 2.8×10^{-6} cm^2 s^{-1} to 12.6×10^{-6} cm^2 s^{-1}.[5]

The Randles-Ševčík equation (equation 3.1) can be used to determine diffusion coefficients (D) from cyclic voltammetry experiments for fully reversible redox processes in solution under a linear diffusion regime, with fast electron transfer kinetics, and if the concentration (c) and the area (A) of the electrode are known.[6,7]

$$I_p = 0.446nFAc\left(\frac{nFvD}{RT}\right)^{\frac{1}{2}} \qquad (3.1)$$

Here n is the number of electrons transferred, F is Faraday's constant, R is the universal gas constant, T is the temperature, I_p is the peak current, and v is the scan rate. A plot of I_p versus $\sqrt{v}$ gives a linear plot where the diffusion coefficient can be evaluated from the slope. However, inaccuracies can arise for systems with (i) slow electron transfer kinetics, (ii) high solution resistance, (iii) high capacitive charging current, (iv) a non-linear diffusion regime, and (v) for systems where the number of electrons transferred is not known absolutely.

Potential step methods at planar disc electrodes can also be used to determine diffusion coefficients. The experiment should begin at a potential where no electron transfer is occurring and be stepped to a potential where the electron transfer is fast enough to immediately deplete all starting material at the electrode surface. In this way, the current recorded at the electrode is limited by the rate of mass transport to the surface at all times. In a stagnant solution the current is usually limited by diffusion, although effects from convection could be observed at long time scales. The diffusion layer thickness (δ) increases with time (t) as the potential is held and can be approximated by equation 3.2.

$$\delta = \sqrt{4Dt} \tag{3.2}$$

As the diffusion layer thickness increases, a change from linear diffusion to radial diffusion may be observed. The dominant mode of diffusion can be determined by using the dimensionless parameter τ, which is the square of the ratio of the diffusion layer thickness to the radius of the disc working electrode.[8-10]

$$\tau = \frac{4Dt}{r^2} \tag{3.3}$$

Here, D is the diffusion coefficient, r is the radius of the disc working electrode, and t is the time length of the potential step. If $\tau \ll 1$, the diffusion layer thickness is thin compared to the radius of the disc and the diffusion to the disc can be considered as linear (or planar). The current-time transient under linear diffusion is quantitatively described by the Cottrell equation (equation 3.4).

$$I = \frac{nFAc\sqrt{D}}{\sqrt{\pi t}} \tag{3.4}$$

A plot of I against $t^{-\frac{1}{2}}$ is linear and the diffusion coefficient can be evaluated from the slope.

If $\tau \gg 1$, the diffusion layer thickness is much larger than the radius of the electrode and the diffusion can be considered to be radial, which leads to a steady-state current (I_{ss}) at long time scales (equation 3.5).

$$I_{ss} = 4nFcDr \tag{3.5}$$

Radial diffusion, which leads to a steady-state current, is most typically observed at microelectrodes with a radius of less than ~100 μm.

If $0.01 < \tau < 50$ the diffusion layer thickness is in the same order of magnitude to the radius of the disc and the current is limited by a combination of planar and radial diffusion.[9] Neither the Cottrell equation nor the steady-state equation give an accurate model for the current response under a mixed diffusion regime. However, combination of these equations can lead to an approximate expression for the current (equation 3.6)

$$I(t) = \frac{\pi^{\frac{1}{2}} nFD^{\frac{1}{2}} cr^2}{t^{\frac{1}{2}}} + 4nFDcr \tag{3.6}$$

Using the slope (k) and intercept (b) of a Cottrell plot (I vs. $t^{-\frac{1}{2}}$) can enable determination of the diffusion coefficient without knowing the concentration (equation 3.7).[11-13]

$$D = \pi \left(\frac{br}{4k}\right)^2 \tag{3.7}$$

However, under mixed diffusion conditions this simplification can give up to 6.8 % error. For errors of less than 1 %, this simplified expression should only be used when $\tau < 0.11$ and $\tau > 15000$.

A more precise expression (equation 3.8) was derived by Shoup and Szabo to model the current at a disc electrode as a function of the dimensionless parameter τ after a potential step.[8]

$$I(t) = 4nFDcr\left[0.7854 + 0.8862\tau^{-\frac{1}{2}} + 0.2146\exp(-0.7823\tau^{-\frac{1}{2}})\right] \tag{3.8}$$

The expression is accurate for all values of τ to within an error of less than 0.6 %.[8,14] When $\tau \gg 1$ or $\tau \ll 1$, the exponential term in equation 3.8 approximates to 1, leading to the approximate expression (equation 3.6).

The methods discussed so far are suitable for determining the diffusion coefficient of a starting material, and often assume the electrogenerated species has the same (or

similar) diffusion coefficient. However, there are numerous reports of the oxidised and the reduced forms of the electroactive species exhibiting different diffusion coefficients.[15-18] For example, the diffusion coefficient of electro-generated superoxide is reported to be at least one order of magnitude lower compared with oxygen in ionic-liquids.[19,20] Similar variances have been found for the $[Ru(NH_3)_6]^{2+/3+}$ redox couple, where a lower diffusion coefficient is reported for the oxidised form due to the increased ion-pairing between the triply charged species and the anion of the supporting electrolyte.[15] The Compton group have used double potential step experiments, coupled with simulation, to determine diffusion coefficients for starting material and electrogenerated species.[15,21,22]

It is important to find low-cost, environmentally friendly solvents for chemical processes. This chapter investigates the electrochemical properties of poly(ethylene glycol) with an average molecular weight of 200 g mol^{-1} (PEG200) as a solvent for electrochemical processes. Double potential step experiments under a mixed diffusion regime are performed at a microdisc electrode. A commercial software package (DigiElch™ Professional) is used for simulations to determine accurate diffusion coefficients for the oxidised and reduced forms of electroactive species.

3.2 Experimental

3.2.1 Chemical reagents

Poly(ethylene glycol) (Sigma-Aldrich, average molecular weight = 200 g mol^{-1}) was used as purchased. Lithium perchlorate ($LiClO_4$, Sigma-Aldrich, ACS reagent, ≥ 95 %), ferrocene (Fc, Fluka, > 98 %), 1,1'-ferrocene dimethanol ($Fc(CH_2OH)_2$, Aldrich, 98 %), 1,1'-ferrocenedicarboxylic acid ($Fc(COOH)_2$, Aldrich, 96 %), and anthraquinone-2-solufonic acid, sodium salt monohydrate (AQS, Aldrich, 97 %) were used as purchased without any further purification.

3.2.2 Instrumentation

Electrochemical impedance spectroscopy (EIS) measurements were collected using a Solartron 1286 electrochemical interface and SI1250 frequency analyser. All other electrochemical measurements were taken using an Autolab PGSTAT12 potentiostat using a two-electrode set up. The vacuum was achieved using an Edwards High Vacuum Pump ES50, reducing the pressure to 0.8 mbar. Elchsoft's DigiElch™ Professional (Version 4F) software was used as an electrochemical simulation and data-fitting package in order to determine diffusion coefficients.

3.2.3 Procedure for voltammetry in vacuo

A sealed electrochemical cell was manufactured for voltammetry to be carried out *in vacuo* at room temperature (Figure 3.1) similar to a design proposed by Evans et al.[23] The cell consists of a cylindrical glass tube with a valve at each end of the tube. These valves can be connected to a gas supply or a vacuum pump as desired. Midway along the cylindrical tube there is a perpendicular protrusion where the working electrode is positioned. The working electrode is held in place by a silicone washer, which forms an air-tight seal when tightened by a screw cap. The disc working electrode is positioned vertically so that the active area of the disc is facing upwards. Silicone tubing is placed around the tip of the working electrode, which acts as a container for the electrolyte. Voltammetry was performed in a 40 μL droplet of solution on the surface of the electrode. The system was subjected to 3 h of vacuum prior to experimentation in order to remove unwanted gases, such as oxygen, and control the humidity levels of the system. A 100 μm diameter platinum disc was used as the working electrode with a silver wire counter/pseudo-reference electrode. A small diameter was used for experiments in PEG200 to reduce the uncompensated resistance in the voltammetry. Prior to experiments the working electrode was polished using alumina paste with particle diameter 0.3 μm in order to remove surface impurities and imperfections. Potentials are stated with respect to a silver wire pseudo-reference electrode. The counter and pseudo-reference electrode could be connected due to the very low currents measured (< 10 nA).

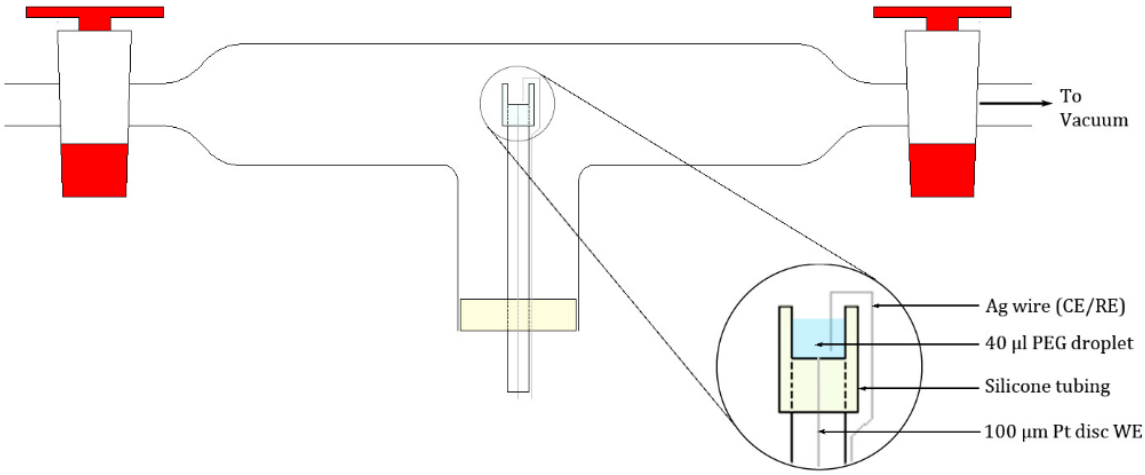

Figure 3.1. A schematic diagram of the electrochemical cell used for 'vacuum voltammetry'. The solution was a 40 µL droplet of solvent on the surface of the working electrode.

3.2.4 Procedure for electrochemical impedance spectroscopy

Electrochemical impedance spectroscopy (EIS) was used to determine the double layer capacitance (C_{dl}) for the 100 µm Pt disc working electrode, and the solution resistance (R_Ω) for a PEG200 solution with 0.02 M lithium perchlorate ($LiClO_4$) electrolyte. EIS was performed *in vacuo*, which removed unwanted gases and controlled the humidity levels in the solution. EIS was performed at 0 V (*vs.* Ag wire) with a potential amplitude of 50 mV. The frequency of modulation was decreased from 100 kHz to 10 Hz. Equivalent circuit fitting was used to determine C_{dl} and R_Ω using the electrical circuit shown in Figure 3.2.

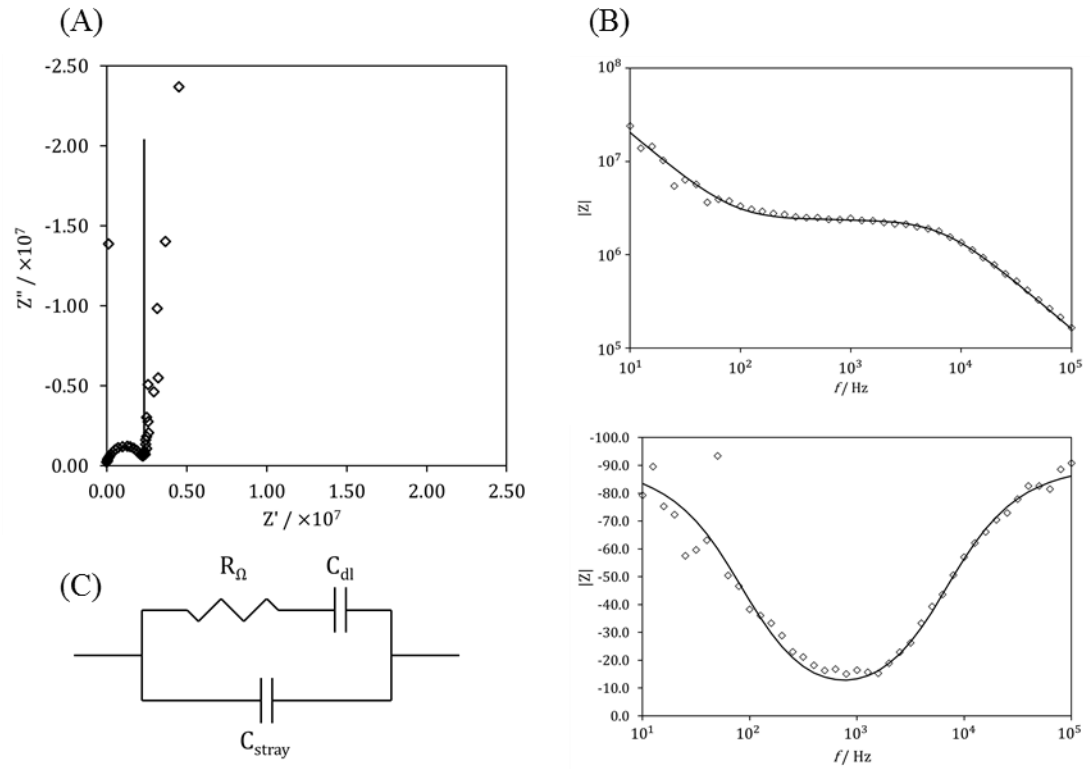

Figure 3.2. A Nyquist plot (**A**) and a Bode plot (**B**) for experimental results (◇) and a simulated fit (solid line) for a 20 mM $LiClO_4$ / PEG200 solution at a 100 μm diameter Pt disc. (**C**) The equivalent circuit used for data fitting analysis.

The solution resistance (R_Ω) and double layer capacitance (C_{dl}) were found to be 2.4 MΩ and 0.8 nF respectively and were used in subsequent electrochemical simulations. C_{stray} represents a stray capacitance with a very small magnitude (~9.9 pF) and is not considered further.

3.2.5 Procedure for diffusion coefficient determination

Voltammetry was performed *in vacuo* in order to determine the diffusion coefficients for a number of redox species. Vacuum conditions were used to remove unwanted gases, such as oxygen, from the PEG200 solution and to control the humidity levels. Overall this helped to reduce the background interferences in the voltammetry measurements and give a more reliable determination of the diffusion coefficient. A 40 μL droplet of solution was placed on the surface of the working electrode and subjected to 3 h of vacuum prior to experimentation. Cyclic voltammetry was used to determine the reversible potential for the redox species with respect to the silver wire reference. A double potential step (chronoamperometry) experiment was performed to determine

the diffusion coefficients of both the reduced (D_{red}) and oxidised (D_{ox}) form of the analyte. The potential was stepped from a value where no electron transfer occurs to a potential where the rate of electron transfer is expected to be fast. This ensures that the current is limited by diffusion rather than slow electrode transfer kinetics. The potential was held for 180 s and then returned to the original value for a further 180 s whilst the current was sampled every 0.5 s. Analysing values of τ (see equation 3.3) for a 180 s potential step at a 100 μm diameter Pt electrode with an estimated diffusion coefficient of 1×10^{-7} cm^2 s^{-1} implies a mixed diffusion regime ($\tau > 0.01$) would be observed for > 99.6 % of the potential step experiment.

To determine diffusion coefficients under a mixed diffusion regime the commercial DigiElch™ Professional (version 4F) software package was used. A DigiElch™ simulation of a potential step experiment using a 2-dimensional semi-infinite diffusion model was shown to agree with the conventional Shoup-Szabo method[8] to within 0.71 % deviation (Figure 3.3). The computer software was used in preference as it allowed the diffusion coefficient for both the oxidised (D_{ox}) and reduced (D_{red}) forms of the redox species to be determined.

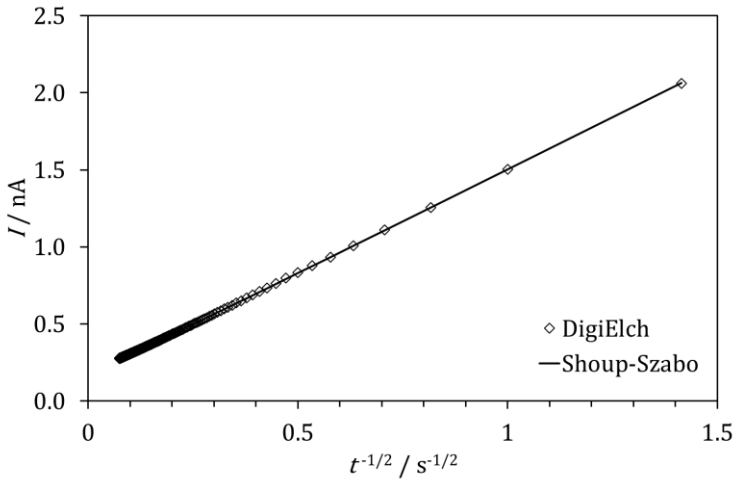

Figure 3.3. A Cottrell plot comparing the Shoup-Szabo equation (solid line) with a simulated current transient using DigiElch (◇) for a 180 s potential step. k_s = 10000 cm s^{-1}, n = 1, $D_{ox} = D_{red}$ = 1×10^{-7} cm^2 s^{-1}, c = 1 mmol dm^{-3}, and r = 50 μm.

The diffusion coefficients were optimised using the data fitting tool on DigiElch™. The software uses an iterative approach to find the diffusion coefficients that minimise the standard deviation between the experimental data points and the simulated current

transient. The simulated current transient was based upon a 2-dimensional (2D) semi-infinite diffusion model at 293.2 K with fast electron transfer (k_s = 10 000 cm s^{-1}) and $\alpha = 0.5$. The solution resistance and double layer capacitance determined from EIS measurements were included in the computer simulation.

The optimised diffusion coefficients (determined from potential step experiments) were then used as fixed parameters to simulate cyclic voltammograms using DigiElch™ software. The simulated cyclic voltammograms were compared with experimental results to verify the values of the optimised diffusion coefficients. The diffusion coefficients for anthraquinone-2-sulfonate (AQS), 1,1'-ferrocene dicarboxylic acid ($Fc(COOH)_2$), and 1,1'-ferrocene dimethanol ($Fc(CH_2OH)_2$) were optimised using this method.

3.3 Results and Discussion

3.3.1 Effect of vacuum on voltammetry

In order to understand the electrochemical responses of redox species in neat poly(ethylene glycol) with average M_w = 200 g mol^{-1} (PEG200), it is necessary to investigate the background processes that underlie all measurements. PEG200 is a hygroscopic liquid at room temperature and is deliquescent at high relative humidity.[24] Although water is an excellent solvent itself, it has been found to reduce the electrochemical window of non-aqueous solvents, such as ionic liquids.[8] The low volatility of PEG200 was utilised and voltammetry was conducted under vacuum conditions in order to control the humidity levels of the PEG200 solution and minimise the effects of water on the voltammetric response. In addition, the application of vacuum also removed unwanted gases, such as oxygen, from the solution and hence helped to prevent the formation of reactive peroxide and/or superoxide species at negative potentials.

Cyclic voltammetry was used to probe the electrochemical window of PEG200 containing 20 mM $LiClO_4$ as electrolyte, in both ambient conditions and after 3 h of

applied vacuum (Figure 3.4). In ambient conditions, the oxidation of PEG200 had an onset potential of *ca.* +0.4 V (vs. Ag) and the reduction of oxygen dominated the signal at potentials more negative than -0.25 V (vs. Ag). After 3 h vacuum, the background signals had been suppressed with the cathodic window of the polymer solvent extended to -1.0 V. These results suggest the complete removal of oxygen from the system under vacuum, which facilitates the studies of redox processes occurring at negative potentials. Deaerating the solution by nitrogen or argon gas purging was found to be ineffective at removing all traces of oxygen from the solution. The determination of diffusion coefficients was therefore carried out using voltammetry under vacuum conditions as this helped to reduce background interferences from the voltammograms.

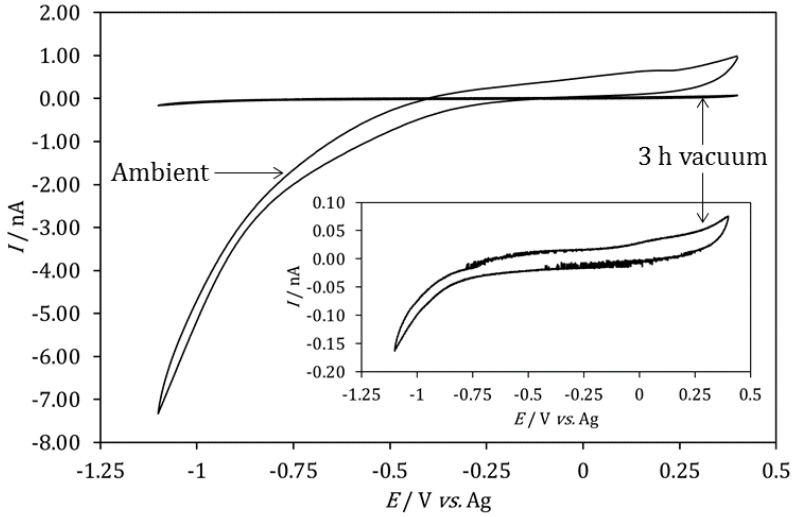

Figure 3.4. A cyclic voltammogram (scan rate 10 mV s^{-1}) showing the solvent limit for a 20 mM $LiClO_4$ / PEG200 solution at a 100 μm diameter Pt disc in ambient conditions and after 3 h of applied vacuum (inset).

3.3.2 Diffusion coefficient analysis: anthraquinone-2-sulfonate

The voltammetric response of anthraquinone-2-sulfonate (AQS) was investigated in PEG200 with 20 mM $LiClO_4$ as electrolyte *in vacuo*. Two possible mechanisms for anthraquinone reduction are shown in Figure 3.5. In the absence of protons the reduction is often observed as two 1-electron reduction steps.[25-28] However, in the presence of protons a single 2-electron, 2-proton reduction peak is usually observed.[29,30] The reduction of anthraquinones has been reported to mediate the reduction of oxygen to form peroxides.[31,32] It is therefore important to remove all traces of oxygen from the system to determine an accurate diffusion coefficient.

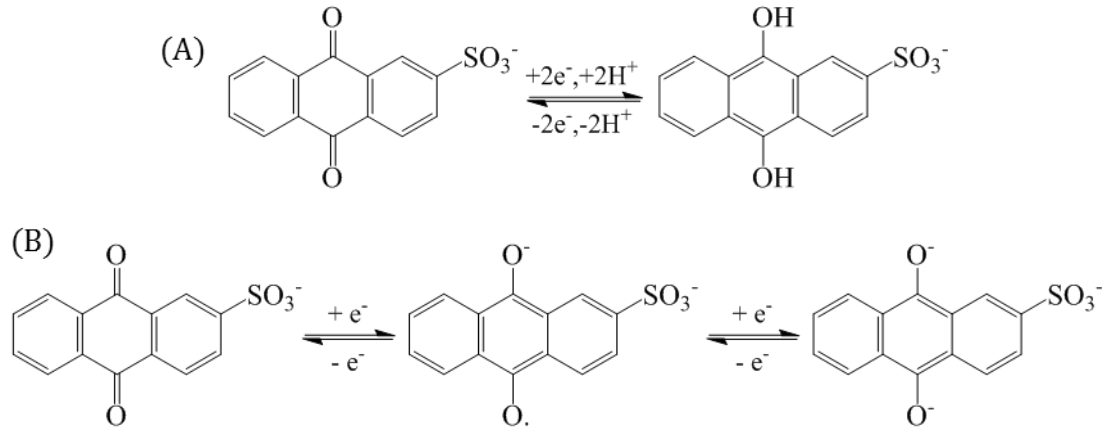

Figure 3.5. Mechanisms for anthraquinone reduction. (**A**) as a single 2-electron reduction in the presence of protons, and (**B**) as two sequential 1-electron reductions (in the absence of protons)

The cyclic voltammogram of AQS under ambient conditions in PEG200 at a 100 μm diameter Pt disc working electrode gave a complex steady-state response, which is likely to be due to the catalytic reduction of oxygen in the solution.[31] However, a quasi-reversible response was observed after 3 h of vacuum with a midpoint potential of −0.80 V and a peak separation of 88 mV. This signal was reproducible after 12 hours of applied vacuum, which suggests neither the polymer solvent nor the redox species are being lost from the system by evaporation. A second reduction process was not observed by scanning to more negative potentials, which suggests the quasi-reversible peak corresponds to a two-electron, two-proton process (Figure 3.6). A degree of asymmetry was observed between the reduction current and the oxidation current. At 10 mV s^{-1} the peak reduction current was ~3.5 times larger in magnitude. An irreversible oxidation peak with an onset potential of −0.25 V (*vs*. Ag) was also apparent at faster scan rates.

The cyclic voltammogram exhibits considerable complexity and a speculative mechanism to account for the redox processes is proposed. Consider the reduction of AQS to proceed via two sequential 1-proton, 1-electron transfer steps, where the second reduction process is more favourable than the first (i.e. the second reduction step has a more positive reduction potential). This causes the AQS redox signal to be observed as a single 2-electron, 2-proton reversible redox peak. The electro-generated final reduction product is anthrahydroquinone-2-sulfonate ($AQSH_2$). The protons required for the reduction steps are provided by the terminal hydroxyl groups on the PEG200

chains. The oxidation of $AQSH_2$ generates protons, which causes a localised increase in proton concentration near to the electrode surface in the unbuffered PEG solution. This favours the initiation of the hydrogen evolution reaction and generates a negative (cathodic) current. The peak in the cyclic voltammogram assigned to the oxidation of $AQSH_2$ has a magnitude that is the net current for the oxidation of $AQSH_2$ (positive current) and the reduction of protons (negative current). Consequently, the magnitude of the $AQSH_2$ oxidation current is lower than expected, which results in a degree of asymmetry in the AQS redox signal. The hydrogen evolved may also have a secondary effect on the voltammetry and is thought to be responsible for the oxidation peak observed at -0.25 V (*vs*. Ag). If the reduction of protons to form hydrogen is considered to be reversible, the charge under the oxidation peak at -0.25 V (*vs*. Ag) should be equivalent to the charge that is 'missing' from the $AQSH_2$ oxidation peak. Consequently, double potential step experiments were performed across a broad potential range (+0.2 V to -1.0 V and back to +0.2 V *vs.* Ag) to try to minimise the systematic errors caused by hydrogen evolution occurring as a background process.

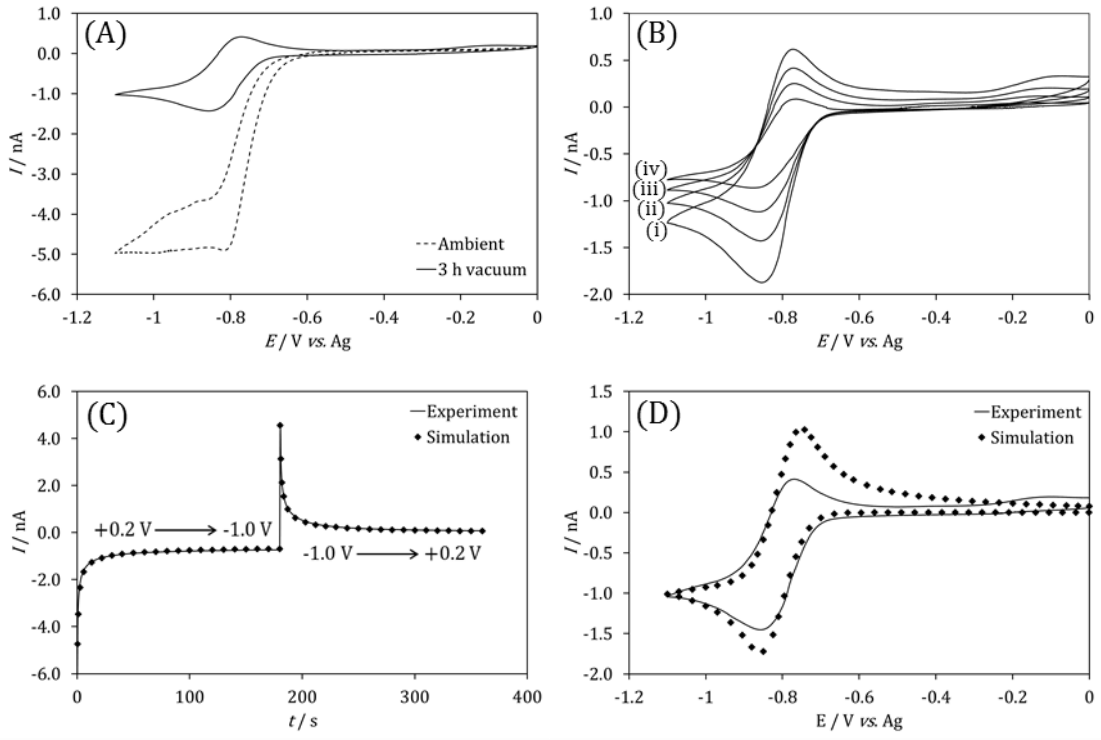

Figure 3.6. Voltammetry for 1 mM anthraquinone-2-sulfonate (AQS) in 20 mM $LiClO_4$ / PEG200 solution at a 100 μm diameter Pt disc. (**A**) Cyclic voltammograms (CVs) in ambient conditions (dashed line) and after 3 h of applied vacuum (solid line). (**B**) CVs after 3 h of vacuum at (i) 20 mV s^{-1}, (ii) 10 mV s^{-1}, (iii) 5 mV s^{-1}, and (iv) 2 mV s^{-1}. (**C**) Current transient for a double potential step experiment (solid line) and simulation (♦). (**D**) Experimental CV (solid line) and simulation (♦) (scan rate 10 mV s^{-1}). $D_{ox} = 1.3 \times 10^{-7}$ cm^2 s^{-1}, $D_{red} = 0.9 \times 10^{-7}$ cm^2 s^{-1}.

The diffusion coefficients were optimised from double potential step experiments using the data fitting tool on DigiElch™. The simulation considered the reduction of AQS as two sequential 1-electron reduction reactions, where the second reduction step had a more positive reduction potential. The redox processes were assumed to be diffusion limited at the potentials stepped to, and the rate of electron transfer (k_s) was therefore assumed to be fast ($k_s = 10\,000$ cm s^{-1}). Background processes, including the hydrogen evolution reaction, were not considered as part of the simulation. The simulation used an iterative approach to simultaneously vary the diffusion coefficients for both the oxidised (D_{ox}) and reduced (D_{red}) form of AQS. The values which gave the lowest standard deviation between simulation and experiment were used as the optimised diffusion coefficients. The optimised values were: $D_{ox} = 1.3 \times 10^{-7}$ cm^2 s^{-1} and $D_{red} = 0.9 \times 10^{-7}$ cm^2 s^{-1}. It should be noted that the optimised value of D_{red} could be affected by the coupled chemistry under the conditions employed.

These values were verified by comparing experimental cyclic voltammograms with simulation. It was found that the peak currents from simulated cyclic voltammograms were larger than those observed by experiment. Despite the apparent overestimation, the values obtained in this study are similar to those previously reported for similar systems in viscous media, which indicates that this simplistic model gives a reasonable approximation to the diffusion coefficients.[33] A more accurate determination of the diffusion coefficients could be achieved by using a more complex computer model that incorporates the underlying background processes. However, inaccuracies could arise as more unknown parameters are included in the model.

3.3.3 Diffusion coefficient analysis: ferrocene

Ferrocene (Fc) is a commonly used redox species that is known to undergo a fully reversible 1-electron oxidation to form a ferrocenium cation (Figure 3.7). The ferrocene redox couple has previously been studied in high molecular weight poly(ethylene glycols) and diffusion coefficients determined.[34-36] However, the diffusion coefficient has not been determined in poly(ethylene glycol) with an average molecular weight of 200 g mol^{-1}.

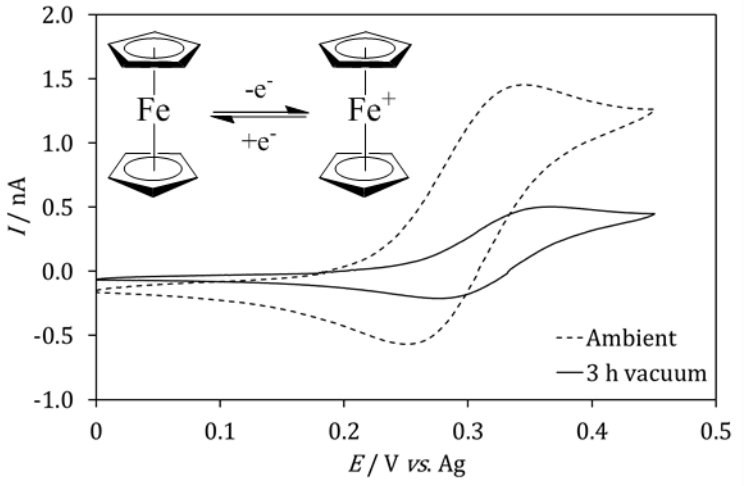

Figure 3.7. Cyclic voltammogram of 1 mM ferrocene in 20 mM $LiClO_4$ / PEG200 in ambient conditions (dashed line) and after 3 h of applied vacuum (solid line).

In ambient conditions the cyclic voltammogram at a 100 μm Pt disc electrode gave a quasi-reversible response with a midpoint potential of +0.30 V (*vs.* Ag) and a peak separation of 90 mV. After 3 h of vacuum the midpoint potential had shifted +27 mV but the peak separation remained constant. The shift is due to unstable potential of the Ag wire pseudo-reference electrode.[37] The peak separation for the $Fc^{0/+}$ redox couple is expected to be ~60 mV due to the fast electron kinetics. The larger than expected peak separation observed in these experiments is due to an uncompensated voltage drop (*IR* drop) caused by the high solution resistance. The magnitude of the peak currents after 3 h of applied vacuum were 65 % lower compared to in ambient conditions. This implies that ferrocene is volatile and a significant amount of material is removed from the solution in the timescale of the experiment whilst under reduced pressure. Consequently, the concentration of the redox species after 3 h of vacuum is unknown. DigiElch™ can be employed to simultaneously determine concentration and diffusion coefficient parameters. However, optimising multiple parameters simultaneously can lead to greater uncertainty and was avoided in this investigation. Subsequent experiments used ferrocene derivatives, such as 1,1'-ferrocene dimethanol and 1,1'-ferrocene dicarboxylic acid, which have the possibility of forming hydrogen bonds with the poly(ethylene glycol) chains. This was expected to prevent evaporation of the redox species under vacuum conditions.

3.3.4 Diffusion coefficient analysis: 1,1'-ferrocene dimethanol

1,1'-ferrocene dimethanol ($Fc(CH_2OH)_2$) is known to undergo a fully reversible 1-electron redox process (equation 3.9). The alcohol groups have the potential to form hydrogen bonds with the poly(ethylene glycol) solvent, which should disfavour the evaporation of $Fc(CH_2OH)_2$ under vacuum conditions.

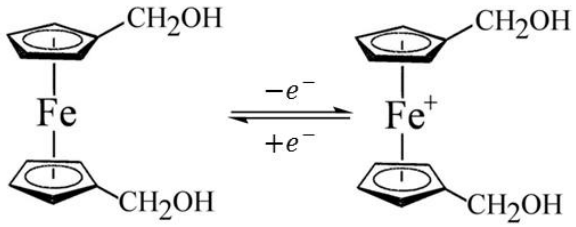

(3.9)

A 100 μm diameter platinum disc working electrode was used to probe the voltammetry of 1 mM $Fc(CH_2OH)_2$ in PEG200 with 20 mM $LiClO_4$ as supporting electrolyte. The cyclic voltammogram in ambient conditions (Figure 3.8A) had a reversible potential of +0.29 V (*vs.* Ag) and a peak separation of 86 mV. After 3 h of applied vacuum, the reversible potential had shifted to +0.31 V (*vs.* Ag) but the peak separation remained constant. The 20 mV shift in reversible potential after vacuum is likely to be due to the unstable nature of the Ag wire pseudo-reference electrode. The magnitude of the peak currents remained constant in ambient conditions and after 3 h of vacuum. This implies that the concentration of the solution remained unchanged and that $Fc(CH_2OH)_2$ is not evaporating to a significant extent (if at all) in the timescale of the experiment. The peak currents were found to remain constant after over 12 h of applied vacuum, which further supports the conclusion that $Fc(CH_2OH)_2$ was not evaporating under vacuum conditions. Since the voltammetry of $Fc(CH_2OH)_2$ remained the same in ambient conditions and after 3 h of applied vacuum, it was possible to proceed with the method outlined above to determine the diffusion coefficients under vacuum conditions.

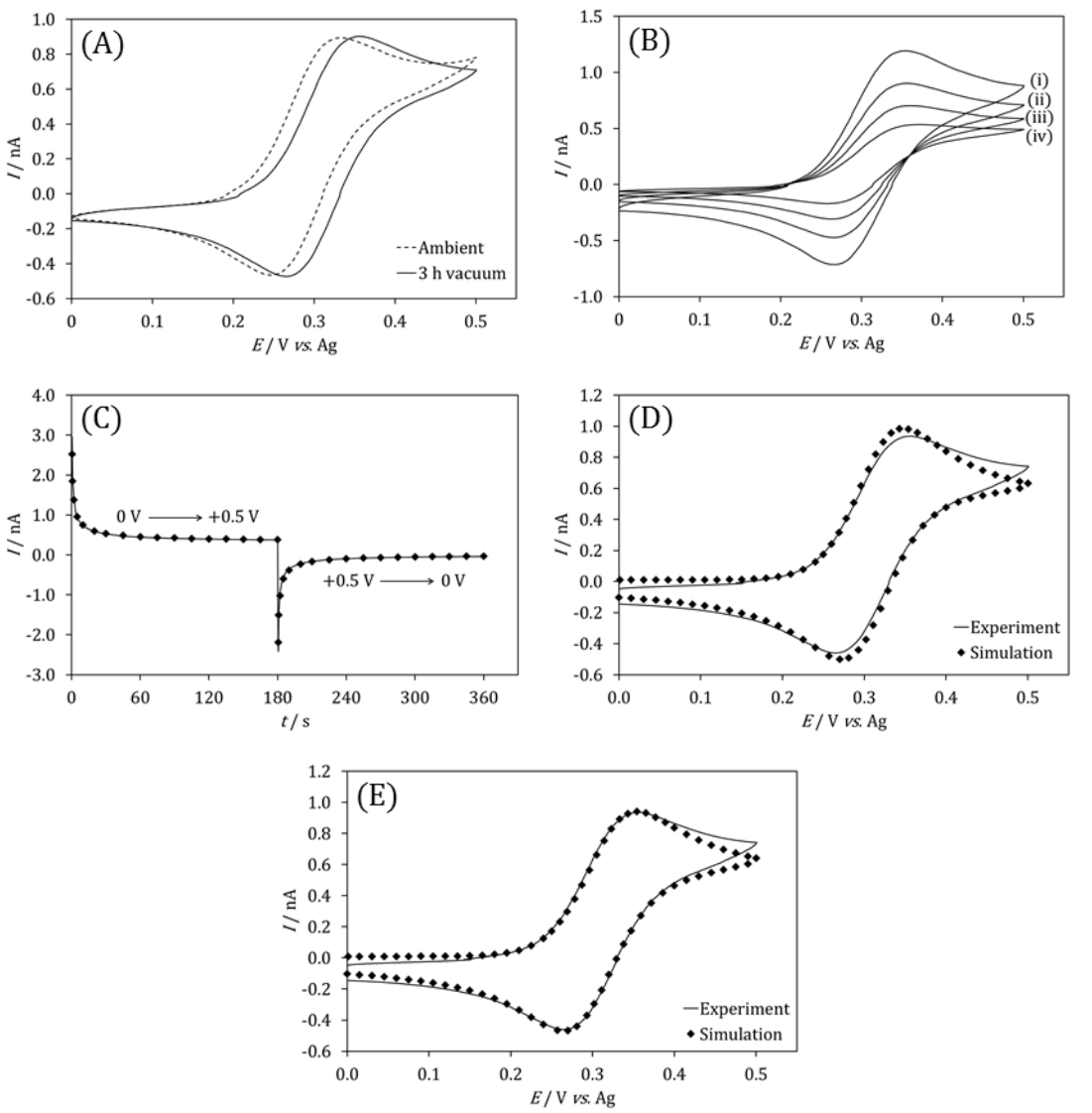

Figure 3.8. Voltammetry of 1 mM $Fc(CH_2OH)_2$ in 20 mM $LiClO_4$ / PEG200 at a 100 μm diameter Pt disc. **(A)** Cyclic voltammograms (scan rate 10 mV s^{-1}) in ambient conditions (dashed line) and after 3 h of applied vacuum (solid line). **(B)** Voltammograms at scan rates of (i) 20 mV s^{-1}, (ii) 10 mV s^{-1}, (iii) 5 mV s^{-1}, and (iv) 2 mV s^{-1}. (**C**) Current transient for a double potential step experiment (solid line) and simulation (♦). Optimised values were $D_{red} = 1.4 \times 10^{-7}$ cm^2 s^{-1} and $D_{ox} = 1.3 \times 10^{-7}$ cm^2 s^{-1}. (**D**) Experimental voltammograms *in vacuo* (solid line) and simulation (♦) assuming fast electron transfer ($k_s = 10\,000$ cm s^{-1}) and (**E**) after optimising the rate of electron transfer ($k_s = 7.9 \times 10^{-4}$ cm s^{-1}).

A double potential step experiment (chronoamperometry) was used to extract the diffusion coefficient of $Fc(CH_2OH)_2$ and the electro-generated ferrocenium cation $\{[Fc(CH_2OH)_2]^+\}$ *in vacuo* (Figure 3.8C). The cyclic voltammogram indicates that the oxidation of $Fc(CH_2OH)_2$ is diffusion controlled at +0.5 V (*vs.* Ag) and the reduction is diffusion controlled at 0 V (*vs.* Ag). The potential was therefore stepped from 0 V to

+0.5 V and back to 0 V (*vs.* Ag). DigiElch™, an electrochemical simulation software package, was used to simulate chronoamperometry (CA) experiments and the data fitting tool was used to optimise D_{red} and D_{ox} simultaneously. Since the electrode processes are diffusion limited in the double potential step experiment, the rate of electron transfer (k_s) was assumed to be fast ($k_s = 10\,000$ cm s^{-1}). The values of D_{red} and D_{ox} were found to be 1.4×10^{-7} cm^2 s^{-1} and 1.3×10^{-7} cm^2 s^{-1} respectively.

The optimised diffusion coefficients were subsequently used as fixed parameters to simulate cyclic voltammograms using DigiElch™. The simulation was compared with experimental results to verify the optimised values of the diffusion coefficients. If the rate of electron transfer (k_s) was assumed to be fast ($k_s = 10\,000$ cm s^{-1}), the simulation gave a higher peak current than found by experiment (Figure 3.8D). However, a lower, optimised value for the rate of electron transfer ($k_s = 7.9 \times 10^{-4}$ cm s^{-1}) gave an improved fit. This is consistent with literature values.[36] Ferrocene derivatives are typically considered to undergo fast electron transfer at platinum electrodes.[3,38,39] The slower electron transfer could be due to the arrangement of the polymer at the metal electrode | polymer solvent interface. It is speculatively proposed that PEG200 adsorbs on the platinum surface at positive potentials, which passivates the electrode to some extent and decreases the rate of electron transfer for the $Fc(CH_2OH)_2^{0/+}$ redox couple. This phenomenon will be discussed further in Chapter 4. The deviation between the simulated cyclic voltammograms and the experimental results > 0.4 V (*vs.* Ag) is due to a background PEG oxidation process, which becomes more significant at more positive potentials.

3.3.5 Diffusion coefficient analysis: 1,1'-ferrocene dicarboxylic acid

1,1'-ferrocene dicarboxylic acid, $Fc(COOH)_2$, undergoes a 1-electron oxidation and reduction process:

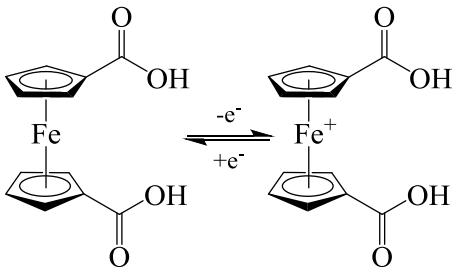

(3.10)

The electron withdrawing dicarboxylic acid substituents cause the reduction potential to be more positive than for the ferrocene or 1,1'-ferrocene dimethanol systems previously discussed.[36] The carboxylic acid substituents can form hydrogen bonds with the PEG200 solvent and $Fc(COOH)_2$ is not removed from the solution under vacuum conditions. The cyclic voltammogram in ambient conditions (Figure 3.9A) has a significant contribution from an irreversible background PEG oxidation process, which has an onset potential of ~0.4 V (*vs.* Ag). The background process was suppressed to some extent after 3 h of vacuum but generates an increasing contribution to the current as the potential is increased. The redox process for $Fc(COOH)_2$ has a reversible potential of ~0.43 V (*vs.* Ag). An oxidation peak could not be assigned with certainty, however, a peak separation of > 150 mV was observed, which is an indication of slow electron transfer across the Pt electrode | PEG200 interface.

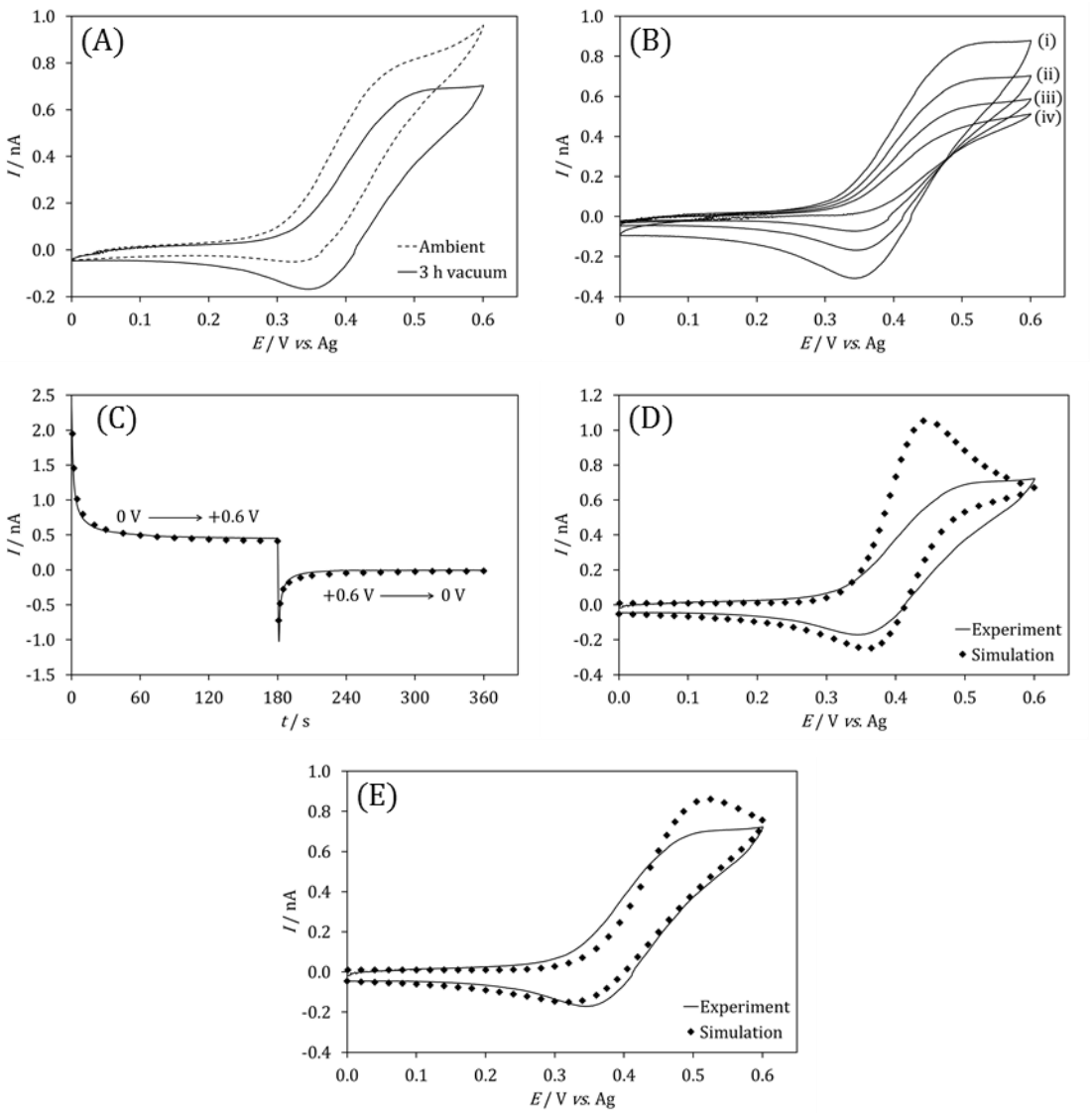

Figure 3.9. Voltammetry of 1 mM $Fc(COOH)_2$ in 20 mM $LiClO_4$ / PEG200 at a 100 µm diameter Pt disc. **(A)** Cyclic voltammograms (scan rate 10 mV s^{-1}) in ambient conditions (dashed line) and after 3 h of applied vacuum (solid line). **(B)** Voltammograms at scan rates of (i) 20 mV s^{-1}, (ii) 10 mV s^{-1}, (iii) 5 mV s^{-1}, and (iv) 2 mV s^{-1}. (**C**) Current transient for a double potential step experiment (solid line) and simulation (♦). Optimised values were $D_{red} = 1.6 \times 10^{-7}$ cm^2 s^{-1} and $D_{ox} = 9.7 \times 10^{-7}$ cm^2 s^{-1}. (**D**) Experimental voltammograms *in vacuo* (solid line) and simulation (♦) assuming fast electron transfer ($k_s = 10\,000$ cm s^{-1}) and (**E**) after optimising the rate of electron transfer ($k_s = 1.2 \times 10^{-4}$ cm s^{-1}).

A double potential step experiment was performed stepping from 0 V to +0.6 V and back to 0 V (*vs.* Ag). The $Fc(COOH)_2$ oxidation process was considered to be limited by diffusion at +0.6 V (*vs*. Ag), and the rate of electron transfer in the simulation was therefore fixed at a high value ($k_s = 10\,000$ cm s^{-1}). A good fit between simulation and experiment was observed in the chronoamperogram using optimised diffusion

coefficients of $D_{red} = 1.6 \times 10^{-7}$ cm^2 s^{-1} and $D_{ox} = 9.7 \times 10^{-7}$ cm^2 s^{-1}. These D values were used as fixed parameters to simulate cyclic voltammograms using DigiElch™. If the rate of electron transfer used in the simulation was fast ($k_s = 10\ 000$ cm s^{-1}), the fit between simulation and experiment was poor (Figure 3.9D). Non-linear data fitting methods were employed to optimise the rate of electron transfer by minimising the standard deviation between simulated and experimental cyclic voltammograms. However, even after optimising the rate of electron transfer ($k_s = 1.2 \times 10^{-4}$ cm s^{-1}), the simulation overestimated the oxidation peak height in the cyclic voltammogram (Figure 3.9E).

Although the optimised diffusion coefficients were reproducible and led to a good fit for potential step experiments, it is suspected that a systematic bias is present in the $Fc(COOH)_2$ optimisation, which is responsible for the poor agreement between simulated and experimental cyclic voltammograms. An irreversible background oxidation process – thought to be PEG200 oxidation – occurs with an onset potential of ~+0.4 V (*vs.* Ag). This could add a significant current to the first step of the chronoamperogram, which was held at +0.6 V (*vs.* Ag) for $Fc(COOH)_2$, and consequently lead to an overestimation of the diffusion coefficients. This highlights the importance of using at least two complementary methods when using non-linear fitting techniques to verify the accuracy of the convergence. The background process was not included in DigiElch™ simulations because the current from PEG200 oxidation could not be distinguished from the current generated by the oxidation of $Fc(COOH)_2$. A more complex model would be needed to incorporate the background process but was not pursued in this study.

The diffusion coefficients determined in this chapter are consistent to those reported for similar systems in polymeric media.[15,36,40,41] The diffusion coefficient values are approximately two orders of magnitude lower than those reported in acetonitrile or aqueous solutions, which can be rationalised by the higher viscosity of the PEG200 solvent. The Stokes-Einstein relation (equation 3.11) states that the diffusion coefficient (D) is inversely proportional to the viscosity (η).

$$D = \frac{k_B T}{6\pi\eta a} \tag{3.11}$$

In this equation k_B is the Boltzmann constant (1.38×10^{-23} J K^{-1}), T is the absolute temperature (in K), and a is the hydrodynamic radius of the species. The viscosity of PEG200 is reported to be 48 cP at 25 °C.[42] The Stokes-Einstein relation could therefore be used to determine the hydrodynamic radius for the three redox species studied. The results are summarised in Table 3.1.

Table 3.1. A table comparing experimentally determined hydrodynamic radii with those reported from literature sources. [a] Literature radii were calculated from literature diffusion coefficients using the Stokes-Einstein relation with a viscosity of 1.0 cP (at 293 K) and slip limit of 6. [b] Diffusion coefficient reported in MeCN – hydrodynamic radius calculated using $\eta = 0.34$ cP (at 293 K) and a slip limit of 4.

Analyte	D_{red} / $\times 10^{-7}$ cm^2 s^{-1}	D_{ox} / $\times 10^{-7}$ cm^2 s^{-1}	a_{red} / Å	a_{ox} / Å	Literature a[a] / Å
AQS	0.9	1.3	5.7	3.8	4.7[30]
$Fc(CH_2OH)_2$	1.4	1.3	3.4	3.6	3.4[43]
$Fc(COOH)_2$	1.6	9.7	3.1	0.5	4.2[b, 39]

3.4 Conclusions

A fundamental study of the voltammetry in PEG200 has been performed with the addition of a suitable electrolyte. Voltammetry was performed *in vacuo*, which was shown to be an effective tool for deaerating non-volatile, viscous media and controlling the humidity levels. The high viscosity of the PEG200 solution results in low diffusion coefficients. Double potential step experiments were performed under a mixed diffusion regime and were analysed using a commercial electrochemical simulation software package. Diffusion coefficients for both oxidised and reduced forms of the electroactive species were determined using non-linear fitting methods. The simulated fit for double potential step experiments was good in all cases studied. The optimised values were verified using cyclic voltammetry, which sometimes resulted in a poor fit, although could be improved by optimisation of the rate of electron transfer. This highlights the importance of using at least two complementary methods when using non-linear fitting methods to ensure the simulation does not give a false convergence.

The diffusion coefficients for 1,1'-ferrocene dimethanol ($Fc(CH_2OH)_2$) and the equivalent electro-generated oxidised species were obtained. Values gave a good fit for both potential step and cyclic voltammetry experiments, which supports the reliability of the values obtained.

Background processes – thought to be the oxidation of PEG200 – were observed to give a significant contribution to the current above +0.4 V (*vs*. Ag), which prevented the accurate determination of diffusion coefficients for 1,1'-ferrocene dicarboxylic acid ($Fc(COOH)_2$). More complex computer models could be used to account for the occurrence of the background processes. However, this was not considered here.

The high viscosity of PEG200 is responsible for low diffusion coefficients and slow mass transport to the electrode surface, which resulted in very low currents. Hydrodynamic methods can be employed to increase the rate of mass transport to the electrode. Chapter 4 discusses a hydrodynamic technique based on Couette flow in a microgap, which is suitable for highly viscous media.

3.5 References

1. S. K. Sharma and A. Mudhoo, eds., *Green Chemistry for Environmental Sustainability*, CRC Press, 2011.
2. D. P. Valencia and F. J. Gonzalez, *Journal of Electroanalytical Chemistry*, 2012, **681**, 121-126.
3. N. G. Tsierkezos and U. Ritter, *Journal of Applied Electrochemistry*, 2010, **40**, 409-417.
4. J. E. Baur and R. M. Wightman, *Journal of Electroanalytical Chemistry*, 1991, **305**, 73-81.
5. T. I. Quickenden and Q. Z. Xu, *Journal of the Electrochemical Society*, 1996, **143**, 1248-1253.
6. J. E. B. Randles, *Transactions of the Faraday Society*, 1948, **44**, 327-&.
7. F. Scholz, A. J. Bard and G. Inzelt, *Electrochemical Dictionary*, Springer-Verlag, Berlin, Heidelberg, 2008.
8. D. Shoup and A. Szabo, *Journal of Electroanalytical Chemistry*, 1982, **140**, 237-245.
9. M. L. Longmire, M. Watanabe, H. Zhang, T. T. Wooster and R. W. Murray, *Analytical Chemistry*, 1990, **62**, 747-752.

10. K. Aoki and J. Osteryoung, *Journal of Electroanalytical Chemistry*, 1981, **122**, 19-35.
11. G. Denuault, M. V. Mirkin and A. J. Bard, *Journal of Electroanalytical Chemistry*, 1991, **308**, 27-38.
12. H. F. Zhou and S. J. Dong, *Journal of Electroanalytical Chemistry*, 1996, **414**, 121-125.
13. H. F. Zhou, G. L. Che and S. J. Dong, *Electroanalysis*, 1997, **9**, 40-44.
14. A. J. Bard and L. R. Faulkner, *Electrochemical methods : fundamentals and applications*, John Wiley, New York ; Chichester, 2nd edn., 2001.
15. Y. Wang, J. G. Limon-Petersen and R. G. Compton, *Journal of Electroanalytical Chemistry*, 2011, **652**, 13-17.
16. E. I. Rogers, D. S. Silvester, D. L. Poole, L. Aldous, C. Hardacre and R. G. Compton, *Journal of Physical Chemistry C*, 2008, **112**, 2729-2735.
17. E. O. Barnes, A. M. O'Mahony, S. R. Belding and R. G. Compton, *Journal of Chemical and Engineering Data*, 2010, **55**, 2219-2224.
18. R. D. Martin and P. R. Unwin, *Journal of Electroanalytical Chemistry*, 1997, **439**, 123-136.
19. M. C. Buzzeo, O. V. Klymenko, J. D. Wadhawan, C. Hardacre, K. R. Seddon and R. G. Compton, *Journal of Physical Chemistry A*, 2003, **107**, 8872-8878.
20. R. G. Evans, O. V. Klymenko, S. A. Saddoughi, C. Hardacre and R. G. Compton, *Journal of Physical Chemistry B*, 2004, **108**, 7878-7886.
21. Y. Wang, E. I. Rogers and R. G. Compton, *Journal of Electroanalytical Chemistry*, 2010, **648**, 15-19.
22. O. V. Klymenko, R. G. Evans, C. Hardacre, I. B. Svir and R. G. Compton, *Journal of Electroanalytical Chemistry*, 2004, **571**, 211-221.
23. R. G. Evans, O. V. Klymenko, C. Hardacre, K. R. Seddon and R. G. Compton, *Journal of Electroanalytical Chemistry*, 2003, **556**, 179-188.
24. J. A. Baird, R. Olayo-Valles, C. Rinaldi and L. S. Taylor, *Journal of Pharmaceutical Sciences*, 2010, **99**, 154-168.
25. M. Bauscher and W. Mantele, *Journal of Physical Chemistry*, 1992, **96**, 11101-11108.
26. N. Gupta and H. Linschitz, *Journal of the American Chemical Society*, 1997, **119**, 6384-6391.
27. A. Gomis-Berenguer, M. Gomez-Mingot, L. Garcia-Cruz, T. Thiemann, C. E. Banks, V. Montiel and J. Iniesta, *Journal of Physical Organic Chemistry*, 2013, **26**, 367-375.
28. V. A. Nikitina, R. R. Nazmutdinov and G. A. Tsirlina, *Journal of Physical Chemistry B*, 2011, **115**, 668-677.
29. M. A. Haque, M. M. Rahman and M. A. B. H. Susan, *Journal of Solution Chemistry*, 2011, **40**, 861-875.
30. C. Batchelor-McAuley, Q. Li, S. M. Dapin and R. G. Compton, *Journal of Physical Chemistry B*, 2010, **114**, 4094-4100.
31. C. E. Banks, G. G. Wildgoose, C. G. R. Heald and R. G. Compton, *Journal of the Iranian Chemical Society*, 2005, **2**, 60-64.
32. A. Sarapuu, K. Vaik, D. J. Schiffrin and K. Tammeveski, *Journal of Electroanalytical Chemistry*, 2003, **541**, 23-29.

33. M. Shamsipur, A. Salimi, S. M. Golabi, H. Sharghi and M. F. Mousayi, *Journal of Solid State Electrochemistry*, 2001, **5**, 68-73.
34. H. F. Zhou and S. J. Dong, *Electrochimica Acta*, 1996, **41**, 2395-2398.
35. H. F. Zhou and S. J. Dong, *Journal of Electroanalytical Chemistry*, 1997, **425**, 55-59.
36. H. F. Zhou, N. Y. Gu and S. J. Dong, *Journal of Electroanalytical Chemistry*, 1998, **441**, 153-160.
37. K. Izutsu, Reference Electrodes for Use in Nonaqueous Solutions in *Handbook of Reference Electrodes*, eds. G. Inzelt, A. Lewenstam and F. Scholz, Springer Berlin Heidelberg, 2013, pp. 145-187.
38. W. R. Fawcett and M. Opallo, *Angewandte Chemie-International Edition in English*, 1994, **33**, 2131-2143.
39. A. D. Clegg, N. V. Rees, O. V. Klymenko, B. A. Coles and R. G. Compton, *Journal of Electroanalytical Chemistry*, 2005, **580**, 78-86.
40. Y. Guo, K. Aoki, J. Chen and T. Nishiumi, *Electrochimica Acta*, 2011, **56**, 3727-3730.
41. M. E. Williams and R. W. Murray, *Journal of Physical Chemistry B*, 1999, **103**, 10221-10227.
42. S. Ottani, D. Vitalini, F. Comelli and C. Castellari, *Journal of Chemical and Engineering Data*, 2002, **47**, 1197-1204.
43. R. W. French, A. M. Collins and F. Marken, *Electroanalysis*, 2008, **20**, 2403-2409.

Chapter 4: Hydrodynamic electrochemistry in poly(ethylene glycol)

Chapter abstract

Electrochemical processes in viscous media, such as poly(ethylene glycol), are often limited by the rate of mass transport to the electrode surface, which results in low current densities. This chapter describes a new hydrodynamic technique suitable for viscous solutions based on an inlaid electrode approaching a rotating wheel (or drum) causing Couette flow in a microgap. A Levich-type equation is derived for the new hydrodynamic technique, which suggests that the limiting current at high overpotentials is proportional to the cube root of the speed of the rotating wheel and to the reciprocal cube root of the distance across the microgap. However, the limiting current is independent of the solution viscosity. The derived Levich-type equation was found to be in good agreement with both COMSOL Multiphysics® simulation and experimental results for a model $Fe(CN)_6^{3-/4-}$ redox couple in aqueous solution. Having previously determined the diffusion coefficient for 1,1'-ferrocene dimethanol in poly(ethylene glycol) with an average molecular weight of 200 g mol^{-1} (PEG200) in Chapter 3, the same redox system was employed using the hydrodynamic microgap Couette flow technique for studies in viscous media. Currents are enhanced by two orders of magnitude under experimental conditions used, however, further current enhancement could be achieved by using faster rotation speeds and smaller gap sizes.

Chapter publications

This chapter has been published in:
C. E. Hotchen, N. V. Nguyen, A. C. Fisher, P. E. Frith, and F. Marken, *ChemPhysChem*, 2015, **16**, 2789-2796.

Special acknowledgements

I would like to thank Paul Frith for constructing the rotating drum apparatus, without which this work could not have been completed. I would also like to thank Viet Nguyen for running COMSOL Multiphysics® simulations and helping to derive the Levich-type expression for a hydrodynamic microgap system under Couette flow.

Chapter contents

4 Hydrodynamic electrochemistry in poly(ethylene glycol)

4.1 Introduction

The fundamental voltammetric studies in Chapter 3 indicated that highly viscous polymer solutions result in slow mass transport to the electrode and low current densities. Hydrodynamic methods are important quantitative techniques in electrochemistry that use forced convection to increase the rate of mass transport to electrodes. This is typically accompanied by a significant enhancement in the current. For example, a high speed rotating disc electrode gave increased currents of over 1 order of magnitude compared with a static solution.[1] Many hydrodynamic methods have been developed for the quantitative study of electrode processes by controlling the flow of solution to the electrode. This is typically achieved by either moving the electrode, for example in rotating disc and rotating ring disc voltammetry[2], or by forcing the flow of solution over a static electrode, for example in wall-jet[3] and wall-tube[4] experiments, and in channel flow devices where one or more coupled electrodes may be under well-defined microfluidic conditions.[5-8] Alternative methods using sono-electrochemistry[9] and microwave-enhanced electrochemistry[10] have also been investigated as methods to enhance currents. A hanging meniscus rotating disc experiment is a variation of the rotating disc electrode, which enables hydrodynamic voltammetry to be performed in microlitre droplets.[11,12] Similarly, a rocking disc alternative has been proposed enabling hydrodynamic measurements to be recorded at a conventional inlaid disc working electrode.[13]

The hydrodynamic techniques mentioned above can be categorised into methods which generate an approximately uniform diffusion layer thickness, for example the rotating disc electrode, and methods with a non-uniform diffusion layer thickness, for example in channel flow electrodes.[14] For static electrodes with a flow across the surface, the highest current density is always observed at the leading edge of the electrode with a diffusion layer that increases in thickness towards the trailing edge. Therefore the resulting current is not only dependent upon the area of the electrode but also the

electrode geometry. A Levich-type expression can be derived to account for the flow parameters at an electrode of particular geometry.[15]

The rotating disc electrode (RDE) is often the favoured hydrodynamic technique because the flux of material to the electrode surface can be controlled with high precision by varying the rotation frequency.[16] However, rotating disc experiments are not so well suited in highly viscous solutions due to (i) an increased contribution from edge effects, which causes a deviation from the Levich equation,[17] and (ii) the very high rotation frequencies required to reach steady state.[18] This chapter aims to develop a hydrodynamic technique based upon Couette flow in a microgap. Couette flow is the shear induced flow caused by the movement of a boundary plate parallel to a second, stationary boundary plate. This generates a linear velocity gradient orthogonal to the boundary plates that is dependent upon the relative velocity of the moving plate but independent of the solution viscosity. Therefore the hydrodynamic voltammetry under Couette flow conditions in a microgap should be a suitable technique for quantitative analytical studies in highly viscous media. The technique could also have applications in bulk electrolyses in highly viscous media.

4.2 Experimental

4.2.1 Chemical reagents

Potassium ferricyanide(III) ($K_3Fe(CN)_6$, Aldrich, 99+ %) was employed as redox species in aqueous solutions containing 1 M potassium nitrate (KNO_3, Sigma-Aldrich, $\geq$ 99.0 %) as background electrolyte. 1,1'-Ferrocene-dimethanol ($Fc(CH_2OH)_2$, Aldrich, 98%) was used as a reversible redox species in liquid poly(ethylene glycol) (PEG200, Sigma-Aldrich, average molecular weight = 200 g mol^{-1}) with 20 mM lithium perchlorate ($LiClO_4$, Sigma-Aldrich, ACS reagent, $\geq$ 95%) as background electrolyte. Experiments were performed at 20 $\pm$ 2 °C.

4.2.2 Instrumentation

All electrochemical measurements were recorded using an Autolab PGSTAT12 potentiostat. For rotating drum experiments, a Physik Instrumente E-665 piezo-positioner (500 μm travel distance) was used to control the distance between the working electrode (250 μm diameter platinum disc) and the rotating drum to the nearest 0.1 μm. A three-electrode set up was employed with a Pt wire counter electrode and a KCl-saturated calomel electrode (SCE) reference. The rotation of the drum was controlled by an IKA®-WERKE EUROSTAR digital overhead stirrer, which allowed the frequency of rotation to be adjusted to the nearest revolution per minute (rpm). COMSOL-Multiphysics® modelling software was used to simulate voltammetry under hydrodynamic conditions.

4.2.3 Procedure for hydrodynamic microgap voltammetry

Hydrodynamic microgap voltammetry was performed using the apparatus shown in Figure 4.1. The system consisted of a motor with a digital readout of the rotation speed, which could be adjusted to the nearest revolution per minute (rpm). The motor is connected via an axle to a 50 mm diameter solid polyether-ether-ketone (PEEK) wheel, which is partially submerged in the solution. This wheel rotates, collecting a thin film of solution on the surface of the wheel. The working electrode (250 μm diameter Pt) is positioned at a distance h above the apex of the drum such that the active area of the electrode is at a tangent to the rotating wheel. The vertical position of the working electrode was controlled to the nearest 0.1 μm by a piezoelectric positioner with a maximum travel distance of 500 μm. The eccentricity in the drum rotation is estimated to be below 5 μm, which is less than 10 % of the smallest distance h employed in this study and assumed insignificant at least in first approximation. Effects from drum roughness and curvature may also be considered as insignificant because the gap between the inlaid disc electrode and the drum ($\leq$ 500 μm) is sufficiently smaller than both the electrode outer diameter (4 mm) and the diameter of the rotating wheel (50 mm). The working electrode was polished using alumina paste (0.3 μm diameter), rinsed and dried using nitrogen prior to experimentation. A KCl-saturated calomel reference electrode (SCE) and Pt wire counter electrode were positioned in the bulk

solution. All electrochemical measurements were performed in an earthed Faraday cage to reduce background interferences. An increase in temperature was noted with longer periods of drum rotation, which is thought to arise from the dissipation of kinetic energy into heat. Therefore a 20 minute delay was employed to keep the temperature of the solution between 20 – 25 °C.

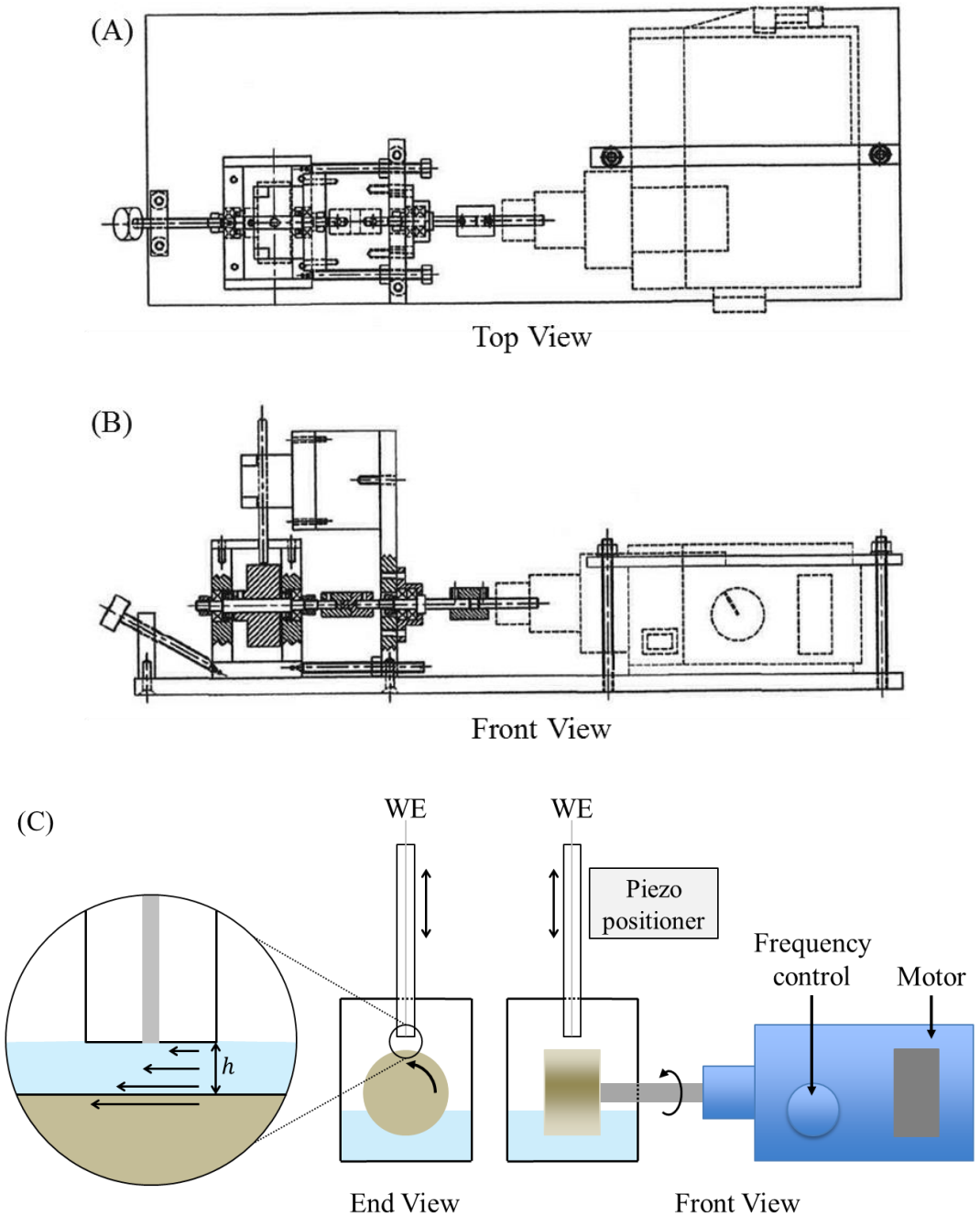

Figure 4.1. CAD technical drawings (**A** and **B**) and a schematic diagram (**C**) of the rotating drum rig. The distance between the working electrode (WE) and the drum (h) is controlled by a piezoelectric positioner. The frequency of rotation can also be varied.

4.2.4 Derivation of a Levich-type expression for hydrodynamic voltammetry under Couette flow

Depending on the hydrodynamic conditions, the measured current approaches a pseudo-steady state value I_{lim}. Two classical cases in the literature are those of the rotating disk electrode (RDE) (equation 4.1)[19] and the rectangular flow channel electrode (FCE) (equation 4.2).[20]

$$I_{lim,RDE} = 1.554nFAc_0D^{\frac{2}{3}}f^{\frac{1}{2}}\nu^{-\frac{1}{6}} \quad (4.1)$$

$$I_{lim,FCE} = 0.925nFAc_0D^{\frac{2}{3}}\left(\frac{4v_f}{h_c^2 d_c x_e}\right)^{\frac{1}{3}} \quad (4.2)$$

In these expressions the mass transport limited current (I_{lim}) is expressed in terms of the number of electrons transferred per molecule diffusing to the electrode surface (n), the Faraday constant (F), the electrode area (A), the bulk concentration of redox active species (c_0), the diffusion coefficient (D), the electrode width and length (w_e and x_e, respectively, inherent in A), the rotation frequency in Hz (f), the solution viscosity (ν), the volume flow rate (v_f), and the channel height and channel width (h_c and d_c respectively). In order to obtain a similar expression for the hydrodynamic microgap under Couette flow conditions[21] simplified parameters need to be defined. The set-up for the rotating drum experiment is inherently three dimensional. However, one can simplify the model to two dimensions as follows. If the active electrode disc diameter (250 μm) and the gap between the electrode and the drum (h) is sufficiently smaller than both the electrode outer diameter (4 mm) and the diameter of the drum (50 mm), the curvature effect of the drum can be ignored. Under these conditions, the Reynold's number (Re) may be defined as:

$$Re = \frac{U_0 h}{\nu} \quad (4.3)$$

In this expression, U_0 is the drum speed ($U_0 = 2\pi \times$ drum radius $\times$ frequency < 10 m s^{-1}) and ν is the kinematic viscosity ($\nu \approx 0.05$ Pa s for PEG200 at 293 K). The Reynold's number for distances h used in this study (50 – 500 μm) is therefore calculated to be < 1000, which satisfies laminar flow requirements.

Assuming the drum curvature to be negligible, the microgap can be considered as two parallel planar boundary plates, one of which is moved at a constant velocity relative to the other with fluid in between. The shear-induced flow generated by the moving

boundary plate has a linear velocity gradient perpendicular to the plates and is described as Couette flow (Figure 4.2).

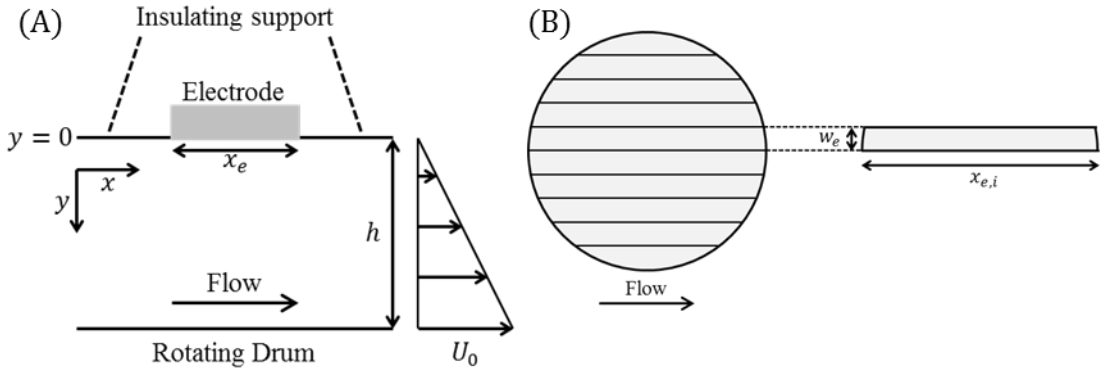

Figure 4.2. (A) 2D model simplification of the hydrodynamic microgap under Couette flow conditions. (**B**) Dividing the inlaid circular disc electrode into N number rectangular strips of equal width (w_e) and with each individual (i^{th}) rectangle having length $x_{e,i}$. The limiting current for the disc is the sum of the current for each individual rectangle.

The derivation of a Levich-type expression for Couette flow under steady state conditions follows methods employed in previous studies.[22] An electrochemical oxidation is considered to be occurring in a mass transport limited region, such that at the electrode surface ($y = 0$), all of the reduced species (R) has been converted to product (O):

$$R \rightleftharpoons O + e^- \tag{4.4}$$

To simplify the calculations, assume the electrode has a rectangular geometry with a width (w_e) going into the page and a length (x_e) going across the page so that the perpendicular distance from the electrode is down the page (y-axis) as shown in Figure 4.2A, where $y = 0$ at the electrode surface. Using these coordinates and considering the mass transport to be under steady state conditions, the mass transport equations can be expressed as:

$$U_y \frac{\partial C_i}{\partial x} = D_i \frac{\partial^2 C_i}{\partial y^2} \tag{4.5}$$

Here U_y denotes the flow velocity at a distance y from the electrode and C_i denotes the concentration of oxidative (C_O) and reductive (C_R) species undergoing the electrochemical transformation. Assuming Couette flow conditions (ie. a linear velocity

gradient in the y-axis) the mass transport equations (4.6 and 4.7) and the boundary conditions (equations 4.8-4.10) can be expressed as:

$$\frac{U_0 y}{h}\frac{\partial C_R}{\partial x} = D_R \frac{\partial^2 C_R}{\partial y^2} \tag{4.6}$$

$$\frac{U_0 y}{h}\frac{\partial C_O}{\partial x} = D_O \frac{\partial^2 C_O}{\partial y^2} \tag{4.7}$$

$$y \to \infty: C_R \to C_{R,bulk}, C_O \to 0 \tag{4.8}$$

$$y = 0:\ D_R \frac{\partial C_R}{\partial y} + D_O \frac{\partial C_O}{\partial y} = 0 \tag{4.9}$$

$$y = 0: \frac{C_R}{C_O} = \exp\left(-\frac{nF}{RT}(E - E^0)\right) = \exp(-\theta) \tag{4.10}$$

In these expressions, $\left(\frac{U_0 y}{h}\right)$ is the flow velocity at a distance y from the electrode, E^0 is the equilibrium potential for the redox couple, E is an externally applied voltage and θ denotes the dimensionless voltage, where $\theta = \frac{nF}{RT}(E - E^0)$. Equation 4.8 is satisfied given that the gap h is a few times larger than the diffusion layer thickness, $\delta_{diff} = \left(\frac{Dhx_e}{U_0}\right)^{\frac{1}{3}}$. The parameter η is introduced to simplify the calculations and is defined by equation 4.11. The variable transformation of η into equations 4.6 and 4.7 yields equations 4.12 and 4.13 respectively.

$$\eta = y\left(\frac{U_0}{xh}\right)^{\frac{1}{3}} \tag{4.11}$$

$$\frac{1}{3D_R}\eta^2 \frac{\partial C_R}{\partial \eta} + \frac{\partial^2 C_R}{\partial \eta^2} = 0 \tag{4.12}$$

$$\frac{1}{3D_O}\eta^2 \frac{\partial C_O}{\partial \eta} + \frac{\partial^2 C_O}{\partial \eta^2} = 0 \tag{4.13}$$

Equations 4.12 and 4.13 can be solved by treating them as linear first order differential equations:

$$\frac{dC_R}{d\eta} = k\exp\left(-\frac{\eta^3}{9C_R}\right) \tag{4.14}$$

$$\frac{dC_O}{d\eta} = k\exp\left(-\frac{\eta^3}{9C_R}\right) \tag{4.15}$$

In these expressions k is an unresolved constant. Suitable integration using the boundary conditions defined in 4.8 leads to equations 4.16 and 4.17.

$$\frac{C_R - C_{R(y=0)}}{C_{R,bulk} - C_{R(y=0)}} = \frac{\int_0^\eta \exp\left(-\frac{\eta^3}{9D_R}\right)d\eta}{\int_0^\infty \exp\left(-\frac{\eta^3}{9D_R}\right)d\eta} \tag{4.16}$$

$$\frac{C_O - C_{O(y=0)}}{-C_{O(y=0)}} = \frac{\int_0^\eta \exp\left(-\frac{\eta^3}{9D_O}\right)d\eta}{\int_0^\infty \exp\left(-\frac{\eta^3}{9D_O}\right)d\eta} \tag{4.17}$$

In these expressions $C_{R(y=0)}$ and $C_{O(y=0)}$ correspond to the concentration of R and O at the electrode surface. The integral in the denominator can be solved by making an appropriate variable transformation, z, where the integral of the exponential function between 0 and infinity becomes the Gamma function.

$$z = \frac{\eta^3}{9D_i} \tag{4.18}$$

$$\int_0^\infty \exp\left(-\frac{\eta^3}{9D_i}\right) d\eta = \left(\frac{D_i}{3}\right)^{\frac{1}{3}} \int_0^\infty z^{-\frac{2}{3}} \exp(-z)\, dz = \left(\frac{D_i}{3}\right)^{\frac{1}{3}} \Gamma\left(\frac{1}{3}\right) = 1.857 D_i^{\frac{1}{3}} \tag{4.19}$$

In these expressions D_i is equivalent to D_R and D_O. A Taylor series expansion of the numerators in equations 4.16 and 4.17 gives a polynomial function (4.20) where each term can be integrated individually to yield equation 4.21.

$$\int_0^\eta \exp\left(-\frac{\eta^3}{9D_i}\right) d\eta = \int_0^\eta \left[1 - \frac{\eta^3}{9D_i} + \frac{1}{2!}\left(\frac{\eta^3}{9D_i}\right)^2 - \frac{1}{3!}\left(\frac{\eta^3}{9D_i}\right)^3 + \cdots\right] d\eta \tag{4.20}$$

$$\int_0^\eta \exp\left(-\frac{\eta^3}{9D_i}\right) d\eta = \eta - \frac{\eta^4}{36D_i} + \frac{\eta^7}{1134D_i^2} - \frac{\eta^{10}}{43740D_i^3} + \cdots \approx \eta \tag{4.21}$$

If η is sufficiently small, the first term in equation 4.21 provides a good approximation to the definite integral of the numerator in equations 4.16 and 4.17. The flux at the electrode surface is therefore calculated using equations 4.22 and 4.23.

$$D_R \left(\frac{\partial C_R}{\partial y}\right)_{y=0} = 0.5384 D_R^{\frac{2}{3}} \left(\frac{U_0}{xh}\right)^{\frac{1}{3}} \left(C_{R,bulk} - C_{R,y=0}\right) \tag{4.22}$$

$$D_O \left(\frac{\partial C_O}{\partial y}\right)_{y=0} = 0.5384 D_O^{\frac{2}{3}} \left(\frac{U_0}{xh}\right)^{\frac{1}{3}} \left(-C_{O,y=0}\right) \tag{4.23}$$

Equations 4.22 and 4.23 can be substituted into equation 4.9 and simplified to give expressions for the surface concentrations, which can be subsequently substituted into equation 4.10 to give:

$$C_{R(y=0)} = C_{R,bulk} - \left(\frac{D_O}{D_R}\right)^{\frac{2}{3}} C_{O(y=0)} = \frac{C_{O(y=0)}}{\exp(\theta)} \tag{4.24}$$

$$C_{O(y=0)} = \left(\frac{D_R}{D_O}\right)^{\frac{2}{3}} \left(C_{R,bulk} - C_{R(y=0)}\right) = C_{R(y=0)} \exp(\theta) \tag{4.25}$$

Appropriate rearrangement and further substitution back into either equation 4.22 or 4.23 yields an expression for the flux at the electrode surface that is independent of surface concentrations:

$$D_R \left(\frac{\partial C_R}{\partial y}\right)_{y=0} = 0.5384 D_R^{\frac{2}{3}} \left(\frac{U_0}{xh}\right)^{\frac{1}{3}} C_{R,bulk} \frac{\exp(\theta)}{\exp(\theta) + \left(\frac{D_R}{D_O}\right)^{\frac{2}{3}}} \tag{4.26}$$

The current at a given potential can be calculated by integrating across the length (x_e) of the electrode surface, which leads to equation 4.28.

$$I = nFw_e \int_0^{x_e} D_R \left(\frac{\partial C_R}{\partial y}\right)_{y=0} dx \tag{4.27}$$

$$I = 0.8076nFw_e D_R^{\frac{2}{3}} U_0^{\frac{1}{3}} x_e^{\frac{2}{3}} h^{-\frac{1}{3}} C_{R,bulk} \frac{\exp(\theta)}{\exp(\theta)+\left(\frac{D_R}{D_O}\right)^{\frac{2}{3}}} \tag{4.28}$$

At very high oxidising potentials (i.e. large $\exp(\theta)$), the transport limiting current simplifies to equation 4.29, where the area of the rectangular electrode is $A = w_e \times x_e$ and the velocity of the wheel is $U_0 = 2\pi r_{drum} f$, where r_{drum} is the radius of the rotating drum (25 mm) and f is the frequency of rotation (in Hz).

$$I_{lim,rectangle} = 0.8076nFAC_{R,bulk} D_R^{\frac{2}{3}} \left(\frac{U_0}{hx_e}\right)^{\frac{1}{3}} \tag{4.29}$$

In this equation, n is the number of electrons transferred, F is Faraday's constant, $C_{R,bulk}$ is the bulk concentration of starting material, and h is the distance between the rotating drum and the electrode. This equation for rectangular electrodes is closely related to equation 4.2 for the channel flow case and it offers a general access to various other shapes of electrodes via a combination of thin rectangular strips. For example, the limiting current at an inlaid circular disc may be modelled by splitting the circular disc into N number of thin rectangular slices, and summing the current for each individual (i^{th}) slice (Figure 4.2B).

$$I_{lim,disc} = 0.8076nFC_{R,bulk} D_R^{\frac{2}{3}} \left(\frac{U_0}{hx_e}\right)^{\frac{1}{3}} \sum_{i=0}^{i=N} w_e x_{e,i} \tag{4.30}$$

Equation 4.30 gives a good approximation for the limiting current at a circular disc if the number of slices (N) is sufficiently high (> 500). When N is high, the corresponding Levich-type equation (4.31) for an inlaid disc electrode (with radius r_0) in the hydrodynamic microgap under Couette flow conditions can be determined.

$$I_{lim,disc} = 0.6866nFC_{R,bulk} A D_R^{\frac{2}{3}} \left(\frac{U_0}{hr_0}\right)^{\frac{1}{3}} \tag{4.31}$$

Furthermore, comparison of equations 4.29 and 4.31 allows a "magic rectangle" case to be considered where the "magic rectangle" has an equal current density to that of a circular disc of equal area. This case arises when the rectangular electrode has an electrode width to electrode length ratio ($w_e : x_e$) of 1.1863 and will result in steady-state current responses identical to those for a circular disc of equal area. This simplification was used in COMSOL® simulations.

4.2.5 Comsol® Simulation

COMSOL® is a multi-physics modelling software and is applied here to verify the Levich-type expression for hydrodynamic voltammetry under Couette flow conditions for a rectangular electrode (equation 4.29). The simplified 2-dimensional (2D) model in Figure 4.2 was coded in COMSOL® with open boundary conditions at open ends. At the moving boundary, constant sliding velocity U_0 is applied. Similarly, a zero velocity condition was used for the stationary electrode casing. Meshing of the simulation domain is based on the finite element approach (FE) to solve partial differential equations (PDEs). Couette flow is simple and the usual unstructured triangular mesh is sufficient. Fine meshing is applied at the boundaries and a structured mesh is used to resolve the fluid boundary layers (Figure 4.3).

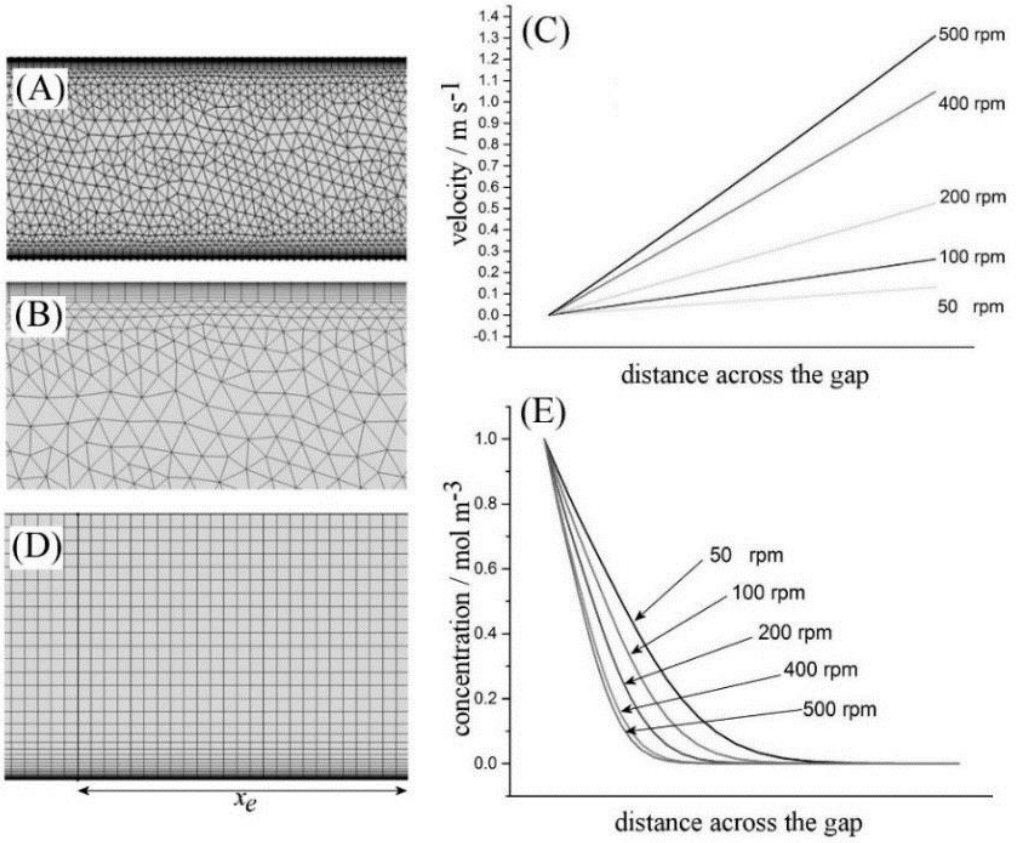

Figure 4.3. Triangular mesh used for COMSOL® computation of Couette flow. (**A**) Overall mesh structure and (**B**) enlargement of the top and bottom edges. (**C**) Velocity profiles at $h = 500$ μm and at various drum rotation rates. (**D**) Structured mesh used for mass transport calculations. Nodes are denser above the electrode surface (bottom) and sparser towards the moving bulk (top). (**E**) Concentration profile for the oxidised form of 1,1'-ferrocene dimethanol ($Fc(CH_2OH)_2$ at the trailing edge for $h = 500$ μm and various drum rotation rates.

Figure 4.3C shows that the velocity profiles for a given h and different rotating frequencies have indeed linear behaviour with respect to the dimension across the gap. The computation makes use of the Electrochemistry Module in COMSOL®, which is specifically developed for electrochemical analysis and related problems. Electrochemical phenomena can be described by the general Nernst-Planck-Poisson (NPP) equation:

$$\frac{\partial C_i}{\partial t} = \nabla.(D_i \nabla C_i) - \underline{v}.\nabla C_i + \frac{nF}{RT}\nabla.(D_i C_i \nabla E) \quad (4.32)$$

If sufficient supporting electrolyte is added to the solution, the migration flux (i.e. the third term) can be ignored, leaving only the diffusion (first) and convective (second) terms. Due to the fluid dynamics having a much shorter timescale compared to mass transport, the Couette flow field $\underline{v}$ can be solved separately and then used as an input to solve equation 4.32. A generic quadrilateral mesh is generated and used for all the mass transport computation. To completely resolve the diffusion layer, a sufficiently small element size near the electrode surface is required. The diffusion layer can be estimated using equation 4.33.

$$\delta_{diff} = \left(\frac{D.h.x_e}{U_0}\right)^{\frac{1}{3}} \approx \left(\frac{10^{-11}\times 10^{-4}\times 10^{-4}}{10}\right)^{\frac{1}{3}} \approx 10^{-7}\text{m} \quad (4.33)$$

Thus the smallest element size should be in the order of 10^{-7} m. The mesh for the mass transport computation is structured as follows. Normal to the electrode surface, an exponential mesh with smallest element size of 10^{-7} m is employed. Furthermore, the element-size growth rate is set to be 1.2, so as to allow for adequate resolution of the diffusion layer. In the direction across the surface, a regular spacing is used. The spacing is chosen such that at least 250 points cover the electrode surface and thus ensure accurate convergence of the current values. The electrochemistry at the electrode is described by the classical Butler-Volmer equation. Oxidation of 1,1'-ferrocene dimethanol ($Fc(CH_2OH)_2$) is expected to have a symmetrical transition state, hence the charge transfer constant (α) is set to 0.5 and the heterogeneous standard rate constant is set to 100 cm s^{-1} assuming reversible conditions. The Levich expression 4.29 is then verified using different combinations of gap h and drum rotation rates f (Table 4.1). The results show a good agreement (within 2 %) between the numerical and theoretical values for the limiting current. The key to accuracy in this simulation is in the meshing for the electrochemical process (Figure 4.3D) and the fact that a high current density is

expected at the leading edge of the electrode. Coarse meshing can lead to an underestimation of the total current.

Table 4.1. Comparison between the COMSOL® simulated limiting current and the Levich-type equation 4.29.

Gap h / μm	Rotation rate f / rpm	Rotation rate / s^{-1}	$I_{simulated}/ I_{Levich}$
50	50	0.833	1.019
50	500	83.3	0.999
500	50	0.833	1.020
500	500	83.3	1.002

To verify the extent of the diffusion layer thickness under the conditions employed here, the concentration profile of the oxidised form of 1,1'-ferrocene dimethanol ($Fc(CH_2OH)_2$) versus distance across the gap (at the trailing edge) has been plotted for different rotation rates (Figure 4.3E).

4.3 Results and discussion

4.3.1 Hydrodynamic microgap voltammetry: $Fe(CN)_6^{3-/4-}$ in aqueous electrolyte

In order to verify the theory based on Couette flow, the hydrodynamic microgap system was tested with 5 mM potassium ferricyanide ($K_3Fe(CN)_6$) as the redox species in an aqueous solution with 1 M KNO_3 as electrolyte (equation 4.34).

$$Fe(CN)_6^{3-} + e^- \rightleftharpoons Fe(CN)_6^{4-} \quad (4.34)$$

The distance, h, between the 250 μm diameter Pt disc working electrode and the rotating drum was initially fixed at 50 μm, whilst the rotation frequency was varied. Cyclic voltammetry measurements were taken using rotation frequencies between 50 and 400 revolutions per minute (rpm). In Figure 4.4A it is shown that limiting currents increased by more than one order of magnitude compared to those recorded in a static solution. Figure 4.4B shows that the limiting reduction current is proportional to the cube root of

the rotation frequency of the rotating drum, which is consistent with equation 4.31. The dotted line shows the theoretical values for a literature diffusion coefficient of $D = 0.65 \times 10^{-9}$ m^2 s^{-1}.[23]

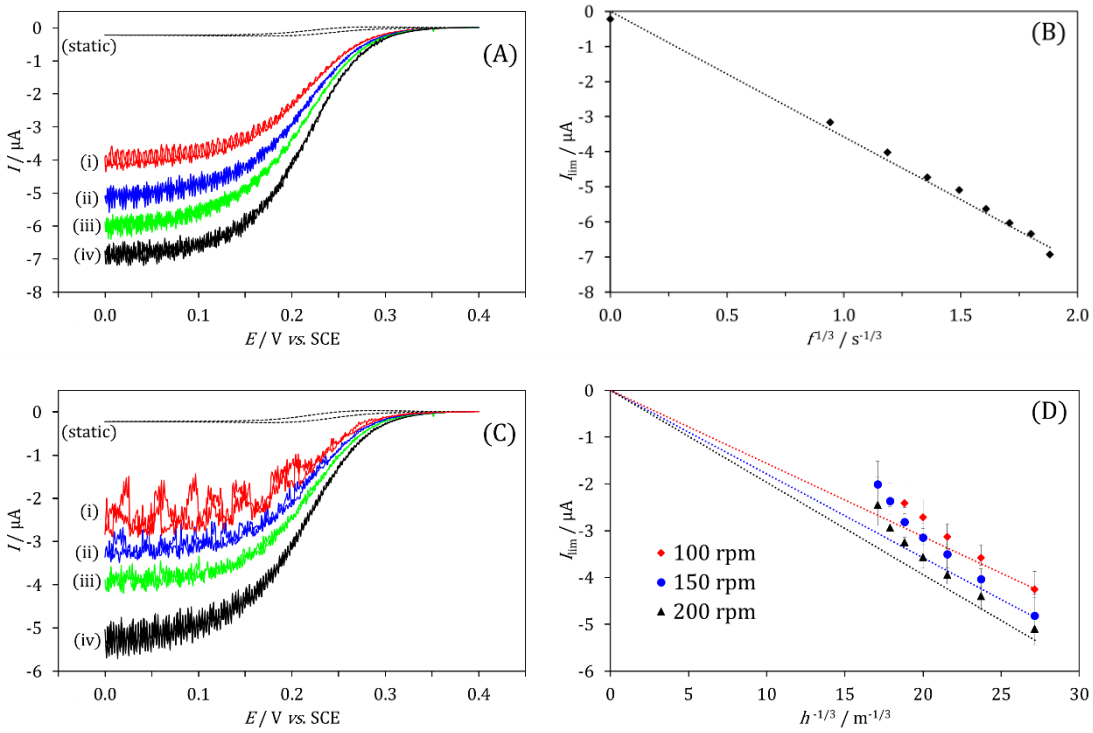

Figure 4.4. (**A**) Cyclic voltammograms (scan rate 10 mV s^{-1}, 250 μm diameter platinum disc, 50 μm microgap) for reduction of 5 mM $K_3Fe(CN)_6$ in 1 M KNO_3 in static solution (dotted) and with a rotation frequency of (i) 100, (ii) 200, (iii) 300, and (iv) 400 rpm. (**B**) Plot of the limiting current for experimental results versus cube root of the rotation frequency in Hz. The dotted line indicates calculated limiting currents based on equation 4.31 (with $D = 0.65 \times 10^{-9}$ m^2 s^{-1}). (**C**) Cyclic voltammograms (scan rate 10 mV s^{-1}, 50 rpm) for reduction of 5 mM $K_3Fe(CN)_6$ in 1 M KNO_3 with (i) 50, (ii) 100, (iii) 150, and (iv) 200 μm gap between the electrode and the rotating drum. (**D**) Plot of the limiting current at 100 rpm, 150 rpm, and 200 rpm versus the reciprocal cube root of the distance with dotted lines indicating calculated limiting currents based on equation 4.31.

Next the effect of the size of the micrgap, h, was investigated using the same 5 mM $K_3Fe(CN)_6$ redox system. Figure 4.4C shows that the voltammetric response became more "noisy" as the size of the microgap increased. This is indicative of a loss of laminar flow conditions at wider gap distances for the aqueous solution of relatively low viscosity. The plot in Figure 4.4D confirms a deviation from linearity at larger microgap distances for all three rotation rates. However, the overall agreement between theory and experiment are excellent and measurements in the more viscous

poly(ethylene glycol) with average molecular weight 200 g mol^{-1} (PEG200) are possible.

4.3.2 Hydrodynamic microgap voltammetry: 1,1'-ferrocene dimethanol in poly(ethylene glycol) electrolyte

Having determined the diffusion coefficient of 1,1'-ferrocene dimethanol ($Fc(CH_2OH)_2$) in PEG200 in Chapter 3, the same system was investigated under hydrodynamic Couette flow conditions using a 250 μm diameter platinum disc working electrode. The microgap was first fixed at 500 μm, whilst the rotation frequency of the drum was varied between 50 rpm and 500 rpm. Cyclic voltammograms for the oxidation of 1 mM 1,1'-ferrocene dimethanol under hydrodynamic Couette flow conditions show steady-state characteristics (Figure 4.5A) and a limiting current typically 50 times larger than those observed under static conditions. A comparison to COMSOL® simulations and to the limiting current predicted by equation 4.31 shows good agreement. There is some evidence for some irreversibility in the electron transfer. The possible reason for this is discussed in more detail below.

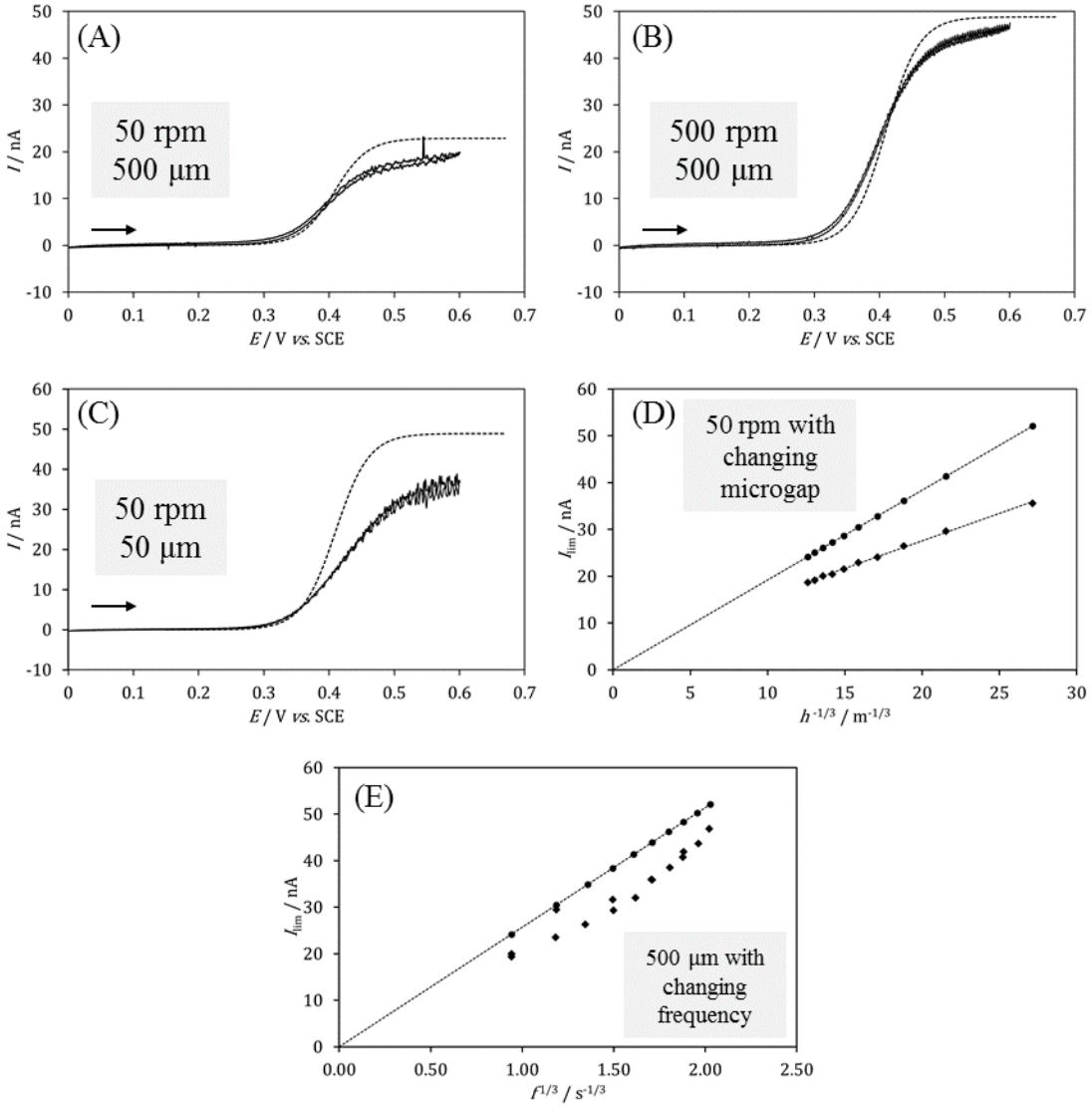

Figure 4.5. Cyclic voltammograms (scan rate 10 mV s^{-1}) comparing experiment (red) and COMSOL® simulation (blue) for the oxidation of 1 mM 1,1'-ferrocene dimethanol in PEG200 with 20 mM $LiClO_4$ at a 250 µm diameter Pt disc electrode under rotating drum conditions: (**A**) 500 µm gap, 50 rpm, (**B**) 500 µm gap, 500 rpm, and (**C**) 50 µm gap, 50 rpm. (**D**) Plot of limiting currents versus $h^{-\frac{1}{3}}$ at 50 rpm. (**E**) Plot of limiting currents versus $f^{\frac{1}{3}}$ at a 500 µm gap.

A plot of the limiting current as a function of the reciprocal cube root of microgap distance h (Figure 4.5D) shows that a mismatch between theoretical and experimental limiting current is observed when going to small gaps (higher shear conditions). Data in Figure 4.5B and 4.5C also show that the apparent irreversibility in the electron transfer to 1,1'-ferrocene dimethanol is more obvious for smaller microgaps and for higher rotation frequency. The frequency dependency (Figure 4.5E) shows a relatively good agreement between experiment and theory, although all data points from

experiment are below those predicted by theory. Given the accurate determination of the diffusion coefficient this is unlikely to be the cause for the deviation. A log-plot analysis (Figure 4.6) can be used to help explain the deviation between experiment and theory for the oxidation of 1,1'-ferrocene dimethanol in PEG200. The simulation data shows a linear slope of 58 mV ($= \frac{RT}{nF} \times 2.303$), which is consistent with fully reversible electron transfer. However, the log-plot for 1,1'-ferrocene dimethanol is split into two regions. Below +0.45 V (*vs.* SCE) a slope value of 80 mV is indicative of a transition to irreversible electron transfer. Above +0.45 V (*vs.* SCE) the slope changes to 176 mV, which cannot be reconciled with slow electron transfer. It is proposed that the underlying interaction between the PEG200 solvent and the platinum surface changes (Figure 4.6) to cause an additional impedance, which leads to a deviation from the expected theoretical limiting current. This is consistent with reports of the adsorption of poly(ethylene glycol) on platinum in acidic solutions.[24] A similar transition in mechanism is present in all experimental datasets and therefore likely to be associated with the partitioning of the 1,1'-ferrocene dimethanol molecule into the surface PEG200 layer. This effect is most pronounced under high mass transport conditions, either for small microgap or for high rotation frequencies.

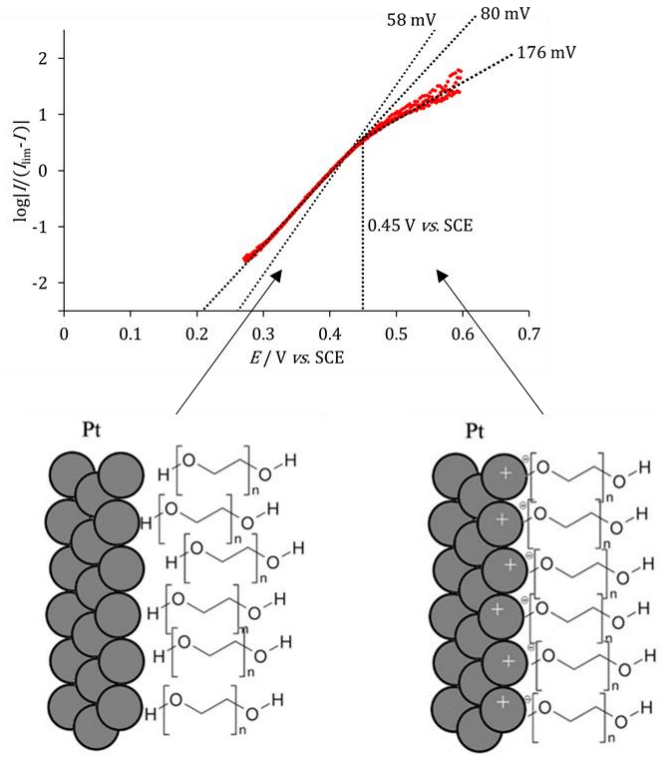

Figure 4.6. (**A**) Log-plot for data in Figure 4.5B indicating a switch in mechanism at +0.45 V (*vs.* SCE). (**B**) Schematic drawings of the proposed chemical changes at the Pt-PEG200 interface.

4.4 Conclusions

A hydrodynamic technique has been developed suitable for highly viscous media to increase the mass transport to the electrode, and hence increase the measured currents. The design is based upon a rotating drum and a piezo-controlled electrode position system, which generates a Couette flow regime at the electrode surface. A Levich-type expression was derived for a rectangular electrode, which was subsequently adapted for a disc electrode geometry, and provided a quantitative model for the hydrodynamic system. The Levich-type expression was found to be independent upon the viscosity of the solution and was consistent with COMSOL® simulations. Both theoretical approaches are fully consistent and verified with a $Fe(CN)_6^{3-/4-}$ redox system in aqueous electrolyte.

The same hydrodynamic microgap system was used to investigate the oxidation of 1,1'-ferrocene dimethanol in the more viscous PEG200. Significant current enhancements were observed in the viscous solvent compared to static conditions. The Levich-type equation and COMSOL® models were generally in agreement with experimental results. However, a deviation between simulation and experiment was observed above +0.45 V (*vs.* SCE), which becomes apparent from analysis of a log-plot. It is proposed that a change in conditions at the platinum-PEG200 electrolyte interface is responsible. Interactions between poly(ethylene glycol) derivatives and carbon electrode surfaces will be discussed in greater detail in Chapters 5 and 6.

Hydrodynamic microgap voltammetry under Couette flow conditions could be a useful tool for enhancing currents in solutions, in particular for highly viscous media such as ionic liquids and other polymer solvents. The technique could have applications in bulk electrolysis (or organic electrosynthesis) reactions, where the turnover could be enhanced by improved mass transport. Analytical systems for probing reaction mechanisms could also be developed using a double band electrode, which would be analogous to voltammetry at a rotating ring disc electrode. The development of a hydrodynamic nanogap system could also be of interest, however, this would require improved precision in the rotation mechanism.

4.5 References

1. C. E. Banks, A. O. Simm, R. Bowler, K. Dawes and R. G. Compton, *Analytical Chemistry*, 2005, **77**, 1928-1930.
2. N. V. Rees and R. G. Compton, *Russian Journal of Electrochemistry*, 2008, **44**, 368-389.
3. J. C. Ball, R. G. Compton and C. M. A. Brett, *Journal of Physical Chemistry B*, 1998, **102**, 162-166.
4. J. V. Macpherson, N. Simjee and P. R. Unwin, *Electrochimica Acta*, 2001, **47**, 29-45.
5. J. A. Cooper and R. G. Compton, *Electroanalysis*, 1998, **10**, 141-155.
6. C. Amatore, N. Da Mota, C. Lemmer, C. Pebay, C. Sella and L. Thouin, *Analytical Chemistry*, 2008, **80**, 9483-9490.
7. C. Amatore, N. Da Mota, C. Sella and L. Thouin, *Analytical Chemistry*, 2007, **79**, 8502-8510.
8. J. Booth, R. G. Compton, J. A. Cooper, R. A. W. Dryfe, A. C. Fisher, C. L. Davies and M. K. Walters, *Journal of Physical Chemistry*, 1995, **99**, 10942-10947.
9. R. G. Compton, J. C. Eklund and F. Marken, *Electroanalysis*, 1997, **9**, 509-522.
10. I. J. Cutress, F. Marken and R. G. Compton, *Electroanalysis*, 2009, **21**, 113-123.
11. H. M. Villullas and M. L. Teijelo, *Journal of Electroanalytical Chemistry*, 1995, **384**, 25-30.
12. H. M. Villullas and M. L. Teijelo, *Journal of Electroanalytical Chemistry*, 1995, **385**, 39-44.
13. S. D. Ahn, P. E. Frith, A. C. Fisher, A. M. Bond and F. Marken, *Journal of Electroanalytical Chemistry*, 2014, **722**, 78-82.
14. I. Streeter and R. G. Compton, *Physical Chemistry Chemical Physics*, 2007, **9**, 862-870.
15. C. M. A. Brett and A. M. O. Brett, *Electrochemistry : principles, methods, and applications*, Oxford University Press, Oxford, 1993.
16. L. Challier, R. Miranda-Castro, D. Marchal, V. Noel, F. Mavre and B. Limoges, *Journal of the American Chemical Society*, 2013, **135**, 14215-14228.
17. J. Legrand, E. Dumont, J. Comiti and F. Fayolle, *Electrochimica Acta*, 2000, **45**, 1791-1803.
18. D. L. Boxall, J. J. O'Dea and R. A. Osteryoung, *Journal of the Electrochemical Society*, 2002, **149**, E468-E471.
19. V. G. Levich, *Physicochemical hydrodynamics*, Prentice-Hall, 1962.
20. R. G. Compton, E. Laborda and K. R. Ward, *Understanding Voltammetry: Simulation of Electrode Processes*, Imperial College Press, 2013.
21. C. Combellas, M. Fermigier, A. Fuchs and F. Kanoufi, *Analytical Chemistry*, 2005, **77**, 7966-7975.
22. W. J. Blaedel and L. N. Klatt, *Analytical Chemistry*, 1966, **38**, 879-&.
23. R. N. Adams, *Electrochemistry at solid electrodes*, Marcel Dekker, 1969.
24. T. Y. Safonova, N. V. Smirnova and O. A. Petrii, *Russian Journal of Electrochemistry*, 2006, **42**, 995-1000.

Chapter 5: Modification of carbon electrodes using poly(ethylene glycol)

Chapter abstract

"Amplified" electron transfer is observed purely based on electron transfer kinetic effects at modified carbon surfaces. This study describes a one-step, anodic electrochemical grafting method for the attachment of poly(ethylene glycol) directly to glassy carbon and boron doped diamond electrodes. Successful grafting was confirmed by XPS. The grafting conditions were optimised as a function of potential and time, and effects of chain length were investigated. Cyclic voltammetry and electrochemical impedance spectroscopy measurements indicate a severe decrease in the apparent rate of heterogeneous electron transfer for the $Fe(CN)_6^{3-/4-}$ redox couple at a PEG-modified carbon electrode. The tunnel distance coefficient (β) was found to be 0.17 $Å^{-1}$, which is suggestive of a diffuse PEG-water interface. The voltammetric response for the more hydrophobic 1,1'-ferrocene dimethanol redox species is not significantly affected at a PEG-modified carbon electrode. It is demonstrated that a low concentration of 1,1'-ferrocene dimethanol can mediate the oxidation and reduction for $Fe(CN)_6^{3-/4-}$ at a PEG-modified carbon electrode, which results in amplified currents for low mediator concentrations. The estimated apparent rate constants for the bimolecular reaction are: $k_{oxidation} = 6 \times 10^5$ mol^{-1} dm^3 s^{-1} and $k_{reduction} = 1 \times 10^5$ mol^{-1} dm^3 s^{-1}. This type of seemingly selective electron transfer and subsequent "amplification" could have future applications in electroanalytical devices.

Chapter publications

This chapter has been published in:
C. E. Hotchen, I. J. Maybury, G. W. Nelson, J. S. Foord, P. Holdway and F. Marken, *Phys. Chem. Chem. Phys.*, 2015, **17**, 11260-11268.

Special acknowledgements

I would like to thank Ian Maybury for his laboratory work as a summer project student. I would also like to thank Geoffrey Nelson for his expertise in XPS analysis and Begbroke Science Park for allowing use of their equipment.

Chapter contents

5 Modification of carbon electrodes using poly(ethylene glycol)

5.1 Introduction

Poly(ethylene glycol) derivatives have many applications from low-volatility additives,[1, 2] in carbon dioxide capture[3] and in cosmetic products.[4, 5] They are also reported to exhibit good anti-biofouling properties, which could prevent non-specific protein adsorption[6-8] and cell adhesion.[9] It is therefore of interest to investigate methods to bind poly(ethylene glycol) derivatives to surfaces.

The modification of surfaces has been widely studied and many methods have been developed to graft organic molecules to electrodes.[10] Self-assembled monolayers (SAMs) of thiols are known to form spontaneously on gold, but the monolayers are thermally unstable, prone to oxidation in air, and desorb in some organic solvents, such as THF.[11, 12] The reduction of diazonium salts on carbon electrodes can form stronger bonds and lead to stable surface modifications.[13, 14] The attachment of alcohols directly to carbon surfaces has also been performed using chemical methods. Wen et al. used a multistep procedure taking several days to modify multi-walled carbon nanotubes (MWCNTs) with poly(ethylene glycol) with an average molecular weight of 4000 g mol^{-1}. The MWCNTs were first treated in nitric acid, which added carboxylic acid functionality to the surface, followed by a functional group conversion to a reactive acid chloride. The acid chloride could then react directly with poly(ethylene glycol) chains. Haemoglobin, a redox active protein, was subsequently immobilised on the PEG-modified MWCNT surface.[15]

An electrochemical grafting approach was introduced by Barbier and Pinson.[16] They used anodic potentials to bind primary amines, such as ethylene diamine, to carbon fibre electrodes[16]. Similar electrochemical methods have been used to graft diazonium cations, arylacetates and alcohols to carbon surfaces.[10, 14] Maeda et al. were the first to report the anodic electrochemical grafting of aliphatic primary alcohols to glassy carbon electrodes.[17] They proposed a mechanism where the carbon electrode generates carbocations on the surface, which undergo nucleophilic attack from alcohols in solution to form ether linkages.[17] The properties of the resulting films, such as

hydrophobicity, closely matched the starting alcohol.[18] The films showed a suppression for the voltammetric response for the $Fe(CN)_6^{3-/4-}$ redox couple, which was attributed to the hydrophobic nature of the grafted films for 1-alkanols.[19] The voltammetric signal could be restored by the addition of a suitable surfactant, such as trimethyldodecyl ammonium bromide.[17] A similar suppression of the voltammetric signal for $Fe(CN)_6^{3-/4-}$ was observed when anodisation was performed in water, however, the signal was not restored with the addition of surfactant.[19] It is thought that the carbon surface oxidised in aqueous solution is covered by anionic functional groups, such as carboxylates, which leads to an electrostatic repulsion towards the $Fe(CN)_6^{3-/4-}$ species and hence gives a depressed voltammetric response.[19] Similar electrostatic repulsions are observed when diols are used as surface modifiers, where the grafting of 1,5-pentanediol completely suppressed the voltammetric signal for ascorbic acid (anionic) but did not affect the voltammetric response for dopamine (neutral).[20, 21] The authors propose that treatment in diols causes anodic oxidation of the terminal hydroxyl group to form a carboxylate.[20]

The electrochemical anodisation of glassy carbon electrodes in oligo(ethylene glycol)s resulted in modified electrodes that were resistant to protein adsorption, whilst maintaining good electrochemical performance.[22, 23] The electrodes were used in high performance liquid chromatography (HPLC) analysis for the detection of acetaminophen in urine samples without the need to remove proteins.[24] The direct anodic modification could also lead to more elaborate surface functionality. For example, a tri(ethylene glycol)-modified glassy carbon electrode was subsequently reacted with the 2,2,6,6-tetramethylpiperidinyl-1-oxyl (TEMPO) radical.[25] The TEMPO-modified surface maintained the catalytic properties of the TEMPO species towards the oxidation of allyl alcohol in the presence of base.[25]

This study aims to follow the procedure developed by Maeda et al. to graft poly(ethylene glycol) to glassy carbon and boron-doped diamond surfaces. The modification is optimised as a function of grafting potential and the effects on the apparent rate of heterogeneous electron transfer for hydrophilic ($Fe(CN)_6^{3-/4-}$) and hydrophobic (1,1'-ferrocene dimethanol) redox systems are investigated. The results imply a highly diffuse poly(ethylene glycol)-water boundary and a high degree of selectivity in the electron transfer process between redox species. A signal

‘amplification’ effect is observed for combined redox systems, where a trace amount of redox mediator shows a high current response due to bimolecular reaction with the second redox system in solution.

5.2 Experimental

5.2.1 Chemical reagents

Poly(ethylene glycol)s with average molecular weight 200 g mol^{-1} (PEG200), 300 g mol^{-1} (PEG300) and 400 g mol^{-1} (PEG400) were obtained from Aldrich and used as the solvent for grafting solutions with lithium perchlorate ($LiClO_4$, Sigma-Aldrich, ≥95.0 %) as electrolyte. Potassium ferricyanide ($K_3Fe(CN)_6$, Sigma-Aldrich, 99 %), potassium ferrocyanide ($K_4Fe(CN)_6$, Fison Scientific, ≥95.0 %), and 1,1’-ferrocene dimethanol ($Fc(CH_2OH)_2$, Aldrich, 98 %) were used as redox probes for voltammetry with potassium nitrate (KNO_3, Sigma-Aldrich, ≥99.0 %) as electrolyte.

5.2.2 Instrumentation

Electrochemical measurements were performed using an Autolab PGSTAT12 potentiostat (Autolab, Utrecht, NL) with platinum wire counter electrode and KCl-saturated calomel reference electrode (SCE) at room temperature (20 ±2 °C). Working electrodes were either a 3 mm diameter glassy carbon (BAS Analytical UK) or a 3 mm diameter bulk-boron-doped diamond (polished to a mirror finish, Diafilm™, Windsor Scientific, UK). The General Purpose Electrochemical Software (GPES) package (version 4.9005, Autolab, Utrecht, NL) was employed for data acquisition with a potential step parameter not higher than 1 mV. Electrochemical impedance spectroscopy (EIS) measurements were performed using a Solartron 1286 potentiostat and 1250 frequency response analyser over a frequency range of 10 kHz to 0.1 Hz with an amplitude of 10 mV. Field emission scanning electron microscopy (FESEM) images were taken using a Jeol 6301F FESEM microscope.

XPS experiments were conducted using a Thermo K Alpha (Thermo Scientific) spectrometer (operating at $\approx 10^{-8} - 10^{-9}$ Torr), a 180° double focussing hemispherical analyser running in constant analyser energy (CAE) mode with a 128-channel detector. A mono-chromated Al Kα radiation source (1486.7 eV) was used. Peak fitting was conducted using XPS Peak Fit (version 4.1) software using Shirley background subtraction. Peaks were referenced to the adventitious carbon C1s peak (284.6 eV) and peak areas were normalised to the photoelectron cross-section of the F1s photoelectron signal using atomic sensitivity factors.[26]

5.2.3 Procedure for anodising carbon electrodes

The method developed by Maeda for grafting 1-alkanols to electrodes was adapted to attach poly(ethylene glycol) to carbon electrodes.[19] The working electrode – either a 3 mm diameter glassy carbon (GC) disc or a 3 mm diameter boron doped diamond (BDD) disc – was polished with wet alumina paste with particle diameter 0.3 μm followed by rinsing with de-ionised water (18.2 MΩ cm^2). Cyclic voltammetry of a solution containing 5 mM $K_3Fe(CN)_6$ and 5 mM $K_4Fe(CN)_6$ in aqueous 0.1 M KNO_3 was performed on the polished electrode in order to confirm that any effects from previous experiments had successfully been removed. The electrode was immersed in a neat poly(ethylene glycol) solution (containing 20 mM $LiClO_4$ as electrolyte) and subjected to a fixed anodic potential for a fixed time. The applied attachment potential and the treatment time needed to be optimised. After the anodic treatment, the working electrode was rinsed with de-ionised water, to remove residual PEG from the electrode surface, and dried using nitrogen. The properties of the electrode after anodisation were investigated using cyclic voltammetry, electrochemical impedance spectroscopy (EIS) and X-ray photoelectron spectroscopy (XPS). The effects of anodisation could be removed by either mechanical polishing or by scanning the potential to +1.5 V (*vs.* SCE) in aqueous 0.1 M KNO_3 solution.

5.3 Results and discussion

5.3.1 Evidence for attachment of poly(ethylene glycol) on carbon electrodes: XPS analysis

X-ray photoelectron spectroscopy (XPS) was used to probe the changes in surface composition after the anodic treatment of boron doped diamond (BDD) and glassy carbon (GC) samples in poly(ethylene glycol) with average molecular weights 200 g mol^{-1} and 400 g mol^{-1} (PEG200 and PEG400 respectively). The anodisation treatment followed the procedure outlined above with an anodisation potential of +1.2 V (*vs.* SCE) held for 20 min.

Survey spectra of BDD (and GC) substrates show photoelectron signals from nearly contaminant free surfaces containing primarily C and O (Figure 5.1). The Al2s and Al2p peaks are likely to arise due to residues from the alumina powder used to polish the carbon surfaces. These peaks are attenuated after the anodic treatment in polyethylene glycol (PEG), which is consistent with the attachment of PEG over-layers to the initial BDD or GC substrate.

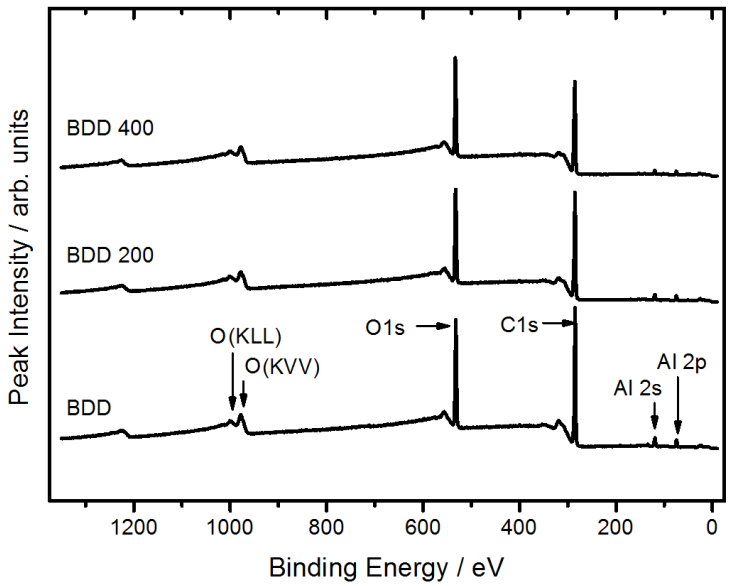

Figure 5.1. Representative XPS survey spectra of (i) a bare boron doped diamond surface (BDD), (ii) a BDD surface after anodisation in PEG200 (BDD 200) and (iii) a BDD surface after anodisation in PEG400 (BDD 400).

The C1s photoelectron signal shows evidence of systematic changes in surface chemistry consistent with PEG attachment (Figure 5.2A). The C1s signal was fitted into five chemical environments as described by Ferro et al.: adventitious carbon (C-C, 284.6 eV), hydrocarbon (C-H, ≈ 285.1 eV), ether (C-O, ≈ 286.1 eV), carbonyl (C=O, ≈ 287.1 eV) and carboxyl (C=O(OH), ≈ 288.1 eV).[27] Notably, as either BDD or GC is treated in PEG, the intensity of the ether component increases in proportion to the PEG chain length (cf. Figure 5.2 and Table 5.1) This result is consistent with the sequential addition of poly(ethylene glycol) moieties to the surface.

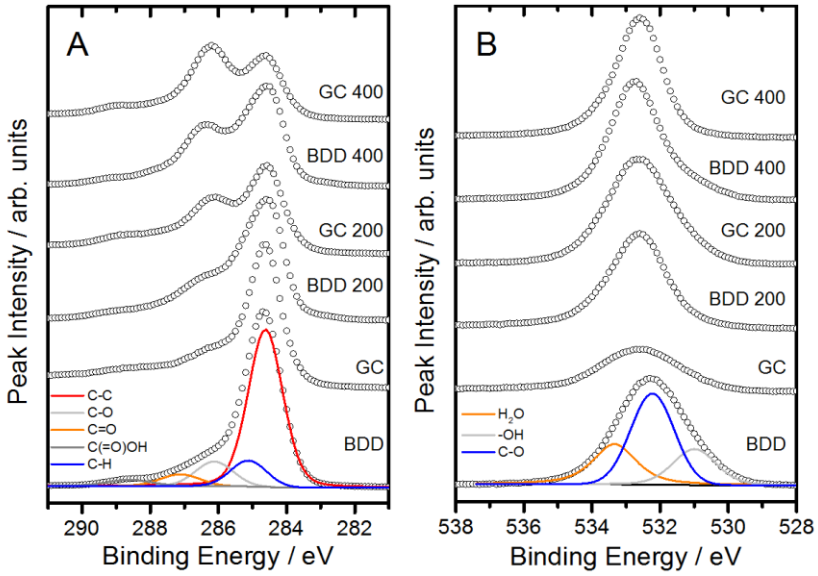

Figure 5.2. Data for C1s (left) and O1s (right) XPS core level spectra of BDD, GC, and PEG-modified BDD and GC, with representative curve fits associated with unmodified BDD shown.

The O1s photoelectron signal (Figure 5.2B) was curve fitted using the model established by Schlapak *et al.* as follows: hydroxyl (-OH, ≈ 531 eV), ether (C-O, ≈ 532.2 eV), water (H_2O, ≈ 533.3 eV).[28] After treatment in PEG, the percentage of ether component in the O1s signal increases in proportion to chain length, whilst the percentage of hydroxyl (-OH) and H_2O decreases. The increase in ether component is consistent with PEG attaching to the surface of the carbon electrode during anodisation. The XPS data suggests that poly(ethylene glycol) covalently binds to both glassy carbon and boron doped diamond surfaces upon anodisation. The anodisation potential can therefore be considered as an *attachment* potential. More quantitative coverage information is difficult to extract from these XPS data, but can be obtained in electrochemical experiments.

Table 5.1. Summary of XPS data for bare and modified samples in terms of ratios and composition.

		% O1s signal			% C1s signal				
Sample	**O1s/C1s**	**OH**	**C-O**	**H_2O**	**C-C**	**C-H**	**C-O**	**C=O**	**C=O(OH)**
BDD	2.58	50	21	29	70	11	11	5	3
BDD200	2.72	18	63	19	51	14	18	13	4
BDD400	2.75	22	66	12	43	16	33	5	3
GC	1.29	12	55	33	66	4	11	11	8
GC200	2.61	9	70	21	46	6	26	10	12
GC400	2.99	2	81	17	28	14	37	14	7

5.3.2 Poly(ethylene glycol) modified carbon electrodes: effects on $Fe(CN)_6^{3-/4-}$ electron transfer

The one electron $Fe(CN)_6^{3-/4-}$ redox couple is often used to detect surface modifications on carbon electrodes and was employed here to probe the changes in electrode behaviour after anodisation.[29, 30]

$$Fe(CN)_{6\ (aq)}^{4-} \rightleftharpoons Fe(CN)_{6\ (aq)}^{3-} + e^- \qquad (5.1)$$

Figure 5.3 shows a typical cyclic voltammogram for the $Fe(CN)_6^{3-/4-}$ redox couple in aqueous 0.1 M KNO_3 at a glassy carbon disc electrode. At 50 mV s^{-1} the voltammetric response appears quasi-reversible with a peak separation (ΔE_p) of 140 mV and a reversible potential (E_0) of +0.19 V (*vs.* SCE). A plot of the peak current (I_p) against the square root of the scan rate ($\sqrt{v}$) followed by analysis using the Randles-Ševčík equation (equation 5.2) allows the diffusion coefficient for the ferrocyanide species to be determined as $D_{ferrocyanide} = 0.6 \times 10^{-5}$ cm^2 s^{-1}, which is consistent with literature values.[31]

$$I_p = 0.466nFAc\sqrt{\frac{nFvD}{RT}} \qquad (5.2)$$

In this expression *n* is the stoichiometric number of electrons transferred, *F* is Faraday's constant, *A* is the electrode area, *c* is the bulk concentration of ferrocyanide, *R* is the universal gas constant (8.314 J K^{-1} mol^{-1}) and *T* is the absolute temperature (in K).

After the anodic treatment of the electrode in PEG400 (with 20 mM $LiClO_4$ electrolyte) the peak separation increased, which is indicative of a decrease in the rate of interfacial electron transfer. Increasing either the treatment time or the anodisation potential systematically increased the peak separation in the cyclic voltammograms (Figure 5.3). Figure 5.3B shows that the redox signal for the $Fe(CN)_6^{3-/4-}$ couple was completely suppressed in the 1 V potential window investigated after an anodic treatment of +1.6 V for 20 minutes in PEG400. These effects were observed at both glassy carbon and boron doped diamond electrodes. It is proposed that the anodic treatment of the electrodes in a PEG solution causes oxidative coupling between the polymer and the carbon substrate to form a PEG layer on the surface of the electrode, which is consistent with reports by Maeda[18].

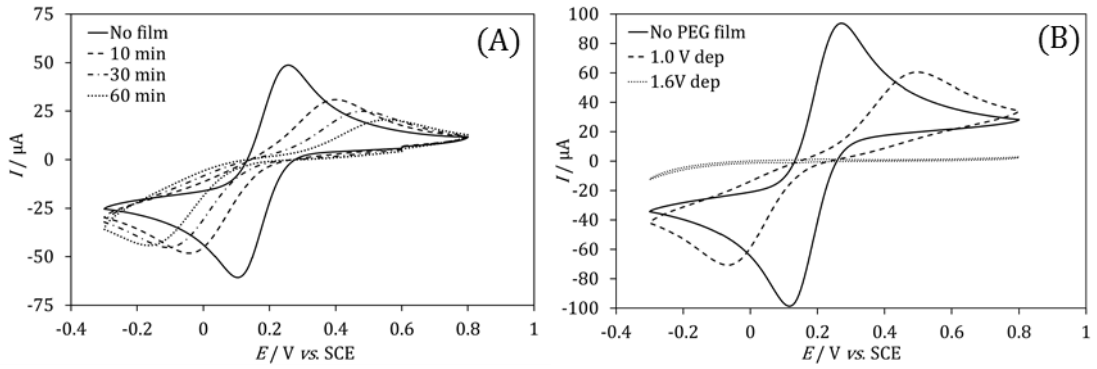

Figure 5.3. (**A**) Cyclic voltammograms (scan rate 50 mV s^{-1}, second cycle shown) for a solution containing 5 mM $K_3Fe(CN)_6$, 5 mM $K_4Fe(CN)_6$ and 0.1 M KNO_3 at a 3 mm diameter glassy carbon working electrode before PEG400 attachment (i), after 10 min (ii), after 30 min (iii), and after 60 min (iv) at +1.2 V (*vs.* SCE). (**B**) As above, but with no PEG film (i) and a PEG400 film attached by anodic treatment for 20 min at (ii) +1.0 V and (iii) +1.6 V (*vs.* SCE).

The standard heterogeneous rate constant for electron transfer (k_0) is a parameter used to measure the rate of electron transfer across an electrode-solution interface. The value of k_0 can be qualitatively observed using cyclic voltammetry but more quantitatively measured using electrochemical impedance spectroscopy (EIS). The effect of the anodic treatment in PEG400 on k_0 was investigated at both glassy carbon (GC) and boron doped diamond (BDD) electrodes. EIS measurements were performed in an aqueous solution containing 5 mM $Fe(CN)_6^{4-}$, 5 mM $Fe(CN)_6^{3-}$ and 0.1 M KNO_3 at open circuit potential (OCP). Nyquist (not shown) and Bode plots show systematic changes as a function of anodisation potential (Figure 5.4). Equivalent circuit data

fitting based upon a simple Randles circuit (Figure 5.4) was used to determine the charge transfer resistance (R_{ct}), which could subsequently be used to calculate the apparent standard rate constant for heterogeneous electron transfer (k_0) for the $Fe(CN)_6^{3-/4-}$ redox couple using equation 5.3.

$$k_0 = \frac{RT}{n^2F^2AcR_{ct}} \tag{5.3}$$

In this expression, R is the universal gas constant (8.314 J K^{-1} mol^{-1}), T is the absolute temperature (in K), n is the stoichiometric number of electrons transferred, F is Faraday's constant, A is the geometric electrode area, and c is the bulk concentration for the case that $c = c_{Fe(CN)_6^{3-}} = c_{Fe(CN)_6^{4-}}$.

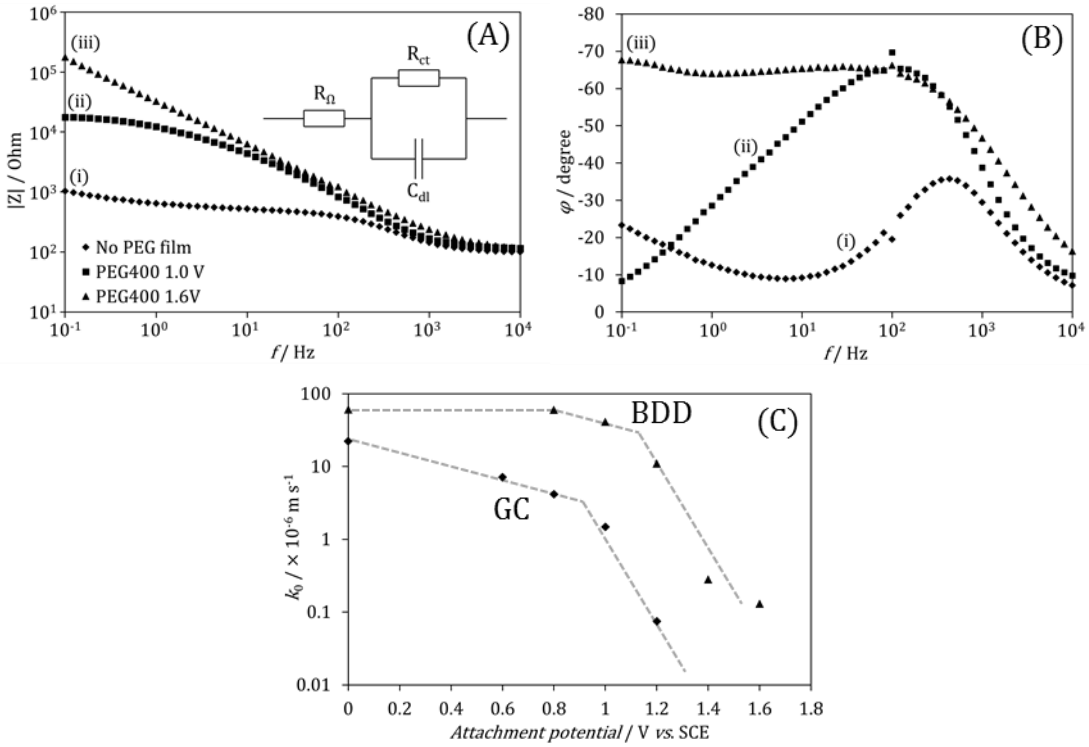

Figure 5.4. (**A, B**) Bode impedance plots for an aqueous solution containing 5 mM $K_4Fe(CN)_6$, 5 mM $K_3Fe(CN)_6$ and 0.1 M KNO_3 at a 3 mm diameter glassy carbon working electrode recorded at OCP (i) without anodic treatment, (ii) anodisation at +1.0 V (*vs.* SCE) for 20 min, and (iii) anodisation at +1.6 V (*vs.* SCE) for 20 min. (**C**) Plot of the apparent standard rate constant for heterogeneous electron transfer as a function of anodisation potential for a glassy carbon (♦) and for a boron doped diamond (▲) electrode. Line provided to aid the eye.

As the attachment potential increased (for a fixed treatment time), the charge transfer resistance (R_{ct}) for the $Fe(CN)_6^{3-/4-}$ redox couple also increased, which indicates a decrease in the apparent rate of electron transfer. The solution resistance (R_Ω) was ~114 Ω in all expeirments and the double layer capacitance (C_{dl}) was ~1.7 μF and

~2.4 μF on glassy carbon and boron doped diamond respectively. R_Ω and C_{dl} were independent of PEG attachment potential and therefore insensitive to the coverage of PEG on the electrode. Poly(ethylene glycol)s and water are known to be highly miscible. It is proposed that the PEG layer formed from the anodic treatment is miscible with aqueous solution, which rationalises the insignificant change in double layer capacitance of the electrode after anodisation. Higher deposition potentials lead to faster rates of oxidative coupling, which appears to result in a more dense PEG film with improved surface coverage. For glassy carbon, an attachment potential of +1.4 V and +1.6 V (*vs.* SCE) gave highly passivating films, with R_{ct} values too low to be quantified accurately under these conditions.

Field emission scanning electron microscopy (FESEM) was used to observe the passivating PEG film on a BDD electrode. The PEG film is very thin and cannot be seen directly by FESEM. Figure 5.5 shows the polycrystalline domains typically observed for a boron doped diamond surface. There are no significant morphology changes after the anodic treatment; however, due to the insulating nature of the PEG layer, modified regions of the electrode appear darker compared to untreated regions. This is most apparent in a low magnification image (Figure 5.5C) comparing a treated region with an untreated region of the electrode.

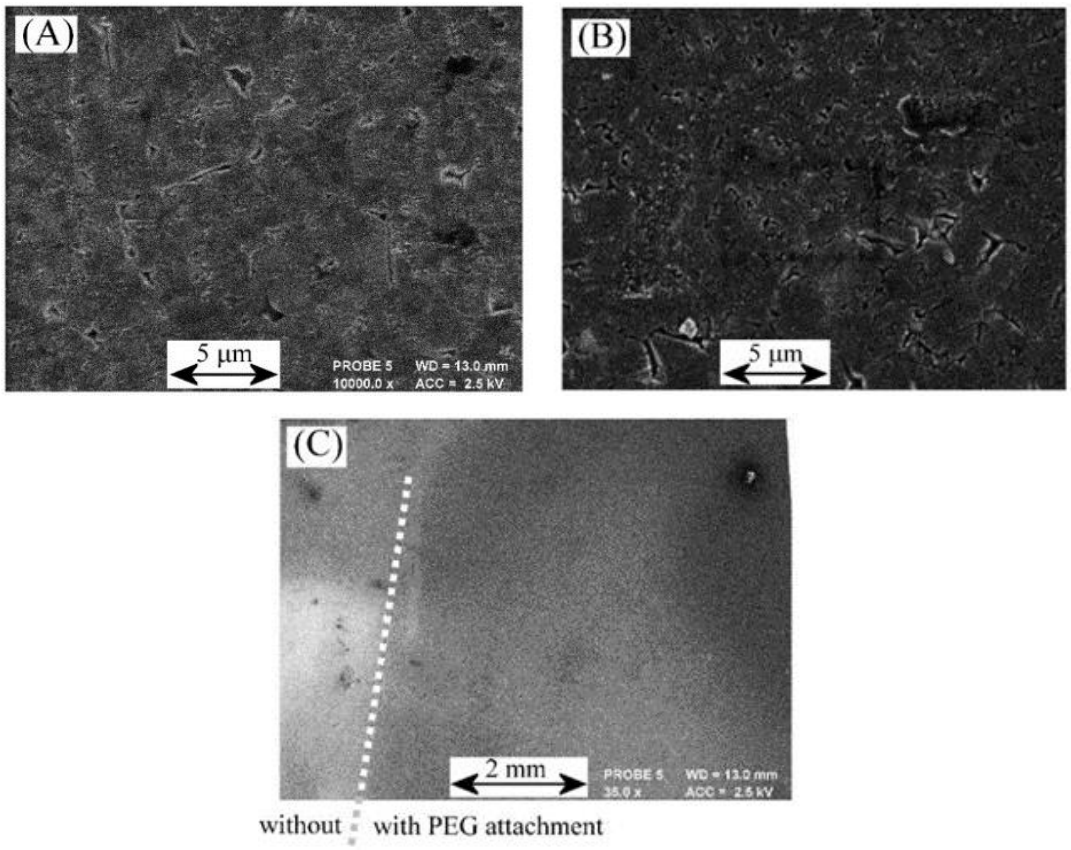

Figure 5.5. Scanning electron micrographs for (**A**) a bare boron doped diamond (BDD) electrode (10,000x), (**B**) a PEG400-modified BDD electrode (20 min at +1.6 V (*vs.* SCE) (10,000x), and (**C**) a low magnification (35x) image showing the interface between bare and PEG400-modified regions of a BDD electrode. The dashed line represents the interface between the modified and unmodified regions of the electrode.

The minimum potential at which electrodes can be modified with a PEG layer is dependent upon the nature of the surface. A threshold potential of +1.0 V (*vs.* SCE) had to be overcome for PEG400 to attach to the boron doped diamond surface. In contrast, signs of PEG attachment were observed on a glassy carbon electrode at an anodisation potential of +0.6 V (*vs.* SCE), although a second threshold potential was also observed at +1.0 V (*vs.* SCE) for higher surface coverages. The presence of two threshold potentials for glassy carbon could reflect the non-uniform surface reactivity of the carbon substrate. This could be different reactivity shown between sp^2 and sp^3 type carbons or different reactivity shown by the graphite edges and planes. The doping level dependent rate of electron transfer at boron-doped diamond may also contribute to the difference in reactivity.[32] At attachment potentials above +1.2 V (*vs.* SCE) for glassy carbon and +1.6 V (*vs.* SCE) for boron doped diamond (for a 20 min attachment), both PEG400-modified electrodes had similarly low k_0 values (10^{-7} – 10^{-8} m s^{-1}) for the

$Fe(CN)_6^{3-/4-}$ redox couple. For both glassy carbon and boron doped diamond, the modified electrodes were somewhat sensitive to redox cycling and detachment of the film was observed with continued potential cycling over a wide potential window in aqueous media. Beyond a potential of +1.2 (*vs.* SCE) in aqueous 0.1 M KNO_3 a rapid degradation of the film was observed and the signal for the $Fe(CN)_6^{3-/4-}$ couple returned to its original quasi-reversible state.

5.3.3 Poly(ethylene glycol) modified carbon electrodes: effect of chain length on electron transfer

Having optimised the attachment parameters, the properties of the PEG-modified electrode can be tuned by altering the chain length of the polymer. Poly(ethylene glycol) with an average molecular weight of 600 g mol^{-1} is a waxy solid at room temperature, however, lower molecular weight PEGs are viscous liquids at room temperature. These liquid PEGs could be used directly to attach to electrode surfaces from neat solutions containing 20 mM $LiClO_4$ using the anodic treatment outlined previously (see section 5.2.3). In order to investigate the effect of PEG chain length, PEG films with average molecular weights 200, 300 and 400 g mol^{-1} were deposited onto a glassy carbon electrode. Electrochemical impedance spectroscopy (EIS) was used to determine the standard rate constant for heterogeneous electron transfer (k_0) for the $Fe(CN)_6^{3-/4-}$ redox couple (Figure 5.6). The solution resistance (R_Ω) and the double layer capacitance (C_{dl}) were independent of PEG chain length. The apparent rate constant for heterogeneous electron transfer sequentially decreased as the average molecular weight of the polymer increased. The higher molecular weight polymers, with longer chains, are likely to form a thicker passivating layer on the electrode surface, which causes an increase in the tunnelling distance for electron transfer. The apparent standard heterogeneous rate constant for electron transfer through a monolayer ($k_{0(monolayer)}$) should follow a Gamov-type relationship and decay exponentially as the tunnelling distance increases (equation 5.4).[33]

$$k_{0(monolayer)} = k_{0(substrate)} \exp(-\beta d) \quad (5.4)$$

In this expression $k_{0(substrate)}$ is the rate of electron transfer without a monolayer present; β is the tunnel distance coefficient, which is $\sim$1 Å^{-1} for alkyl chains;[34, 35] and d is the tunnel distance, which can be approximated for an alkyl chain (in Å) by $d = 5.6 + 1.3x$, where x is the number of CH_2 units in the alkyl chain. When PEG attaches to a glassy carbon electrode, it forms an insulating layer and can be considered in a similar way to an insulating alkyl chain layer. However, unlike alkyl chains, PEG is miscible with water and is unlikely to form a completely separate phase in aqueous solution. As the chain length of the polymer increases, the thickness of the insulating layer does so accordingly and the apparent rate of electron transfer is reduced. The gradient of a plot of $\ln(k_{0(monolayer)})$ against the tunnelling distance (d) can be used to determine the tunnel distance coefficient (β) (Figure 5.6). At large tunnelling distances (or high molecular weight PEGs) β was found to be $\sim$1 Å^{-1}, which is in agreement with expected values for alkyl chains ($\beta = 1$ Å^{-1}). However, at short tunnelling distances (or low molecular weight PEGs) β was found to be $\sim$0.17 Å^{-1}, which is considerably lower than predicted. The lower than expected β value implies that the $Fe(CN)_6^{3-/4-}$ species is able to penetrate some way into the PEG layer through the diffuse phase boundary and/or that the surface coverage of the PEG layer is incomplete.

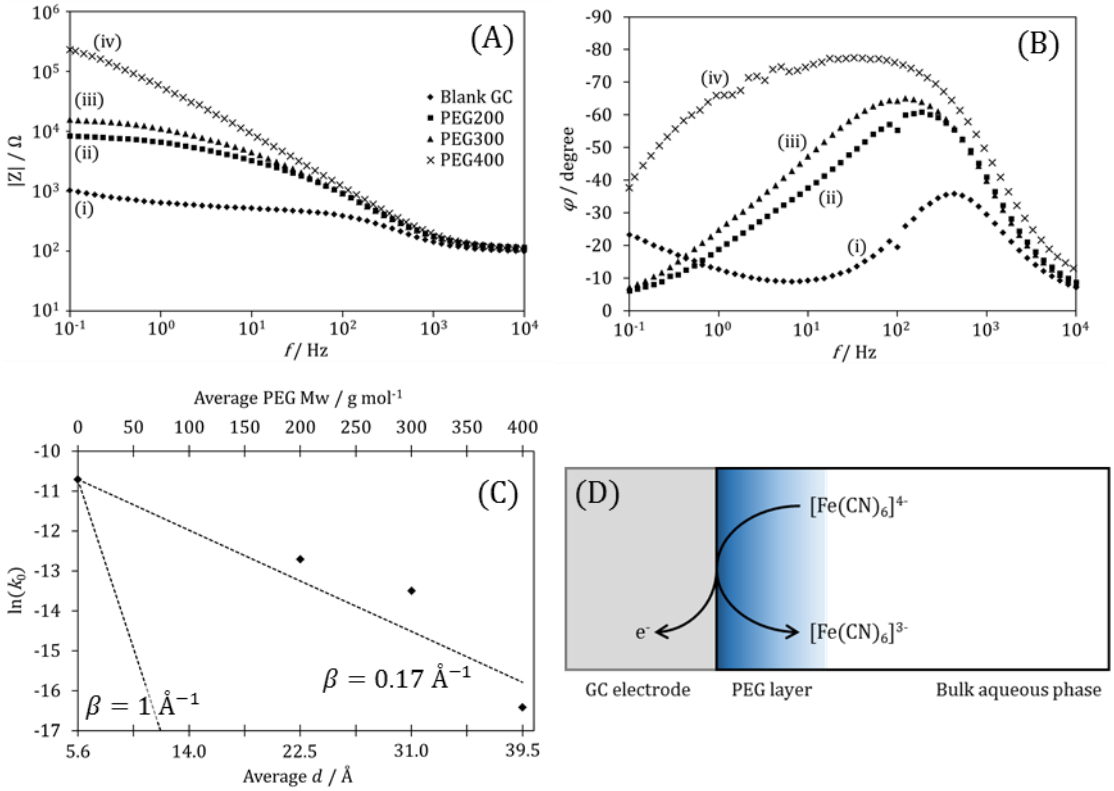

Figure 5.6. (**A**, **B**) Bode impedance plots for a solution containing 5 mM $K_4Fe(CN)_6$, 5 mM $K_3Fe(CN)_6$ and 0.1 M KNO_3 at a 3 mm diameter glassy carbon working electrode recorded at OCP (i) with no PEG film, (ii) PEG200-GC, (iii) PEG300-GC, and (iv) PEG400-GC after anodic treatment at +1.2 V (*vs.* SCE) for 20 min. (**C**) Plot of $\ln(k_0)$ as a function of PEG average molecular weight. Also shown is the tunnelling distance (d, in Å), which is approximated by $d = 5.6 + 3.9n$ (where n is the number of (O-CH_2-CH_2) units). (**D**) Schematic drawing of the interfacial electron transfer. The colour gradient of the PEG layer is indicating the diffuse phase boundary layer.

5.3.4 Poly(ethylene glycol) modified carbon electrodes: effect on 1,1'-ferrocene dimethanol electron transfer

Although PEG is completely miscible with water, a thin, dense film of PEG attached to an electrode could be considered as a separate surface phase with a diffuse phase boundary to the bulk solution. Species which are insoluble in PEG will not be able to penetrate far into the PEG film, whereas compounds that solubilise in PEG should pass through the diffuse boundary layer unhindered. Voltammetry using the more hydrophobic 1,1'-ferrocene dimethanol ($Fc(CH_2OH)_2$) redox system demonstrates this phenomenon.

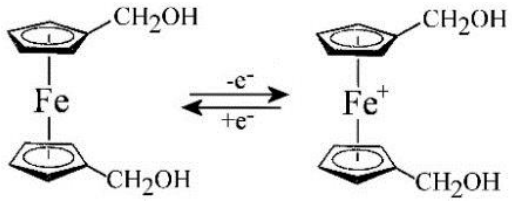

The voltammetry for 0.5 mM $Fc(CH_2OH)_2$ was investigated at a glassy carbon electrode prior to and after surface modification with PEG (Figure 5.7). Prior to modification, the cyclic voltammogram had a reversible potential (E_0) at +0.23 V (*vs.* SCE) and a peak separation (ΔE_p) of 85 mV. These highly reversible characteristics did not change after modification with different weight PEGs. Randles- Ševčík analysis (using equation 5.2) allowed a diffusion coefficient in aqueous 0.1 M KNO_3 of $D_{1,1'-ferrocene\ dimethanol} = 0.6 \times 10^{-9}$ m^2 s^{-1} to be determined, which is consistent with previous reports.[36] This voltammetric behaviour was observed on both glassy carbon and boron doped diamond electrodes.

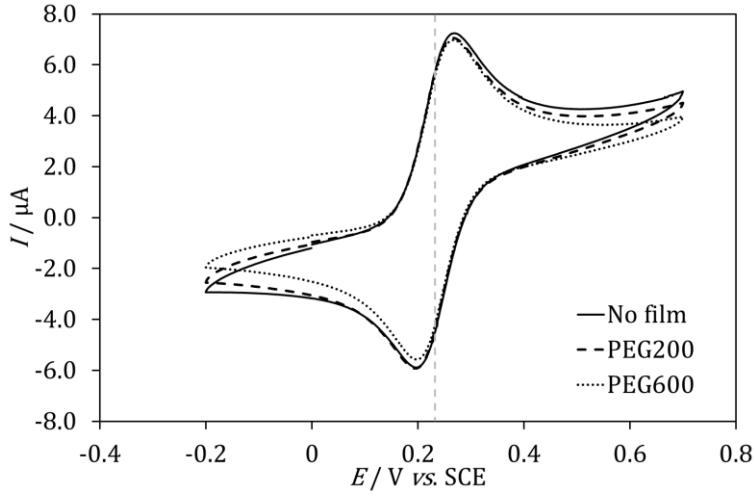

Figure 5.7. Cyclic voltammogram (scan rate 50 mV s^{-1}, second cycle) for the oxidation of 0.5 mM $Fc(CH_2OH)_2$ in 0.1 M KNO_3 with different PEG length surface modifications on glassy carbon.

After PEG attachment, the rate of electron transfer appears to remain fast for the $Fc(CH_2OH)_2^{0/+}$ redox system and was found to be independent upon attachment time, attachment potential and length of the attached PEG chain. It is proposed that the rate of electron transfer does not change for $Fc(CH_2OH)_2^{0/+}$ at a PEG modified glassy carbon (or boron doped diamond) electrode because the redox system can diffuse more deeply into the PEG layer when compared with the more hydrophilic $Fe(CN)_6^{3-/4-}$ species. Consequently there is less effect on the electron tunnelling distance.

The apparent selectivity between $Fe(CN)_6^{3-/4-}$ and $Fc(CH_2OH)_2^{0/+}$ redox couples at PEG modified carbon electrodes could have implications and applications in electrochemical sensing, for example when exploited for suppressing unwanted background current responses or when "amplifying" the signal for low concentration mediators. The mediated oxidation of potassium ferrocyanide ($K_4Fe(CN)_6$) using a $Fc(CH_2OH)_2$ mediator was investigated further.

5.3.5 Poly(ethylene glycol) modified carbon electrodes: mediated processes

It has been shown that a PEG modified carbon electrode (either glassy carbon or boron doped diamond) suppresses the electron transfer for the $Fe(CN)_6^{3-/4-}$ redox couple. However, the rate of electron transfer for the $Fc(CH_2OH)_2^{0/+}$ redox couple is not significantly altered. At unmodified carbon electrodes the oxidation of $K_4Fe(CN)_6$ and $Fc(CH_2OH)_2$ have similar electron transfer kinetics and have reversible potentials of +0.19 V and +0.23 V (*vs.* SCE) respectively. The marginally more positive reversible potential of $Fc(CH_2OH)_2$ implies that it is thermodynamically feasible for $Fc(CH_2OH)_2$ to mediate the oxidation of ferrocyanide(II). $Fc(CH_2OH)_2$ has previously been employed as a redox mediator in protein electrochemistry.[37] $Fc(CH_2OH)_2$ is employed here to mediate the oxidation of potassium ferrocyanide ($K_4Fe(CN)_6$) at a PEG400 modified glassy carbon electrode (PEG400-GC).

PEG400-GC electrodes were prepared using an attachment potential of +1.6 V (*vs.* SCE) for 20 minutes. Cyclic voltammetry was performed with these electrodes in solutions containing different amounts of $K_4Fe(CN)_6$ and $Fc(CH_2OH)_2$. Initially a fixed 10 mM concentration of $K_4Fe(CN)_6$ was used as the concentration of $Fc(CH_2OH)_2$ was increased from 0 to 50 μM (Figure 5.8A) The mediated electron transfer can be observed for concentrations as low as 5 μM $Fc(CH_2OH)_2$, which had a gradually increasing, kinetically limited current (Figure 5.8A(ii) and 5.8A(iii)). This suggests that at low concentrations of $Fc(CH_2OH)_2$ mediator, the rate of the mediated step is limiting the current. The gradually increasing nature of the kinetically limited current with applied potential suggests either (i) the rate is in part limited by slow (non-Butler-Volmer) $Fc(CH_2OH)_2$ oxidation at the electrode surface or (ii), perhaps less likely, the positive applied potential can affect the bimolecular electron transfer, for example by allowing $Fe(CN)_6^{4-}$ to penetrate further into the PEG layer. At concentrations greater

than 50 μM $Fc(CH_2OH)_2$, a peak-shaped current response was observed as mass transport started to limit the current.

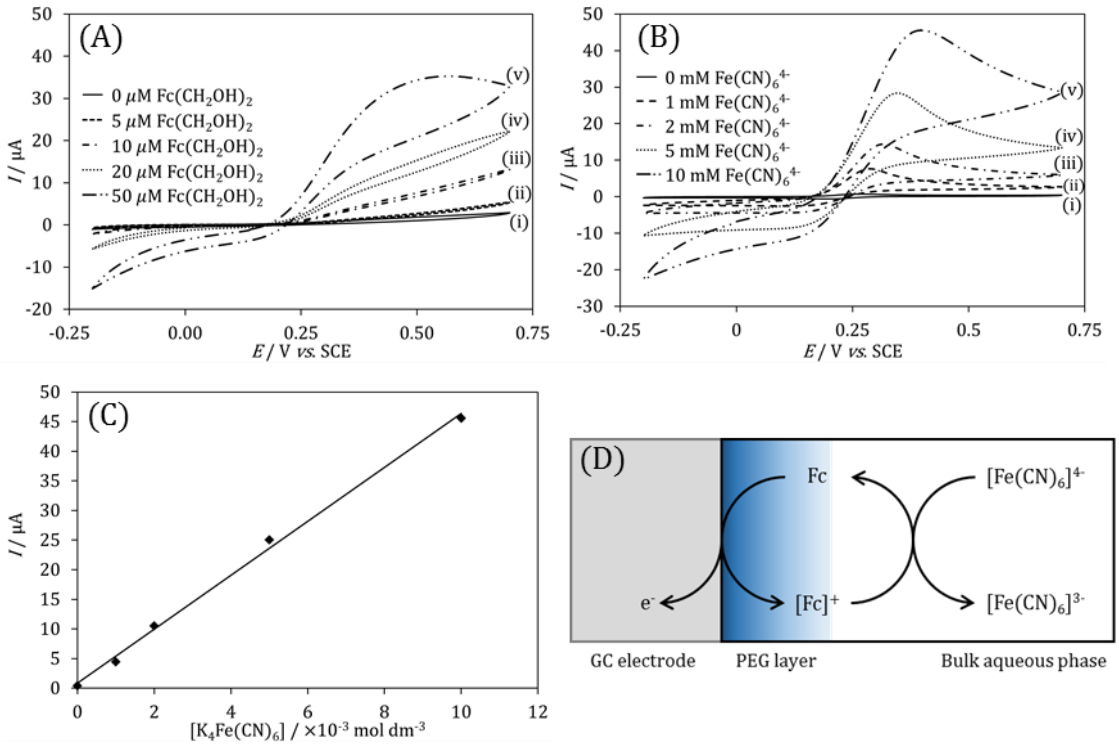

Figure 5.8. (**A**) Cyclic voltammograms (scan rate 50 mV s^{-1}, second cycle) at a PEG400-GC electrode (attachment at +1.6 V (*vs*. SCE) for 20 min) for aqueous solutions containing fixed 10 mM $K_4Fe(CN)_6$ and 0.1 M KNO_3 concentration with (i) 0 μM, (ii) 5 μM, (iii) 10 μM, (iv) 20 μM, (v) 50 μM of $Fc(CH_2OH)_2$. (**B**) As above, but with a fixed 100 μM $Fc(CH_2OH)_2$ concentration and with (i) 0 mM, (ii) 1 mM, (iii) 2 mM, (iv) 5 mM and (v) 10 mM of $K_4Fe(CN)_6$. (**C**) Linear plot of peak current against $K_4Fe(CN)_6$ concentration. (**D**) Schematic diagram of the mediated electron transfer process.

For a solution containing 10 mM $K_4Fe(CN)_6$ and low $Fc(CH_2OH)_2$ concentrations, the current is kinetically limited implying that the electrochemical step is the slowest step. In the same 10 mM $K_4Fe(CN)_6$ solution but at high $Fc(CH_2OH)_2$ concentrations, the current is limited by diffusion, which suggests depletion of the $K_4Fe(CN)_6$ concentration from the electrode. For a concentration of 10 μM $Fc(CH_2OH)_2$ and 10 mM $K_4Fe(CN)_6$, the response can be considered as a transition between these two limiting cases. The limiting current (I_{lim}) for this transition case is 13 μA, which corresponds to a diffusion layer thickness ($\delta_{diffusion}$) of:

$$\delta_{diffusion} = \frac{FADc}{I_{lim}} \approx 310 \text{ nm} \qquad (5.5)$$

This was determined using a diffusion coefficient of $D = 0.6 \times 10^{-9}$ m^2 s^{-1}.[36] Since this is the transition case between a kinetically limited and diffusion limited process, $\delta_{diffusion}$ is approximately equal to the reaction layer thickness ($\delta_{reaction}$). The homogeneous bimolecular rate constant for oxidation of $K_4Fe(CN)_6$ ($k_{forward}$) can therefore be approximated using equation 5.6.

$$\delta_{diffusion} \approx \delta_{reaction} = \sqrt{\frac{D}{k_{forward}[\mathrm{Fe(CN)_6^{4-}}]}} \quad (5.6)$$

The bimolecular rate constant for the oxidation of $K_4Fe(CN)_6$ (forward reaction) was estimated as 6×10^5 mol^{-1} dm^3 s^{-1}. Forward and backward rate constants are linked by equation 5.7, which enables the backward rate constant ($k_{backward}$) to be estimated as $k_{backward} \approx 1 \times 10^5$ mol^{-1} dm^3 s^{-1}.

$$\Delta G = -nF\Delta E_0 = -RT \ln \frac{k_{forward}}{k_{backward}} \quad (5.7)$$

For a fixed concentration of $Fc(CH_2OH)_2$ in the solution, the voltammetric current response increases with $K_4Fe(CN)_6$ concentration (Figure 5.8) The oxidation peak current shows an approximately linear increase with $K_4Fe(CN)_6$ concentration, which is consistent with a bimolecular mediation mechanism. It is interesting to note that the redox mediation mechanism operates for both oxidation and reduction reactions due to the small difference in reversible potential for the two redox systems. The negative currents observed in Figure 5.8A and 5.8B are indicative of the reduction of $K_3Fe(CN)_6$ back to $K_4Fe(CN)_6$. The mediator effect of $Fc(CH_2OH)_2$ is versatile and could have potential future applications in electrochemical sensors at PEG-modified electrodes.

Digital simulation (using DigiElch Professional, Version 4.F) allowed the values of all kinetic and thermodynamic parameters (E_0, D, $k_{forward}$ and $k_{backward}$) to be verified. All experiments investigating the mediated oxidation of $K_4Fe(CN)_6$ were compared with digital simulations (Figure 5.9).

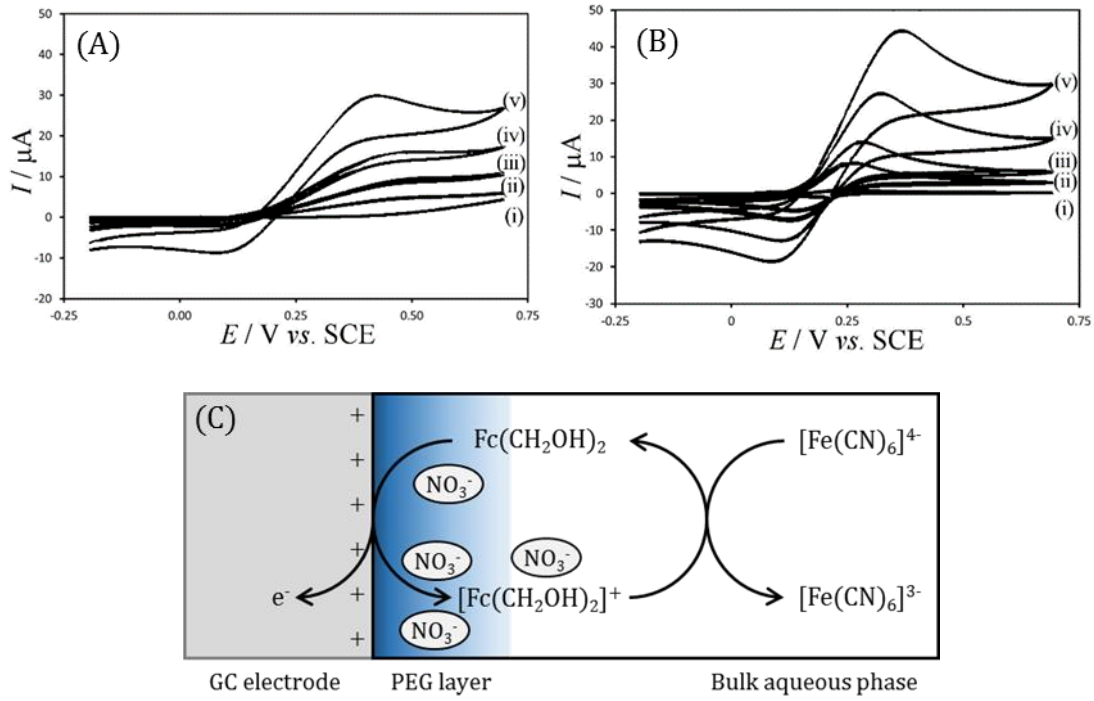

Figure 5.9. (**A**) Digital simulation of cyclic voltammograms (scan rate 50 mV s^{-1}, second cycle) for fixed 10 mM $K_4Fe(CN)_6$ in 0.1 M KNO_3 concentration with (i) 0 μM, (ii) 5 μM, (iii), 10 μM, (iv) 20 μM, (v) 50 μM of $Fc(CH_2OH)_2$. (**B**) As above, but with a fixed 100 μM $Fc(CH_2OH)_2$ concentration and with (i) 0 mM, (ii) 1 mM, (iii) 2 mM, (iv) 5 mM and (v) 10 mM of $K_4Fe(CN)_6$. Parameters for digital simulation were as given in the text and included an additional uncompensated resistance as described by Table 5.2. (**C**) Schematic drawing indication the stabilising role of nitrate anions in the PEG film.

The relatively good match of experiment and theory verifies the parameters derived above, but also reveals a further effect. The simulated fit is improved by introducing an uncompensated resistance (R_u) that is inversely proportional to the mediator concentration (Table 5.2). This suggests a higher concentration of mediator reduces the uncompensated resistance in the voltammogram, which could be explained by the formation of a $[Fc(CH_2OH)_2]^+[NO_3]^-$ complex in the PEG layer at oxidising potentials. The gradually increasing limiting current as a function of potential could also indicate that the uncompensated resistance is potential dependent, which also could suggest the formation of a $[Fc(CH_2OH)_2]^+[NO_3]^-$ complex in the PEG layer (Figure 5.9C).

Table 5.2. A table showing the uncompensated resistance required in digital simulations at each $Fc(CH_2OH)_2$ concentration.

$[Fc(CH_2OH)_2]$ / μM	R_u / kΩ
5	40
10	20
20	10
50	4
100	2

5.4 Conclusions

Poly(ethylene glycol) of average molecular weight 200, 300 and 400 g mol^{-1} was electrochemically grafted to glassy carbon and boron-doped diamond electrode surfaces at anodic potentials. The thickness and coverage of the grafted poly(ethylene glycol) films was dependent upon grafting potential, time and poly(ethylene glycol) chain length. Voltammetry at PEG-modified carbon surfaces indicates that the heterogeneous rate of electron transfer for hydrophilic redox systems, such as $Fe(CN)_6^{3-/4-}$, is impeded compared to an untreated electrode. In contrast, the electron transfer for 1,1'-ferrocene dimethanol, a more hydrophobic species, was not significantly affected by the PEG-modification.

A combination of the two redox species in solution resulted in a mediated electrochemical response whereby the hydrophobic ferrocene derivative mediates the oxidation of the hydrophilic ferrocyanide(II) species. Further studies on the mediation mechanism could be beneficial. The apparent selectivity of the modified carbon electrodes allows for trace amounts of hydrophobic redox material to be detected if a suitable hydrophilic redox mediator is present in high concentrations in the bulk. This could lead to electroanalytical applications, in particular for the detection of trace hydrophobic drug molecules. The limit of detection for this mediated process is given by the rate of the bimolecular electron transfer, which depends on the reversible potentials for hydrophobic analyte mediator and hydrophilic amplifier redox systems.

Further studies using a range of ferrocene mediator derivatives at modified carbon electrodes will be discussed in chapter 6.

5.5 References

1. H.-F. Zhou, Q.-H. Fan, Y.-Y. Huang, L. Wu, Y.-M. He, W.-J. Tang, L.-Q. Gu and A. S. C. Chan, *Journal of Molecular Catalysis a-Chemical*, 2007, **275**, 47-53.
2. Z.-Z. Yang, Q.-W. Song and L.-N. He, *Capture and Utilization of Carbon Dioxide with Polyethylene Glycol*, Springer, 2012.
3. O. Aschenbrenner and P. Styring, *Energy & Environmental Science*, 2010, **3**, 1106-1113.
4. C. Fruijtier-Polloth, *Toxicology*, 2005, **214**, 1-38.
5. J. Chen, S. K. Spear, J. G. Huddleston and R. D. Rogers, *Green Chemistry*, 2005, **7**, 64-82.
6. R. K. Bose, S. Nejati, D. R. Stufflet and K. K. S. Lau, *Macromolecules*, 2012, **45**, 6915-6922.
7. A. J. Downard and A. bin Mohamed, *Electroanalysis*, 1999, **11**, 418-423.
8. H. Maeda, T. Okada, Y. Matsumoto, K. Katayama, Y. Yamauchi and H. Ohmori, *Analytical Sciences*, 1999, **15**, 633-639.
9. S. Kaneko, H. Nakayama, Y. Yoshino, D. Fushimi, K. Yamaguchi, Y. Horiike and J. Nakanishi, *Physical Chemistry Chemical Physics*, 2011, **13**, 4051-4059.
10. A. J. Downard, *Electroanalysis*, 2000, **12**, 1085-1096.
11. C. Vericat, M. E. Vela, G. Benitez, P. Carro and R. C. Salvarezza, *Chemical Society Reviews*, 2010, **39**, 1805-1834.
12. J. B. Schlenoff, M. Li and H. Ly, *Journal of the American Chemical Society*, 1995, **117**, 12528-12536.
13. J. Pinson and F. Podvorica, *Chemical Society Reviews*, 2005, **34**, 429-439.
14. P. Allongue, M. Delamar, B. Desbat, O. Fagebaume, R. Hitmi, J. Pinson and J. M. Saveant, *Journal of the American Chemical Society*, 1997, **119**, 201-207.
15. Y. Wen, H. Wu, S. Chen, Y. Lu, H. Shen and N. Jia, *Electrochimica Acta*, 2009, **54**, 7078-7084.
16. B. Barbier, J. Pinson, G. Desarmot and M. Sanchez, *Journal of the Electrochemical Society*, 1990, **137**, 1757-1764.
17. H. Maeda, Y. Yamauchi, M. Hosoe, T. X. Li, E. Yamaguchi, M. Kasamatsu and H. Ohmori, *Chemical & Pharmaceutical Bulletin*, 1994, **42**, 1870-1873.
18. H. Maeda, M. Itami, Y. Yamauchi and H. Ohmori, *Chemical & Pharmaceutical Bulletin*, 1996, **44**, 2294-2299.
19. H. Maeda, T. X. Li, M. Hosoe, M. Itami, Y. Yamauchi and H. Ohmori, *Analytical Sciences*, 1994, **10**, 963-965.
20. H. Maeda, Y. Yamauchi, M. Yoshida and H. Ohmori, *Analytical Sciences*, 1995, **11**, 947-952.

21. H. Maeda, T. Kitano, C. Z. Huang, K. Katayama, Y. Yamauchi and H. Ohmori, *Analytical Sciences*, 1999, **15**, 531-536.
22. H. Maeda, M. Itami, K. Katayama, Y. Yamauchi and H. Ohmori, *Analytical Sciences*, 1997, **13**, 721-727.
23. B. Guo, J. Anzai and T. Osa, *Chemical & Pharmaceutical Bulletin*, 1996, **44**, 860-862.
24. H. Maeda, K. Katayama, R. Matsui, Y. Yamauchi and H. Ohmori, *Analytical Sciences*, 2000, **16**, 293-298.
25. H. Maeda, Y. Saka-iri, T. Ogasawara, C. Z. Huang, Y. Yamauchi and H. Ohmori, *Chemical & Pharmaceutical Bulletin*, 2001, **49**, 1349-1351.
26. C. D. Wagner, in *Practical Surface Analysis*, eds. D. Briggs and M. P. Seah, J. Wiley and Sons, New York, Editon edn., 1990, vol. 1.
27. S. Ferro, M. Dal Colle and A. De Battisti, *Carbon*, 2005, **43**, 1191-1203.
28. R. Schlapak, D. Caruana, D. Armitage and S. Howorka, *Soft Matter*, 2009, **5**, 4104-4112.
29. L. Xiong, C. Batchelor-McAuley, K. R. Ward, C. Downing, R. S. Hartshorne, N. S. Lawrence and R. G. Compton, *Journal of Electroanalytical Chemistry*, 2011, **661**, 144-149.
30. K. K. Cline, L. Baxter, D. Lockwood, R. Saylor and A. Stalzer, *Journal of Electroanalytical Chemistry*, 2009, **633**, 283-290.
31. R. N. Adams, *Electrochemistry at solid electrodes*, Marcel Dekker, 1969.
32. R. G. Compton, J. S. Foord and F. Marken, *Electroanalysis*, 2003, **15**, 1349-1363.
33. A. Kiani, M. A. Alpuche-Aviles, P. K. Eggers, M. Jones, J. J. Gooding, M. N. Paddon-Row and A. J. Bard, *Langmuir*, 2008, **24**, 2841-2849.
34. H. Z. Yu, H. B. Shao, Y. Luo, H. L. Zhang and Z. F. Liu, *Langmuir*, 1997, **13**, 5774-5778.
35. J. R. Winkler and H. B. Gray, *Journal of the American Chemical Society*, 2014, **136**, 2930-2939.
36. R. W. French, A. M. Collins and F. Marken, *Electroanalysis*, 2008, **20**, 2403-2409.
37. A. Konash and E. Magner, *Analytical Chemistry*, 2005, **77**, 1647-1654.

Chapter 6: Interfacial electron shuttling processes across Kolliphor® EL modified glassy carbon electrodes

Chapter abstract

A PEGylated castor oil, Kolliphor® EL (formerly known as Cremophor EL), is used to demonstrate the attachment of complex molecules to glassy carbon surfaces using an anodic grafting method. The attachment was confirmed by XPS. Cyclic voltammetry and electrochemical impedance spectroscopy indicates that the rate of heterogeneous electron transfer for $Fe(CN)_6^{3-/4-}$ is suppressed at the modified electrode due to the hydrophilic redox species being unable to cross a hydrophobic Kolliphor® EL layer. However, hydrophobic ferrocene derivatives used in low concentrations (< 50 μM) can be employed as electron shuttle molecules to mediate the electron transfer to $Fe(CN)_6^{3-/4-}$. The electron shuttle ability for five ferrocene derivatives was assessed and found to decrease in the order: dimethylaminomethyl ferrocene > *n*-butyl ferrocene > ferrocene dimethanol > ferrocene acetonitrile > ferrocene acetic acid. The electron shuttle ability is proposed to be influenced by (i) the reversible potential for mediator molecule, (ii) heterogeneous electron transfer kinetics for the mediator molecule, (iii) electrostatic interactions, and (iv) an ability to bind or aggregate at the electrode surface.

Chapter publications

This chapter has been published in:
K. Nekoueian, C. E. Hotchen, M. Amiri, M. Sillanpää, G. W. Nelson, J. S. Foord, P. Holdway, A. Buchard, S. C. Parker and F. Marken, *ACS Appl. Mater. Interfaces*, 2015, **7**, 15458-15465.

Special acknowledgements

I would like to thank Khadijeh Nekoueian for her experimental work, Geoffrey Nelson for his expertise in XPS analysis and Begbroke Science Park for allowing use of their equipment. I would also like to thank Steve Parker for using computational methods to determine the size of the Kolliphor® EL molecule.

Chapter contents

6 Interfacial electron shuttling processes across Kolliphor® EL modified glassy carbon electrodes

6.1 Introduction

Surface modified electrodes have uses in electroanalytical applications, electrochromic devices and can allow selectivity between redox species.[1-4] Chemical surface modification methods can often be lengthy, multi-step processes where the modifier molecule may require specific functionality, and hence a complex synthesis prior to grafting. Electrochemical grafting methods can allow the attachment of a variety of functional groups, such as diazonium salts, amines and alcohols, in a single electrochemical step.[5] The surface coverage and thickness of resulting films can be controlled by optimising the grafting potential and attachment time. The previous chapter described an electrochemical attachment method adapted from Maeda et al.[6] to graft poly(ethylene glycol) to glassy carbon and boron-doped diamond electrodes. This chapter aims to demonstrate the attachment of a more complex molecule, Kolliphor® EL (formerly known as Cremophor EL), to glassy carbon surfaces.

Kolliphor® EL (CAS number 61791-12-6, MW ≈2486 g mol^{-1}) is a PEGylated castor oil (Figure 6.1) synthesised from the reaction of castor oil with ethylene oxide in the molar ratio 1:35.[7] Kolliphor® EL is a viscous non-ionic surfactant at room temperature and is able to solubilise a range of hydrophobic species, including hydrophobic drug molecules. It is consequently used as an excipient in the formulation for a range of drugs, such as Paclitaxel (anti-cancer), diazepam (sedative) and propofol (anaesthetic), to increase the bioavailability of the therapeutics *in vivo* and allow oral administration.[8]

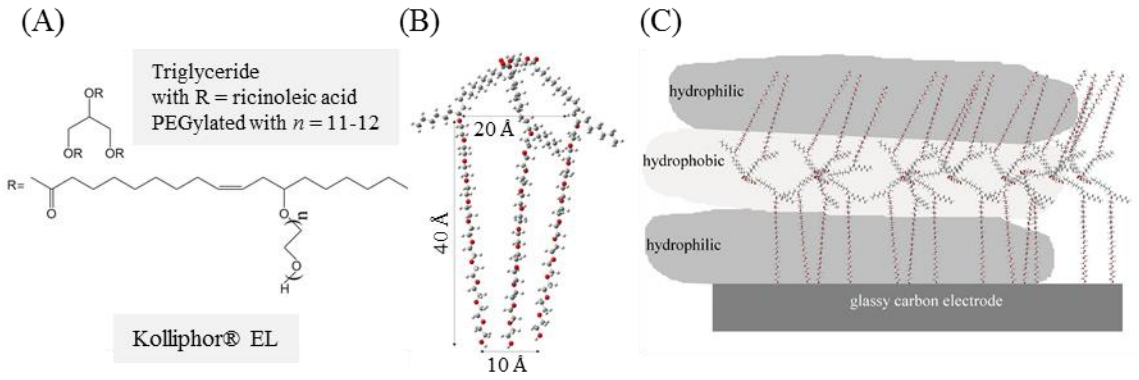

Figure 6.1. (A) Molecular structure of the main component in Kolliphor® EL and (B) 3-dimensional rendering (GaussView 5.0) showing the approximate diameter of 3-5 nm. (C) Schematic drawing of a Kolliphor® EL monolayer with a hydrophobic region resulting from the triglyceride.

The terminal hydroxyl groups of the poly(ethylene glycol) chains in Kolliphor® EL are susceptible to oxidation and are likely to bind to carbon surfaces.[6] After grafting, a hydrophobic layer could be established (Figure 6.1C), which could facilitate the transport of hydrophobic species across the Kolliphor® EL layer, whilst excluding hydrophilic species. In this study Kolliphor® EL is anodically attached to glassy carbon surfaces where it acts as a barrier to electron transfer for hydrophilic species. However, hydrophobic ferrocene derivatives can penetrate or bind to the Kolliphor® EL layer, which can enhance the interfacial electron transfer.

A low limit of detection and high sensitivity are desired for electroanalytical devices. The analytical response of electrochemical sensors can be enhanced by using redox cycling methods, such as generator-collector electrode devices[9], or by incorporating enzyme[10] or nanoparticle[11] catalysts into the device. This study aims to covalently attach Kolliphor® EL to a glassy carbon surface using an anodic grafting method.[12,13] The heterogeneous rate of electron transfer for the oxidation of ferrocyanide(II) is severely suppressed at a Kolliphor® EL modified electrode. However, the voltammetric response can be partially or fully restored in the presence of a hydrophobic ferrocene derivative, which acts as an electron shuttle molecule across the Kolliphor® EL layer (Figure 6.2).

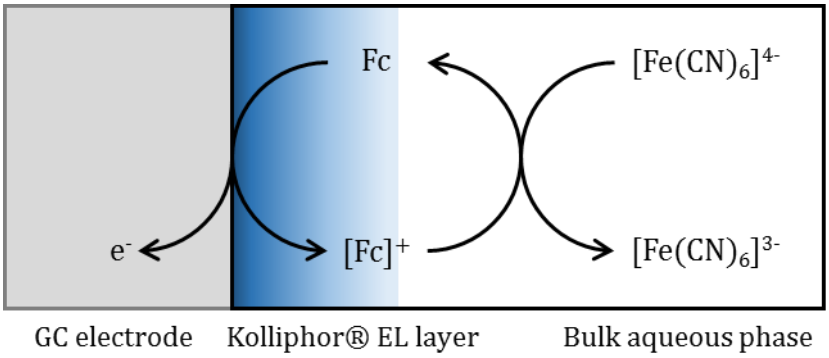

Figure 6.2. Schematic drawing of the amplification mechanism for the low concentration ferrocene (Fc) redox process in the presence of the suppressed $Fe(CN)_6^{3-/4-}$ electron transfer.

Very low concentrations of ferrocene derivatives can therefore be detected as relatively large currents. A range of ferrocene derivatives are assessed in their "shuttle ability" to restore the voltammetric response to ferrocyanide(II) oxidation. A quantitative study reveals the parameters that govern the electron shuttle process. Future applications are envisaged in the enhancement of other electron transfer processes, for example in analytical drug or explosives detection.

6.2 Experimental

6.2.1 Chemical reagents

Kolliphor® EL (CAS number 61791-12-6, MW ca. 2450 g mol^{-1}; previously known as Cremophor EL, Aldrich) is a PEGylated castor oil derivative (Figure 6.1). Lithium perchlorate ($LiClO_4$, Sigma-Aldrich, ≥ 95 %, ACS reagent) was used as background electrolyte in neat Kolliphor® EL solutions. 1,1'-ferrocene dimethanol ($Fc(CH_2OH)_2$, Aldrich, 98 %), ferrocene acetic acid (FcAcOH, Aldrich, 98 %), ferrocene acetonitrile (FcMeCN, Aldrich), *n*-butyl ferrocene (BuFc, Alfa Aesar, 98 %, oil), *N*,*N'*-dimethylaminomethyl ferrocene ($MeFcNMe_2$, TCI Europe, oil), potassium ferrocyanide(II) ($K_4Fe(CN)_6$, Fisons, 98 %) and potassium ferricyanide(III) ($K_3Fe(CN)_6$, Aldrich, 99+ %) were used as redox species in aqueous solutions

containing 0.1 M potassium nitrate (KNO_3, Sigma-Aldrich, ≥ 99.0 %) as background electrolyte.

6.2.2 Instrumentation

All electrochemical measurements were performed using an Ivium Compactstat 104 Model B08084 (Ivium Technologies NL). A step potential of 1 mV was used in cyclic voltammetry experiments. Electrochemical impedance spectroscopy (EIS) was performed at open circuit potential (OCP = 0.19 V (*vs*. SCE)) with an amplitude of 10 mV in a solution containing 5 mM $K_4Fe(CN)_6$, 5 mM $K_3Fe(CN)_6$ and 0.1 M KNO_3 electrolyte. The frequency was varied from 10 kHz to 0.01 Hz. Equivalent circuit data fitting was carried out using ZView software.

X-ray photoelectron spectroscopy (XPS) experiments were performed using a Thermo K Alpha (Thermo Scientific) spectrometer (operating at $\approx 10^{-8} - 10^{-9}$ Torr), a 180 ° double focusing hemispherical analyser running in constant analyser energy (CAE) mode with a 128-channel detector. A monochromated Al Kα radiation source (1486.7 eV) was used. Peak fitting was performed with XPS Peak Fit (version 4.1) software using Shirley background subtraction. Peaks were referenced to the adventitious carbon C1s peak (284.6 eV) and peak areas were normalised to the photoelectron cross-section of the F1s photoelectron signal using atomic sensitivity factors.[14,15]

6.2.3 Procedure for attachment of Kolliphor® EL

Kolliphor® EL is a viscous liquid and can be employed directly as a solvent in electrochemical experiments after addition of a suitable electrolyte. In this investigation a solution of 20 mM $LiClO_4$ in Kolliphor® EL was employed for the electrode modification process. The anodisation process previously described in Chapter 5 (+1.6 V (*vs.* SCE) for 20 min) was employed to attach the PEGylated castor oil to a 3 mm diameter glassy carbon disc electrode. The electrode was then rinsed with water (with resistivity not less than 18.2 MΩ cm^2) to remove any residual Kolliphor® EL from the electrode and dried using nitrogen. The surface modification was confirmed by XPS and the electron transfer processes across the Kolliphor® EL interface were investigated using cyclic voltammetry and electrochemical impedance spectroscopy.

6.2.4 Evidence for attachment of Kolliphor® EL: XPS analysis

The surface modification was confirmed by XPS using two independently prepared samples (K1 and K2) (Figure 6.3). Survey spectra show photoelectron signals from contaminant free surfaces containing C and O (Figure 6.3A). The C1s photoelectron signals show evidence for a PEG-like interface. The C1s spectra could be fitted into four chemical environments: adventitious carbon and hydrocarbon (284.6 eV), ether (C-O, ≈ 286.1 eV), carbonyl (C=O, ≈ 287.1 eV) and carboxyl (C=O(OH), ≈ 288.1 eV).[16] The O1s photoelectron signal in Figure 6.3C was curve fitted using the model established by Schlapak et al.[17] as follows: hydroxyl (-OH, ≈ 531 eV), ether (C-O, ≈ 532.2 eV), water (H_2O, ≈ 533.5 eV).

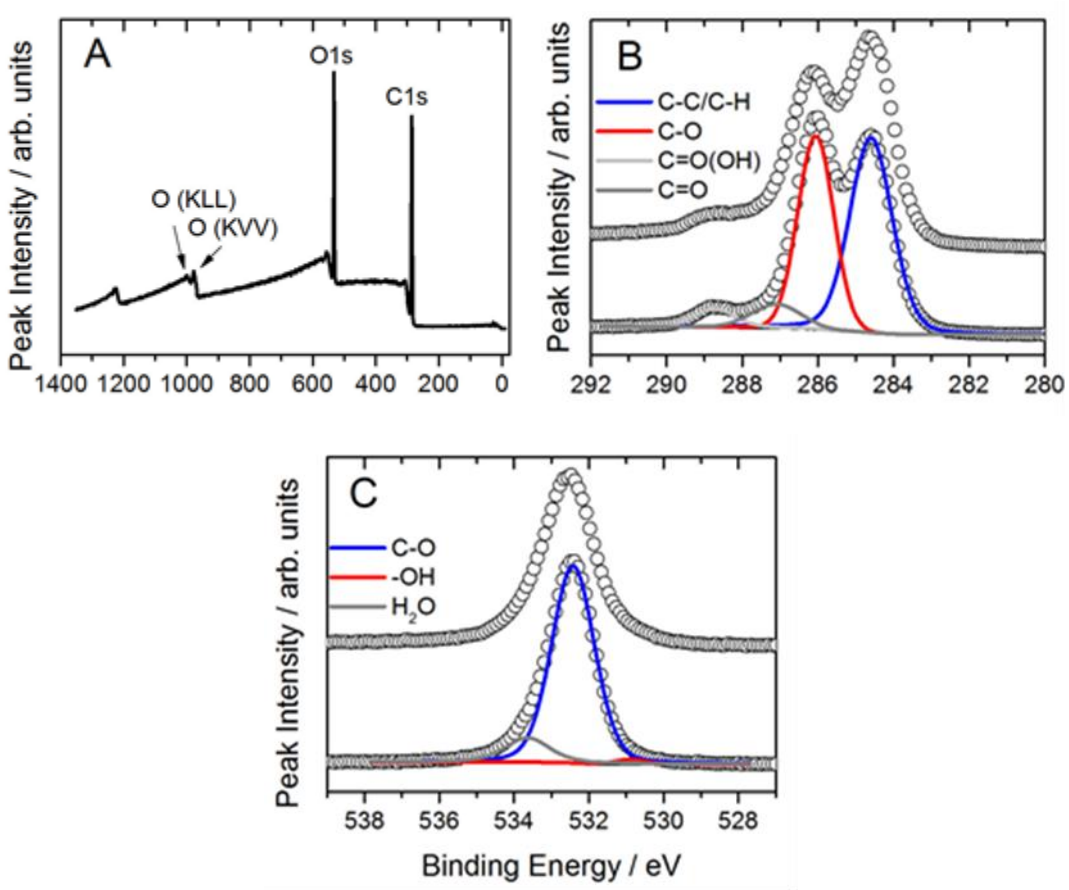

Figure 6.3. (**A**) Representative survey XPS spectra of Kolliphor® EL modification of glassy carbon. XPS core level spectra of modified substrate (**B**) C1s and (**C**) O1s. Representative curve fits are shown for C1s and O1s and for two independently investigated samples (dotted lines K1, bottom, and K2, above; Table 6.1).

The spectra shown in Figure 6.3 are consistent with PEG-like surface chemistry, with a contribution from C-O from repeated poly(ethylene glycol) units dominating the observe photoelectron signal. The presence of hydroxyl and water O1s signals suggests that trace water is present within the interface, which is to be expected as water binds strongly to PEG. XPS data are summarised in Table 6.1. Variation between samples K1 and K2 suggests some position dependence and/or sample to sample variability. Key changes in comparison to the bare glassy carbon surface are (i) an increase in O1s/C1s ratio mainly due to C-O, (ii) and increase in C1s for C-O, and (iii) an increase in O1s for C-O.

Table 6.1. XPS ratios and surface composition for two independently investigated samples with Kolliphor® EL (K1 and K2) and a bare glassy carbon substrate (GC). Peak integration methods based on literature models for C1s[16] and O1s[17] were employed.

		C1s composition / %				O1s composition / %		
Sample	**O1s/C1s**	**C-C**	**C-O**	**C=O**	**C=O(OH)**	**OH**	**H_2O**	**C-O**
K1	2.94	39.1	50.2	6.4	4.3	1.3	12.6	86.1
K2	3.12	54.7	33.8	4.8	6.7	5.3	12.8	81.9
GC	1.29	66.0	11.0	11.0	8.0	12.0	33.0	55.0

6.3 Results and discussion

6.3.1 Effects on heterogeneous electron transfer due to Kolliphor® EL grafting

The ferrocyanide ($Fe(CN)_6^{3-/4-}$) redox system is commonly used to probe the effects of surface modification of electrode surfaces on voltammetry.[18] The system was employed here to investigate the effects of attaching Kolliphor® EL to glassy carbon electrodes on the rate of electron transfer. The cyclic voltammetry of a polished 3 mm glassy carbon electrode showed a quasi-reversible response with a reversible potential (E_0) of +0.19 and a peak separation (ΔE_p) of 120 mV (Figure 6.4A).

$$Fe(CN)_6^{3-} + e^- \rightleftharpoons Fe(CN)_6^{4-} \quad (6.1)$$

Kolliphor® EL is a non-ionic surfactant used as an excipient in drug formulations in order to increase the solubility of hydrophobic therapeutics in the body.[7] An anodic

treatment of +1.6 V for 20 minutes in Kolliphor® EL at a glassy carbon electrode caused the non-ionic surfactant to graft to the electrode surface. The voltammetry for the $Fe(CN)_6^{3-/4-}$ redox couple was sensitive to the Kolliphor® EL modified carbon surface and completely suppressed the redox signal across a 1 V potential window (Figure 6.4A). Kolliphor® EL has an approximate diameter of 1-2 nm (Figure 6.1) and is assumed to form a monolayer on the carbon surface, which appears to be sufficient to severely reduce the rate of heterogeneous electron transfer. The effect can be reversed by mechanical polishing.

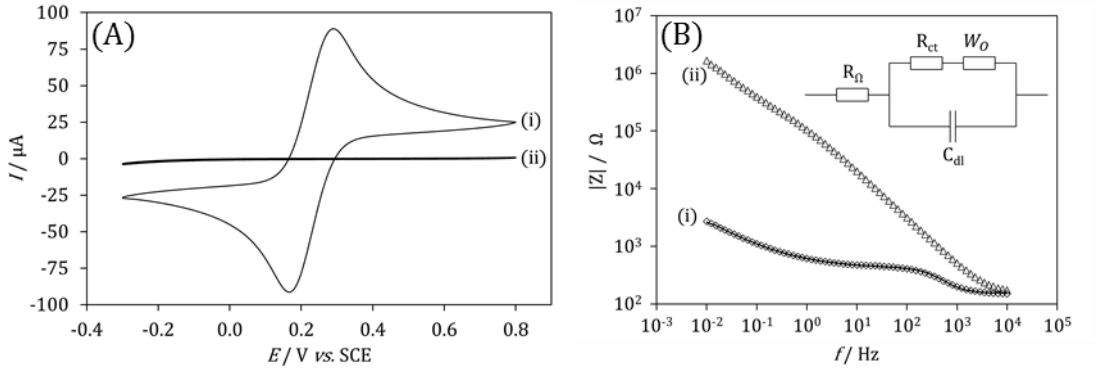

Figure 6.4. (A) Cyclic voltammogram (scan rate 50 mV s^{-1}) and (**B**) a Bode plot of an aqueous solution containing 5 mM $K_4Fe(CN)_6$, 5 mM $K_3Fe(CN)_6$ and 0.1 M KNO_3 at a 3 mm diameter glassy carbon disc electrode (i) before and (ii) after modification with Kolliphor® EL.

Electrochemical impedance analysis was used to explore the effect in the time domain and reveal kinetic information concerning the rate of electron transfer. Impedance data at an unmodified 3 mm glassy carbon electrode can be modelled satisfactorily using a Randles circuit, which consists of the solution resistance (R_Ω), the charge transfer resistance (R_{ct}), the double layer capacitance (C_{dl}) and an "Open" Warburg element (W_O) (Figure 6.4B). The "Open" Warburg element is used to describe the semi-infinite diffusion of redox species to the electrode surface and is characterised by a 45 ° linear region to the Nyquist plot at low frequencies. Equivalent circuit data fitting was performed using ZPlot Software, which gave: $R_\Omega = 154\ \Omega$, $R_{ct} = 266\ \Omega$, $C_{dl} = 1.8$ µF, $W_p = 0.5$, $W_T = 107$, and $W_R = 6310\ \Omega$.

The electrochemical impedance response at a Kolliphor® EL modified electrode was predominantly associated with capacitive charging currents. The values for solution

resistance and double layer capacitance were not significantly affected by the anodic modification. However, the Randles circuit was not a suitable model for the modified electrode and a good fit was not possible, in particular at low frequencies. It is thought that additional complexity in the system is apparent at low frequencies. This could arise due to remaining porosity in the Kolliphor® EL film, which could also be associated with some slow electron transfer occurring in the low frequency region (< 1 Hz). The Kolliphor® EL modification process strongly suppressed the electron transfer for the $Fe(CN)_6^{3-/4-}$ redox couple and trace concentrations of guest molecules (or mediators) may now be added to explore the effect of possible electron shuttling mechanisms.

6.3.2 Ferrocene mediators at Kolliphor® EL modified glassy carbon electrodes

Kolliphor® EL modified glassy carbon electrodes severely suppress the rate of the electron transfer for the hydrophilic $Fe(CN)_6^{3-/4-}$ redox couple. In contrast, a range of hydrophobic ferrocene derivatives are seemingly insensitive towards the Kolliphor® EL film and no significant changes are observed in the rate of electron transfer. This is consistent with the less hydrated ferrocene derivatives being able to penetrate into the hydrophobic Kolliphor® EL region more easily than the more hydrophilic $Fe(CN)_6^{3-/4-}$ species. Ferrocene derivatives with a more positive reversible potential (E_0) compared with ferrocyanide can be used as "electron shuttle molecules" or redox mediators. The ability of five ferrocene derivatives (ferrocene dimethanol, ferrocene acetonitrile, ferrocene acetic acid, dimethylaminomethyl ferrocene and butyl ferrocene) to act as electron shuttle molecules is investigated.

1,1'-ferrocene dimethanol ($Fc(CH_2OH)_2$) is a partially water soluble species that undergoes a one-electron oxidation. It is used here in low concentrations (0, 5, 10 and 50 μM) to lower the electron transfer impedance between the electrode and $Fe(CN)_6^{4-}$ species, which is present in high concentrations in the bulk. The voltammetric response without $Fc(CH_2OH)_2$ shows negligible oxidation current. However, a peak current of 35 μA was obtained at 50 μM concentrations, which is nearing the diffusion limited current for $Fe(CN)_6^{4-}$ oxidation at an unmodified electrode (Figure 6.5). The underlying signal for $Fc(CH_2OH)_2$ remains insignificant in this experiment, and the voltammetric response is due to a mediated electron transfer process. A systematic change in the low frequency region (< 10 Hz) of electrochemical impedance measurements is consistent

with a flow of Faradaic current arising from a mediated electron transfer process (Figure 6.5B). The analysis of electrochemical impedance data will be discussed in more detail later.

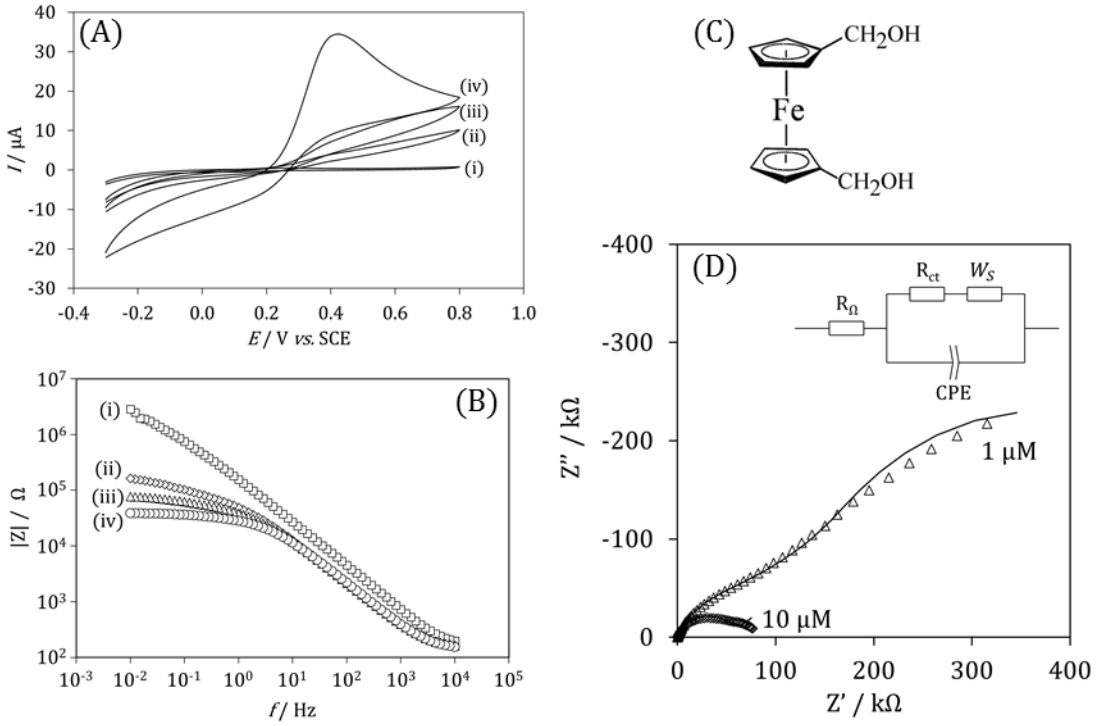

Figure 6.5. (A) Cyclic voltammogram (scan rate 50 mV s^{-1}) and **(B)** a Bode plot of a solution containing 5 mM $K_4Fe(CN)_6$, 5 mM $K_3Fe(CN)_6$ and 0.1 M KNO_3 with (i) 0 µM, (ii) 5 µM, (iii) 10 µM and (iv) 50 µM 1,1'-ferrocene dimethanol (structure shown in (**C**)). (**D**) Nyquist plot of the same system with 1 µM (△) and 10 µM (◇) 1,1'-ferrocene dimethanol. The solid line is a simulated model using the equivalent circuit shown.

Similar effects on the voltammetry are observed when using ferrocene-acetonitrile (Fc(MeCN)) as the electron shuttle molecule (Figure 6.6). However, the magnitudes of the peak oxidation currents are lower compared with ferrocene dimethanol (discussed above) and less cathodic current is observed on the reverse scan.

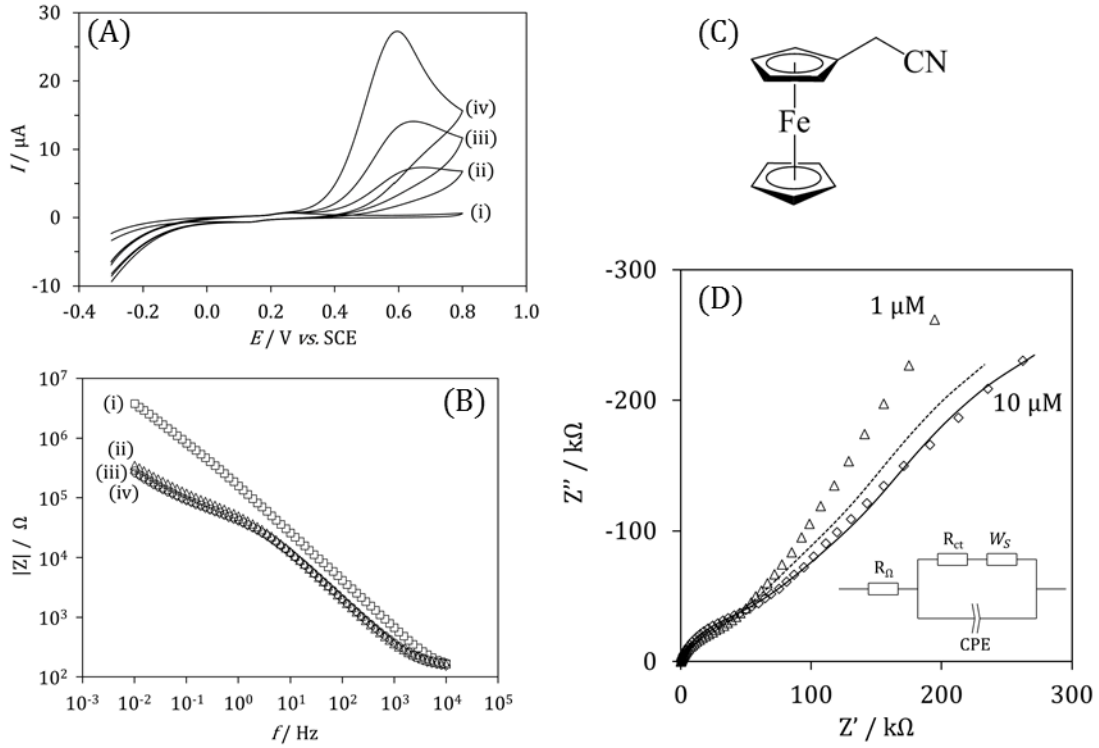

Figure 6.6. (A) Cyclic voltammogram (scan rate 50 mV s^{-1}) and **(B)** a Bode plot of a solution containing 5 mM $K_4Fe(CN)_6$, 5 mM $K_3Fe(CN)_6$ and 0.1 M KNO_3 with (i) 0 µM, (ii) 5 µM, (iii) 10 µM and (iv) 50 µM ferrocene acetonitrile (structure shown in (**C**)). (**D**) Nyquist plot of the same system with 1 µM (△) and 10 µM (◇) ferrocene acetonitrile. The solid line is a simulated model using the equivalent circuit shown.

The voltammetric data for five ferrocene derivatives at a Kolliphor® EL modified glassy carbon electrode in the presence of 5 mM $K_4Fe(CN)_6$ is summarised in Table 6.2. The reversible potential for the $Fe(CN)_6^{3-/4-}$ redox couple is +0.19 V (*vs*. SCE) (E_0), which is more negative compared with all five of the ferrocene derivatives used as electron shuttles in this investigation. If the reversible potential for the ferrocene mediator is more positive, it is thermodynamically more favourable for the ferrocene derivative to mediate the oxidation of the ferrocyanide(II) species (and less favourable to mediate the reduction of the ferricyanide(III) species). A more favourable mediated oxidation process should be accompanied by larger anodic currents. However, the magnitude of the anodic currents may also be affected by the rate of heterogeneous electron transfer for the ferrocene derivative at the Kolliphor® EL modified glassy carbon electrode. The rate of heterogeneous electron transfer can be approximated by using the peak separation of a 50 µM ferrocene derivative solution (without $Fe(CN)_6^{4-}$) at a Kolliphor® EL modified glassy carbon electrode. A wider peak separation is

indicative of slower heterogeneous electron transfer kinetics, which could limit the electron shuttle rate and lower anodic currents in the mediated oxidation process. Therefore the lower anodic peak currents for ferrocene acetonitrile compared to ferrocene dimethanol is likely to be due to a combination of slower heterogeneous electron transfer kinetics and the mediated oxidation being less thermodynamically favourable.

Table 6.2. Summary of data from voltammetry for solutions containing 50 μM ferrocene derivative in 0.1 M KNO_3 (scan rate 50 mV s^{-1}) at a Kolliphor® EL modified glassy carbon electrode. Note that signals, in particular for ferrocene acetonitrile, dimethylaminomethyl ferrocene and *n*-butyl ferrocene, are complicated by interactions with the electrode surface.

	E_0^a / V *vs.* SCE	**ΔE_p^a / V**
Ferrocene-dimethanol	0.28	0.11
Ferrocene-acetonitrile	0.21	0.22
Ferrocene acetic acid	0.20	0.22
Dimethylamino-methyl ferrocene	0.27	0.10
n-butyl ferrocene	0.22	0.04

Based on the data from Table 6.2, ferrocene acetonitrile and ferrocene acetic acid should have similar electron shuttle abilities towards the mediated oxidation of $K_4Fe(CN)_6$. However, although ferrocene acetic acid shows signs of mediating the oxidation of $K_4Fe(CN)_6$, the anodic currents are considerably lower in cyclic voltammetry (Figure 6.7). The seemingly poor electron shuttle ability can be attributed to the mediator species existing as a negatively charged ferrocene acetate at neutral pH. The electrostatic repulsion between the anionic mediator and the $Fe(CN)_6^{4-}$ complex slows the rate of the bimolecular electron transfer reaction. Electrochemical impedance spectroscopy at the equilibrium potential indicates that a higher ferrocene acetic acid concentration leads to lower impedance at frequencies less than 10 Hz.

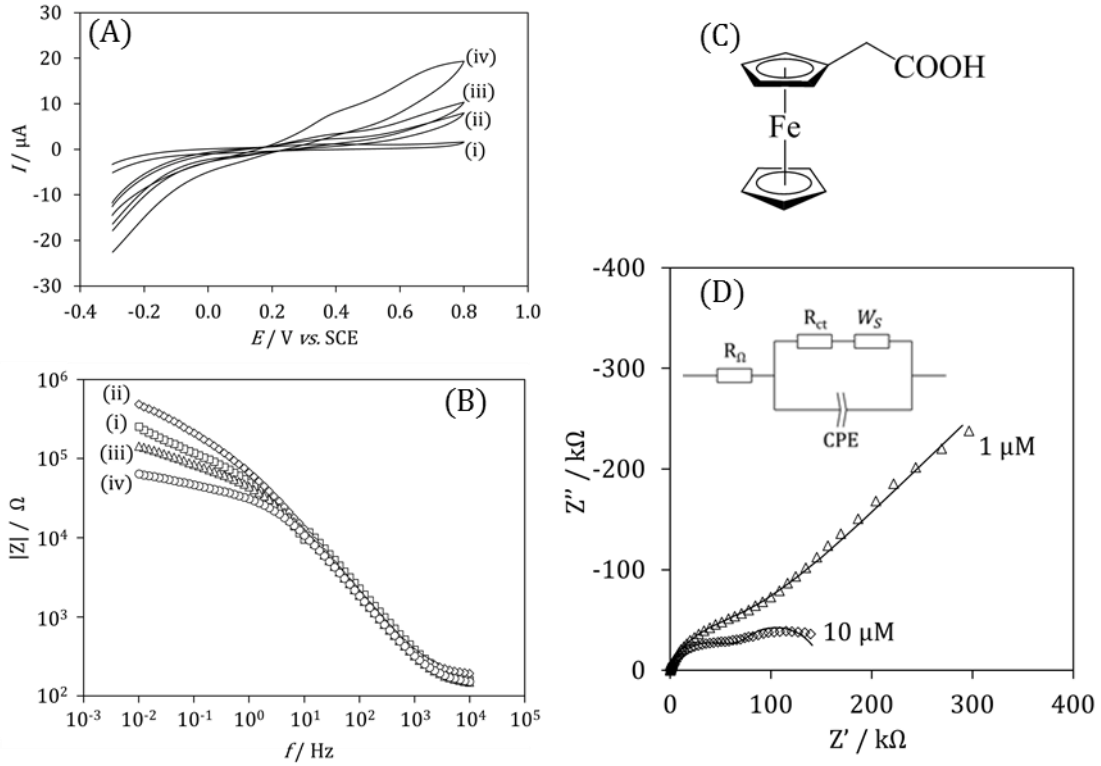

Figure 6.7. (A) Cyclic voltammogram (scan rate 50 mV s^{-1}) and **(B)** a Bode plot of a solution containing 5 mM $K_4Fe(CN)_6$, 5 mM $K_3Fe(CN)_6$ and 0.1 M KNO_3 with (i) 0 µM, (ii) 5 µM, (iii) 10 µM and (iv) 50 µM ferrocene acetic acid (structure shown in (**C**)). (**D**) Nyquist plot of the same system with 1 µM (△) and 10 µM (◇) ferrocene acetic acid. The solid line is a simulated model using the equivalent circuit shown.

Dimethylaminomethyl ferrocene is an oil at room temperature and exists as a cationic species in aqueous solution at pH 7. The cyclic voltammetry of 5 mM $K_4Fe(CN)_6$ with up to 50 µM dimethylaminomethyl ferrocene is consistent with redox mediator activity (Figure 6.8). As the concentration of the ferrocene redox mediator increases, the peak current shifts to a more negative potential. A sharp anodic peak is observed at 50 µM dimethylaminomethyl ferrocene concentrations, with a peak current similar to that found for a 5 mM $K_4(CN)_6$ solution at an unmodified glassy carbon electrode. This implies the dimethylaminomethyl ferrocene derivative is an effective electron shuttle molecule. Table 6.2 suggests that the electron shuttle ability for dimethylaminomethyl ferrocene should be similar to 1,1'-ferrocene dimethanol, however, the former ferrocene derivative causes larger anodic currents and therefore appears to be a more effective mediator. The unusually sharp peak and larger anodic currents may be attributed to the cationic dimethylaminomethyl ferrocene species having favourable electrostatic interactions with the ferrocyanide species and the electrode surface. At

high concentrations, the oil may aggregate at the electrode surface, which could be partially responsible for the sharp anodic peak.

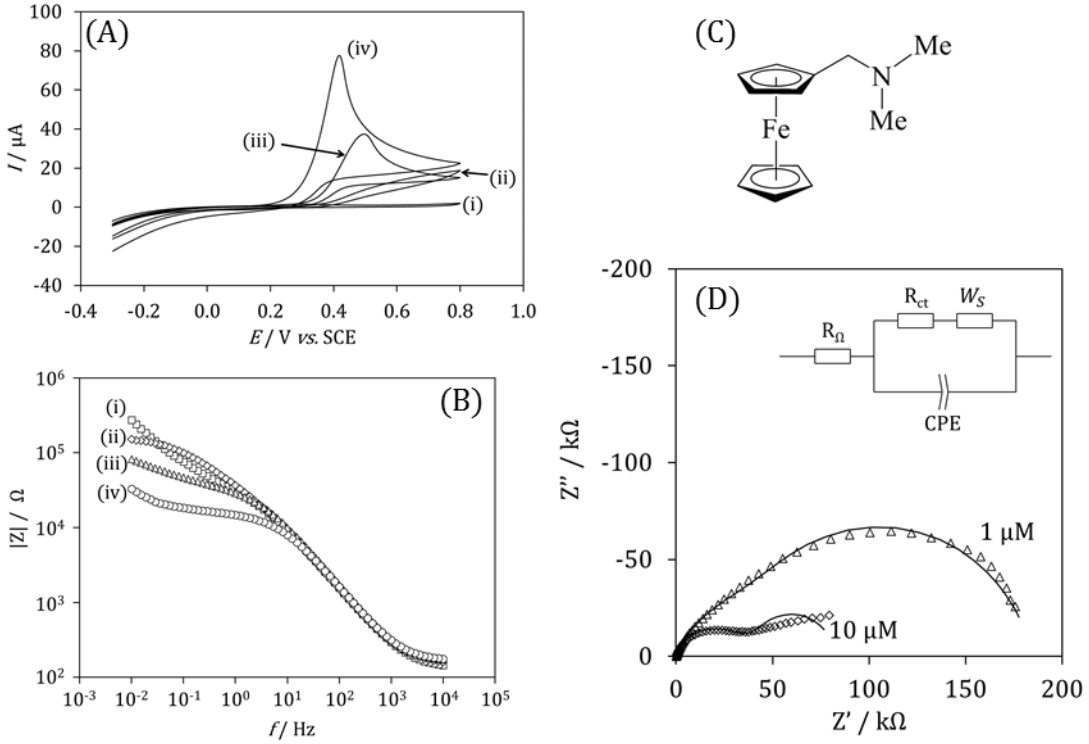

Figure 6.8. (A) Cyclic voltammogram (scan rate 50 mV s^{-1}) and **(B)** a Bode plot of a solution containing 5 mM $K_4Fe(CN)_6$, 5 mM $K_3Fe(CN)_6$ and 0.1 M KNO_3 with (i) 0 µM, (ii) 5 µM, (iii) 10 µM and (iv) 50 µM dimethylaminomethyl ferrocene (structure shown in (**C**)). (**D**) Nyquist plot of the same system with 1 µM (△) and 10 µM (◇) dimethylaminomethyl ferrocene. The solid line is a simulated model using the equivalent circuit shown.

The fifth ferrocene derivative to be examined as a redox mediator was *n*-butyl ferrocene. Similar to dimethylaminomethyl ferrocene, it exists as an oil at room temperature. Due to its hydrophobic nature it is only partially soluble in aqueous solution. A 50 µM nominal concentration caused a mediated response with a sharp peak current of 57 µA at +0.26 V (*vs*. SCE), which is likely to be due to aggregation of the lipophilic mediator at the Kolliphor® EL modified glassy carbon electrode surface (Figure 6.9).

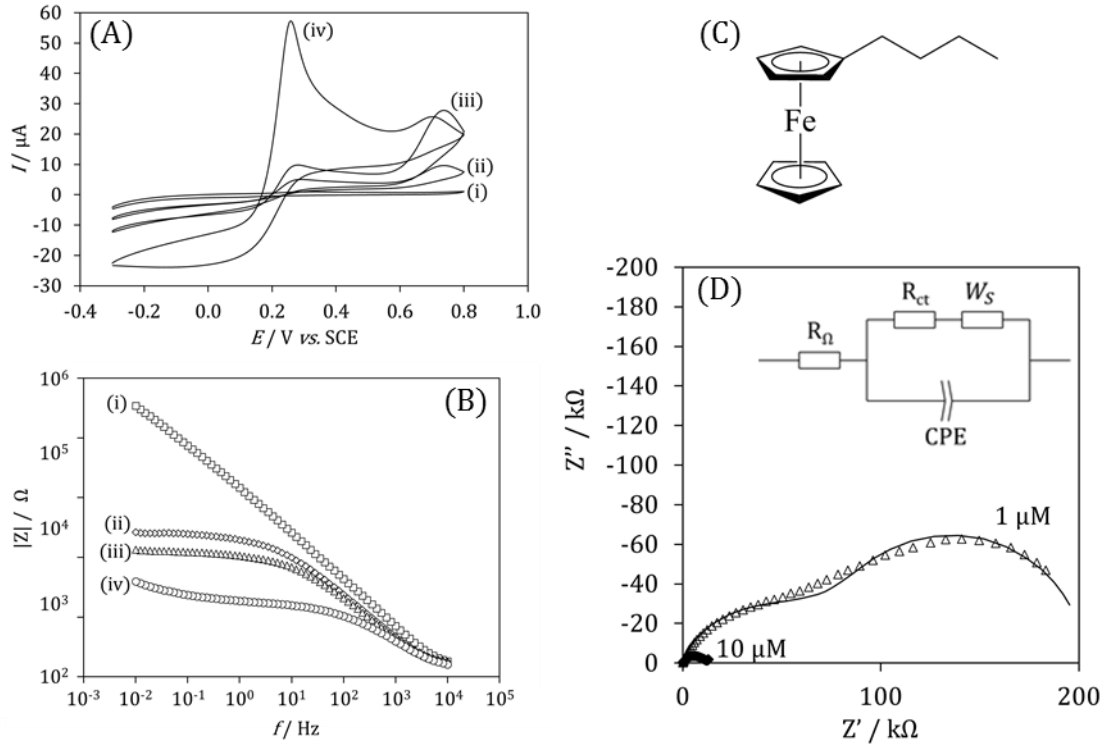

Figure 6.9. (A) Cyclic voltammogram (scan rate 50 mV s^{-1}) andn (B) a Bode plot of a solution containing 5 mM $K_4Fe(CN)_6$, 5 mM $K_3Fe(CN)_6$ and 0.1 M KNO_3 with (i) 0 µM, (ii) 5 µM, (iii) 10 µM and (iv) 50 µM *n*-butyl ferrocene (structure shown in (**C**)). (**D**) Nyquist plot of the same system with 1 µM (△) and 10 µM (◇) *n*-butyl ferrocene. The solid line is a simulated model using the equivalent circuit shown.

Five ferrocene derivatives have been employed to investigate their ability electron shuttle molecules or redox mediators towards the oxidation of potassium ferrocyanide ($K_4Fe(CN)_6$) at Kolliphor® EL modified glassy carbon electrodes. All five ferrocene derivatives have a reversible potential more positive than for potassium ferrocyanide, and all exhibited some electron shuttle ability. The mediator ability was improved for ferrocene derivatives with (i) a more positive reversible potential, (ii) a faster rate of heterogeneous electron transfer for the ferrocene derivative at the Kolliphor® EL modified glassy carbon electrode, (iii) an ability to aggregate or bind to the Kolliphor® EL layer, and (iv) favourable electrostatics between the mediator and $Fe(CN)_6^{3-/4-}$ couple.

6.3.3 Mechanism of ferrocene mediators at Kolliphor® EL modified electrode

Electrochemical impedance spectroscopy (EIS) was used to help extract mechanistic information concerning the mediated oxidation of potassium ferrocyanide ($K_4Fe(CN)_6$) at a Kolliphor® EL modified glassy carbon electrode. The equivalent circuit used for data fitting is shown in Figure 6.10. R_Ω is the solution resistance and R_{ct} is the charge transfer resistance. A constant phase element (CPE) was used to account for non-ideal capacitive behaviour at the Kolliphor® EL modified surface, which arises due to heterogeneity and porosity in the Kolliphor® EL layer. A short (or closed) Warburg (W_s) is a circuit element used to describe a diffusion limited process with a finite diffusion layer thickness. The presence of $K_4Fe(CN)_6$ in the bulk solution donates electrons to the electro-generated ferrocenium species, which limits the diffusion layer thickness. If the $K_4Fe(CN)_6$ concentration is not significantly depleted, for example at low ferrocene mediator concentrations, the use of a short Warburg element is an acceptable description of the mechanism.

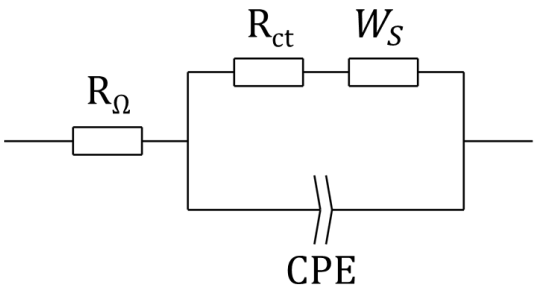

Figure 6.10. Equivalent circuit employed for data fitting analysis to represent electrochemical impedance measurements at a Kolliphor® EL modified glassy carbon electrode.

Table 6.3. Summary of data from electrochemical impedance spectroscopy measurements taken at equilibrium potential from solutions containing 5 mM $K_4Fe(CN)_6$, 5 mM $K_3Fe(CN)_6$ in 0.1 M KNO_3 and with ferrocene derivative at stated concentration. Parameters obtained using equivalent circuit in Figure 6.10 with W_P = 0.5 and $\delta_{app} = (W_T \times D)^{1/2}$ with $D = 0.6 \times 10^{-9}$ m^2 s^{-1} as an approximate value[19] used for all ferrocene derivatives. A short Warburg element was selected to reflect the electron transfer to $Fe(CN)_6^{3-/4-}$.

	[Fc] / μM	R_Ω **/ Ω**	R_{ct} **/ Ω**	W_R **/ kΩ**	W_T **/ s**	CPE_T **/ μF**	CPE_P	δ_{app} **/ μm**
Ferrocene-dimethanol	1	127	9177	524	38.9	2.84	0.796	153
	10	134	5073	268	5.16	2.78	0.798	56
Ferrocene-acetonitrile	1	137	2958	690	82.5	2.39	0.816	222
	10	150	5332	635	67.3	2.30	0.835	201
Ferrocene acetic acid	1	123	7815	1720	393	2.32	0.843	486
	10	132	6063	89	11.8	2.58	0.832	84
Dimethylamino-methyl ferrocene	1	135	6180	123	2.82	4.01	0.795	41
	10	138	3092	335	19.0	2.69	0.838	107
n-butyl ferrocene	1	130	6557	139	8.14	1.82	0.789	70
	10	127	1117	127	222	3.94	0.743	365

The data is Table 6.3 summarises the results from quantitative data fitting using the equivalent circuit shown in Figure 6.10. Data fitting was performed using ZView Software. The solution resistance (R_Ω) did not change to a significant degree throughout all experiments. Similarly, the apparent capacitance (CPE_T) for the Kolliphor® EL modified electrode remains reasonably constant for all ferrocene derivatives and is similar to the double layer capacitance for an unmodified 3 mm glassy carbon electrode. There is not a clear trend in the change in charge transfer resistance (R_{ct}) as a function of mediator concentration nor a correlation between R_{ct} and the structure of the ferrocene derivative. The W_T parameter for the short Warburg element is linked to the apparent diffusion layer thickness (δ_{app}) of the ferrocene derivative by equation 6.2.

$$\delta_{app} = (W_T \times D)^{\frac{1}{2}} \qquad (6.2)$$

The diffusion coefficient (D) was approximated to be 0.6×10^{-9} m^2 s^{-1} for all ferrocene derivatives and allowed an approximate diffusion layer thickness to be determined.[19] The values of δ_{app} ranged from 41 μm to 486 μm, which is considerably larger than the expected thickness of the Kolliphor® EL grafted layer (< 10 nm). It is

therefore concluded that the bimolecular reaction between ferrocene mediator and $Fe(CN)_6^{3-/4-}$ is likely to occur well within the solution phase (Figure 6.2). The large values of the apparent diffusion layer thickness (δ_{app}) could suggest that other physical processes, such a slow bimolecular electron transfer or additional heterogeneous electron transfer, may be hidden within the data. As the concentration of dimethylaminomethyl ferrocene and *n*-butyl ferrocene increases, the apparent diffusion layer thickness also increases, which can be attributed to a greater depletion of the $Fe(CN)_6^{4-}$ concentration from the electrode surface. However, ferrocene dimethanol, ferrocene acetonitrile and ferrocene acetic acid show a *decrease* in δ_{app} as the concentration of ferrocene derivative is increased, which is also suggestive of the occurrence of underlying physical processes that have not been accounted for. These trends are also observed in the corresponding data for 5 μM and 50 μM ferrocene derivative (data not shown).

The apparent diffusion layer thickness can be used to gauge the efficiency of the electron shuttling process, where a short diffusion layer thickness corresponds to efficient mediated oxidation (assuming no depletion of the $Fe(CN)_6^{4-}$ concentration, which is reasonable at low ferrocene derivative concentration). The electron shuttling ability for the five ferrocene derivatives at 1 μM concentration was dimethylaminomethyl ferrocene > *n*-butyl ferrocene > ferrocene dimethanol > ferrocene acetonitrile > ferrocene acetic acid. The most effective redox mediator was found to be dimethylaminomethyl ferrocene, which exhibited the smallest apparent diffusion layer thickness of $\delta_{app} = 41$ μm at 1 μM concentration. It is likely that dimethylaminomethyl ferrocene can bind or accumulate in the Kolliphor® EL layer and favourable electrostatic interactions can facilitate the electron shuttle process.

6.4 Conclusions

This chapter describes an anodic grafting method to attach Kolliphor® EL to glassy carbon electrode surfaces and demonstrates that complex PEGylated systems can be attached to carbon substrates. The voltammetry of $Fe(CN)_6^{3-/4-}$ was entirely suppressed at a Kolliphor® EL modified glassy carbon electrode, however, anodic currents could

be restored by addition of suitable hydrophobic ferrocene mediators. Kolliphor® EL is used to increase the solubility of hydrophobic drug molecules and allows hydrophobic species to diffuse across the membrane, whilst excluding hydrophilic species. Ferrocene derivatives have been shown to carry electrons across the Kolliphor® EL interface and the electron shuttle ability for five ferrocene derivatives has been assessed for the mediated oxidation of $Fe(CN)_6^{4-}$.

The cyclic voltammetry of the mediated process appears to show an irreversible oxidation process. The reversible potentials for all five ferrocene derivatives is more positive than for $Fe(CN)_6^{3-/4-}$ and the mediated oxidation process is therefore faster than the reduction process, which leads to the observed irreversibility in the cyclic voltammogram. The electron shuttle efficiency was improved for ferrocene derivatives with a more positive reversible potential, exhibiting faster heterogeneous electron transfer across the Kolliphor® EL film, an ability to aggregate in the Kolliphor® EL film due to hydrophobicity, and favourable electrostatic interactions. Dimethylaminomethyl ferrocene was found to be the most effective mediator and could be detected at very low concentrations (< 1 μM) in the future.

The Kolliphor® EL modified glassy carbon electrodes could be used to test a wider range of different hydrophobic electron shuttle molecules with an aim of electroanalytical detection of low concentration hydrophobic redox active molecules, such as drugs. A wider range of hydrophobic redox mediators could be tested with an aim to lower the limit of detection of the mediator species.

6.5 References

1. D. Mandler and S. Kraus-Ophir, *Journal of Solid State Electrochemistry*, 2011, **15**, 1535-1558.
2. O. I. Aksimentyeva, O. I. Konopelnyk and D. O. Poliovyi, *Molecular Crystals and Liquid Crystals*, 2011, **536**, 160-165.
3. C. E. Hotchen, I. J. Maybury, G. W. Nelson, J. S. Foord, P. Holdway and F. Marken, *Physical Chemistry Chemical Physics*, 2015, **17**, 11260-11268.
4. H. Maeda, Y. Yamauchi, M. Yoshida and H. Ohmori, *Analytical Sciences*, 1995, **11**, 947-952.
5. A. J. Downard, *Electroanalysis*, 2000, **12**, 1085-1096.
6. H. Maeda, Y. Yamauchi, M. Hosoe, T. X. Li, E. Yamaguchi, M. Kasamatsu and H. Ohmori, *Chemical & Pharmaceutical Bulletin*, 1994, **42**, 1870-1873.
7. H. Gelderblom, J. Verweij, K. Nooter and A. Sparreboom, *European Journal of Cancer*, 2001, **37**, 1590-1598.
8. R. Berthelsen, R. Holm, J. Jacobsen, J. Kristensen, B. Abrahamsson and A. Mullertz, *Molecular Pharmaceutics*, 2015, **12**, 1062-1071.
9. E. O. Barnes, G. E. M. Lewis, S. E. C. Dale, F. Marken and R. G. Compton, *Analyst*, 2012, **137**, 1068-1081.
10. X. Wang and G. Pang, *Sensor Review*, 2015, **35**, 30-42.
11. Y. Si, Z. Sun, N. Zhang, W. Qi, S. Li, L. Chen and H. Wang, *Analytical Chemistry*, 2014, **86**, 10406-10414.
12. H. Maeda, M. Hosoe, T. X. Li, M. Itami, Y. Yamauchi and H. Ohmori, *Chemical & Pharmaceutical Bulletin*, 1996, **44**, 559-564.
13. H. Maeda, M. Itami, Y. Yamauchi and H. Ohmori, *Chemical & Pharmaceutical Bulletin*, 1996, **44**, 2294-2299.
14. C. D. Wagner, L. E. Davis, M. V. Zeller, J. A. Taylor, R. H. Raymond and L. H. Gale, *Surface and Interface Analysis*, 1981, **3**, 211-225.
15. C. D. Wagner, Appendix in *Practical Surface Analysis*, eds. D. Briggs and M. P. Seah, J. Wiley and Sons, New York, 2nd edn., 1990, vol. 1.
16. S. Ferro, M. Dal Colle and A. De Battisti, *Carbon*, 2005, **43**, 1191-1203.
17. R. Schlapak, D. Caruana, D. Armitage and S. Howorka, *Soft Matter*, 2009, **5**, 4104-4112.
18. L. Xiong, C. Batchelor-McAuley, K. R. Ward, C. Downing, R. S. Hartshorne, N. S. Lawrence and R. G. Compton, *Journal of Electroanalytical Chemistry*, 2011, **661**, 144-149.
19. R. W. French, A. M. Collins and F. Marken, *Electroanalysis*, 2008, **20**, 2403-2409.

Chapter 7: One-step electroless growth of nano-fibrous platinum catalyst from "paint-on" $PtCl_6^{2-}$ solution in poly(ethylene glycol)

Chapter abstract

A one-step electroless deposition of nano-fibrous platinum electro-catalysts is developed, which utilises the mild reducing nature of poly(ethylene glycol) (PEG). An inorganic platinum precursor (K_2PtCl_6) is dissolved in PEG and applied to a tin-doped indium oxide (ITO) glass substrate. The deposition process is conducted by a rapid heating to 500 °C in air. Upon heating, PEG acts as the reducing agent to form nano-fibrous platinum, but also evaporates from the system. After 30 min of treatment, all organic species had been removed to leave an electrochemically active platinum deposit. The deposit exhibited platinum oxidation and hydrogen adsorption peaks characteristic of a polycrystalline platinum surface. A slight increase in catalytic activity (per electrochemically active surface area) is observed towards methanol oxidation compared to a conventional 2 mm polycrystalline platinum macro-disc electrode.

Chapter publications

This chapter has been published in:
C. E. Hotchen, G. Attard, S. D. Bull and F. Marken, *Electrochim. Acta*, 2014, **137**, 484-488.

Special acknowledgements

I would like to thank Gary Attard for his expert advice on methanol oxidation at platinum electrodes.

Chapter contents

7 One-step electroless growth of nano-fibrous platinum catalyst from "paint-on" $PtCl_6^{2-}$ solution in poly(ethylene glycol)

7.1 Introduction

Platinum is known for its high catalytic activity towards many substrates, such as in the oxygen reduction reaction, hydrogen evolution reaction and towards methanol oxidation. Consequently platinum has found many applications as an electrode material in fuel cells,[1] solar cells,[2] and in water electrolysis systems.[3] Catalysts are often expensive materials, and it is important to develop systems where the catalytic activity (and surface area) is high, whilst keeping the amount of catalyst used to a minimum. Nanoparticles are considered to be useful catalytic materials since they have a high active surface area whilst keeping the bulk (inactive) area to a minimum.

Single crystal experiments have shown that each facet of a platinum crystal can have varying degrees of catalytic activity. For example, Silva *et al.* report that a Pt(100) surface is most active towards the electro-oxidation of D-mannitol.[4] However, Herrero *et al.* report that the highest current for methanol electro-oxidation is observed on a Pt(110) surface. The corrugated Pt(110) surface has many highly reactive sites, however, interactions between the platinum surface and the electrolyte anions also play a role in the oxidation current observed.[5] It is therefore very important to be able to control the shape and size of platinum deposits to maximise the catalytic activity.

The growth of platinum nanoparticles has been widely studied and methods to control the shape of nanoparticles have been reviewed.[6-8] Ye *et al.* use a pulse electrodeposition method to show how the shape of platinum nano-crystals can be influenced by additives. A high molecular weight poly(ethylene glycol), PEG10000, was found to cause the growth of "clump-like crystal aggregations".[9] The formation of platinum nano-flowers has been reported on carbon substrates[10] and on tin-doped indium oxide (ITO) glass[11] from sulphuric acid solutions. Thin metal layers can also be formed using the Pechini method (also known as the polymeric precursor method).[12] This process

involves the calcination of a metal salt precursor dissolved in ethylene glycol in the presence of citric acid, and has been used to form platinum electro-catalysts.[13]

Carbon is commonly used as a substrate for platinum electrocatalysts, in particular as a cathode in fuel cells where platinum is catalytic towards the oxygen reduction reaction (ORR).[14-16] However, alternative materials, such as ITO glass, are being investigated as a more stable scaffold material.[17,18] Pt deposits on ITO glass have also been used as an effective counter electrode in dye-sensitized solar cell applications.[11] Literature reports suggest that alloying tin into platinum improves the activity of the catalyst towards methanol oxidation.[19,20] However, only a limited increase in the catalytic activity of platinum on ITO has been observed compared with bulk polycrystalline platinum.[21]

The polyol process is a method where an inorganic metal precursor solution is dissolved in a polyol solution and heated under reflux above 85 °C. The polyol, often ethylene glycol, acts as a reducing agent to form metal colloids, which are stabilised in solution by the polyol and can be later filtered for use in catalysis.[14] The high dielectric constant for polyols allows good solubility for a number of inorganic precursors, which makes the technique suitable for the synthesis of a wide range of metal nanoparticles, including platinum.[22] Furthermore, optimising the reaction conditions and the use of additives in the reaction mix can give good control over the size and shape of the colloids,[23-26] which are two important properties that can affect the catalytic activity of the particles.[7]

The synthetic route for the formation of nano-catalysts should be kept as simple as possible and avoid complex purification steps that add cost to the process. One-step processes, which do not require the use of inert atmospheres, are therefore desirable. The non-toxic, non-volatile and reducing properties of poly(ethylene glycol) are utilised in this chapter to develop a one-step method for the electroless deposition of nano-fibrous platinum catalysts, which are formed directly by the atmospheric thermolysis of a $PtCl_6^{2-}$ precursor. The electrochemically active surface area of Pt nano-fibrous deposits is determined and the catalytic activity of the platinum deposits towards methanol electro-oxidation is investigated.

7.2 Experimental

7.2.1 Chemical reagents

Poly-(ethylene-glycol) (Sigma-Aldrich, average molecular weight = 200 g mol^{-1}) was used as the solvent for nanoparticle preparation. Potassium hexachloroplatinate(IV) (K_2PtCl_6, Sigma-Aldrich, 99.99 % metal basis) was used as the precursor for Pt deposits with an indium-tin-oxide (ITO) glass substrate (Image Optics, Basildon, 15 Ohm per square). Sulphuric acid (H_2SO_4, BDH, 98 %) and methanol (MeOH, Fisher Scientific, HPLC Grade), were used as analytes to investigate the structure and catalytic activity of the Pt deposits, respectively.

7.2.2 Instrumentation

Heating was performed using a TSH12 furnace (Elite Thermal Systems Ltd.). Field emission scanning electron microscopy (FESEM) images were taken using a JEOL FESEM6301F microscope. All electrochemical measurements were performed using an Autolab PGSTAT12 potentiostat (Autolab, Utrecht, NL) and using a three-electrode configuration with a platinum wire counter electrode and KCl-saturated calomel reference electrode (SCE) at room temperature (20 $\pm$ 2 °C). The GPES software package (version 4.9005, Autolab, Utrecht, NL) was employed for data acquisition with a potential step of 1 mV.

7.2.3 Procedure for nanoparticle fabrication

A solution of either 5 mM, 10 mM, or 20 mM potassium hexachloroplatinate(IV) (K_2PtCl_6) was prepared by stirring in PEG200 at room temperature. Sonication and heating were avoided. A 20 μL volume of the resulting solution was placed on the ITO glass substrate and distributed over an area of ca. 1 cm^2. The sample temperature was ramped (10 °C per minute) from room temperature to 500 °C and then maintained for 30 minutes. The samples were gradually cooled to room temperature and rinsed with deionised water (resistivity 18.2 MΩ cm) to remove any remaining soluble inorganics. The structure of the platinum deposits was observed using FESEM imaging, and

energy-dispersive X-ray (EDX) analysis was used for elemental analysis. The crystallinity and the electrochemically active surface area (ESA) of the Pt deposits were determined using cyclic voltammetry in aqueous 0.5 M H_2SO_4 solution.

7.3 Results and discussion

7.3.1 Electroless formation of nano-fibrous platinum from PEG solution

The thermolysis of K_2PtCl_6 solutions in PEG200 yielded platinum deposits on ITO-coated glass substrates. Figure 7.1A and 7.1B show FESEM images for the nanofibrous platinum (appearing as micron-sized aggregates of smaller nano-scale fibres) formed from 10 mM $PtCl_6^{2-}$ solution. EDX analysis (not shown) of the deposit confirmed that the fibrous deposit was composed of Pt metal without any significant traces of K or Cl residues from the precursor.

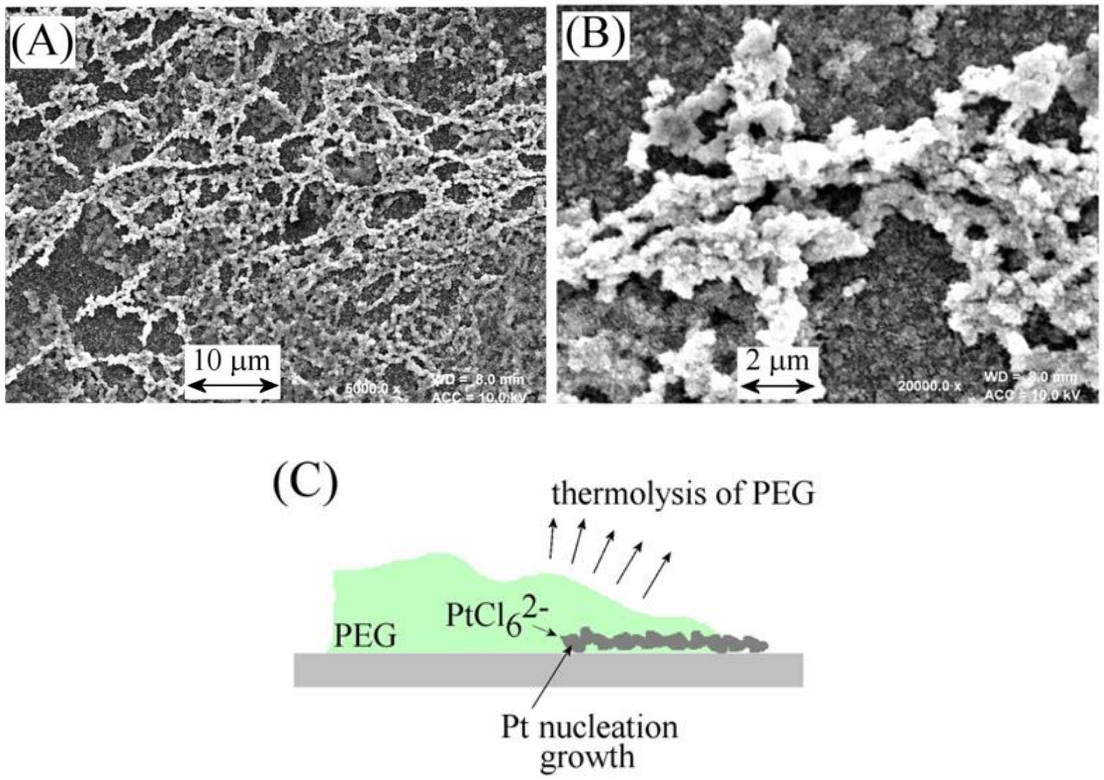

Figure 7.1. FESEM images of Pt deposits from thermolysis of 10 mM K_2PtCl_6 / PEG200 solution at (**A**) 5,000× and (**B**) 20,000× magnification. (**C**) Schematic drawing of the thermolysis process.

The surface coverage appeared to increase with $PtCl_6^{2-}$ concentration with the characteristic nanofibrous appearance remaining. PEG is a mild reducing agent, which reduces the Pt(IV) in a multi-step process to Pt metal with an increasing rate as the temperature is elevated. The high temperatures also cause the polymer solvent to evaporate (boiling point ~250 ^oC[27]) and hence prevent further reactions from occurring. A schematic drawing summarising this complex multi-step mechanism is shown in Figure 7.1C.

7.3.2 Voltammetric characterisation of nano-fibrous platinum in H_2SO_4

The platinum deposits on ITO were investigated by cyclic voltammetry in aqueous 0.5 M H_2SO_4 in order to determine the electrochemically active surface area of the electrodes (Figure 7.2A). The two peaks at -0.09 V and -0.17 V (*vs.* SCE) correspond to weak and strong H adsorption (H_{ads}) on the Pt surface consistent with poly-crystalline bulk platinum (Figure 7.2B). Repeated cycling up to +1.3 V (*vs.* SCE) helped to clean and activate the Pt surface, which caused the H_{ads} peaks to become more clearly resolved. The hydrogen evolution reaction (HER) occurs at potentials more negative than -0.21 V (*vs.* SCE).

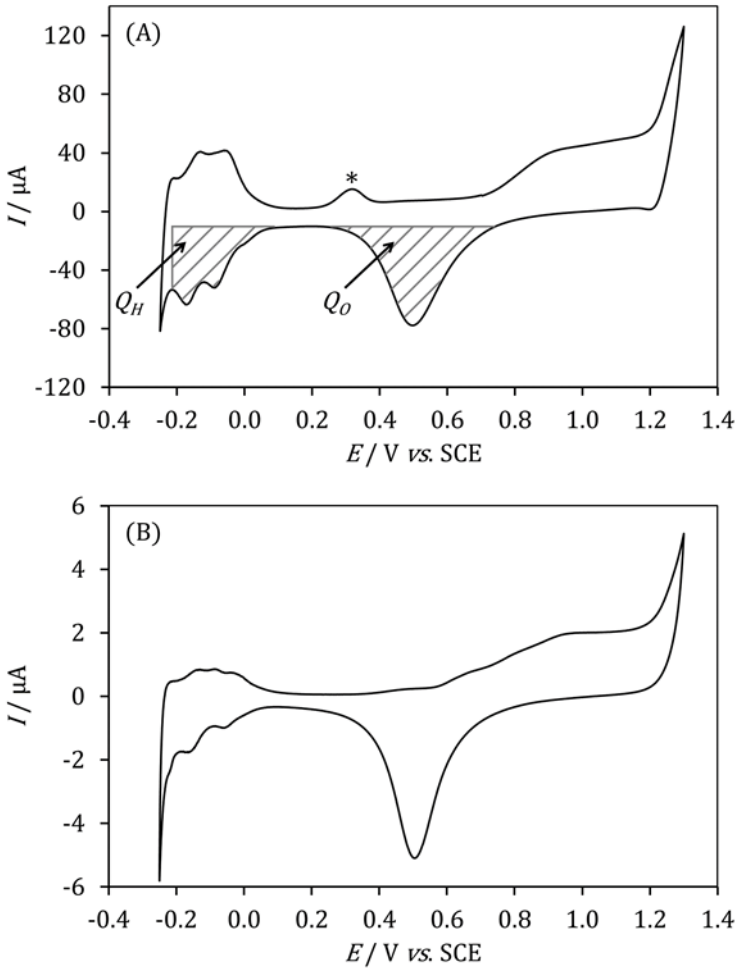

Figure 7.2. (**A**) Cyclic voltammograms (scan 5, scan rate 5 mV s^{-1}) for the platinum deposit (formed from 20 mM K_2PtCl_6) immersed in 0.5 M H_2SO_4. (**B**) As above but for a conventional 2 mm diameter Pt disc electrode.

The oxidation of the platinum surface and back reduction to platinum metal is centred at approximately +0.7 V (*vs*. SCE). A further anodic process occurs at +1.2 V (*vs*. SCE), which is indicative of the electrolyte oxidation. A peak response at +0.3 V (*vs.* SCE) (indicated by *) is observed in addition to the conventional platinum processes and is attributed to an interaction with the underlying ITO substrate. The same peak response has been reported by Liu *et al*..[28] The peak at +0.3 V (*vs.* SCE) is only observed after the potential has been swept into the hydrogen evolution region and therefore could be linked to the ITO substrate being reduced.

The electrochemically active surface area (ESA) of the Pt deposits can be calculated using H-adsorption peaks,[29] carbon monoxide oxidation[30], or (with less precision) the PtO_x/PtOH desorption [31] region of the cyclic voltammogram. In the H-adsorption region

of the cyclic voltammogram it can be assumed that hydrogen achieves a full monolayer coverage by forming 1:1 linkages with every electrochemically active site on platinum. The amount of hydrogen adsorbed is therefore proportional to the electrochemically active surface area of the electrode and can be calculated by using the charge under the H-adsorption peaks. A similar methodology can be followed when using the PtO_x/PtOH desorption peak, however, this is less reliable since oxygen can form multiple oxide layers. The charge under both the PtO_x/PtOH desorption peak (Q_O) and the charge in the H_{ads} region (Q_H) were calculated. However, only the more reliable Q_H value was used to calculate the ESA (see deviations in Q_O/Q_H in Table 7.1). The charge density used was 210 μC cm^{-2} [7] and data are summarised in Table 7.1.

Table 7.1. Summary of the electrochemical data (obtained in 0.5 M H_2SO_4 or in 0.5 M H_2SO_4 /0.5 M MeOH) and electrochemically active surface area (ESA, from H_{ads} region assuming 210 μC cm^{-2} [7]) and methanol oxidation catalysis data (see text) for nanofibrous Pt deposits on ITO with different catalyst loadings compared to a conventional 2 mm diameter Pt disc electrode.

	Q_H: Charge under $H_{adsorption}$ region / mC	**Q_O: Charge under $(PtO_x/PtOH)_{desorption}$ peak / mC**	**Q_O/Q_H**	**ESA / cm^2**	**Current density J_p for MeOH oxidation / μA cm^{-2}**
2 mm diameter Pt disc	0.05	0.15	2.93	0.24	50.9
Sample 1 (5 mM $PtCl_6^{2-}$)	1.02	1.79	1.75	4.87	96.5
Sample 2 (10 mM $PtCl_6^{2-}$)	1.23	2.31	1.88	5.86	79.7
Sample 3 (20 mM $PtCl_6^{2-}$)	2.14	3.64	1.70	10.2	106

The roughness factor is a dimensionless parameter often used to describe the surface roughness of a material and is calculated using equation 7.1.

$$\text{Roughness factor} = \frac{\text{Electrochemically active surface area}}{\text{Geometric surface area}} \quad (7.1)$$

The estimate of electrochemically active surface area suggests a roughness factor of ~8 for a 2 mm diameter platinum disc electrode. A substantially higher roughness factor was found for all nano-fibrous samples. A positive correlation between $PtCl_6^{2-}$ concentration and ESA was found, which, given the similar feature size for nano-fibrous deposits, suggests that the amount of platinum on the ITO surface increases with precursor concentration. Interestingly, the Q_O/Q_H ratio seems to be lower for the nano-fibrous deposits, which could be linked to curvature or disorder effects,[32] or perhaps more likely to substrate effects such as slower growth of the oxide film on ITO.

7.3.3 Voltammetric characterisation of nano-fibrous platinum in the catalytic oxidation of methanol

The catalytic electro-oxidation of MeOH on a Pt electrode has been studied extensively on polycrystalline and single crystal platinum due to its importance in advancing the technology for direct methanol fuel cells (DMFCs).[33,34] The catalytic activity of the nano-fibrous Pt structures towards methanol was investigated using a 0.5 M MeOH solution in 0.5 M H_2SO_4 electrolyte. The voltammetry showed a characteristic oxidation peak current at +0.6 V (*vs.* SCE) on the positive scan. This oxidation peak was independent of scan rate (with appropriate background subtraction), which is indicative of a kinetically controlled (catalytic) process rather than one limited by diffusion (Figure 7.3A). A MeOH oxidation peak was also observed when scanning in the negative direction with an onset potential that coincides with the potential of the PtO_x/PtOH desorption region. The removal of oxides from the Pt surface leaves behind a clean and highly catalytic Pt region, which rapidly converts MeOH into products. The peak current of both MeOH oxidation peaks (from positive and negative-going scans) increases with MeOH concentration (Figure 7.3B), but plateaus at concentrations greater than 1 M MeOH.

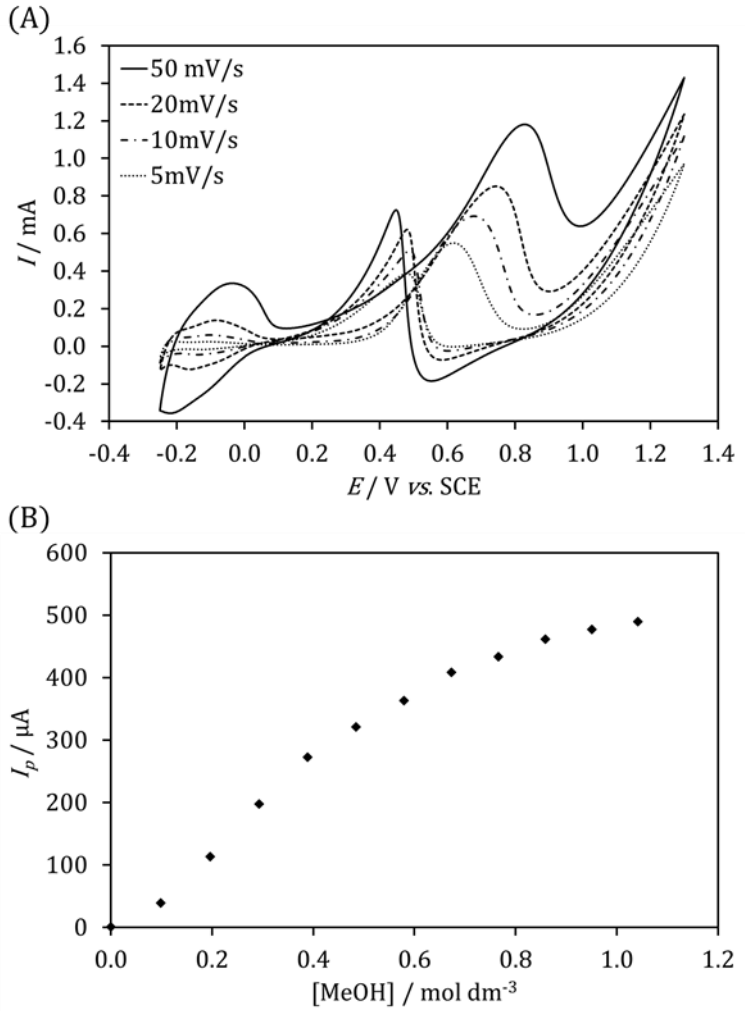

Figure 7.3. (**A**) Cyclic voltammograms (scan rates: 5, 10, 20, 50 mV s^{-1}) for the oxidation of 0.5 M MeOH in 0.5 M H_2SO_4 using sample **3** as the working electrode. (**B**) Plot of the methanol oxidation peak current versus methanol concentration.

A comparison of the peak current density for the MeOH oxidation process (for the positive scan) at a constant MeOH concentration can be used as a measure of the catalytic activity of the Pt nano-fibrous structure. The peak current density (j_p) is the quotient of the peak current (I_p) and the electrochemically active surface area (ESA) (equation 7.2).

$$j_p = \frac{I_p}{ESA} \tag{7.2}$$

Figure 7.4 shows cyclic voltammograms in the presence of 0.5 M methanol for nano-fibrous Pt electrodes deposited from different concentration $PtCl_6^{2-}$ precursor solutions. The peak current density was calculated for each electrode and compared with a polished 2 mm diameter Pt disc. It was observed that a positive potential window up to +1.3 V (*vs.*SCE) was required to maintain a good electrocatalytic response.

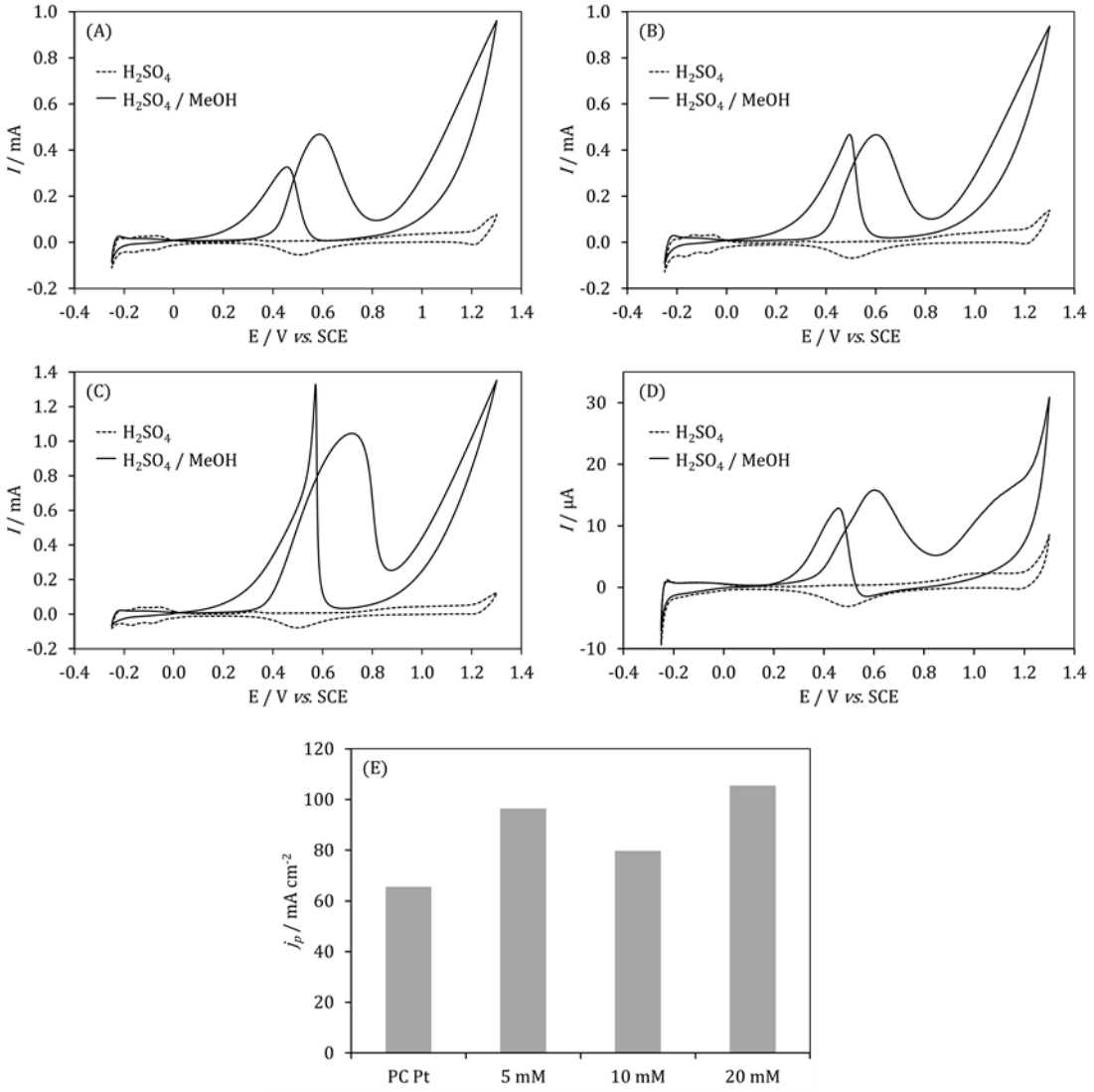

Figure 7.4. Cyclic voltammograms (scan rate 5 mV s^{-1}) for platinum electrodes immersed in 0.5 M H_2SO_4 without (solid line) and with (dashed line) 0.5 M MeOH for (**A**) the deposit formed from 5 mM $PtCl_6^{2-}$, (**B**) the deposit formed from 10 mM $PtCl_6^{2-}$, (**C**) the deposit formed from 20 mM $PtCl_6^{2-}$, and (**D**) a commercial 2 mm diameter platinum disc electrode. (**E**) Bar graph showing the peak current density (from positive scan) for the electro-oxidation of MeOH for the four types of electrodes (estimated error *ca.* $\pm$ 30 %).

The catalytic methanol oxidation appears most pronounced for the nano-fibrous platinum from the 20 mM precursor solution. The sharp peak-like current observed during the negative-going potential sweep is probably caused by a combination of the substrate resistance delaying the onset of the methanol oxidation and the formation of a highly active platinum surface after PtO_x/PtOH desorption.[35,36] The bar graph in Figure 7.4E shows a comparison of all four types of electrode (including a commercial 2 mm diameter polished Pt disc for comparison). Errors are estimated at $\pm$ 30 % and

only a minor increase in catalytic activity (or current density) was observed for nano-fibrous platinum. This is consistent with literature reports for nano-platinum on ITO [21,28]. The long term stability of the nano-fibrous platinum on ITO is limited. Performing 100 potential cycles in 0.5 H_2SO_4 with 0.5 M methanol, a clear decrease in the catalytic current was observed with sizeable areas of the platinum deposits detaching form the ITO surface. To increase the usefulness of these electrodes, the long term stability and uniformity of the platinum nano-fibrous deposits should be improved.

7.4 Conclusions

A one-step method for the synthesis of nano-fibrous platinum deposits from a PEG200 precursor solution in atmospheric conditions at 500 °C has been demonstrated. Upon heating the poly(ethylene glycol) solvent reduces the Pt(IV) species to metallic platinum, whilst simultaneously evaporating to leave a metallic platinum deposit on the substrate. The deposits form a network of nano-fibrous polycrystalline platinum structures on the surface with a high surface area. The electrocatalytic reactivity of the Pt deposits towards methanol oxidation was determined. Only a slight increase in catalytic activity was observed when compared to bulk polycrystalline platinum. Many parameters could affect the quality and activity of the platinum deposits and the procedure could be optimised further. For example, the ramping rate, maximum heating temperature, maximum heating time, cooling rate, and precursor solution composition could all influence the nature of the metal deposits. This method could also be of interest for the formation of mixed-metal catalysts. These nano-fibrous catalysts are most suited toward direct methanol fuel cell or electrochemical sensing applications. However, the long term stability and uniformity of the films must be improved to be useful electrode materials.

7.5 References

1. O. T. Holton and J. W. Stevenson, *Platinum Metals Review*, 2013, **57**, 259-271.
2. M.-Y. Yen, C.-C. Teng, M.-C. Hsiao, P.-I. Liu, W.-P. Chuang, C.-C. M. Ma, C.-K. Hsieh, M.-C. Tsai and C.-H. Tsai, *Journal of Materials Chemistry*, 2011, **21**, 12880-12888.
3. S. Marini, P. Salvi, P. Nelli, R. Pesenti, M. Villa, M. Berrettoni, G. Zangari and Y. Kiros, *Electrochimica Acta*, 2012, **82**, 384-391.
4. A. J. Silva, L. Proenca, M. I. S. Lopes, I. Fonseca, A. Rodes and A. Aldaz, *Electrochimica Acta*, 2001, **46**, 3147-3155.
5. E. Herrero, K. Franaszczuk and A. Wieckowski, *Journal of Physical Chemistry*, 1994, **98**, 5074-5083.
6. Z. Peng and H. Yang, *Nano Today*, 2009, **4**, 143-164.
7. J. Chen, B. Lim, E. P. Lee and Y. Xia, *Nano Today*, 2009, **4**, 81-95.
8. G. J. Leong, M. C. Schulze, M. B. Strand, D. Maloney, S. L. Frisco, H. N. Dinh, B. Pivovar and R. M. Richards, *Applied Organometallic Chemistry*, 2014, **28**, 1-17.
9. F. Ye, L. Chen, J. Li, J. Li and X. Wang, *Electrochemistry Communications*, 2008, **10**, 476-479.
10. M. Zhang, J.-J. Lv, F.-F. Li, N. Bao, A.-J. Wang, J.-J. Feng and D.-L. Zhou, *Electrochimica Acta*, 2014, **123**, 227-232.
11. T.-L. Hsieh, H.-W. Chen, C.-W. Kung, C.-C. Wang, R. Vittal and K.-C. Ho, *Journal of Materials Chemistry*, 2012, **22**, 5550-5559.
12. R. G. Freitas, R. T. S. Oliveira, M. C. Santos, L. O. S. Bulhoes and E. C. Pereira, *Materials Letters*, 2006, **60**, 1906-1910.
13. F. L. S. Purgato, P. Olivi, J. M. Leger, A. R. de Andrade, G. Tremiliosi-Filho, E. R. Gonzalez, C. Lamy and K. B. Kokoh, *Journal of Electroanalytical Chemistry*, 2009, **628**, 81-89.
14. H.-S. Oh, J.-G. Oh and H. Kim, *Journal of Power Sources*, 2008, **183**, 600-603.
15. Z. C. Tang, D. S. Geng and G. X. Lu, *J. Colloid Interface Sci.*, 2005, **287**, 159-166.
16. S. Hirano, J. Kim and S. Srinivasan, *Electrochimica Acta*, 1997, **42**, 1587-1593.
17. Y. Liu and W. E. Mustain, *Journal of the American Chemical Society*, 2013, **135**, 530-533.
18. S. Zhao, A. E. Wangstrom, Y. Liu, W. A. Rigdon and W. E. Mustain, *Electrochimica Acta*, 2015, **157**, 175-182.
19. A. Velazquez-Palenzuela, F. Centellas, E. Brillas, J. Antonio Garrido, C. Arias, R. Maria Rodriguez and P.-L. Cabot, *International Journal of Hydrogen Energy*, 2013, **38**, 16418-16426.
20. J. Florez-Montano, G. Garcia, J. L. Rodriguez, E. Pastor, P. Cappellari and G. A. Planes, *Journal of Power Sources*, 2015, **282**, 34-44.
21. G. Chang, M. Oyama and K. Hirao, *Journal of Physical Chemistry B*, 2006, **110**, 1860-1865.
22. F. Fievet and R. Brayner, The Polyol Process in *Nanomaterials: A Danger or a Promise?*, eds. R. Brayner, F. Fievet and T. Coradin, Springer, London, 2013.

23. T. Herricks, J. Y. Chen and Y. N. Xia, *Nano Letters*, 2004, **4**, 2367-2371.
24. J. Y. Chen, T. Herricks and Y. N. Xia, *Angewandte Chemie-International Edition*, 2005, **44**, 2589-2592.
25. B. Liu, Z.-W. Chia, Z.-Y. Lee, C.-H. Cheng, J.-Y. Lee and Z.-L. Liu, *Journal of Power Sources*, 2012, **206**, 97-102.
26. S.-B. Han, Y.-J. Song, J.-M. Lee, J.-Y. Kim, D.-H. Kim and K.-W. Park, *Bulletin of the Korean Chemical Society*, 2009, **30**, 2362-2364.
27. J.-F. Li, Z.-L. Xu, H. Yang, C.-P. Feng and J.-H. Shi, *Journal of Applied Polymer Science*, 2008, **107**, 4100-4108.
28. J. Liu, C. Zhong, X. Du, Y. Wu, P. Xu, J. Liu and W. Hu, *Electrochimica Acta*, 2013, **100**, 164-170.
29. Y. Ohkubo, S. Seino, S. Kageyama, J. Kugai, T. Nakagawa, K. Ueno and T. A. Yamamoto, *Journal of Nanoparticle Research*, 2014, **16**.
30. E. M. Crabb, R. Marshall and D. Thompsett, *Journal of the Electrochemical Society*, 2000, **147**, 4440-4447.
31. B. E. Conway, *Progress in Surface Science*, 1995, **49**, 331-452.
32. S. Guerin, B. E. Hayden, C. E. Lee, C. Mormiche, J. R. Owen, A. E. Russell, B. Theobald and D. Thompsett, *Journal of Combinatorial Chemistry*, 2004, **6**, 149-158.
33. T. H. M. Housmans and M. T. M. Koper, *Journal of Physical Chemistry B*, 2003, **107**, 8557-8567.
34. X. Li and A. Faghri, *Journal of Power Sources*, 2013, **226**, 223-240.
35. N. Cheng, R. A. Webster, M. Pan, S. Mu, L. Rassaei, S. C. Tsang and F. Marken, *Electrochimica Acta*, 2010, **55**, 6601-6610.
36. Y. E. Seidel, A. Schneider, Z. Jusys, B. Wickman, B. Kasemo and R. J. Behm, *Langmuir*, 2010, **26**, 3569-3578.

Chapter 8: Conclusions and future work

Solvents play a critical role in the success of a reaction and it is becoming increasingly more important to find environmentally benign solvents for many chemical and electrochemical processes. Poly(ethylene glycol) has been identified as a non-toxic, inexpensive, non-volatile and environmentally benign material. The electrochemical properties and potential uses of the solvent have been investigated.

Voltammetry under vacuum conditions has been demonstrated as a method to remove unwanted gases and to control the humidity of non-volatile liquids. Double potential step experiments were coupled with computer simulations to determine the diffusion coefficients of anthraquinone-2-sulfonate, 1,1'-ferrocene dicarboxylic acid and 1,1'-ferrocene dimethanol under mixed diffusion conditions in poly(ethylene glycol) with an average molecular weight of 200 g mol^{-1} (PEG200). Cyclic voltammetry simulations using the optimised diffusion coefficients showed an overestimation of the peak currents for 1,1'-ferrocene dicarboxylic acid and for anthraquinone-2-sulfonate due to the presence of underlying background processes. However, the diffusion coefficients determined for 1,1'-ferrocene dimethanol ($D_{ox} = 1.3 \times 10^{-7}$ cm^2 s^{-1} and $D_{red} = 1.4 \times 10^{-7}$ cm^2 s^{-1}) gave a good fit between simulation and experiment for both potential step and cyclic voltammetry. The values were therefore deemed reliable. The low diffusion coefficient values and the corresponding low currents were attributed to the high viscosity of the PEG200 solution.

In order to enhance currents in viscous electrolyte media, a new hydrodynamic technique was developed. The technique was based upon an inlaid disc electrode approaching a rotating drum so that laminar Couette flow conditions were established in the microgap between the electrode and the rotating wheel. A Levich-type equation, that is geometry dependent, was derived for the hydrodynamic system under Couette flow conditions in a microgap. The Levich-type equation indicated that the limiting current was proportional to the cube root of the rotation speed, but independent upon the viscosity of the solution. Experiments confirmed the validity of the Levich-type equation and the technique successfully caused an increase of two orders of magnitude in the limiting current. Further current enhancements could be achieved by using faster

rotation speeds and developing a similar system with nano-sized distances between electrode and rotating drum. However, improvements to further minimise drum irregularities must be made before nano-size gaps could give reliable data. The hydrodynamic method under Couette flow conditions successfully enhanced currents at an electrode surface in PEG200 and would be suitable for a range of other viscous solvents. This technique could also be used for electrosynthetic applications using highly viscous solvents.

An electrochemical anodic grafting method was developed for the attachment of poly(ethylene glycol) to glassy carbon and boron doped diamond electrodes. XPS data analysis was consistent with poly(ethylene glycol) modified surfaces. Furthermore, the grafting of a more complex, PEGylated species, namely Kolliphor® EL, was also demonstrated on glassy carbon surfaces. The simple electrochemical attachment of poly(ethylene glycols) could enable facile surface modifications with other complex molecules, such as PEGylated redox active proteins, which could lead to interesting surface properties.

The grafting of PEG derivatives to carbon surfaces caused a severe decrease in the rate of heterogeneous electron transfer for the $Fe(CN)_6^{3-/4-}$ redox couple, which was demonstrated by cyclic voltammetry and electrochemical impedance spectroscopy. It is proposed that the hydrophilic $Fe(CN)_6^{3-/4-}$ couple cannot penetrate far into the PEG layer, which causes an apparent decrease in the heterogeneous rate of electron transfer. However, the rate of heterogeneous electron transfer for more hydrophobic species is unimpeded by the presence of the PEG layer. It was found that low concentrations (< 50 μM) of ferrocene derivatives can act as electron shuttle molecules and mediate the oxidation (and to a lesser extent the reduction) of the $Fe(CN)_6^{3-/4-}$ redox couple. The mediated response causes an amplification in current that would typically be expected. Consequently, very low concentrations (< 1 μM) of mediator could be detected, which could have future applications in electroanalytical sensing devices, in particular bio-medical devices. PEG is known to exhibit anti-fouling properties and it would be of interest if these PEG-modified electrodes were resistant to protein adsorption, however, this has not been explored in the current study. Further improvements on the stability of the PEG films must also be made for these modified electrodes to give reliable electroanalytical readings.

A one-step electroless deposition was developed whereby poly(ethylene glycol) was used as the solvent and reducing agent for the formation of nano-fibrous platinum deposits from a platinum(IV) salt precursor solution. The catalytic activity of the resulting platinum deposits towards the electro-oxidation of methanol was assessed. Only slight increases in electro-catalytic activity were observed when compared to a polished, polycrystalline platinum disc electrode. The electroless deposition technique could be adapted to synthesise a wide range of metallic deposits, including perhaps alloys. Further optimisation of the thermolysis technique could help control the shape and uniformity of the deposits on the chosen substrate.

In summary, a range of electrochemical methods have been developed for the study of redox processes in viscous polymer solvents, in particular poly(ethylene glycol). The often low volatility of polymer solvents enables processes to be performed *in vacuo*, which allows the atmosphere and humidity levels to be controlled. These properties could be of particular interest in carbon capture technologies, where the highly absorbing nature of poly(ethylene glycol) towards carbon dioxide could be utilised. Volatile products from the electro-reduction of carbon dioxide could be extracted under reduced pressure. Such viscous solvents suffer from slow mass transport effects, which can make voltammetry troublesome. However, hydrodynamic methods can be used to overcome this limitation. An anodic grafting method was also developed for the surface modification of poly(ethylene glycol), which could have uses in electroanalytical applications. However, further improvements on the film stability must be made in order for reliable sensing devices to be manufactured. Finally, a one-step electroless deposition method was developed for the formation of nano-fibrous metallic deposits. The technique could be adapted for a wide range of metal (or mixed metal) deposits for catalytic applications.

Many methods are available to study and exploit the advantageous properties of polymer solvents for electrochemical processes. In particular, poly(ethylene glycol) is a low cost, non-toxic, environmentally benign solvent that has been shown to be a suitable solvent in electrochemical systems.